STUDY OF TWO-DIMENSIONAL SHOCK TUBE FLOWS BY FOLLOWING PARTICLE TRAJECTORIES USING A MULTIPLY PULSED LASER SCHLIEREN SYSTEM

by

David Keith Walker

B.Sc., University of Wales, 1965

M.Sc., University of Victoria, 1971

A DISSERTATION SUBMITTED IN PARTIAL FULFILLMENT
OF THE REQUIREMENTS FOR THE DEGREE OF
DOCTOR OF PHILOSOPHY
in the Department of
Physics

We accept this dissertation as conforming
to the required standard

..

..

..

.

.

University of Victoria

May 1974

Supervisor: Professor John M. Dewey

ABSTRACT

A system for recording the trajectories of non-planar shocks and particle tracers within a shock tube flow has been developed.

The optics consists of a double-pass schlieren system with a multiply pulsed ruby laser as light source. The laser is synchronized with a high speed framing camera. A grid of ammonium chloride tracers is injected into the flow field, and the motion of the tracers behind the Mach reflection of intermediate strength shocks has been recorded.

Analysis of the trajectories has yielded the space and time variation of the physical properties within the flow field.

.....

TABLE OF CONTENTS

		Page
ABSTRACT		ii
LIST OF TABLES		v
LIST OF FIGURES		vi
LIST OF SYMBOLS		ix
ACKNOWLEDGEMENTS		x
CHAPTER 1	INTRODUCTION	1
CHAPTER 2	SHOCK INTERACTION STUDIES	5
	2.1 One-dimensional interactions	5
	2.2 Oblique interaction	7
CHAPTER 3	PARTICLE TRAJECTORY ANALYSIS	20
	3.1 INTRODUCTION	20
	3.2 Theory	20
	3.3 Applications	25
	3.4 Experimental methods	30
CHAPTER 4	EXPERIMENTAL PROCEDURES	35
	4.1 The optical system	35
	4.2 The light source	45
	4.3 The Pockels cell driver	63
	4.4 The test section mirror	64
	4.5 The particle tracers	69
	4.6 Synchronization and monitoring	72

Page

CHAPTER 5 ANALYSIS OF DATA 77

5.1 Digitization 77

5.2 Reduction of digitized data 79

5.3 Determination of density 83

5.4 Determination of particle velocity 84

5.5 Pressure and temperature 90

CHAPTER 6 DISCUSSION AND CONCLUSIONS 96

LIST OF TABLES

Table No.		Page
5.3.1	Determination of areas from digitized data	85
5.3.2	Density values for Fig. 5.3.1	87
5.3.3	Density values for Fig. 5.3.2	89
5.4.1	Velocity values for Fig. 5.4.1	92
A.1.1	Density values, 30°, Mach 1.34, 190 μs	108
A.1.2	Density values, 30°, Mach 1.34, 289 μs	110
A.1.3	Density values, 30°, Mach 1.34, 387 μs	112
A.1.4	Velocity values, 30°, Mach 1.34, 190 - 289 μs	114
A.1.5	Velocity values, 30°, Mach 1.34, 289 - 387 μs	116
A.2.1	Density values, 10°, Mach 1.35, 349 μs	121
A.2.2	Density values, 10°, Mach 1.35, 442 μs	123
A.2.3	Velocity values, 10°, Mach 1.35, 349 - 442 μs	125
A.3.1	Density values, 10°, Mach 1.21, 345 μs	129
A.3.2	Density values, 10°, Mach 1.21, 437 μs	131
A.3.3	Density values, 10°, Mach 1.21, 532 μs	133
A.3.4	Velocity values, 10°, Mach 1.21, 345 - 437 μs	135
A.3.5	Velocity values, 10°, Mach 1.21, 437 - 532 μs	137
A.4.1	Density values, 30°, Mach 1.20, 232 μs	142
A.4.2	Density values, 30°, Mach 1.20, 328 μs	144
A.4.3	Density values, 30°, Mach 1.20, 423 μs	146
A.4.4	Velocity values, 30°, Mach 1.20, 232 - 328 μs	148
A.4.5	Velocity values, 30°, Mach 1.20, 328 - 423 μs	150

LIST OF FIGURES

Figure No.		Page
2.1.1	Wave diagram illustrating a shock interaction	6
2.2.1	Interaction of a shock wave with a wedge	8
2.2.2	Comparison of theory and experiment in regular and Mach reflection	11
2.2.3	Interaction of a strong shock with a wedge	13
2.2.4	The results of Ludloff and Friedmann (1955)	14
3.3.1	Geometry of two gas flows	26
3.3.2	Element of air at two different times in a two-dimensional shock tube flow	28
3.4.1	Cigarette smoke tracers behind a reflected shock	32
3.4.2	Schlieren photographs of spot heated elements of air . .	33
4.1.1	Schlieren system using lenses	37
4.1.2	Z-pass schlieren	40
4.1.3	Double pass schlieren system	42
4.2.1	Laser shadowgraph of Mach reflection	46
4.2.2	Optical components within the modified laser cavity . . .	47
4.2.3	Flash tube and conventional lasing output	49
4.2.4	Conventional lasing output	50
4.2.5	Double crystal transverse Pockels cell components	53
4.2.6	Pockels cell assembly	55
4.2.7	Crystal cut and crystal axes	56

Figure No.

		Page
4.2.8	Experimental testing of Pockels cell modulator	57
4.2.9	Laser Q-switched pulse	61
4.2.10	A series of Q-switched pulses	62
4.3.1	Pockels cell driver circuit	65
4.3.2	Pockels cell driver unit	66
4.3.3	Pockels cell and driver within the laser cavity	67
4.5.1	Formation of particle tracers	70
4.6.1	Shutter pulse output	74
4.6.2	Laser light detector	75
5.1.1	High speed film record	78
5.2.1	Projection of film record	80
5.3.1	Particle positions, 30°, Mach 1.20, 214 μs	86
5.3.2	Particle positions, 30°, Mach 1.20, 326 μs	88
5.4.1	Velocity vectors, 30°, Mach 1.20, 214 - 326 μs	91
5.5.1	Mean ratios, 30°, Mach 1.20, 214 μs	94
5.5.2	Mean ratios, 30°, Mach 1.20, 326 μs	95
A.1.1	Particle positions, 30°, Mach 1.34, 190 μs	107
A.1.2	Particle positions, 30°, Mach 1.34, 289 μs	109
A.1.3	Particle positions, 30°, Mach 1.34, 387 μs	111
A.1.4	Velocity vectors, 30°, Mach 1.34, 190 - 289 μs	113
A.1.5	Velocity vectors, 30°, Mach 1.34, 289 - 387 μs	115

Figure No. Page

A.1.6 Mean ratios, 30°, Mach 1.34, 190 μs 117

A.1.7 Mean ratios, 30°, Mach 1.34, 289 μs 118

A.1.8 Mean ratios, 30°, Mach 1.34, 387 μs 119

A.2.1 Particle positions, 10°, Mach 1.35, 349 μs 120

A.2.2 Particle positions, 10°, Mach 1.35, 442 μs 122

A.2.3 Velocity vectors, 10°, Mach 1.35, 349 - 442 μs 124

A.2.4 Mean ratios, 10°, Mach 1.35, 349 μs 126

A.2.5 Mean ratios, 10°, Mach 1.35, 442 μs 127

A.3.1 Particle positions, 10°, Mach 1.21, 345 μs 128

A.3.2 Particle positions, 10°, Mach 1.21, 437 μs 130

A.3.3 Particle positions, 10°, Mach 1.21, 532 μs 132

A.3.4 Velocity vectors, 10°, Mach 1.21, 345 - 437 μs 134

A.3.5 Velocity vectors, 10°, Mach 1.21, 437 - 532 μs 136

A.3.6 Mean ratios, 10°, Mach 1.21, 345 μs 138

A.3.7 Mean ratios, 10°, Mach 1.21, 437 μs 139

A.3.8 Mean ratios, 10°, Mach 1.21, 532 μs 140

A.4.1 Particle positions, 30°, Mach 1.20, 232 μs 141

A.4.2 Particle positions, 30°, Mach 1.20, 328 μs 143

A.4.3 Particle positions, 30°, Mach 1.20, 423 μs 145

A.4.4 Velocity vectors, 30°, Mach 1.20, 232 - 328 μs 147

A.4.5 Velocity vectors, 30°, Mach 1.20, 328 - 423 μs 149

A.4.6 Mean ratios, 30°, Mach 1.20, 232 μs 151

A.4.7 Mean ratios, 30°, Mach 1.20, 328 μs 152

A.4.8 Mean ratios, 30°, Mach 1.20, 423 μs 153

LIST OF SYMBOLS

General notation

a sound speed

c_p specific heat at constant pressure

c_v specific heat at constant volume

D density ratio

d density

M shock Mach number (shock speed/speed of sound ahead of shock)

P pressure ratio

p pressure

R universal gas constant (gas constant per mole)

t time

T absolute temperature or temperature ratio

u longitudinal to free stream component of particle velocity

v transverse to free stream component of particle velocity

x longitudinal co-ordinate (parallel to incident flow)

y transverse co-ordinate (perpendicular to incident flow)

γ ratio of specific heats (c_p / c_v)

ACKNOWLEDGEMENTS

I wish to thank Dr. J.M. Dewey for his guidance and encouragement in the supervision of this project. I also wish to thank Mr. L.N. Scotten for his technical assistance.

The University of Victoria, the National Research Council, and the Defence Research Board are gratefully acknowledged for their financial support.

CHAPTER 1

INTRODUCTION

When a disturbance moves through a medium at a velocity greater than the velocity of sound within that medium, so-called shock waves develop, characterized by extremely rapid changes in the physical properties of the medium. Supersonic aircraft, spacecraft re-entering the atmosphere, the flight of a bullet, and the bursting of a balloon are all familiar examples of phenomena which produce shock waves. When these shock waves encounter obstacles, or density changes in the medium through which they are travelling, reflection and refraction occur. Theoretical prediction of the behaviour of shock waves upon reflection and refraction has proved to be difficult, other than in very simple configurations, because of the non-linear nature of the equations describing shock wave motion.

The process of shock reflection and refraction has been studied experimentally both in the laboratory and in large scale field experiments. The shocks may reflect off solid obstacles, or off each other. If the shocks are arranged to reflect off each other then the reflection process may be studied in a situation uninfluenced by boundary layer effects.

The first experimental work on shock wave reflection was carried out by Mach and his associates (1878). In this work it was observed that in certain cases a single incident shock in oblique reflection

could produce not one but two reflected shocks. This phenomena where three shocks intersect at one point has since been named Mach reflection. Subsequently, Gvozdeva *et al.* (1969) have discovered that in the oblique reflection of strong shocks a double Mach configuration may result from a single incident shock.

In the laboratory, reflection of shock waves off solid obstacles is conveniently studied in a shock tube, an instrument first used by Vieille (1899). It was not until the 1940's that experimental studies of shock reflection were systematically undertaken. Today the subject continues to provide problems for both the theoretical and experimental worker. Even for the comparatively simple case of normal reflection of a shock at the end of a shock tube, Dumitrescu and Popescu (1970) can write that the problem is far from settled. The interaction processes between the reflected shock, the boundary layer, and the contact surface affects the duration and uniformity of the hot region in the shock tube in a way not yet fully understood. When the shock is obliquely incident the complexity of the process is increased, and a number of interesting phenomena are observed. It is found, for instance, that oblique reflection sometimes results in a higher peak pressure at the reflecting surface than does normal reflection as reported by Von Neumann (1943). This phenomena was of importance to the early investigators who were interested in assessing the damage caused by blast waves.

In the next chapter a survey of the theoretical and experimental work done on shock reflection and refraction will be given.

The mathematical problem involves the solution of a system of differential equations with appropriate boundary conditions. There has been no analytical solution of the general problem. In order that the analysis should become tractable, various simplifying assumptions have been made. The analyses generally have as their basis equations expressing conservation of mass, momentum and energy. In some cases experimental measurements have indicated what assumptions may be made, and have been able to resolve ambiguities occurring in the mathematics. Experimental measurements have also been used to check various analyses, and to supply information which will help in the integration of a system of differential equations. It will be seen in the next chapter that there has sometimes been marked divergence between theory and experiment in the development of this subject.

Much of the experimental and theoretical work has been concerned with the behaviour of the shock fronts, and has dealt with the flow field between shocks only inasmuch as it directly affects the movement of the shocks. Theoretical calculations of the flow field have been made for some few specific cases, and comparison made with experimental data. Apart from interferometric determinations of the density field there is very little experimental data recording properties throughout the flow field.

In the present experimental work, which can be applied to a number of interaction processes, a method is employed which is capable of determining all of the physical properties within the whole field

in a two-dimensional shock tube flow. This method uses a technique of particle trajectory analysis which will be described in Chapter 3. In this technique both shocks and particle trajectories can be followed on the same photographic record so that considerably more information about the flow can be obtained than would be possible from pictures recording shocks alone. Many shock tube workers have gathered data about a particular shock tube flow by using repeated firings with the same initial conditions. In this way the spatial and time resolution of recording instruments can be extended with the assumption that each firing produces exactly the same shock tube flow. The validity of this assumption will be referred to later in this thesis. Using the present experimental technique, all data about a particular flow is collected during a single shock tube firing. Hence any doubt about the reproducibility of repeated firings is removed. To the author's knowledge this is the first time shock and particle trajectories in a shock tube flow have been recorded simultaneously.

CHAPTER 2

SHOCK INTERACTION STUDIES

2.1 One-dimensional interactions

The simplest type of shock interaction is that of a normal collision. This may be the interaction of a shock with the interface between two media, with another shock, or with a rarefaction wave. A wave diagram illustrating the interaction of a shock wave with a contact surface in a shock tube is shown in Fig. 2.1.1. The dashed line denoting the contact surface separates the gas which was originally at the diaphragm of the shock tube from that which has been compressed and heated by the shock wave. Across a contact surface there is, in general, a change in type, temperature, and density of the gas, whereas velocity is unchanged. The trajectories of shock waves are shown in the distance-time plane where distance is measured along the shock tube. In all cases of a one-dimensional flow for which the boundary layer effects are ignored, a solution of the interaction within a perfect gas is made by use of the Rankine-Hugoniot equations. These equations relate the conditions on either side of an entropy change and are derived using conservation of mass, momentum and energy. For normal shock reflection at the end wall of a shock tube, the boundary condition used is that the particle velocity at the wall be zero. Bradley (1962), and Gaydon and Hurle (1963) give a treatment of this interaction process. The modification of this idealized interaction behaviour by imperfect gas effects, boundary layers, rarefaction waves, and contact surfaces is a subject yet to be fully explored.

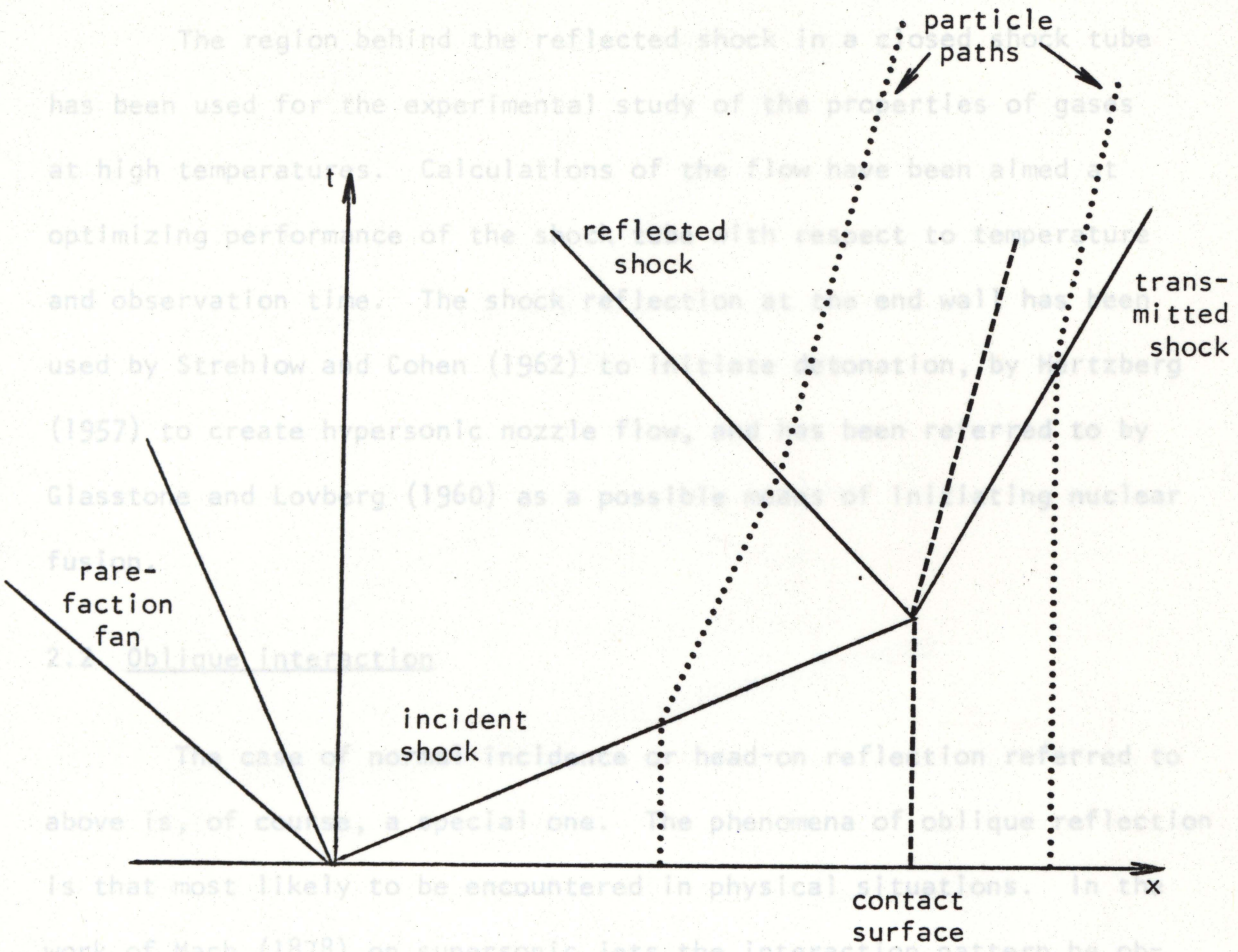

Fig. 2.1.1 A wave diagram illustrating the interaction of a shock wave with a contact surface in a shock tube. The dotted lines show particle paths; the dashed line shows the position of the contact surface. Also shown is the rarefaction fan moving away from the diaphragm.

The region behind the reflected shock in a closed shock tube has been used for the experimental study of the properties of gases at high temperatures. Calculations of the flow have been aimed at optimizing performance of the shock tube with respect to temperature and observation time. The shock reflection at the end wall has been used by Strehlow and Cohen (1962) to initiate detonation, by Hertzberg (1957) to create hypersonic nozzle flow, and has been referred to by Glasstone and Lovberg (1960) as a possible means of initiating nuclear fusion.

2.2 Oblique interaction

The case of normal incidence or head-on reflection referred to above is, of course, a special one. The phenomena of oblique reflection is that most likely to be encountered in physical situations. In the work of Mach (1878) on supersonic jets the interaction pattern he observed was a stationary one. Lean (1946) studied the stationary pattern of shock waves produced between wedges placed in a wind tunnel and measured the angles between the shocks.

In an effort to understand the interaction of blast waves with structures, Von Neumann (1943), Polachek and Seeger (1943), and Bleakney and Taub (1949) made calculations on the interaction of a shock with a wedge. Smith (1945) made extensive experimental measurements of the reflection process in a shock tube. Some of the shock configurations which have been studied are shown in Fig. 2.2.1. In regular reflection the incident and reflected shocks meet at a point on the wedge.

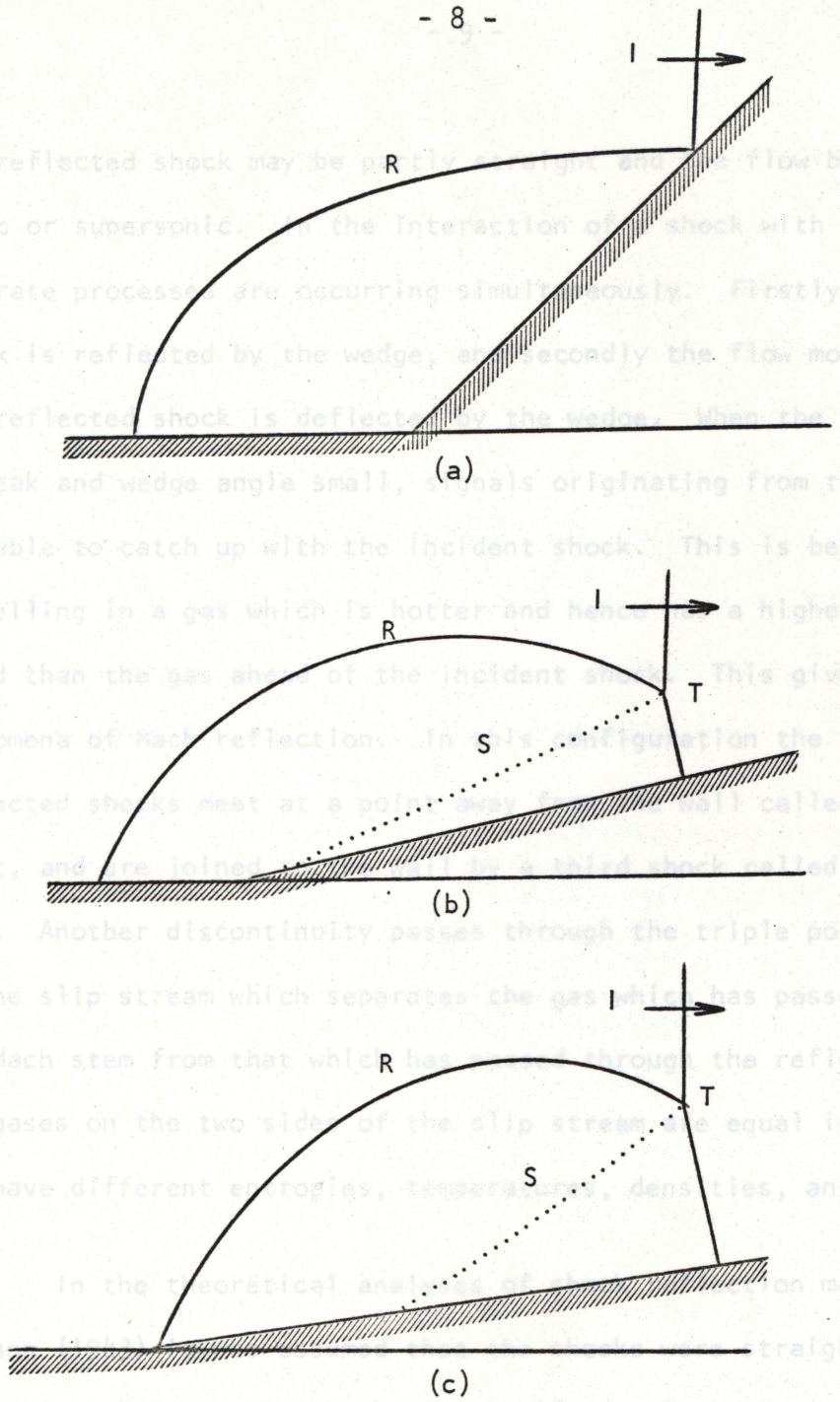

Fig. 2.2.1 Some possible configurations for the interaction of a shock wave with a wedge.

(a) Regular reflection, (b) Mach reflection with detached bow shock,

(c) Mach reflection with attached bow shock.

I--incident shock, R-- reflected shock, T--triple point, S--slip stream

The reflected shock may be partly straight and the flow behind it subsonic or supersonic. In the interaction of a shock with a wedge two separate processes are occurring simultaneously. Firstly the incident shock is reflected by the wedge, and secondly the flow moving behind the reflected shock is deflected by the wedge. When the incident shock is weak and wedge angle small, signals originating from the wedge corner are able to catch up with the incident shock. This is because they are travelling in a gas which is hotter and hence has a higher velocity of sound than the gas ahead of the incident shock. This gives rise to the phenomena of Mach reflection. In this configuration the incident and reflected shocks meet at a point away from the wall called the triple point, and are joined to the wall by a third shock called the Mach stem. Another discontinuity passes through the triple point. This is the slip stream which separates the gas which has passed through the Mach stem from that which has passed through the reflected shock. The gases on the two sides of the slip stream are equal in pressure, but have different entropies, temperatures, densities, and velocities.

In the theoretical analyses of shock reflection made by Von Neumann (1943) it was assumed that the shocks were straight, and that the regions between the shocks were uniform. The extent to which these assumptions are valid has subsequently been clarified by interferometric studies. The Rankine-Hugoniot equations were applied across shocks, and it was required that behind the reflected wave the flow should be parallel to the wall. In the case of Mach reflection, use was made of the experimental observation that the shock configurations remain geometric-

ally similar at all times. Such a flow is termed pseudo-stationary. The analysis was successful in predicting the angles of incidence and reflection for the case of regular reflection, but for Mach reflection serious discrepancies were encountered which have yet to be fully resolved (Fig. 2.2.2). Firstly, the theoretically calculated angle at which the regular reflection pattern goes over into Mach reflection did not agree with experiment, and secondly the theory was clearly inadequate for predicting the angles between shocks in the case of Mach reflection of weak shocks. These discrepancies are pointed out by Bleakney and Taub (1949) in a review article.

Several attempts were made to resolve the discrepancies referred to above. Bargmann (1945), by assuming the regions above and below the reflected shock were uniformly of the same entropy, and by restricting his analysis to weak shocks at glancing incidence, was able to obtain solutions for the entire flow field. Guderley (1947) developed an analysis restricted to weak incident shock waves which placed a centered isentropic flow expansion at the triple point.

Lighthill (1949, 1950) treated the problem of the diffraction of shocks of arbitrary strength at convex and concave corners of small angle. He calculated the pressure distribution on the rigid boundary. Ting and Ludloff (1950) outlined a method in which they treat the interaction as a time-dependent perturbation problem. Again the analysis is for shocks of arbitrary strength at glancing incidence, and in this case both the pressure and density fields were determined. In a review

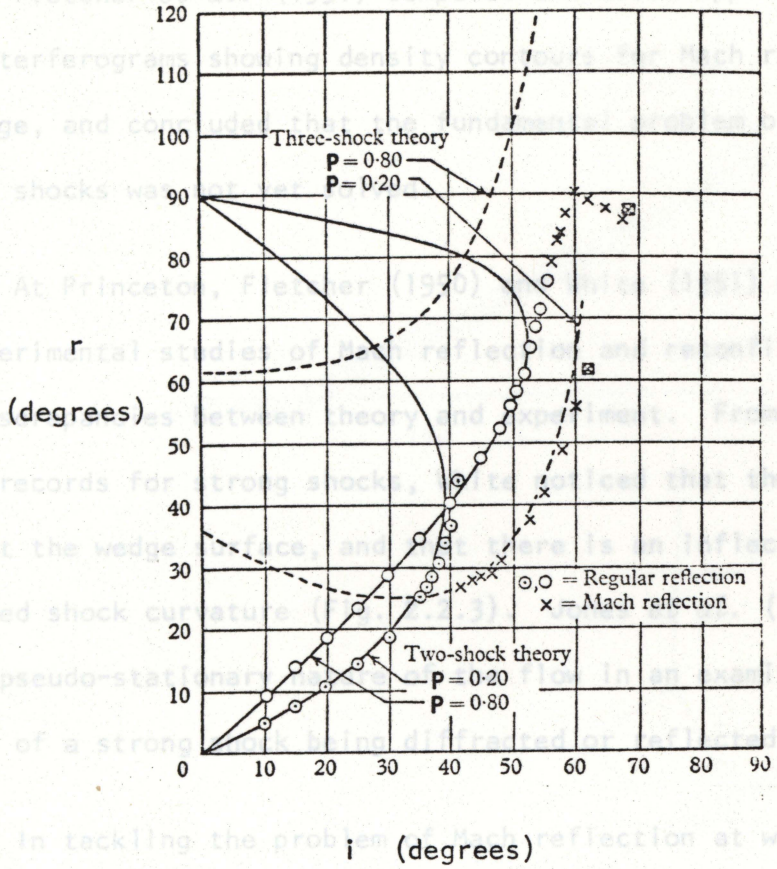

Fig. 2.2.2 Comparison of theory and experiment in regular and Mach reflection. P = pressure ratio across shock; i and r are the angles made by the incident and reflected shocks respectively with the wedge in the case of regular reflection, and with the path of the triple point in the case of Mach reflection. (Pack 1964)

article Fletcher *et al.* (1951) compared the above approximate treatment with interferograms showing density contours for Mach reflection at a 10° wedge, and concluded that the fundamental problem of Mach reflection of weak shocks was not yet solved.

At Princeton, Fletcher (1950) and White (1951) made theoretical and experimental studies of Mach reflection and reconfirmed that there were discrepancies between theory and experiment. From his interferometric records for strong shocks, White noticed that the slip stream curls at the wedge surface, and that there is an inflection in the reflected shock curvature (Fig. 2.2.3). Jones *et al.* (1951) made use of the pseudo-stationary nature of the flow in an examination of the problem of a strong shock being diffracted or reflected at a corner.

In tackling the problem of Mach reflection at wedges of finite angle, Ludloff and Friedmann (1955) used a numerical difference scheme to compute the isentrops throughout the flow field from the experimentally determined isopycnics. Their results for a 38° wedge are shown in Fig. 2.2.4.

Jahn (1956) made extensive studies in a shock tube of the refraction of a shock wave at the interface between two media. The theoretical analysis of this situation closely parallels the analysis for Mach reflection. His measurements found similar discrepancies to those reported earlier for the shock reflection problem. Sternberg (1959), by using the analogy between the flow of a current in an electric tank and compressible flow, finds that for Mach reflection

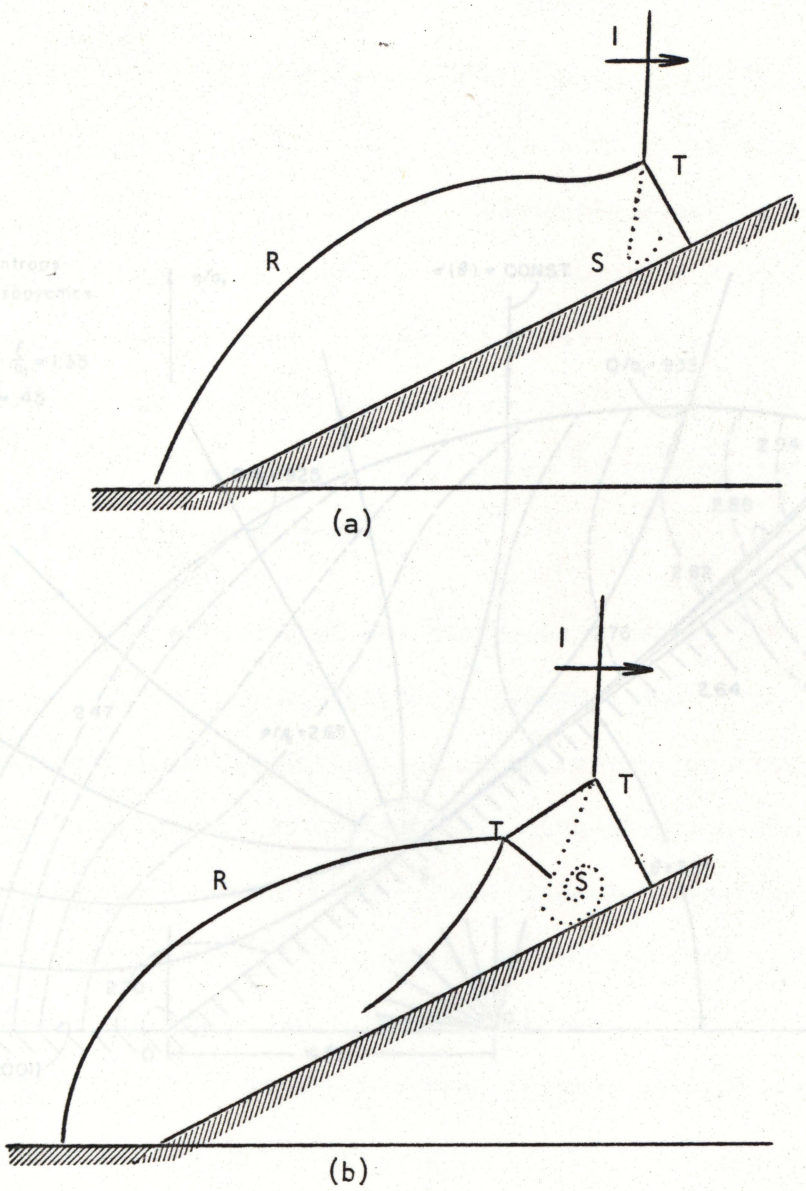

Fig. 2.2.3 Some possible configurations for the interaction of a strong shock with a wedge.

(a) Irregular Mach reflection with kinked reflected shock.

(b) Irregular Mach reflection with second triple shock system (Gvozdeva *et al.* 1969).

I--incident shock, R--reflected shock, T--triple point, S--slip stream.

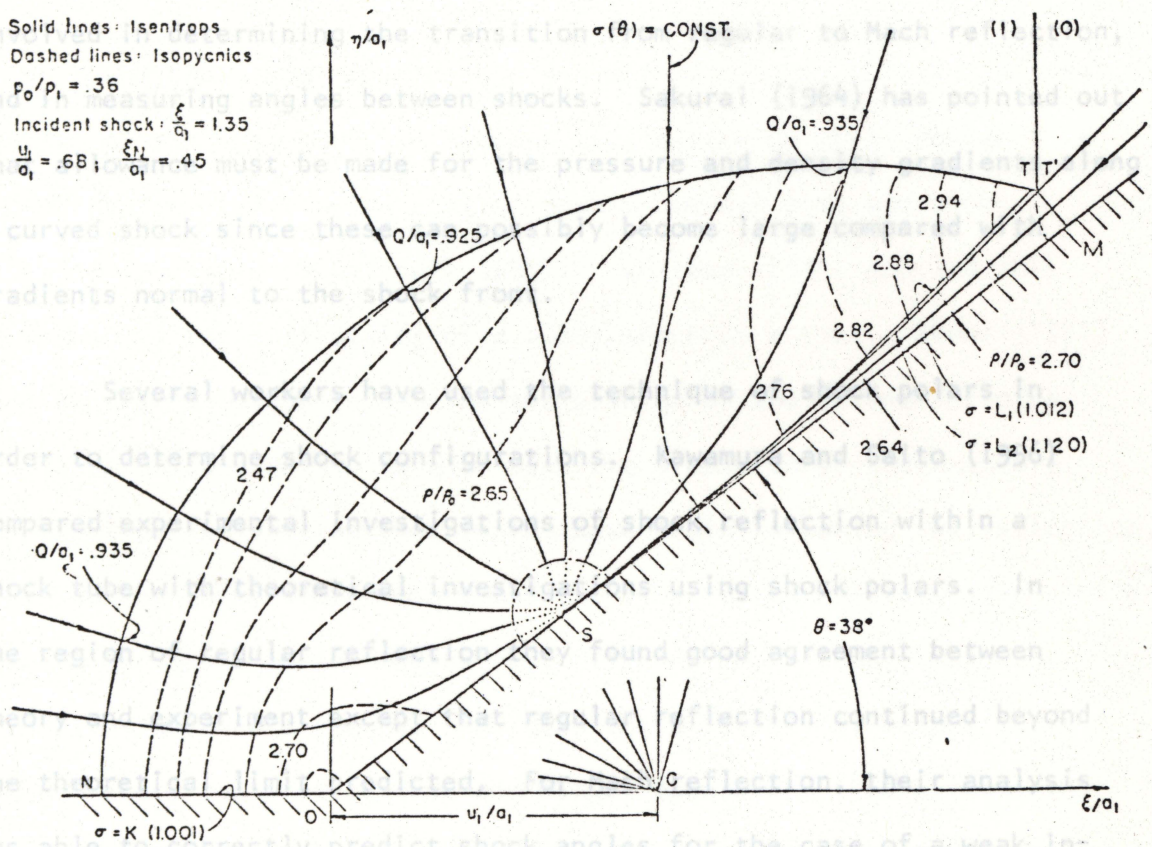

Fig. 2.2.4 The results of Ludloff and Friedmann (1955) for the flow over a 38° wedge.

the shock waves are so strongly curved near the triple point that angles between shocks would not be able to be determined accurately in the laboratory. Smith (1959, 1962) deals with the experimental difficulties involved in determining the transition from regular to Mach reflection, and in measuring angles between shocks. Sakurai (1964) has pointed out that allowance must be made for the pressure and density gradients along a curved shock since these can possibly become large compared with gradients normal to the shock front.

Several workers have used the technique of shock polars in order to determine shock configurations. Kawamura and Saito (1956) compared experimental investigations of shock reflection within a shock tube with theoretical investigations using shock polars. In the region of regular reflection they found good agreement between theory and experiment except that regular reflection continued beyond the theoretical limit predicted. For Mach reflection, their analysis was able to correctly predict shock angles for the case of a weak incident shock, where the flow behind the reflected shock was subsonic. Previous theories had failed in this region. Henderson (1966) and Law (1970) have also made use of shock polars. The latter investigated theoretically and experimentally the diffraction of strong shock waves in oxygen in dissociation equilibrium, for wedge angles from 25° to 60°. He was able to successfully predict from usual gas-dynamic considerations without requirements from chemical kinetics the appearance of a second triple shock system in irregular Mach reflection. He also obtained an approximate solution for the first

triple point trajectory angle as a function of incident shock Mach number and the wedge angle for dissociated oxygen. An analysis was also made for oblique shock wave relations with imperfect gas effects.

Whitham (1957) developed a new method for the solution of the problem of the propagation of shocks by considering their movement in individual ray tubes using a relationship between area and shock strength developed by Chisnell (1957). Whitham (1959) applied this technique to the diffraction of a plane shock by a cone. Skews (1971) used Whitham's method to examine the problem of the reflection of a triple point at a wall. He also used the simple three-shock theory and examined the interactions in the wave train following the reflection. He found the three-shock theory and the interaction analysis gave similar results for small corner angles, but differed considerably from the results of Whitham's theory. He found the experimental values lay between these two predictions, and tended toward the theoretical prediction for the limiting case of zero wall angle. Mölder (1960) reports theoretical and experimental work on the interaction of unequal oblique shock waves in a steady flow at a free stream Mach number of 2.48. He found the theory, based on the Rankine-Hugoniot equations, well substantiated by the experimental results. Heilig (1970) reports extensive theoretical and experimental studies of the reflection of a shock wave at a curved surface, and makes use of the approximate method of Whitham (1957) referred to previously. Ter-Minassiants (1969) has extended the method of Lighthill (1950) to the case of regular reflection at a wedge of finite angle. He considers the motion as a small pertur-

bation of the uniform flow of the gas, moving with a constant velocity behind the plane reflected shock front. Prasse (1972) has also examined the problem of Mach reflection with particular emphasis on the curvature of the reflected shock. He gives an analytic description of the curved part of the reflected shock from which the particle velocities below the reflected shock can be calculated. He also investigated the affect of the wedge corner upon the shape of the reflected shock.

Some workers have applied numerical integration techniques to the shock interaction problem. Von Neumann (1950) introduced an artificial viscosity term so that the difference equations corresponding to the differential equations of the exact formulation could be used throughout the entire calculation, even across shocks. The work of Ludloff and Friedmann (1955) using a numerical difference scheme has been referred to previously. Recently Yagla (1973) determined the properties throughout the flow field for the cases of Mach reflection and Prandtl-Meyer expansion. In this method a transformation of the governing equations is made so that the boundary conditions might become amenable to numerical computation. The results are compared with the experimental results of Dewey (1973) for the case of Mach reflection at a 10° wedge, and with the exact analytic solution for the Prandtl-Meyer expansion problem.

From this review it can be seen that in shock interaction studies emphasis has been on determining shock configurations rather than the properties throughout the flow field. There have been exact

analytic solutions of the shock interaction problem for specialized cases, and approximate solutions for more general cases, but there has been no exact solution for the general case. Few experimental measurements of the properties throughout the flow field have been reported except for the measurement of density by interferometry.

Male and Chelsom (1968) used pressure gauges to determine the pressure on the surface of a wedge in Mach reflection, and concluded that accurate measurement of the peak wall pressure must await the development of considerably smaller gauges. Gvozdeva *et al.* (1969) report using one millimetre diameter pressure gauges, and platinum resistance thermometers.

Interferometry has been used by several workers to determine the density contours in the flow. As far as the author is aware there have been no experimental measurements of either temperature or particle velocity in the flow field associated with Mach reflection. Bleakney (1950) has determined pressure from density interferograms by making the assumption that all changes are isentropic and adiabatic after the incident shock has passed. For his work, this approximation produces an error of no more than a few percent. In general, however, the flow field associated with shock waves is of varying entropy. This means that the measurement of one physical property of a gas element does not lead directly to knowledge of any other property when the entropy of the gas element is unknown. The entropy history of a gas element can be determined, however, if the trajectory of a gas element is followed. This is the method used in the particle trajectory analysis

technique. The work of this thesis, therefore, has been aimed at measurement of all of the physical properties within a two-dimensional shock tube flow. How this has been achieved will be detailed in the succeeding chapters.

CHAPTER 3

PARTICLE TRAJECTORY ANALYSIS

3.1 Introduction

In this chapter, the theory and the experimental technique of particle trajectory analysis will be described. The basis of the method is that in some way individual particles within a gas should be marked so that particle trajectories may be followed. Then in theory, as will be explained in the next section, the macroscopic properties of the gas at any time and any place in the flow may be determined. Section 3.3 will indicate some of the flow visualization techniques that have been used in gas flows.

3.2 The theory of particle trajectory analysis

There are two ways in which a fluid flow may be conveniently described. Using the method attributed to Euler, the whole flow field is described by giving the properties as a function of space and time coordinates. Using the method of Lagrange, the state of an individual element within the fluid is given as a function of time, the element being identified by its space coordinates at a particular arbitrary time, usually time zero.

In particular trajectory analysis we take the Lagrangian viewpoint and follow the history of individual elements of gas, these elements being marked by inertialess tracers of the gas flow. Suppose that at time t_0 the physical properties of an element of gas having position

coordinates (x_0, y_0, z_0) and volume v_0 are known. At some later time t after the element has been moved and deformed by the gas flow it has volume v and coordinates (x, y, z). Using the principle of the conservation of mass, we can then say that the density of the element at time t is given by

$$d = d_0 \frac{v}{v_0}$$

where d_0 is the density at time t_0. Hence by following elements of gas within the flow the density at any time and any position can be determined if the volume of the gas element is known.

The pressure of the element at that time may now be determined provided its entropy change from its ambient value is known. This can be determined from the strength of any shock through which it may have passed. The Rankine-Hugoniot relations are used for this determination. These relate the pressure ratio to the density ratio across a shock, and the entropy change to the pressure and density ratios. They are derived using conservation of mass, momentum, and energy across a shock. If P and D are the pressure and density ratios across a shock, and S is the entropy jump across a shock then these relations are

$$P = \frac{1 - D\left(\frac{\gamma-1}{\gamma+1}\right)}{D - \left(\frac{\gamma-1}{\gamma+1}\right)}$$

and

$$S = c_v \ln\left[P\left(\frac{1}{D}\right)^{\gamma}\right]$$

where γ is the ratio of specific heat at constant pressure (c_p) to that at constant volume (c_v).

Alternatively, the ratios across a shock may be written as a function of the shock Mach number, defined as the ratio of the speed of the shock to the speed of sound in the gas into which the shock is travelling. The equations giving the ratios across a shock as a function of its Mach number are now commonly called the Rankine-Hugoniot equations. They are

$$P = \frac{2\gamma M^2 - (\gamma-1)}{\gamma + 1}$$

$$D = \frac{(\gamma+1)M^2}{(\gamma-1)M^2 + 2}$$

$$T = \frac{\left[\gamma M^2 - \left(\frac{\gamma-1}{2}\right)\right]\left[\left(\frac{\gamma-1}{2}\right)M^2 + 1\right]}{\left(\frac{\gamma+1}{2}\right)^2 M^2}$$

where M is the shock Mach number, and P, D, T the pressure, density, and temperature ratios across the shock.

In the region between shocks we may use the isentropic equation of state to give the pressure of the gas element at any time. If d_s and p_s are the density and pressure of a gas element just after it has passed through a shock, then assuming perfect gas behaviour, the pressure at any point in the region between shocks is given by

$$p = p_s \left(\frac{d_s}{d}\right)^{\gamma}$$

Here γ is the ratio of specific heats for the gas. The densities d and d_s are determined as previously described.

In this way, using the Rankine-Hugoniot equations across shocks and the isentropic equation of state in the regions between shocks, the pressure of all gas elements within the flow field can be determined.

It should be noted that, in order to determine the pressure field from the density, we need to follow the history of individual elements of gas. The interferometric method is capable of giving an accurate Eulerian picture of the density field, but the pressure cannot be determined from this without a knowledge of the entropy field. For shocks of constant strength, commonly called steady shocks, the entropy field is known in terms of the shock Mach number. Bleakney (1950) has used the isentropic equation of state throughout the whole flow field, but for shocks of intermediate strength and unsteady shocks, this approximation is not valid.

Once the pressure and density of a gas element are known, its temperature may then be determined. Assuming that we are dealing with flows of Mach number such that the perfect gas equation is applicable, we may use the thermal equation of state to write

$$\frac{p}{d} = RT$$

where R is the characteristic gas constant for the particular gas. The temperature of a gas element immediately after passing through a shock will also be given by the appropriate Rankine-Hugoniot equation.

Once the temperature of the gas is known everywhere, then the velocity of sound can also be determined throughout the flow field. Finally, observation of particle trajectories gives direct information about the particle velocity, and vorticity within the flow. It is emphasised that the density, velocity, and vorticity can be derived directly from the coordinates of tracers using only the equation of continuity, whereas pressure, temperature, and velocity of sound require the Rankine-Hugoniot equations, and an equation of state for their determination.

This, then, is the technique of particle trajectory analysis. As described above, the technique assumes the equation of state for a perfect gas in order that the pressure and temperature may be determined. This means that for gas flows in air the technique is applicable up to about Mach 2.5. However, it is theoretically possible to apply the technique to determine the pressure without using an equation of state. This would involve application of the Lagrangian momentum equation. If the pressure of a gas element is known at a certain time, then the pressure at any later time may be determined if the acceleration-time history of the particle is known. Application of Newton's second law of motion to the element at any instant would require that its mass multiplied by its acceleration should equal the net force on the element. This net force will be due to the pressure gradient in the flow field. Thus, the pressure of any element of gas of known mass can be obtained from a Lagrangian integration of its acceleration. The practical difficulties involved in this procedure may, however, limit its applicability. In the next section

the application of the particle trajectory analysis technique to several specific gas flows of Mach number less than 2.5 will be described.

3.3 Applications of the particle trajectory analysis technique

Dewey (1971) has used particle trajectory analysis to determine the properties within the flow produced by a spherical blast wave. For this case, particles move in straight lines along radii of the sphere formed by the shock wave. Thus, if r is the radial coordinate at time t of a gas element which had radial coordinate r_0 at time t_0 (Fig. 3.3.1 a) then conservation of mass requires

$$4\pi r_0^2 \, \Delta r_0 \, d_0 = 4\pi r^2 \, \Delta r \, d$$

where Δr_0 and Δr are the dimensions of the gas element measured along a radius vector at time t_0 and t respectively, and d_0, d are the corresponding densities. Hence, the density of the gas element at time t is given by

$$d = d_0 \left(\frac{r_0^2}{r^2} \right) \left(\frac{\Delta r_0}{\Delta r} \right).$$

By determining a continuous functional relationship between r_0 and r, interpolation may be used to determine the ratio $\Delta r_0 / \Delta r$ at any desired point in space and time. Once the density is known everywhere, the other gas properties may be determined as described in the last section. Similarly the properties behind a cylindrical expanding shock wave could be obtained. In this case the density relationship would be

$$d = d_0 \left(\frac{r_0}{r} \right) \left(\frac{\Delta r_0}{\Delta r} \right).$$

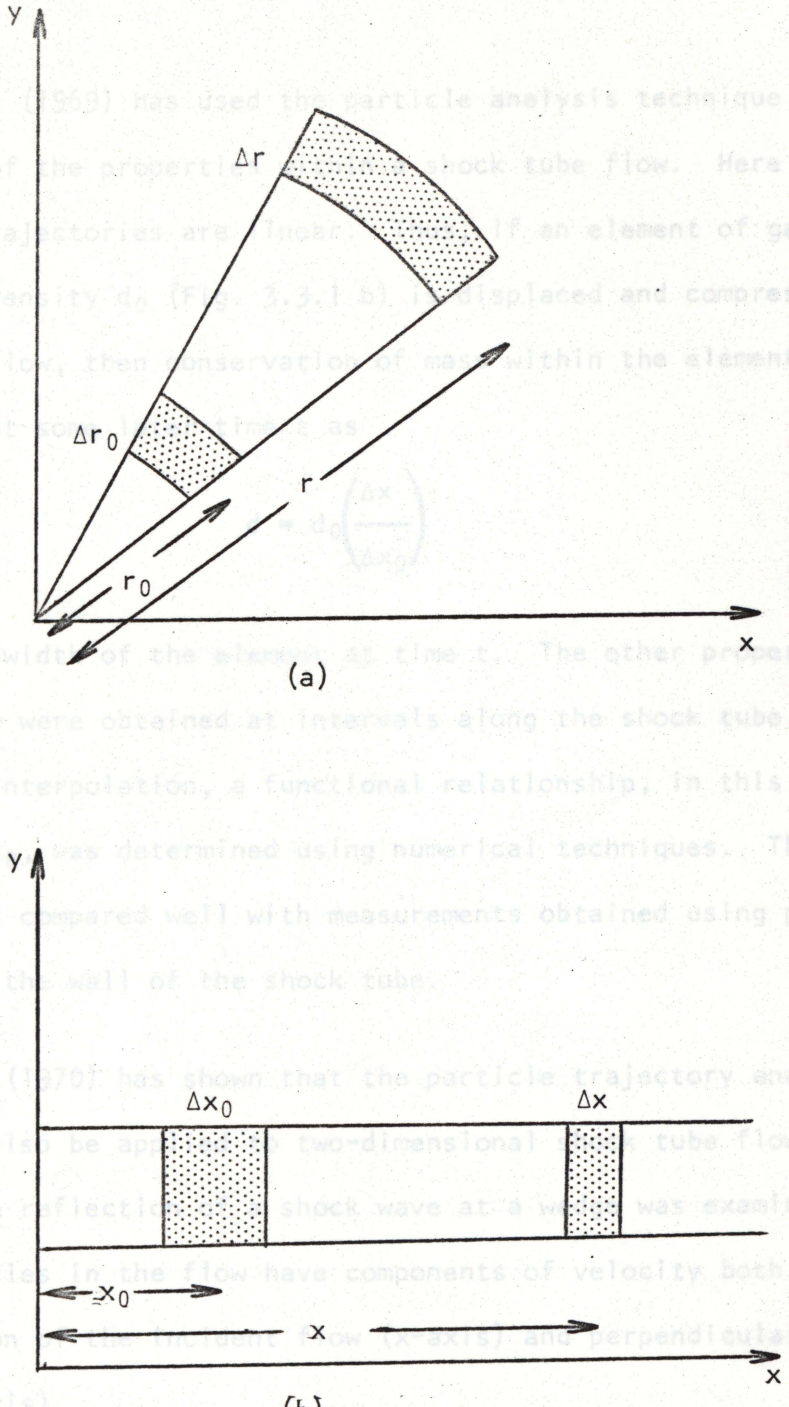

Fig. 3.3.1 Geometry of two gas flows to which particle trajectory analysis has been applied.

(a) Section through a spherical expanding shock wave showing the same gas element at two different times.

(b) Section through a shock tube showing a gas element at two different times in a linear flow.

Whitten (1969) has used the particle analysis technique for the determination of the properties within a shock tube flow. Here again the particle trajectories are linear. Thus, if an element of gas of width Δx_0 and density d_0 (Fig. 3.3.1 b) is displaced and compressed by a shock tube flow, then conservation of mass within the element gives its density d at some later time t as

$$d = d_0\left(\frac{\Delta x}{\Delta x_0}\right)$$

where x is the width of the element at time t. The other properties within the flow were obtained at intervals along the shock tube. Again, to facilitate interpolation, a functional relationship, in this case between x and x_0, was determined using numerical techniques. The results of the analysis compared well with measurements obtained using pressure transducers in the wall of the shock tube.

Walker (1970) has shown that the particle trajectory analysis technique may also be applied to two-dimensional shock tube flows. In particular Mach reflection of a shock wave at a wedge was examined. Here the particles in the flow have components of velocity both parallel to the direction of the incident flow (x-axis) and perpendicular to this direction (y-axis).

Consider an element of air at time t_0 defined by the four particles (1, 2, 3, 4) at its corners (Fig. 3.3.2). Suppose this element is displaced and deformed by a two-dimensional shock tube flow. Let the density, pressure, temperature, and velocity of sound at time t_0 be denoted

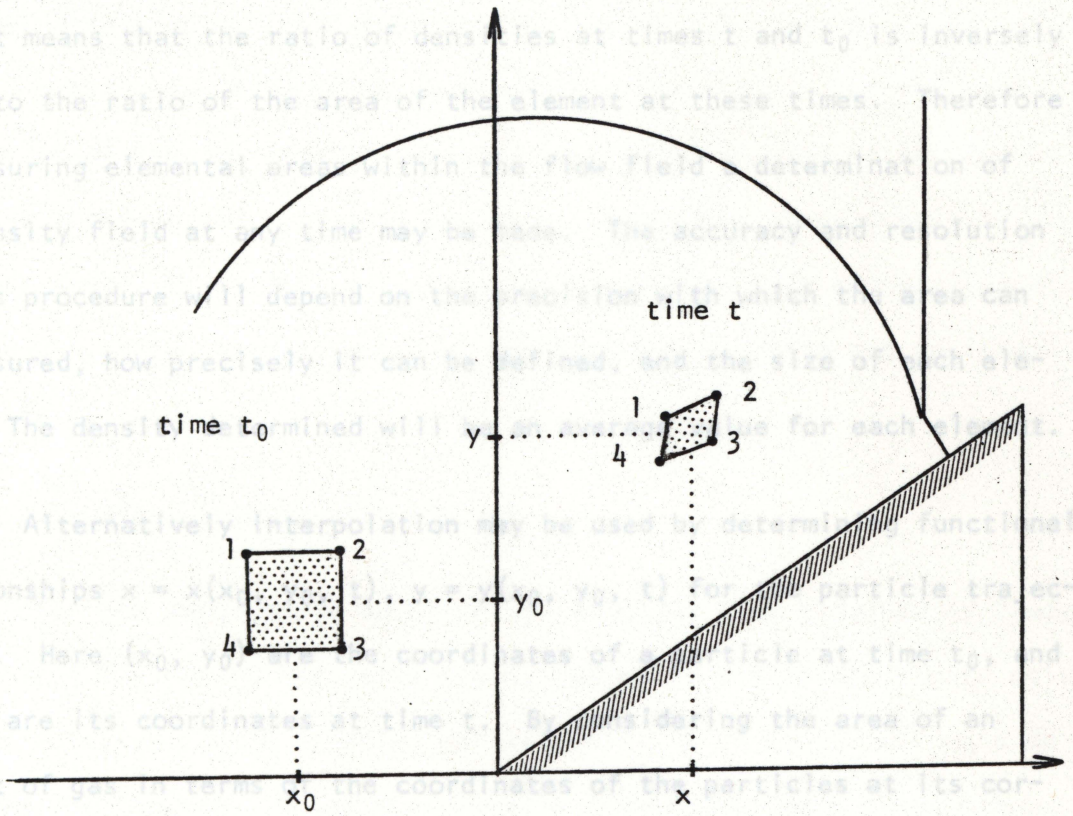

Fig. 3.3.2 Element of air at two different times in a two-dimensional shock tube flow.

by d_0, p_0, t_0 and a_0 respectively and the corresponding properties at time t be d, p, t, and a. Conservation of mass for the gas within the element means that the ratio of densities at times t and t_0 is inversely equal to the ratio of the area of the element at these times. Therefore by measuring elemental areas within the flow field a determination of the density field at any time may be made. The accuracy and resolution of this procedure will depend on the precision with which the area can be measured, how precisely it can be defined, and the size of each element. The density determined will be an average value for each element.

Alternatively interpolation may be used by determining functional relationships $x = x(x_0, y_0, t)$, $y = y(x_0, y_0, t)$ for the particle trajectories. Here (x_0, y_0) are the coordinates of a particle at time t_0, and (x, y) are its coordinates at time t. By considering the area of an element of gas in terms of the coordinates of the particles at its corners, it can be shown (Walker 1970) that

$$d_0\ (x_0, y_0, t_0) = J\ d(x, y, t)$$

where

$$J = \begin{vmatrix} \frac{\partial x}{\partial x_0} & \frac{\partial x}{\partial x_0} \\ \frac{\partial y}{\partial y_0} & \frac{\partial y}{\partial y_0} \end{vmatrix}$$

J is the Jacobian of the transformation $(x_0, y_0, t_0) \rightarrow (x, y, t)$. Thus by evaluating the partial derivatives within the Jacobian from empirically determined functional relationships the density at any point and any time may be determined.

In certain cases, interpolation of this kind might tend to obscure real variations in the properties of the flow. Once the density has been determined the other properties may then be determined as described previously if the shock trajectories are known. For the Mach reflection of a shock wave at a wedge, some elements will be shocked by both the incident and reflected shocks, some will be shocked only by the Mach stem. Since the reflected shock is curved, and of continuously varying curvature, determination of its strength at different positions and times is required.

3.4 Experimental methods

For the large scale spherically symmetric flow examined by Dewey (1971), the air was marked using trails formed by a chlorosulphonic acid mixture released from a spinning mortar shell. Elements of air were defined by the intersection of these trails with radial grid lines drawn on the photographic record.

Whitten (1969) formed trails perpendicular to the incident flow by drawing cigarette smoke through small holes in the wall of the shock tube. The one-dimensional motion of these trails was recorded using a high-speed camera.

For two-dimensional particle trajectory analysis we need to mark discrete points within the flow. Experiments to produce smoke puff grids on a large scale in the field have been reported by Holsgrove and Klymchuk (1970), and Holsgrove *et al.* (1971).

In the laboratory, several methods of producing particle tracers for a two-dimensional shock tube flow have been considered. The present author has used trails of cigarette smoke moving horizontally across the shock tube. These are shown in Fig. 3.4.1. In this arrangement, only a single line of tracers could be observed during one experiment. Data about the flow was gathered from a number of experiments. The separation of the wedge, and the initial tracer positions was altered for each experiment. This procedure was unsatisfactory in that several different experiments were required, and the reproducibility of the experimental conditions was uncertain.

Attempts to produce a grid of particle tracers led to the use of a thin vertical tungsten wire which was heated just before the arrival of the shock by discharging a capacitor through it. The wire was coated at intervals with several different organic and inorganic substances in order to produce smoke puffs. None of the substances investigated gave a smoke sufficiently dense enough to be seen with conventional high speed photography.

In another technique investigated, the wire was thermally insulated at intervals using sleeving. Heating the wire produced small spots of warm air which were clearly visible using schlieren photography. These tracers are shown in Fig. 3.4.2. We require, however, that the particle tracers should be true indicators of the flow. Rudinger and Somers (1960) have shown experimentally that elements of gas, which have densities different to that of a surrounding flow, do not move with the

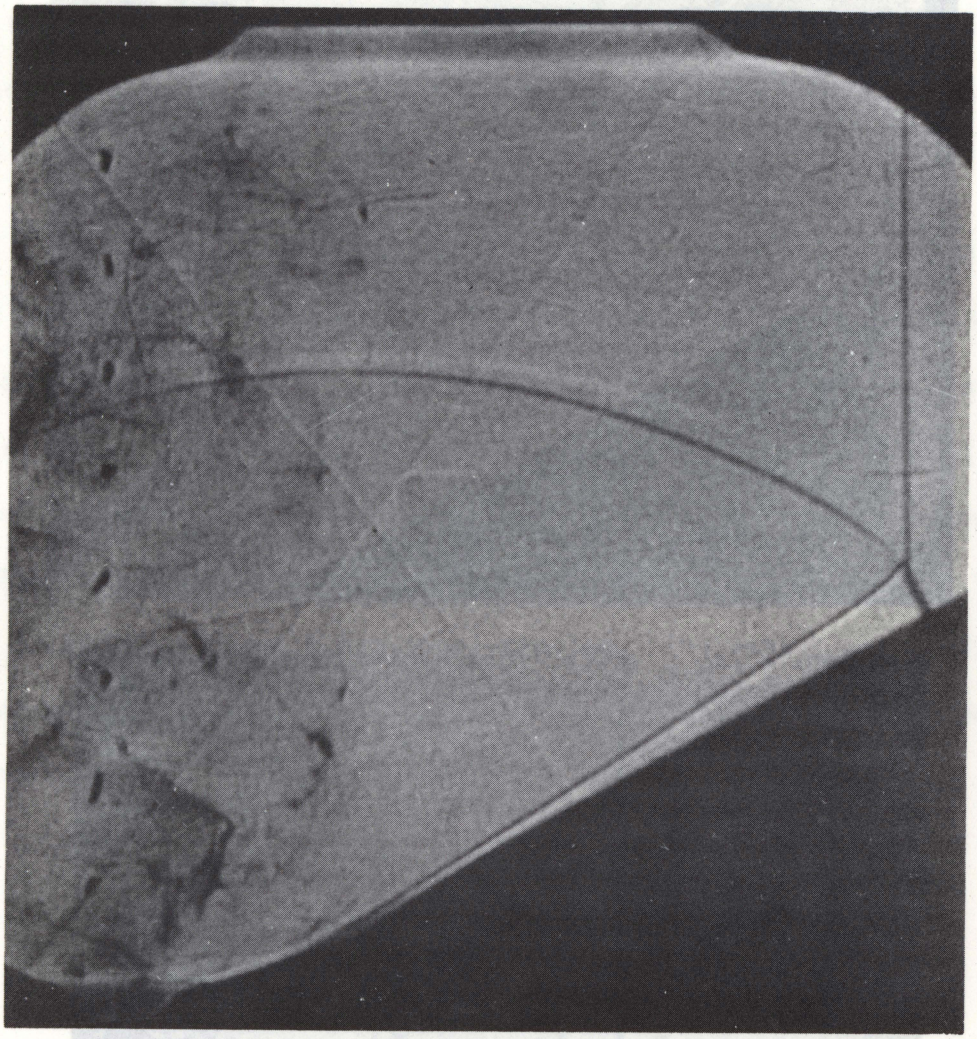

Fig. 3.4.1 Cigarette smoke tracers behind a reflected shock.

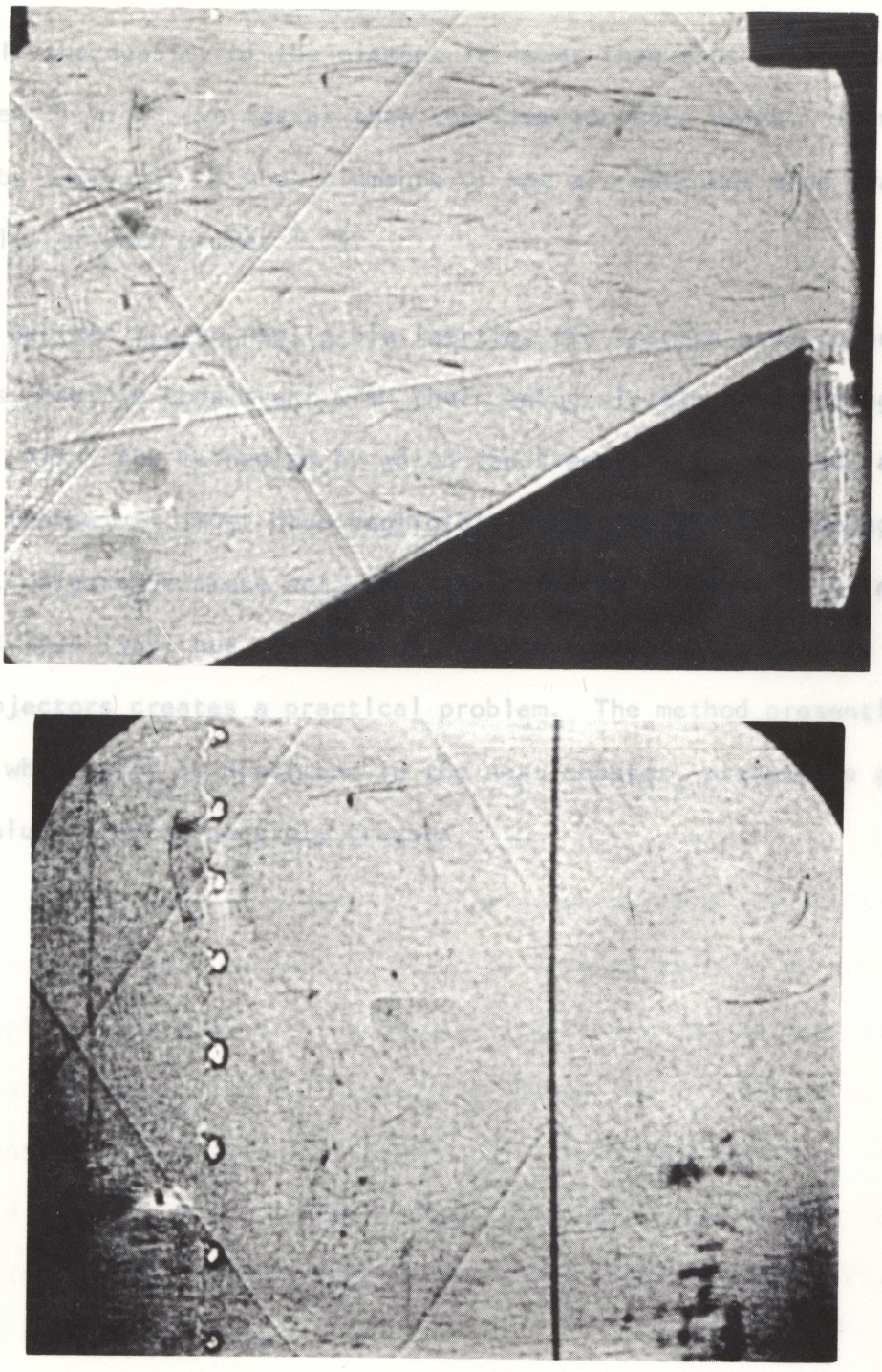

Fig. 3.4.2 Schlieren photographs of spot heated elements of air. Upper picture shows elements heated by wires passing perpendicular to the plane of the photograph. The lower picture shows elements produced by a vertical wire (on left) thermally insulated at intervals.

flow. If the density of the element is lower than that of the surrounding gas, then it will move faster than the flow and *vice versa*. It was observed by Dewey (1973) that elements of hot air were not true tracers for a flow of Mach number 1.15.

Besides having negligible inertia, the tracers need to be as small as possible consistent with their being visible on a photographic record. Also, the mechanism by which the tracers are produced, and the tracers themselves, must have negligible affect on the flow being studied. Cigarette smoke satisfies the criteria of negligible inertial lag (Muirhead 1959) but, because of its tar content, its passage through small injectors creates a practical problem. The method presently adopted which will be described in the next chapter, produces a grid of ammonium chloride particle tracers.

CHAPTER 4

EXPERIMENTAL PROCEDURES

4.1 The optical system

In photographing transient phenomena, such as the motion of the shock waves and the particles in the flow behind the shock waves, the exposure time must be sufficiently brief that the image on the film is not blurred, and long enough for there to be adequate exposure of the film. In the last century Mach (1878), using a spark as the light source, photographed shock waves using a technique attributed to Töepler (1866) and now commonly called schlieren photography. In this method density discontinuities not normally visible appear on the photographic record. Boys (1892), also using a spark lamp source, was able to take a photograph of the shock waves around a bullet penetrating a glass plate using the shadowgraph technique, which is similar to that of schlieren photography. Developments of the spark lamp light source have aimed at decreasing exposure time, increasing intensity, and producing a succession of sparks for cine photography. Cranz and Schardin (1929) developed a multiple spark camera capable of very high framing rates using a series of spark sources, whilst other workers have multiply pulsed a single spark gap.

In previous work in this laboratory single pictures showing shock waves (Fig. 3.4.1) were taken using shadow or schlieren photography with a spark lamp light source. Particle trajectories were

photographed separately using a high speed rotating prism camera running at five thousand frames per second. At this speed the exposure time was twenty microseconds, and the particle tracers were brightly illuminated so that the light which they scattered was visible on the photographic record.

In the present system, using the same high speed camera, the particles and shocks are recorded simultaneously with an exposure time of about thirty nanoseconds. This is achieved by using a multiply pulsed ruby laser as a light source along with a schlieren optical system.

The principles underlying the design and operation of a schlieren optical system will be explained with reference to a system employing lenses and then the particular adaptation of the system used in this work will be described.

A small intense source of light, placed at the focus of a convex lens L1 (Fig. 4.1.1) produces a nearly parallel beam passing through the test section in which the density discontinuities being examined occur. This beam is then brought to a focus at the point K by a lens L2, usually called the schlieren head. A photographic image can be recorded directly at M1, or using a camera objective lens L3 a reduced image can be formed at M2. In considering the operation of this system the focussing of two images will be discussed.

First, the lenses L1 and L2 together focus an image of the source at K. Shown in Fig. 4.1.1 are two extreme pencils of rays passing through

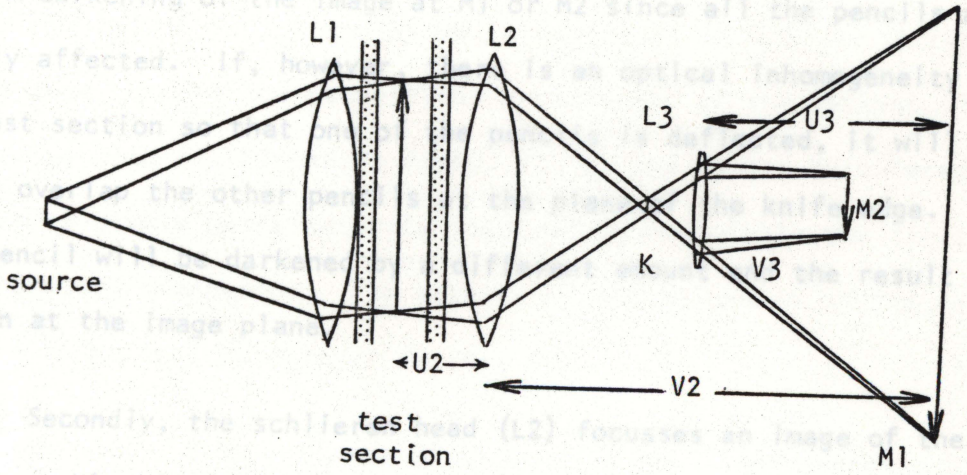

Fig. 4.1.1 Schlieren system using lenses

the test section. It will be noted that each of these pencils fills the entire test section, that all the pencils completely overlap in the plane of the source image at K, and that although the rays passing through the test section are not strictly parallel, because of the finite size of the source, the pencils themselves are parallel. In schlieren photography, introduction of a knife edge at K leads to a uniform darkening of the image at M1 or M2 since all the pencils are equally affected. If, however, there is an optical inhomogeneity in the test section so that one of the pencils is deflected, it will no longer overlap the other pencils at the plane of the knife edge. Thus this pencil will be darkened by a different amount and the result will be seen at the image plane.

Secondly, the schlieren head (L2) focusses an image of the test section at M1. Actually, one plane in the test section can be precisely in focus, but there will usually be sufficient depth of field for the other points in the test section to be sufficiently sharp. In the absence of a knife edge at K, as in the shadowgraph system, there will still be a variation in the intensity of the image at M1 or M2 due to bending of rays of light in the test section. This variation, however, will not be so marked as in the case of the schlieren arrangement.

Applying the thin lens formula to the schlieren head and the objective separately, we have the relationships

$$\frac{1}{U2} + \frac{1}{V2} = \frac{1}{F2} \qquad (4.1.1)$$

$$\frac{1}{U3} + \frac{1}{V3} = \frac{1}{F3} \qquad (4.1.2)$$

where the object and image distances are as shown in Fig. 4.1.1 and F2, F3 are the focal lengths of the schlieren head and objective respectively.

The total magnification of the image of the test section due to L2 and L3 will be given by

$$\text{Magnification} = \frac{V2}{U2} \cdot \frac{V3}{U3} \qquad (4.1.3)$$

The relationships contained in equations (4.1.1) to (4.1.3) can be used to determine the geometrical arrangement of the system. In this laboratory, with F1, F2 and F3 fixed, U1, U2 and U3 are calculated and adjusted to give a satisfactorily focussed system within the limits of the laboratory dimensions. The details of the alignment of the optical system will be described later in this section.

There are many variants of this basic schlieren system. Usually when the field of view is large the lenses L1 and L2 are replaced by curved mirrors. Shown in Fig. 4.1.2 is a so-called Z-pass schlieren arrangement which has previously been used in this laboratory. One disadvantage of this system is the off-axis position of the source. This introduces astigmatic aberrations of the image, although coma can be virtually eliminated by a symmetrical arrangement of components on either side of the test section. In most work the astigmatic aberration is of no consequence, and indeed is quite small when long focal length mirrors are used so that the off-axis angle is small. When quantitative measurements are to be made from the photographic record, however, this aberration can be of importance. Several schemes have been proposed for the correction of this astigmatism. Prescott and Gayhart (1951) have intro-

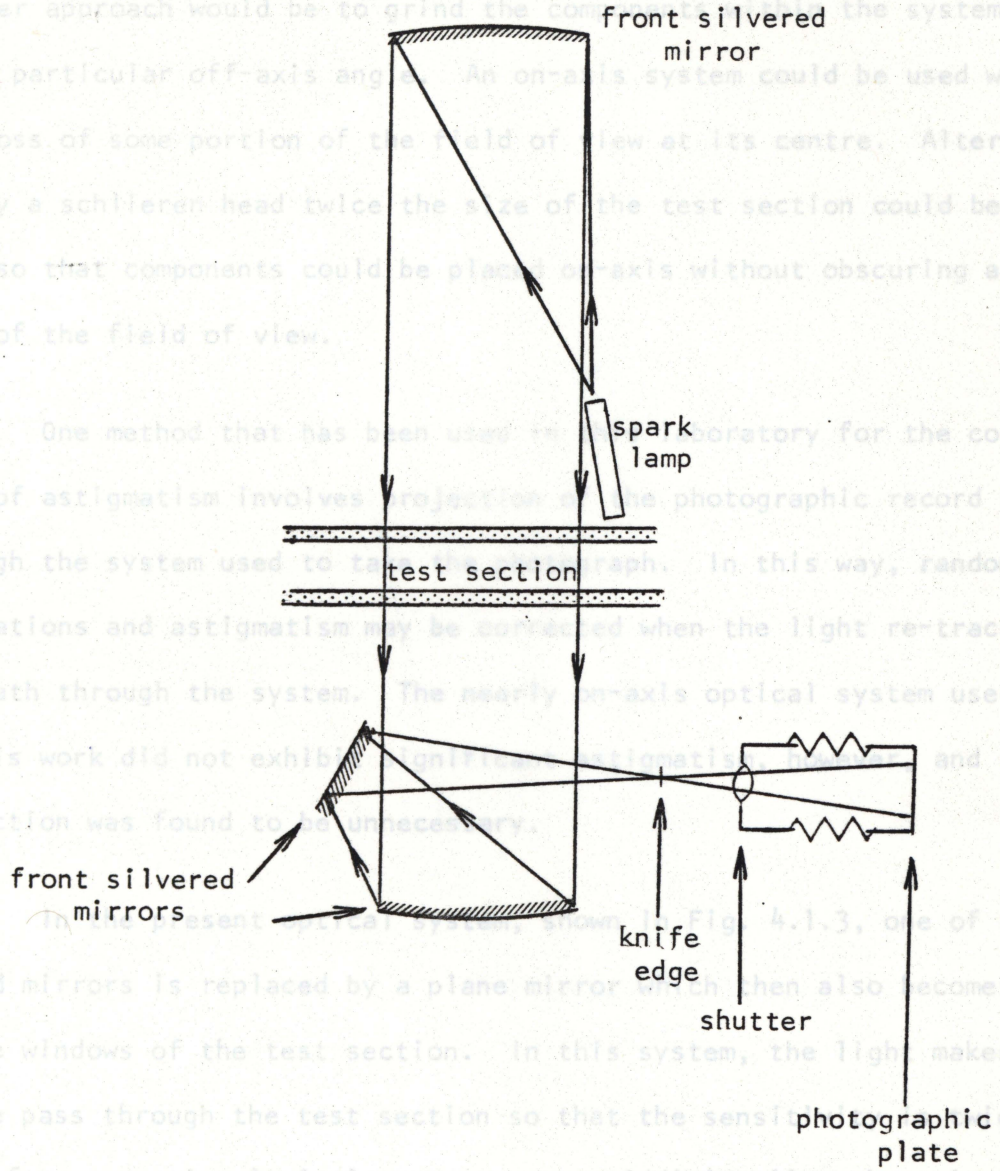

Fig. 4.1.2 Z-pass schlieren system

duced a cylindrical lens between the source and the schlieren head. Another approach would be to grind the components within the system for a particular off-axis angle. An on-axis system could be used with the loss of some portion of the field of view at its centre. Alternatively a schlieren head twice the size of the test section could be used so that components could be placed on-axis without obscuring any part of the field of view.

One method that has been used in this laboratory for the correction of astigmatism involves projection of the photographic record back through the system used to take the photograph. In this way, random aberrations and astigmatism may be corrected when the light re-traces its path through the system. The nearly on-axis optical system used in this work did not exhibit significant astigmatism, however, and such projection was found to be unnecessary.

In the present optical system, shown in Fig. 4.1.3, one of the curved mirrors is replaced by a plane mirror which then also becomes one of the windows of the test section. In this system, the light makes a double pass through the test section so that the sensitivity is twice that of a conventional single pass system. Additionally, there is only one test section window contribution to optical imperfections in the system. In general, the sensitivity of a schlieren system is directly proportional to the focal length of the schlieren head, and inversely proportional to the size of the source (Liepmann and Roshko 1957).

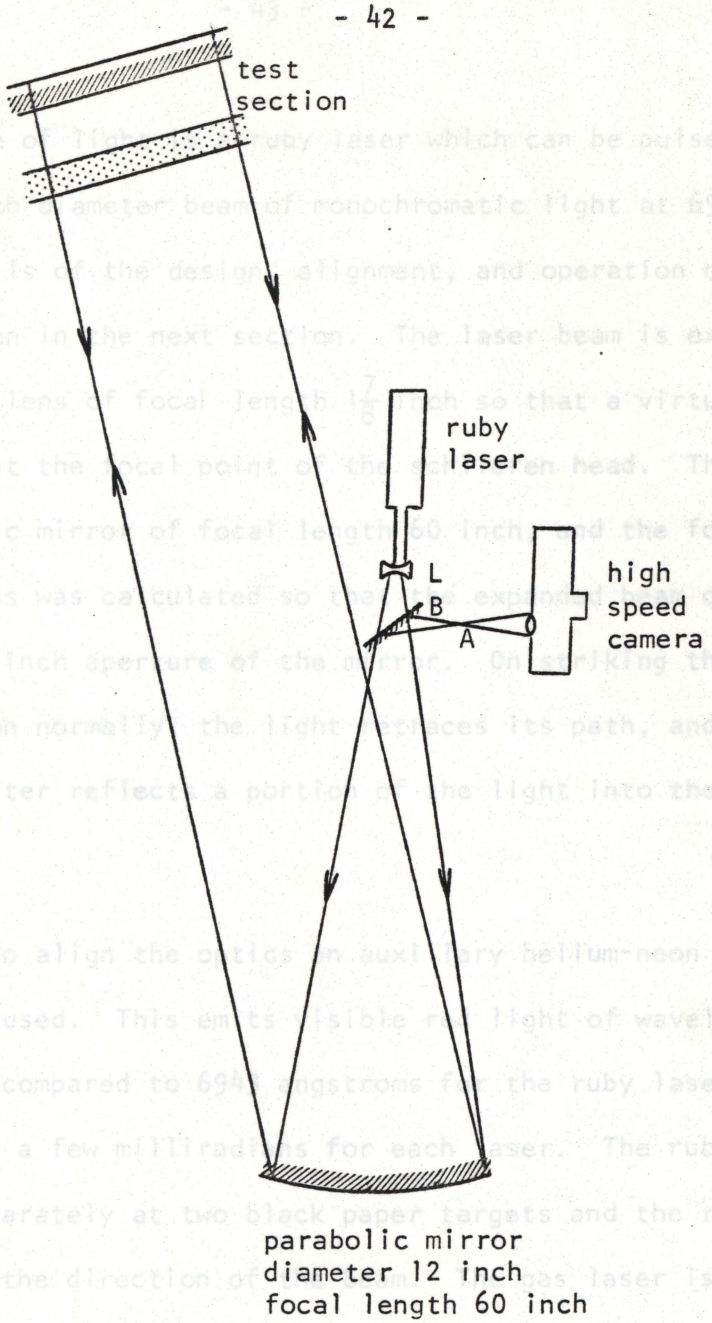

Fig. 4.1.3 Double pass schlieren system

A--1 mm aperture B--50% beam splitter L--diverging lens, focal length $1\frac{7}{8}$ inch.

Camera objective focal length 5.3 cm. Parabolic mirror to test section 129 inch.

The source of light is a ruby laser which can be pulsed, and produces a 3/8 inch diameter beam of monochromatic light at 6943 angstroms. The details of the design, alignment, and operation of this laser will be given in the next section. The laser beam is expanded using a diverging lens of focal length $1\frac{7}{8}$ inch so that a virtual point source is formed at the focal point of the schlieren head. The schlieren head is a parabolic mirror of focal length 60 inch, and the focal length of the concave lens was calculated so that the expanded beam of light just fills the 12 inch aperture of the mirror. On striking the mirror in the test section normally, the light retraces its path, and on return the 50% beam splitter reflects a portion of the light into the high speed camera lens.

In order to align the optics an auxiliary helium-neon gas laser and collimator is used. This emits visible red light of wavelength 6328 angstroms as compared to 6943 angstroms for the ruby laser. The beam divergence is a few milliradians for each laser. The ruby laser is first fired separately at two black paper targets and the resulting burn holes define the direction of the beam. The gas laser is then *interposed between the ruby laser and the schlieren head, and aligned using the burn marks on the targets. The centres of all components are* aligned using the unexpanded beam, and then final adjustments are made with the concave expanding lens in place. During this process a grid is placed in the test section so that if the test section mirror is not perpendicular to the incident beam a double image is produced at the camera.

The pulses of light from the ruby laser are so short that no shuttering is required in the camera. It was, therefore, possible to pass the light through a single objective lens which was placed in the position that would normally be occupied by the eyepiece in conventional operation of the camera. In this way, the four reflecting surfaces and eighteen air-glass surfaces, which are an integral part of the Hycam re-imaging optics, were bypassed. When focussing, a ground glass screen with a focussing mark on it was placed at the film plane, and the image of this was projected through the front of the camera using this re-imaging optics. The image was examined and focussed on a screen placed in front of the camera lens.

The method whereby framing of the photographic record was achieved during a film run will be described in Section 4.6. A considerable amount of light emitted by the ruby laser was lost to the film record in the optical system. Besides the losses at reflecting surfaces, half of the light was lost each time the beam passed through the beam splitter. Nevertheless, there was still more than sufficient light at the camera to adequately expose a high speed film. Accordingly a number of films were investigated in order that an optimum compromise between resolution and sensitivity might be made. The 16 mm high speed film record was to be enlarged to at least the actual size of the test section for the purpose of analysis. A resolution of 10-20 lines per millimeter is reasonable if an image is to be viewed only as a contact print, since this is the resolution of the eye at a reasonable reading distance. If, however, the image is to be enlarged then the resolution

of the original negative should be better than 10-20 lines per millimeter by the enlargement ratio, which in this particular case was approximately sixty times. Film resolutions range from 25 lines per millimeter for polaroid film up to 2,000 lines per millimeter for Kodak High Resolution Plates. Clearly there is nothing to be gained by choosing a film with a resolution far exceeding the resolving power of the optical system. In the final analysis the sufficiency of the resolution of the film was judged by examining an enlargement made from the negative. The film used was Kodak Plus-X pan, and although this is relatively insensitive to the red end of the visible spectrum it was adequate for this application. Should greater sensitivity and resolution be required, then a film with extended red sensitivity could be used. The Plus-X pan film was developed for 10 minutes at 70° F in Kodak Microdol-X.

4.2 The light source

The light source used was a modified Holobeam series 300 ruby laser. The way in which this laser was adapted so that the output from it could be controlled will be described in this section. The pulses of light emitted by a laser are more intense, and much shorter than those from a spark lamp. Additionally the beam emitted is monochromatic, plane polarized, and highly collimated. A shadowgraph taken using this laser is shown in Fig. 4.2.1.

The components within the modified laser cavity are shown schematically in Fig. 4.2.2. A 3/8 inch diameter by 3 inch long ruby rod with a 0.05% chromium dopant level and having plane anti-reflectance

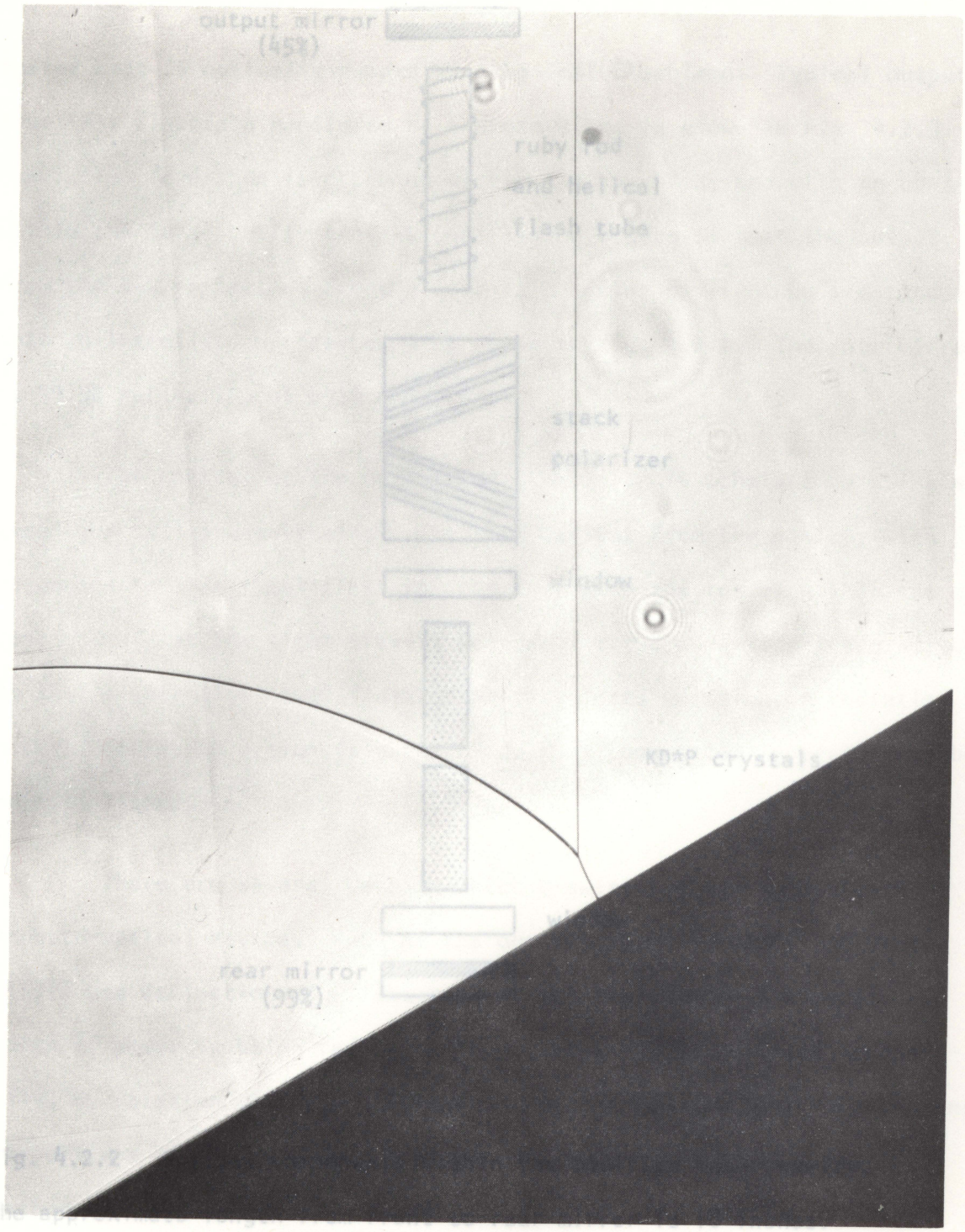

Fig. 4.2.1 Laser shadowgraph of Mach reflection. The exposure time was approximately 30 nanoseconds. The interference effects caused by particles of dust on the optical components can be seen.

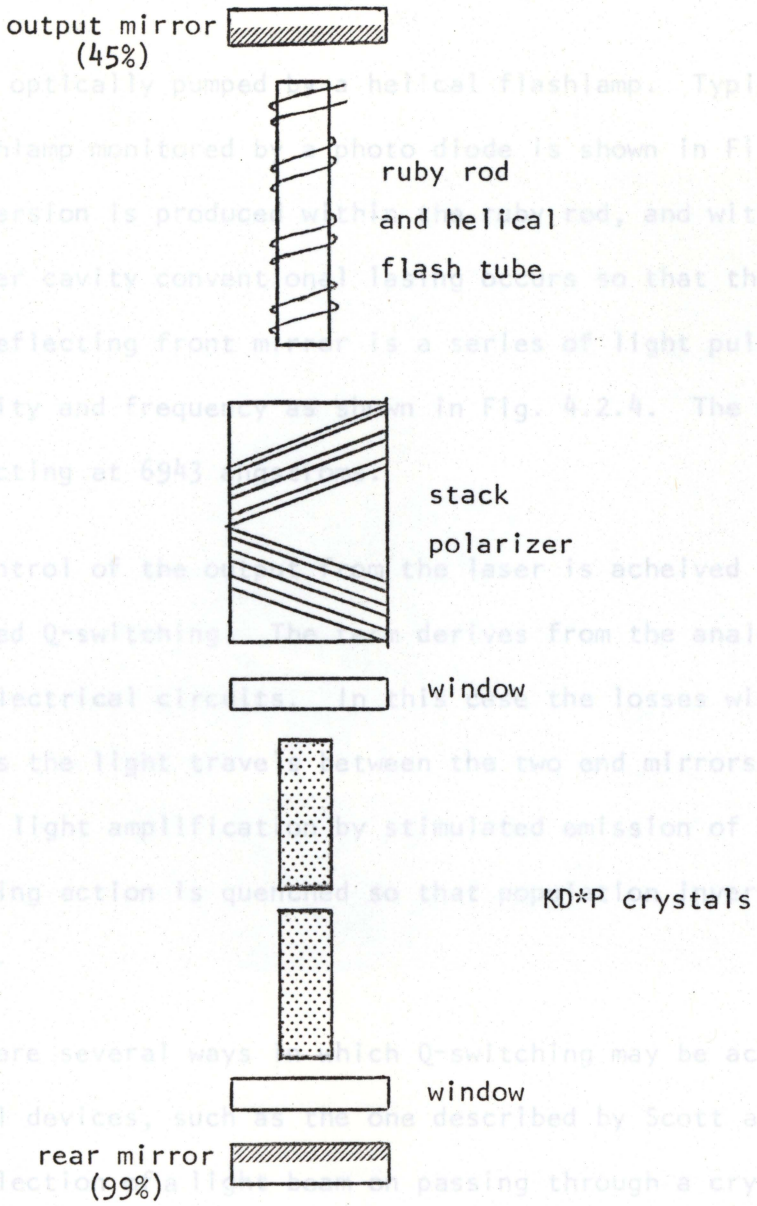

Fig. 4.2.2 Optical components within the modified laser cavity. The approximate length from front to rear mirror is 18 inches.

coated ends is optically pumped by a helical flashlamp. Typical output from this flashlamp monitored by a photo diode is shown in Fig. 4.2.3. Population inversion is produced within the ruby rod, and with no control within the laser cavity conventional lasing occurs so that the output from the 45% reflecting front mirror is a series of light pulses random both in intensity and frequency as shown in Fig. 4.2.4. The rear mirror is 99.9% reflecting at 6943 angstroms.

The control of the output from the laser is acheived by using a technique called Q-switching. The term derives from the analogy with resonance in electrical circuits. In this case the losses within the laser cavity as the light travels between the two end mirrors are adjusted so that either light amplification by stimulated emission of radiation occurs, or lasing action is quenched so that population inversion may be re-established.

There are several ways in which Q-switching may be achieved. Acousto-optical devices, such as the one described by Scott and deWit (1972) use deflection of a light beam on passing through a crystal into which rf power is being fed. The Q-switching may be achieved mechanically, by rotation of one of the end mirrors of the cavity. When the end mirrors are almost parallel, a Q-switched pulse is emitted. Another method uses a class of magneto-optical devices which depend upon the Faraday effect. This is the rotation of the plane of polarization produced when polarized light passes through a crystal subjected to a magnetic field.

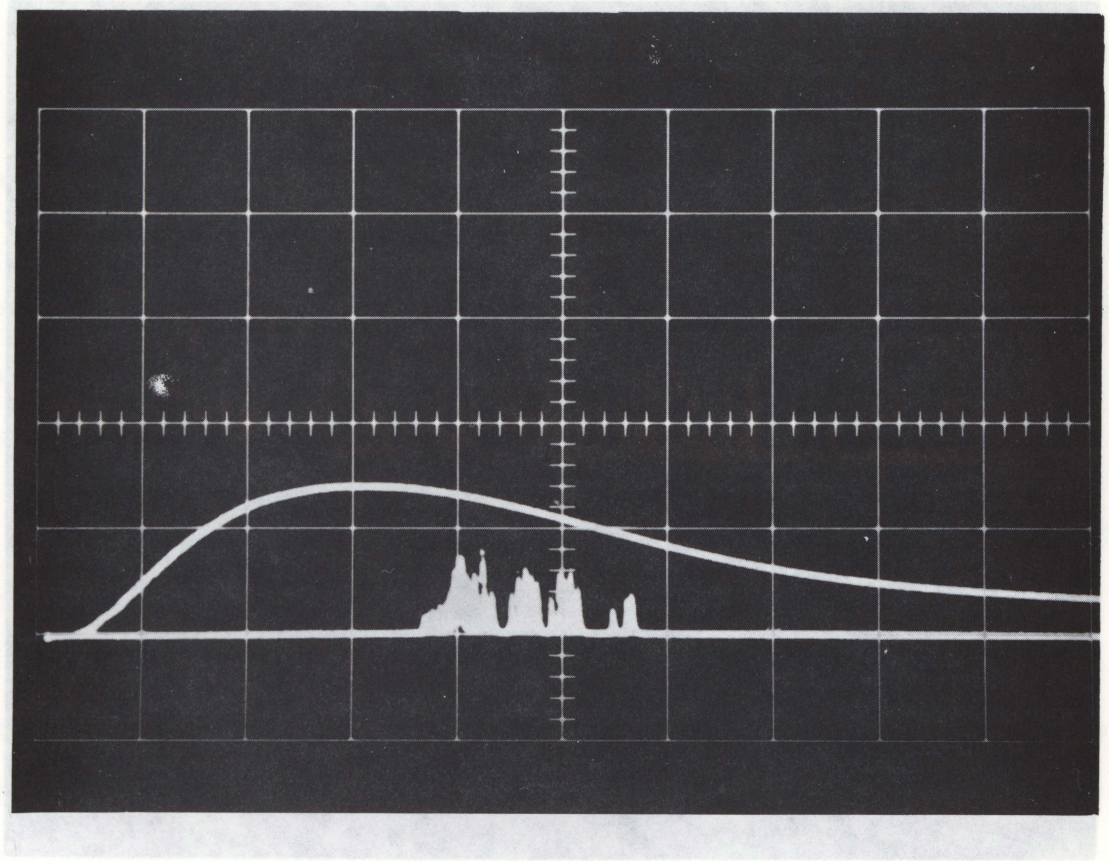

Fig. 4.2.3 Flash tube and conventional lasing output. The light detector is shown in Fig. 4.6.2. Sweep rate 0.2 ms/cm, sensitivity 0.2 v/cm. Both traces were triggered by initiation of the flash tube firing, and stored on a Tektronix type 549 storage oscilloscope. For the upper (flash tube) trace the detector replaced the output mirror. For the conventional lasing trace, the detector was placed behind the rear mirror and covered with several layers of light diffuser.

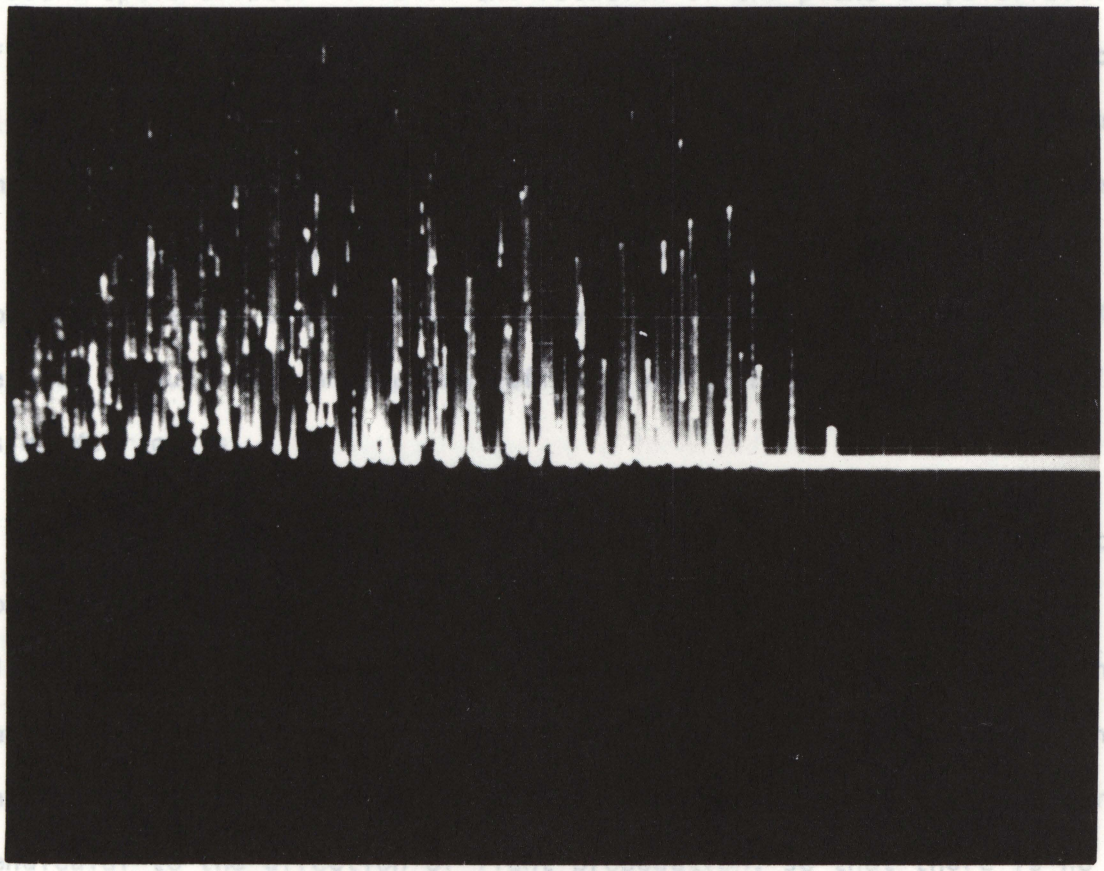

Fig. 4.2.4 Conventional lasing output, showing individual nature of the random pulses. Sweep rate 0.1 ms/cm, sensitivity 0.5 v/cm. The photograph was taken with 10,000 A.S.A. polaroid film on a Tektronix type 547 oscilloscope, using the detector shown in Fig. 4.6.2.

The most widely used laser modulator is that employing the electro-optic effect. This is the rotation of the plane of polarization of polarized light on passing through a substance across which an electric field is applied. Devices using liquids are called Kerr cells, and those employing crystals are called Pockels cells, each being named after the discoverer of the appropriate electro-optic effect. In most applications Pockels cells are preferred since they require less voltage than the Kerr cell to produce the same optical effect, and do not employ toxic liquids as do Kerr cells.

The Pockels effect may be applied in either of two ways. In the longitudinal arrangement, the light propagates along the direction of the electric field. One disadvantage of this arrangement is that the light has to travel through the electrodes supplying the electric field. In the transverse Pockels cell the direction of the electric field is perpendicular to the direction of light propagation, so that there is no electrode problem, and a further advantage is that it requires less voltage than the longitudinal arrangement to produce a given optical effect. In the transverse modulator the light travels perpendicular to the optic axis of the crystal, whilst for the Kerr cell the light travels along the optic axis. Since the optic axis is the one direction in the crystal along which the optical properties are isotropic, this means that even in the absence of an electric field there is, for a single crystal transverse Pockels cell, temperature dependent anisotropy in the direction of light propagation.

Wentz (1964) reported a novel Q-switching device which used two crystals operating in the transverse mode, by means of which he was able to produce laser pulses of 30 nanosecond duration at repetition rates in excess of 400 kilohertz. Rowlands (1967) has also adopted this type of modulator to produce multiple pulsing of a ruby laser, which was used as a light source in high speed photography of dynamic photoelasticity. This double crystal transverse Pockels cell arrangement was the modulator adopted in this work. The Holobeam laser as purchased was capable of giving a single Q-switched pulse using a longitudinal Pockels cell driven by five thousand volts. A new Pockels cell was built and the laser cavity re-designed so that the laser could be multiply pulsed using a 500 volt driver.

The component parts of the re-designed Pockels cell are shown in Fig. 4.2.5. Two crystals of potassium di-deuterium phosphate, each 4 cm × 1 cm × 1 cm, are enclosed in a container made of delrin (trade name for a composition of acetal resins manufactured by E.I. duPont de Nemours & Co. Inc.) machined so that the crystals are aligned as accurately as possible. Connections to the crystals were made through terminal posts which contacted with the gold plated sides of the crystals. The end windows were antireflectance coated, and could be adjusted so that they were parallel with each other and with the end faces of the crystal. This adjustment was made using the reflection of the beam from a helium-neon laser at the surfaces within the Pockels cell. The cell was filled with spectro-quality tetrachloroethylene as an index matching fluid, and sealed using viton (trade name for a composition of synthetic

Fig. 4.2.5 Double crystal transverse Pockels cell components.

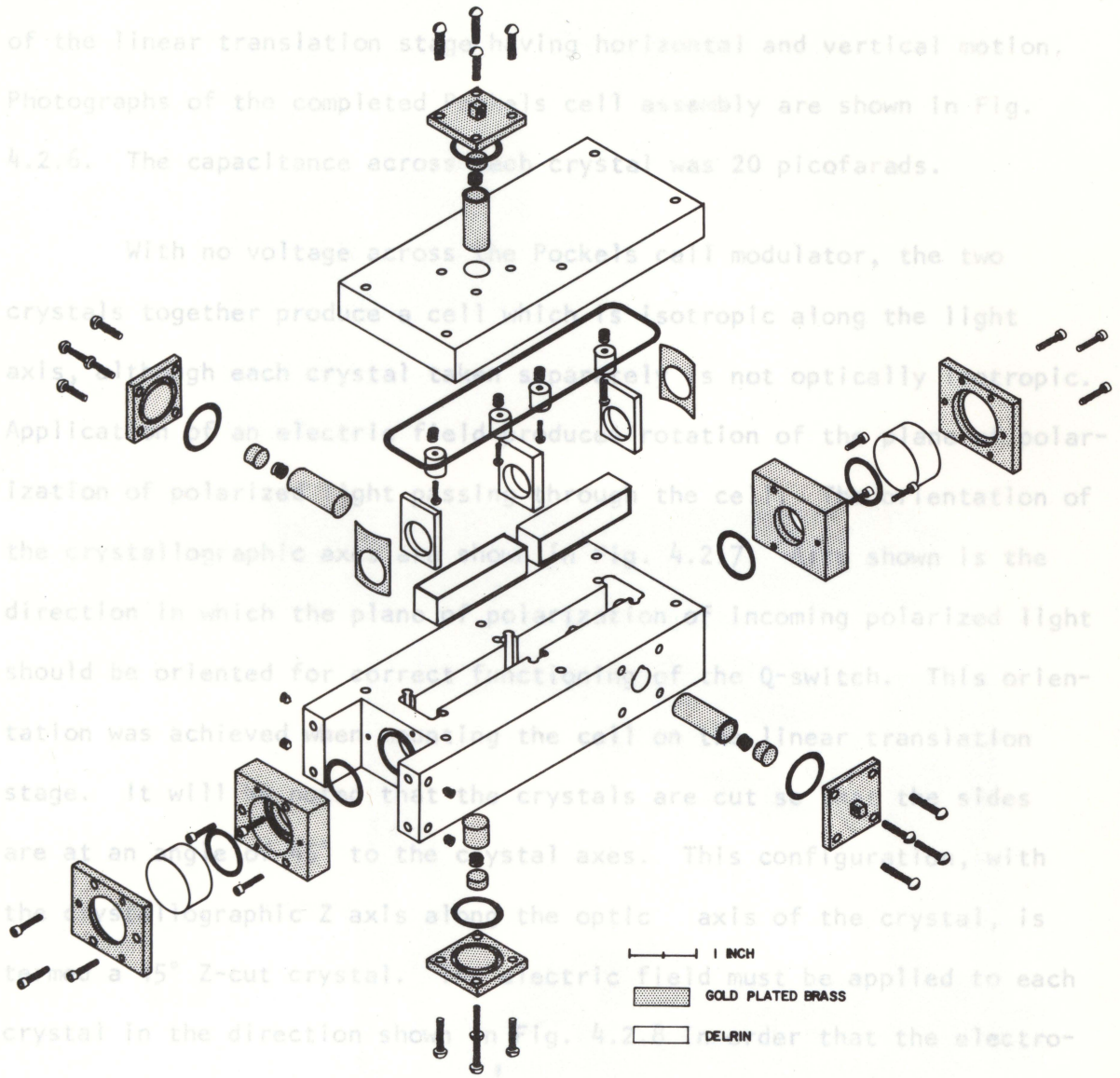

Fig. 4.2.5 Double crystal transverse Pockels cell components.

rubbersmanufactured by E.I. duPont de Nemours & Co. Inc.) O-rings on the windows, terminal posts, and lid. The cell was mounted within the cavity of the linear translation stage having horizontal and vertical motion. Photographs of the completed Pockels cell assembly are shown in Fig. 4.2.6. The capacitance across each crystal was 20 picofarads.

With no voltage across the Pockels cell modulator, the two crystals together produce a cell which is isotropic along the light axis, although each crystal taken separately is not optically isotropic. Application of an electric field produces rotation of the plane of polarization of polarized light passing through the cell. The orientation of the crystallographic axes are shown in Fig. 4.2.7. Also shown is the direction in which the plane of polarization of incoming polarized light should be oriented for correct functioning of the Q-switch. This orientation was achieved when mounting the cell on the linear translation stage. It will be noted that the crystals are cut so that the sides are at an angle of 45° to the crystal axes. This configuration, with the crystallographic Z axis along the optic axis of the crystal, is termed a 45° Z-cut crystal. The electric field must be applied to each crystal in the direction shown in Fig. 4.2.8 in order that the electro-optic effect of each should be additive. The correct direction of the electric field for each crystal was determined by placing the Pockels cell modulator between a mirror and a piece of polaroid acting as a polarizer. The polarity of 500 volts across the crystals was adjusted until light from a helium-neon laser on passing through the polarizer and the cell, and then returning through the cell on being reflected

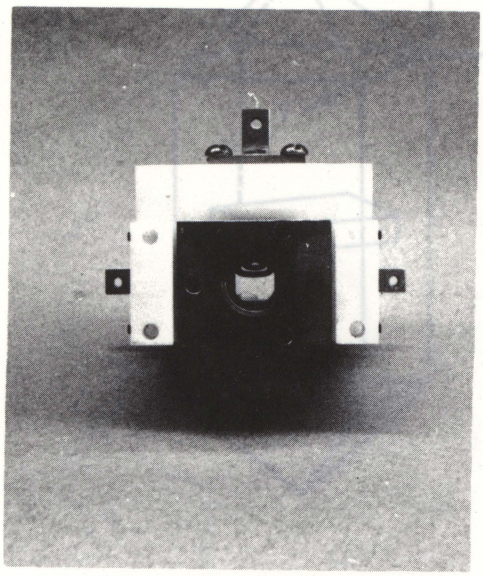

(a)

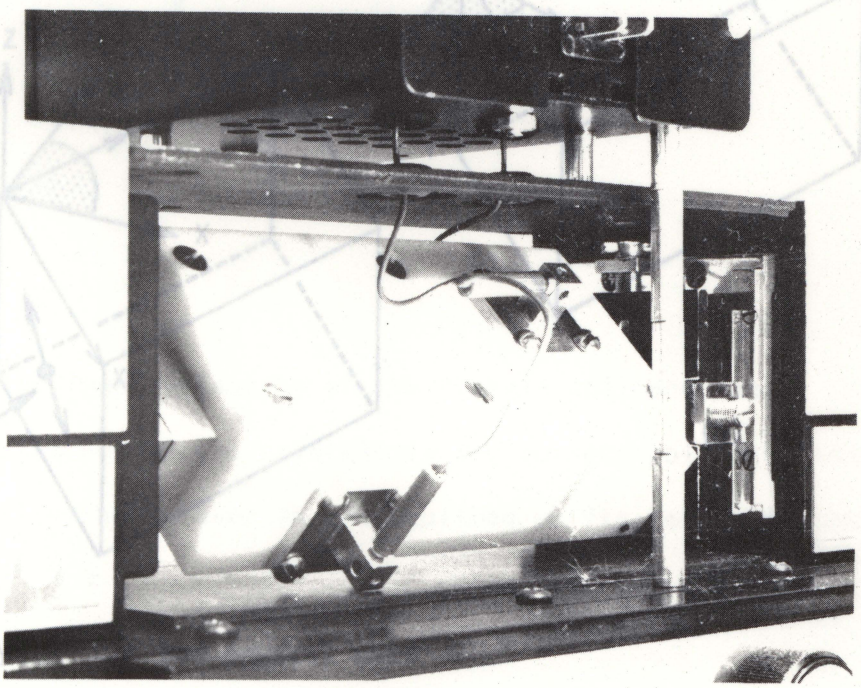

(b)

Fig. 4.2.6 Pockels cell assembly (a) end view (b) side view

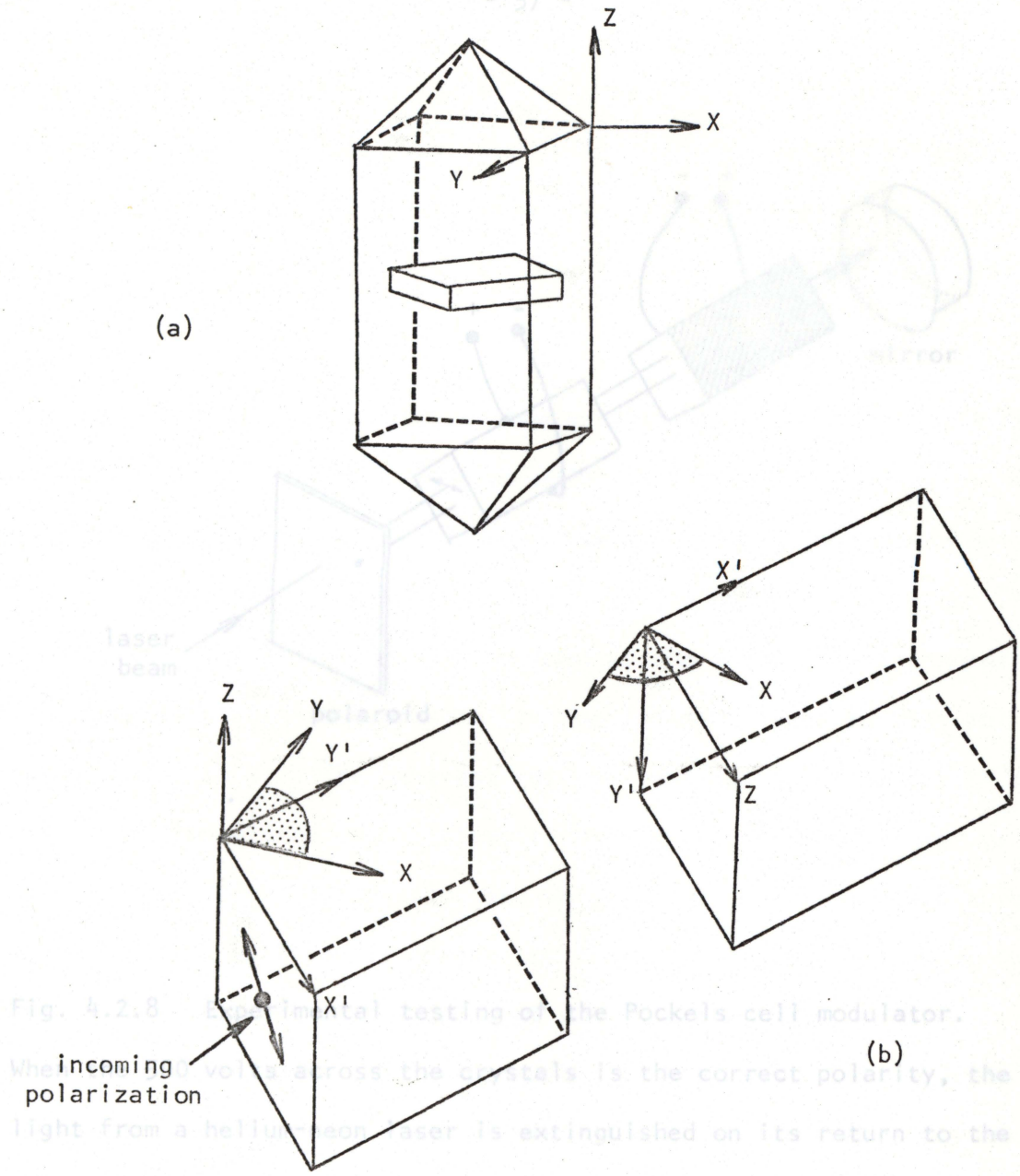

Fig. 4.2.7 Crystal cut and crystal axes

(a) 45° Z-cut crystal

(b) Orientation of crystallographic axes, X, Y, Z, and induced birefringent axes, X', Y', Z', in a double crystal transverse Pockels cell.

The optic axis is co-incident with the Z and Z' axes.

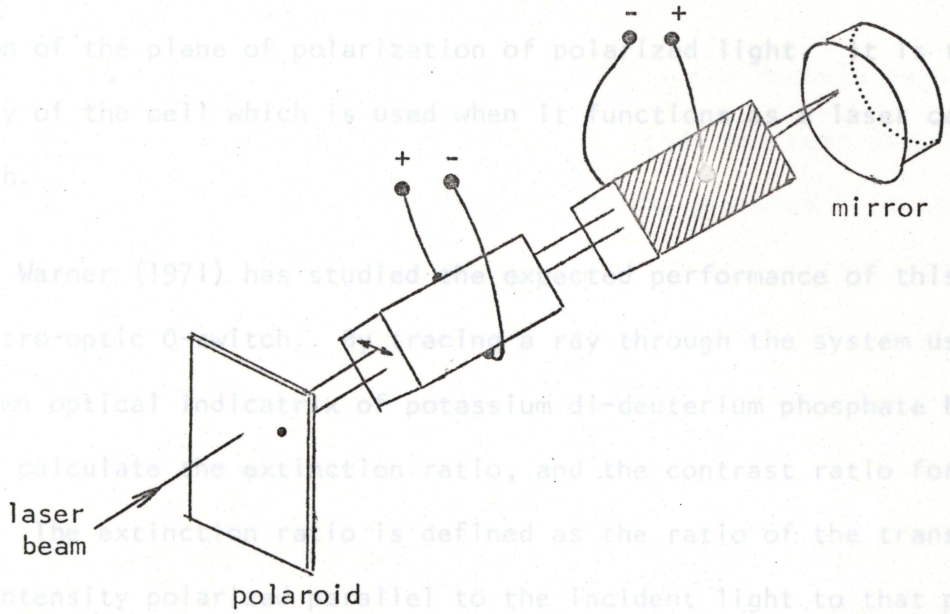

Fig. 4.2.8 Experimental testing of the Pockels cell modulator. When the 500 volts across the crystals is the correct polarity, the light from a helium-neon laser is extinguished on its return to the polaroid.

by the mirror, was extinguished by the piece of polaroid acting as an analyser. Thus, a double pass through the cell produces a 90 degree rotation of the plane of polarization of polarized light. It is this property of the cell which is used when it functions as a laser cavity Q-switch.

Warner (1971) has studied the expected performance of this type of electro-optic Q-switch. By tracing a ray through the system using the known optical indicatrix of potassium di-deuterium phosphate he was able to calculate the extinction ratio, and the contrast ratio for the switch. The extinction ratio is defined as the ratio of the transmitted light intensity polarized parallel to the incident light to that polarized perpendicular to it. The contrast ratio is defined as the ratio of maximum to minimum transmitted light intensity when an increasing voltage is applied to the cell. In particular, Warner concluded first that these ratios depend significantly on the two crystals being within about one fifth of a wavelength of the same optical thickness, and secondly deviation of the crystallographic axes with respect to the geometrical alignment results in a shift of the field of view of the Q-switch away from the system axis. These two factors determine the allowable tolerances in the Pockels cell design.

The working of the modulator within the laser cavity will be explained with reference to Fig. 4.2.2. It is necessary that all the optical surfaces within the cavity should be as parallel as possible. It has previously been mentioned that the windows within the Pockels cell were made parallel with each other and with the crystal end faces

by superimposing the reflections of a helium-neon gas laser beam from each surface. The gas laser was again used with the cell inside the cavity to bring the optical surfaces parallel. The Pockels cell was first adjusted with respect to the ruby rod, then the rear and front mirrors were brought into alignment. Since the distance from the ruby laser to the alignment laser was approximately twenty feet during this process the parallelism of the surfaces which was attained is of the order of a few seconds of arc. This parallelism is essential for laser action to occur.

The ruby rod is first optically pumped by discharging a capacitor charged to 3.8 kilovolts through the helical flash lamp. This causes the build-up of population inversion. The c-axis of the ruby is vertical, so that the light emitted by the ruby rod which is horizontally polarized becomes strictly plane polarized after passing through a stack polarizer. This consists of two series of glass plates set at the Brewster angle to the incident light, and arranged so that there is no net translation of the light beam. With the voltage applied to the Pockels cell, the plane of polarization of the beam returning to the stack polarizer is at right angles to the plane of polarization of the outgoing beam, so that very little light returns to the ruby. Under these circumstances light amplification cannot occur, and population inversion within the ruby rod continues to increase. When the voltage across the Pockels cell is reduced to zero the returning beam passes through the stack polarizer, and causes stimulated emission. In this way the light radiation within the cavity builds up and a giant Q-switched pulse is emitted through the output

mirror. One of these Q-switched pulses is shown in Fig. 4.2.9. The magnitude of this pulse far exceed those occurring during conventional lasing. If now the Pockels cell modulator is again switched on, population inversion can be re-established and another Q-switched pulse emitted.

In this way, a series of pulses were produced having magnitude comparable to that of a single Q-switched pulse. A photograph showing a series of such pulses is shown in Fig. 4.2.10. Wentz (1964) has reported repetition rates in excess of 400 kilohertz for this type of device.

Whether or not light amplification within the laser cavity will occur depends on the losses within the system. These include losses due to absorption by components within the cavity and losses of light from the cavity. In particular, the reflectivity of the output mirror is a compromise between what is required to ensure light amplification within the cavity, and what is required to enable a considerable proportion of the light to emerge from the cavity as a Q-switched pulse. The output mirror also determines the laser build-up time. When the reflectivity of the mirror is large a high proportion of the light energy is reflected back into the cavity so that the laser build-up time is short. It was found necessary to replace the 22% reflecting mirror used in the original laser cavity which employed a single crystal longitudinal Pockels cell, by a 45% reflecting mirror in order to compensate for the increased cavity length, and the increased losses due to the double crystal Pockels cell.

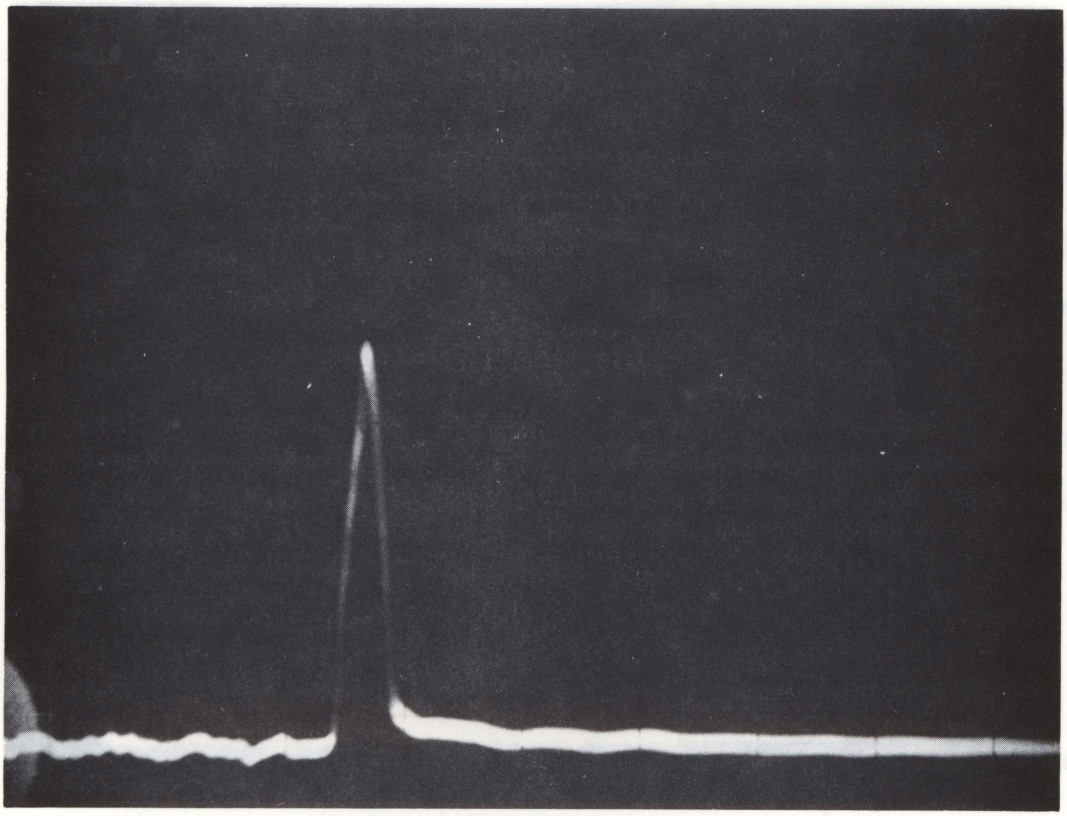

Fig. 4.2.9 A laser Q-switched pulse, monitored using the detector shown in Fig. 4.6.2 with a pinhole aperture in front of the photo-diode. Recording was made on 10,000 A.S.A. Polaroid film using a Tektronix type 546 oscilloscope. The oscilloscope sweep rate was 200 ns/cm, and its sensitivity was 5 v/cm. Triggering occurred on the switching of the Pockels cell.

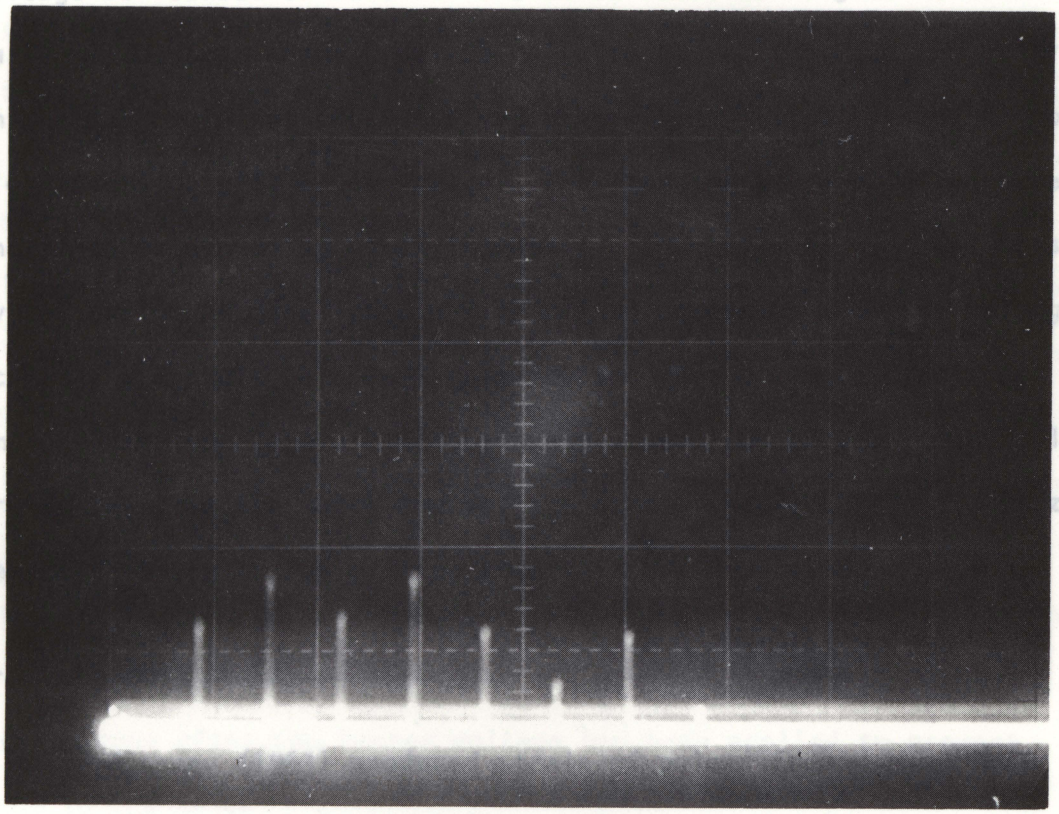

Fig. 4.2.10 A series of Q-switched pulses, monitored using the detector shown in Fig. 4.6.2 with a pinhole aperture in front of the photo-diode. The pulses were recorded on 3,000 A.S.A. Polaroid film using a Tektronix type 546 oscilloscope with a sweep rate of 50 μs/cm and sensitivity 5 v/cm.

It is important for efficient Q-switching that the Pockels cell voltage be reduced to zero for a time at least as long as it takes for build-up to occur and a Q-switch pulse to be emitted. On the other hand this time should not be excessive, otherwise re-establishment of population inversion will be curtailed. The laser build-up time decreases as the flash tube pumping power increases. The build-up time was measured by triggering an oscilloscope with pulses occurring when the voltage across the Pockels cell fell to zero, and when a single Q-switched pulse emerged from the laser. In subsequent production of Q-switched pulse trains the time for which the voltage across the Pockels cell was zero was adjusted to be far greater than this build-up time.

4.3 The Pockels cell driver

Fourney (1963) produced a train of pulses from a ruby laser using a Kerr cell as an optical modulator. He reported pulse rates exceeding a million per second. The electronics involved in the switching of several kilovolts at this rate are both inelegant and costly. Only 500 volts is required to drive the double crystal transverse Pockels cell used in this work. For efficient Q-switching, the pulse applied to the cell should have very short rise and fall times so that energy within the cavity does not leak away during a switching cycle. Several methods for producing 500 volt pulses with short rise and fall times were investigated. In particular, avalanche transistors were considered. It appears, however, that at the present time semi-conductors are not able to cope with the voltages and repetition rates demanded here.

Accordingly, the Pockels cell driver adopted was that used by Rowlands (1967) and employs vacuum tubes. The circuit for the Pockels cell driver is shown in Fig. 4.3.1. The circuit is arranged so that the fall time of the pulse emitted by the driver is shortened by the turn-on time of one of the tubes. Photographs of the completed driver unit are shown in Fig. 4.3.2. The driver was triggered using 50 volt pulses from a Hewlett Packard model 214A pulse generator. The pulse generator itself was triggered by pulses from the high speed camera as will be explained in Section 4.6. The driver unit was mounted directly over the Pockels cell modulator. A photograph showing the driver and modulator within the laser cavity is shown in Fig. 4.3.3. External to the Pockels cell driver a unit was built to supply the heaters of the tubes, and to switch the high voltage from a Fluke model 412 B power supply to the plates. This was done after the heater voltage had been applied to prevent damage to the tubes.

4.4 The test section mirror

Several possibilities were investigated for the test section mirror. It was required that the mirror be of satisfactory optical quality, and that it be drilled with a grid of fine holes for the injection of the smoke tracers.

As a first attempt, a piece of 1/8 inch thick back-silvered plexi-glass was laminated to a piece of 2 inch thich plexi-glass which had been drilled with a grid of 1/8 inch diameter holes. Fine holes were then drilled through the 1/8 inch thick plexi-glass. The optical

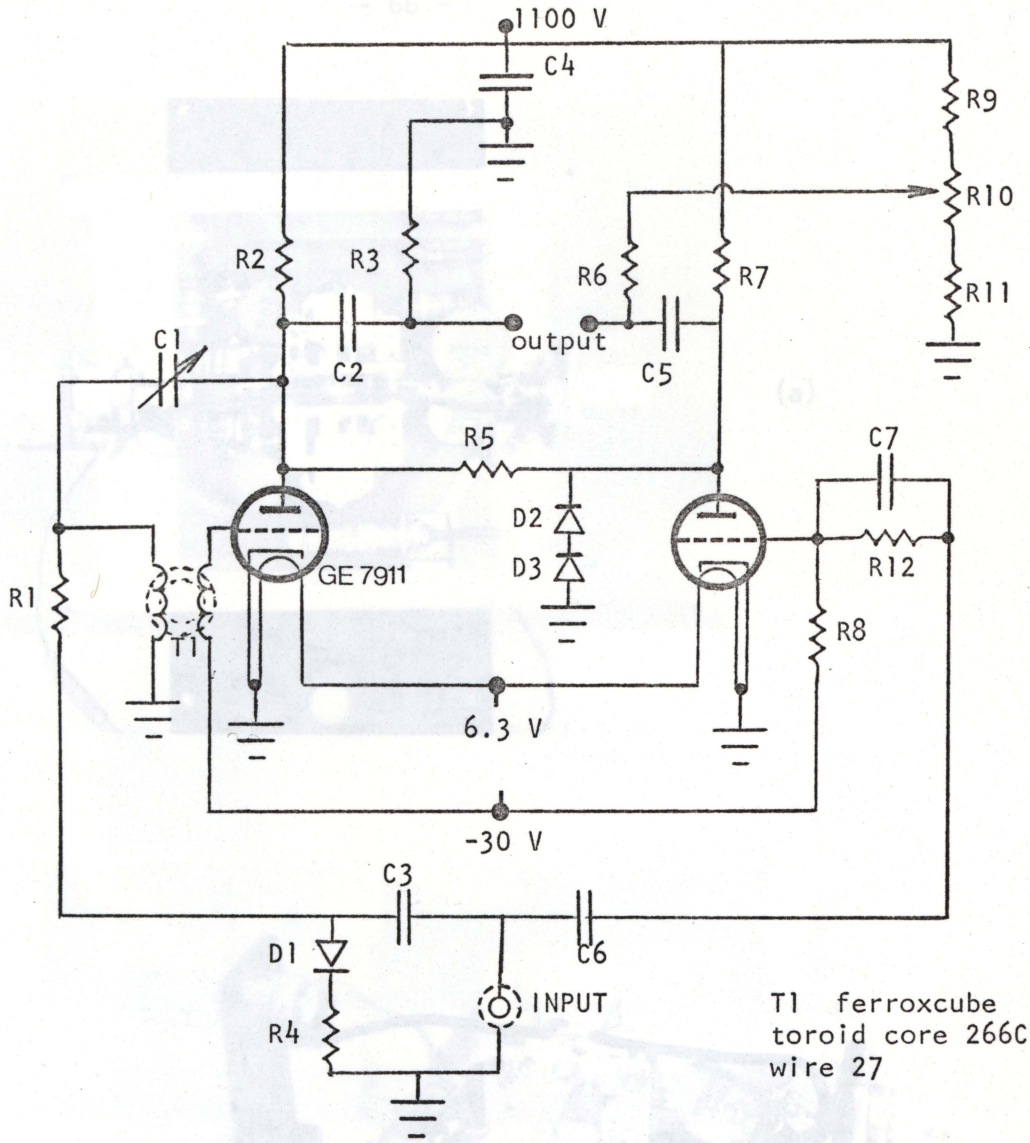

T1 ferroxcube
toroid core 266CT1254C4
wire 27

R1	51 Ohm ½ watt	C1	5-50 pf, 1250 volt JFD type VC55C
R2	7.5 kilohm 2 watt	C2	.002 mfd 3 kV disc ceramic
R3	1.5 megohm 1 watt	C3	2200 pf 300 V disc ceramic
R4	91 Ohm ½ watt	C4	same as C2
R5	7.5 kilohm 2 watt	C5	same as C2
R6	1.5 megohm 2 watt	C6	.01 mfd disc ceramic
R7	5 kilohm 2 watt	C7	390 pf disc ceramic
R8	5 kilohm ½ watt	D1	1N 914
R9	500 kilohm 1 watt	D2 & D3	UTR 61 unitrode diode
R10	500 kilohm ½ watt		
R11	500 kilohm 1 watt		
R12	91 ohm ½ watt		

Fig. 4.3.1 Pockels cell driver circuit

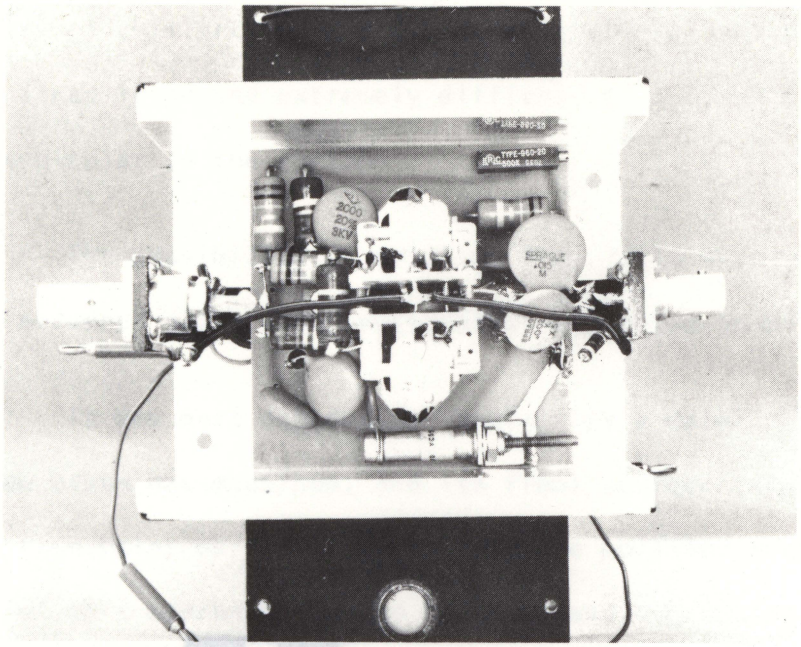

(a)

(b)

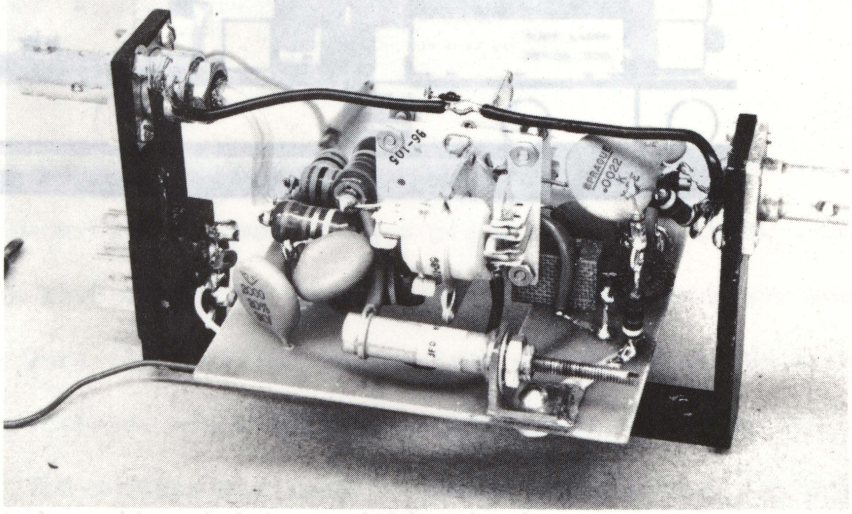

Fig. 4.3.2 Pockels cell driver unit (a) top view (b) side view

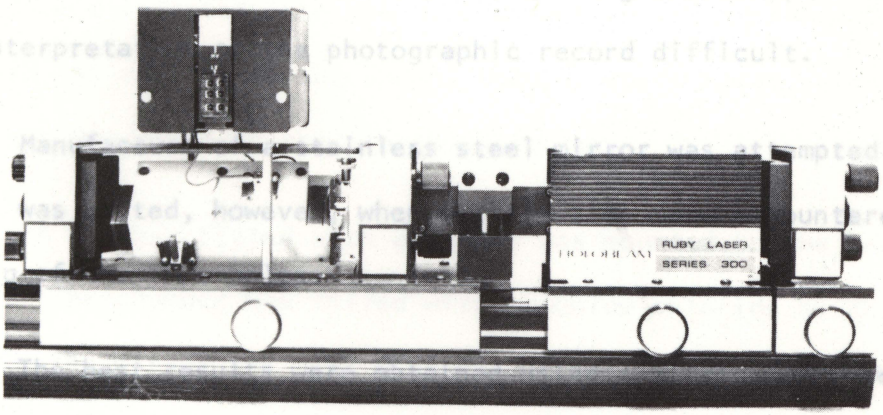

Fig. 4.3.3 Pockels cell and driver within the laser cavity.

quality of this arrangement was unsatisfactory, and the tracers were poor since it proved extremely difficult to drill the plexi-glass exactly perpendicular to the surface.

The possibility of drilling fine holes through 1/4 inch thick back silvered glass was investigated, but found to be impractical.

It was next decided to manufacture a metal mirror. A piece of yellow brass was machined, and its front surface lapped and polished. Then fine holes were drilled through the polished surface. The reflectivity of this mirror proved to be poor, and a granularity in the finish made interpretation of the photographic record difficult.

Manufacture of a stainless steel mirror was attempted. This project was halted, however, when difficulties were encountered in the drilling of the fine holes.

The best results were obtained using a mirror made from aluminum. This mirror was made by first machining a piece of 1 inch thick aluminum to the dimensions 25.4 cm × 7.62 cm. A grid of holes 1 cm apart and 1/8 inch in diameter were then drilled in the back of the mirror to within 1/16 inch of the surface. Then 13/1000 inch diameter holes were drilled to the surface. The surface was roughly ground using a lead lap and 150 grit carborundum. The surface was fine ground and roughly polished using 800 and 3200 mesh emery powder in turn with a Buehler (2120 Greenwood Street, Evanston, Illinois, U.S.A.) "Texmet" polishing cloth placed on an optically flat steel plate. Finally, the surface was optically polished using 5 micron magnesium oxide powder and Buehler "Microcloth" on the steel plate.

The optical quality of the finished mirror, as measured by its performance in the double-pass schlieren system, was satisfactory, and it produced a satisfactory grid of particle tracers. The quality of these tracers depended in part on how accurately the grid of holes in the mirror was drilled. A photograph showing typical particle tracers is given in Fig. 5.1.1.

4.5 The particle tracers

Tracers of ammonium chloride were selected for this work. These tracers were injected into the window section of the shock tube, just prior to the arrival of the shock, through small holes in the mirror which was described in the previous section.

A chamber fitted with a piston was mounted to the back of the mirror. The chamber was filled with ammonium chloride by covering the holes in the mirror and then drawing out the piston. As shown in Fig. 4.5.1 the air entering passes equally over concentrated hydrochloric acid and concentrated ammonium hydroxide. This produced the ammonium chloride, which was then bubbled through water to reduce large particles and substances which might corrode the mirror. In each experiment the tracers were injected into the test section by connecting the chamber to a bottle of air pressurized to 4 inches of mercury. This was done using a solenoid valve, so that the time of application of the pressure could be precisely controlled.

The application of this pressure produced laminar jets of smoke. These jets gradually broadened as they moved across the shock tube. The

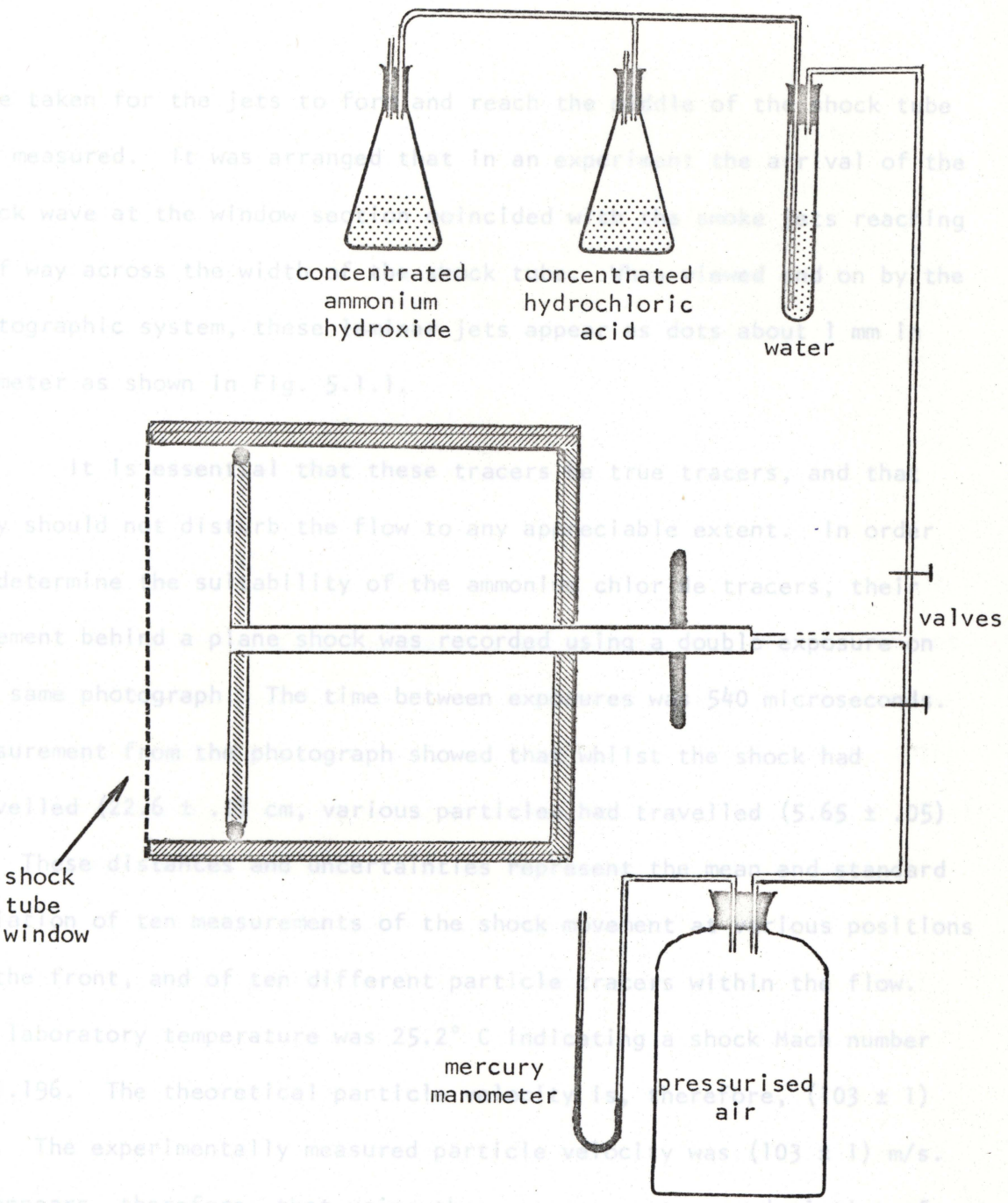

Fig. 4.5.1 Formation of particle tracers.

time taken for the jets to form and reach the middle of the shock tube was measured. It was arranged that in an experiment the arrival of the shock wave at the window section coincided with the smoke jets reaching half way across the width of the shock tube. When viewed end on by the photographic system, these laminar jets appear as dots about 1 mm in diameter as shown in Fig. 5.1.1.

It is essential that these tracers be true tracers, and that they should not disturb the flow to any appreciable extent. In order to determine the suitability of the ammonium chloride tracers, their movement behind a plane shock was recorded using a double exposure on the same photograph. The time between exposures was 540 microseconds. Measurement from the photograph showed that whilst the shock had travelled (22.6 ± .1) cm, various particles had travelled (5.65 ± .05) cm. These distances and uncertainties represent the mean and standard deviation of ten measurements of the shock movement at various positions on the front, and of ten different particle tracers within the flow. The laboratory temperature was 25.2° C indicating a shock Mach number of 1.196. The theoretical particle velocity is, therefore, (103 ± 1) m/s. The experimentally measured particle velocity was (103 ± 1) m/s. It appears, therefore, that using these measurements, no deviation of these particles from true tracers could be detected for the flow behind a Mach 1.2 shock.

Using formulae developed by Hoenig (1957) relating the drag force on a particle to its mass and acceleration, it was calculated that for an ammonium chloride particle one micron in diameter in the particular flow

we are here concerned with, the particle reaches 95% of the stream velocity after 0.5 microsecond. Shirley and Sheldon (1972) have reported particle charging of the dust particles in the flow behind shock waves. This phenomena, however, did not appear to affect the motion of the ammonium chloride particles which were used as tracers in this work. vom Stein and Pfeifer (1972) report that particles 0.1 - 1.0 micron in diameter are capable of following within a few microseconds, flow velocity variations of at least 200 m/sec.

4.6 Synchronization and monitoring

It was arranged that the smoke tracers were well formed, yet not appreciably diffused just before the arrival of the shock at the window section. This was done by triggering a delay circuit at the instant the power was applied to the high speed camera. The camera required 350 feet of film to run through before it was at full speed, which was nominally 11,000 frames per second. Attempts were made to splice 25 feet of film to 350 feet of leader but the splice was found to be unacceptable when the camera was running at full speed. Accordingly a continuous length of film was used several times, the relevant portion being developed after each experimental run. Approximately 500 milliseconds before the camera was at full speed, the solenoid controlling the formation of the particle tracers was switched on for half a second and then switched off. These times were found by trial to give the best formed smoke trails. When the camera was at full speed, a micro-switch within it activated the solenoid which fired the shock tube. A piezo-electric

transducer placed 1 metre from the diagram then monitored the arrival of the shock wave. The signal from this transducer was delayed using the circuit within a Tektronix type 549 oscilloscope and at an appropriate time initiated firing of the laser flash tube. A gating circuit then allowed the pulses from the Pockels cell driver to be applied to the Pockels cell. It was arranged that this gate opened at the time population inversion was first established, which was taken to be the time at which conventional lasing first began.

In order that the high speed pictures should be correctly framed the triggering of the pulse generator which supplied the pulses to the Pockels cell was effected externally. A photo-diode and a source of light were mounted on either side of the camera shutter. The pulses from this unit and the resulting output from the pulse generator are shown in Fig. 4.6.1.

To measure the time between pictures the output from the laser was monitored. The detector shown in Fig. 4.6.2 was covered with a pin-hole aperture and placed behind the rear mirror of the laser. The output from this detector could be direct recorded on a tape recorder, or fed directly into a time-interval counter. Assuming a constant camera speed over the few inches of film where the photographic record appeared, the time between all frames was taken to be the same as the time interval between the first two frames. Since the laser pulses were nanoseconds in width, this time interval could be measured to at least a tenth of a microsecond. Usually 4 - 6 pictures were recorded

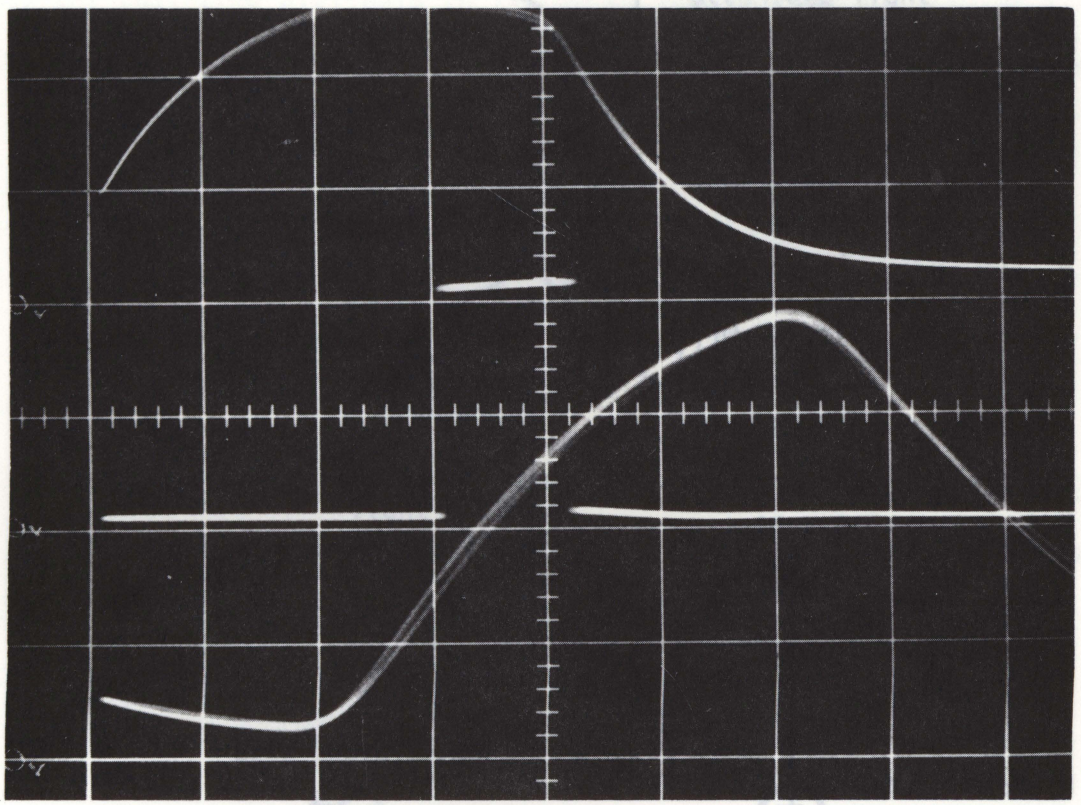

Fig. 4.6.1 Shutter pulse output with sweep rate 10 μs/div.
The top trace was obtained by monitoring the light passing through the high speed camera to the eyepiece, using the detector shown in Fig. 4.6.2. The bottom trace shows the shutter pulse output obtained from the photodiode within the camera. The shutter pulse output triggered the signal generator the output of which is the middle trace.

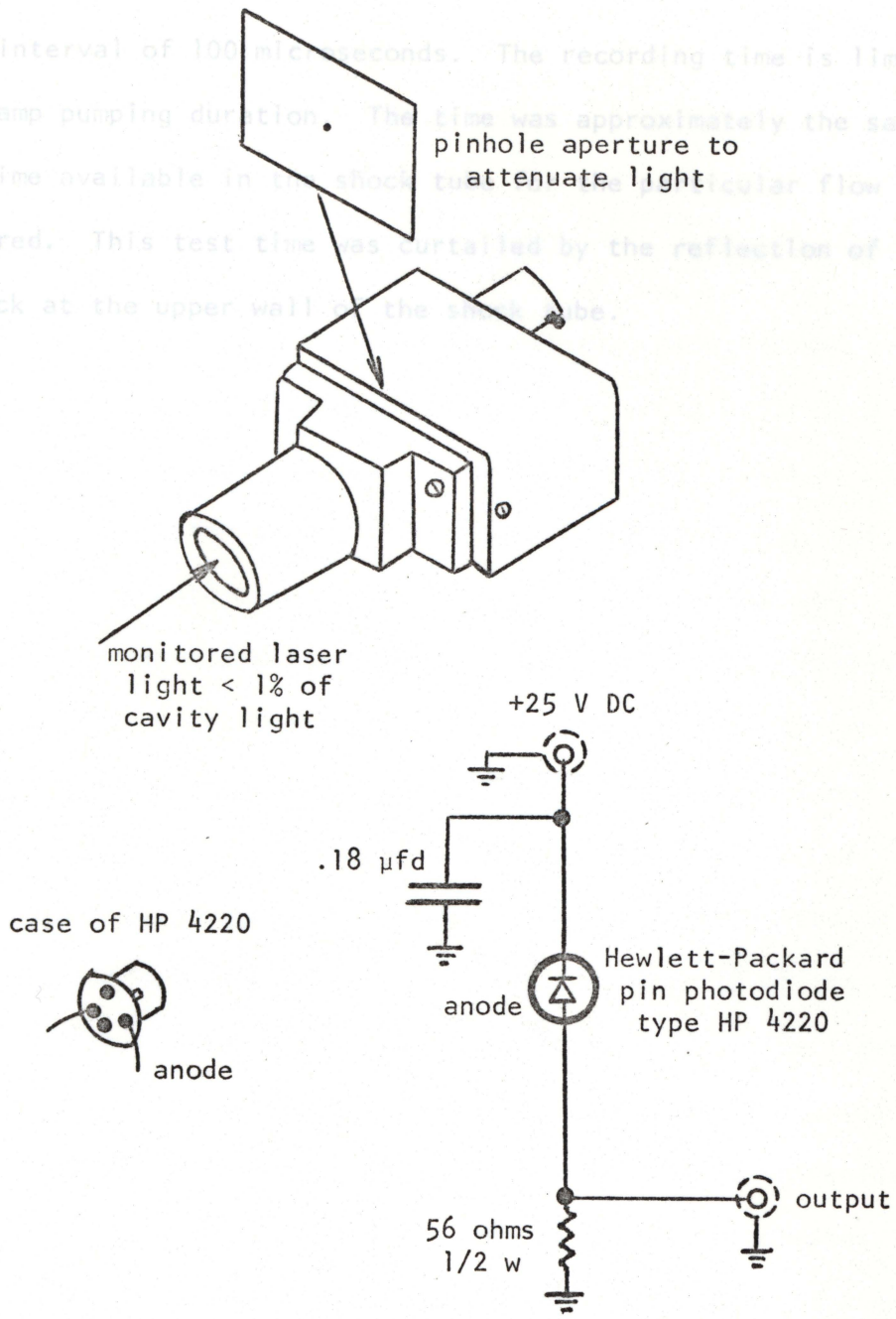

Fig. 4.6.2 Laser light detector

with a frame interval of 100 microseconds. The recording time is limited by the flashlamp pumping duration. The time was approximately the same as the test time available in the shock tube for the particular flow being considered. This test time was curtailed by the reflection of the reflected shock at the upper wall of the shock tube.

CHAPTER 5

ANALYSIS OF DATA

5.1 Digitization

The high-speed film record, which was obtained as described in the last chapter, was projected using an Analyst Movie Projector (L-W Photo Inc., 1547 Cabrito Road, Van Nuys, California 91406, U.S.A.). A print of a typical frame from such a film record is shown in Fig. 5.1.1. The image was projected onto a screen incorporated into the working surface of a Graf-Pen sonic digitizer (Science Accessories Corporation, 65 Station Street, Southport, Connecticut 06490, U.S.A.). The screen was formed by attaching a three foot square piece of back projection material to the transparent table of the digitizer. The position of a point on the screen was recorded simultaneously on a teletype and on paper tape. Recording was initiated by bringing the fine tip of the Graf-Pen down onto the screen. This produced a small spark. The times taken for the spark to reach strip microphones, placed along two edges of the working surface, were then converted by the Graf-Pen electronics into two four-digit numbers proportional to the cartesian coordinates of the point. It was found important to keep the Graf-Pen upright when making a reading, since the spark was generated a small distance above the surface of the table. A simple holder was built which kept the pen perpendicular to the working surface. With this addition, co-ordinates could be recorded with an accuracy of 1/10%.

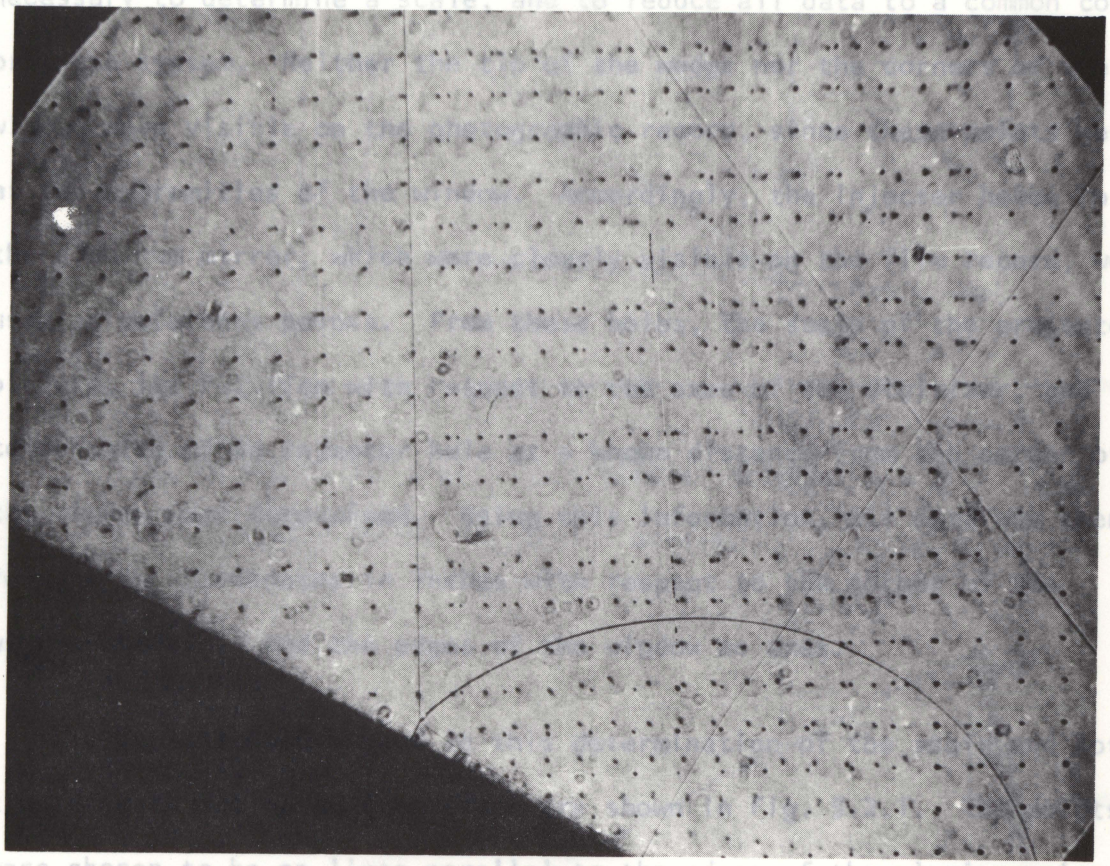

Fig. 5.1.1 High speed film record showing the reflection of a Mach 1.2 shock at a 30° wedge 214 microseconds after the incident shock reaches the corner.

5.2 Reduction of digitized data

For each projected frame of the high speed film record, it was necessary to determine a scale, and to reduce all data to a common coordinate system. Neither the tip of the wedge nor the corners of the window were visible on the photographic record, since these points were at the extremities of the window. Accordingly, the injector holes in the aluminum mirror, which were clearly visible on the film record, were used as reference points. From these holes, the scale of the projected picture, its rotation with respect to the axes of the digitizer, and the coordinates of an injector hole at a known distance from the corner of the window were determined. Using this information, all data was then reduced to coordinates in inches with respect to the corner of the window as origin and the edges of the window as axes.

Typical points used in this determination of the scale and rotation of each projected film frame are shown in Fig. 5.2.1. The points were chosen to be on lines parallel to the edges of the aluminum mirror. The lines were chosen to be in different areas of the picture, and the scale and rotation determined from each.

For a pair of points (1, 2) having digitized coordinates (X_1, Y_1), (X_2, Y_2), their separation in Graf-Pen units is given by

$$\text{SEPARATION} = [(X_2 - X_1)^2 + (Y_2 - Y_1)^2]^{\frac{1}{2}}$$

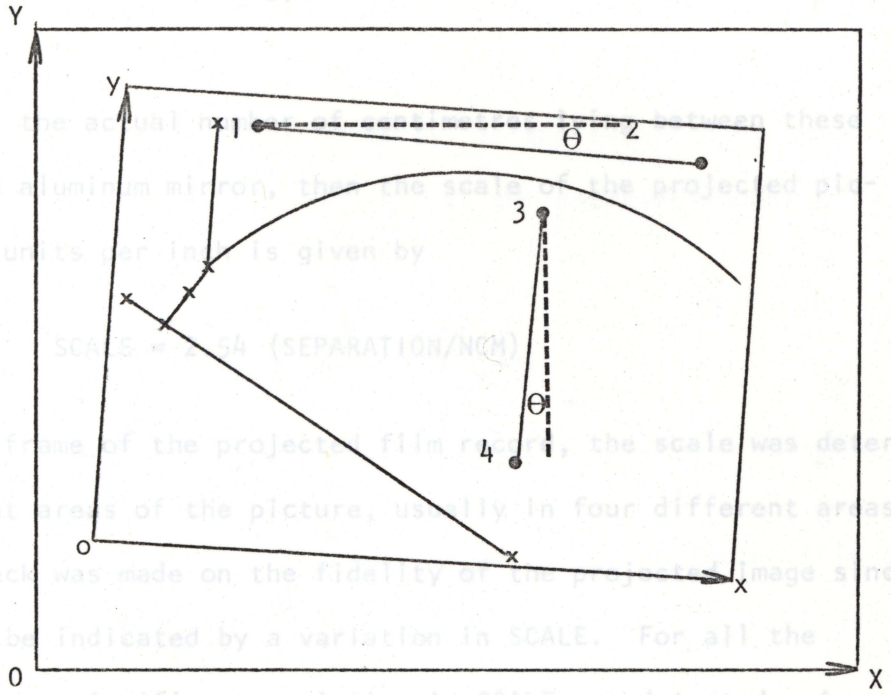

(X, Y) digitizer axes; 0, digitizer origin;

(x, y) window axes; o, window origin.

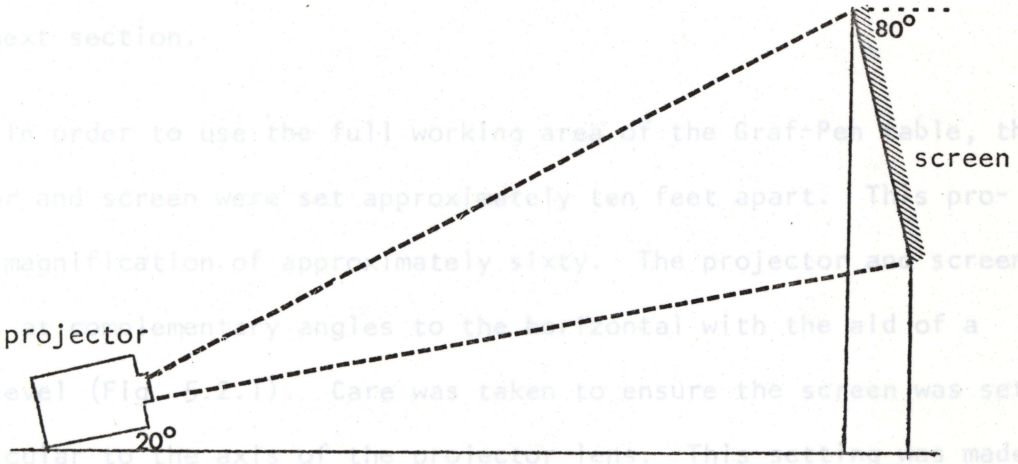

Fig. 5.2.1 Projection of film record.

If NCM is the actual number of centimetres lying between these two points on the aluminum mirror, then the scale of the projected picture in Graf-Pen units per inch is given by

$$SCALE = 2.54\ (SEPARATION/NCM)$$

For each frame of the projected film record, the scale was determined in different areas of the picture, usually in four different areas. In this way a check was made on the fidelity of the projected image since distortion could be indicated by a variation in SCALE. For all the frames digitized, no significant variation in SCALE was detected. A visual check on the fidelity of the projected image could also be made by placing a straight edge along rows and columns of injector holes. The overall accuracy of the data acquisition system will be discussed in the next section.

In order to use the full working area of the Graf-Pen table, the projector and screen were set approximately ten feet apart. This produced a magnification of approximately sixty. The projector and screen were set at complementary angles to the horizontal with the aid of a spirit level (Fig. 5.2.1). Care was taken to ensure the screen was set perpendicular to the axis of the projector lens. This setting was made by projecting a precision grid and then moving the screen until no distortion in the projected image could be measured. Alignment of the projected image so that lines of injector holes were parallel to the axes of the digitizer proved to be excessively tedious. Therefore, the rotation of each frame with respect to the axes of the digitizer was

determined. For a pair of injector holes (1, 2) the rotation of the line joining them, with respect to the axis of the digitizer running across the page in Fig. 5.2.1, is

$$\text{ARC COS } [(X_2 - X_1)/\text{SEPARATION}]$$

and also $$\text{ARC SIN } [(Y_1 - Y_2)/\text{SEPARATION}]$$

For a pair of points such as (3, 4) the rotation of the projected film frame with respect to the digitizer axes is

$$\text{ARC COS } [(Y_3 - Y_4)/\text{SEPARATION}]$$

and also $$\text{ARC SIN } [(X_3 - X_4)/\text{SEPARATION}]$$

Once an average angle of rotation had been determined, the coordinates of the corner of the aluminum mirror, which was to be the origin, could be calculated. The coordinates in Graf-Pen units are

$$XO = XD - (XA \text{ COS } \theta + YA \text{ SIN } \theta) \text{ . SCALE}$$

$$YO = YD - (-XA \text{ SIN } \theta + YA \text{ COS } \theta) \text{ . SCALE}$$

where (XD, YD) are the digitized coordinates of a point whose coordinates in inches, with respect to axes along the edges of the mirror and with origin at the corner of the mirror, are (XA, YA).

Once the origin had been determined in Graf-Pen units, the coordinates in inches of any point having digitized coordinates (XD, YD) is given by

abscissa: $[(XD - XO) \cos\theta - (YD - YO) \sin\theta]/SCALE$

ordinate: $[(XD - XO) \sin\theta + (YD - YO) \cos\theta]/SCALE$

In this way all digitized data was converted into coordinates, in inches, with respect to the corner of the window behind the wedge as origin and the sides of the window as axes. These operations were performed by a computer program.

The positions of the wedge and of the shocks were also digitized. Two points were recorded on the reflecting surface of the wedge, two points on the incident shock, one of which was the triple point, and also several points on the Mach stem. These points are marked with an "x" in Fig. 5.2.1. For the reflected shock, the digitized points were chosen sufficiently close to each other so that a reasonable representation of the curved shock could be obtained by joining straight line segments.

Finally, the smoke tracers were digitized, moving the Graf-Pen down each column of tracers in turn.

5.3 Determination of density

Using the coordinates of each smoke tracer obtained as described in the last section, the area of each quadrilateral formed by four tracers was calculated. For the four tracers shown in Fig. 3.3.2 having coordinates (x_1, y_1), (x_2, y_2), (x_3, y_3), (x_4, y_4), we have:

$$AREA = \tfrac{1}{2}[(x_4 - x_1) \cdot (y_2 - y_3) - (x_2 - x_3) \cdot (y_4 - y_1)]$$

In order to measure the accuracy of this method of area determination, a sample of points on a precision grid were digitized and the area of each quadrilateral was calculated. The results are given in Table 5.3.1 and show a standard (root mean square) deviation of 2%. Also a sample of holes in the aluminum mirror were digitized so that an indication of the accuracy of the area determination, including the production of the highspeed film record and its subsequent projection, could be obtained. The results are given in Table 5.3.1 and show a standard deviation of 3%.

Since the smoke tracers were formed on a centimetre grid, the density of an element of air after it has been shocked is given by

$$\text{DENSITY} = 1/(2.54^2 \cdot \text{AREA})$$

In this way, the density of each element of air, defined by four smoke tracers, was calculated with the aid of a computer program.

Typical results of this determination of the density field for two successive film frames are given in Figs. 5.3.1, 5.3.2 and Tables 5.3.2, 5.3.3. The figures show the grid of particle tracers and the tables give the density values within the grid. Other results are given in the Appendix.

5.4 Determination of particle velocity

The average particle velocity in the interval between two successive film frames was also calculated. For a particle moving

0.99	0.97	1.02	0.99	1.03	1.01	1.04
1.00	1.03	1.00	0.98	1.04	0.98	1.01
0.98	0.99	1.02	0.96	1.03	0.98	1.05
1.00	0.97	1.00	0.97	1.00	0.97	1.03
1.00	1.01	1.03	1.01	1.04	1.02	1.01
0.99	1.01	1.00	1.00	1.01	1.02	1.02
0.97	1.00	0.96	0.97	0.99	0.98	0.98
0.99	1.03	1.00	0.97	1.03	1.04	1.01
0.98	1.00	1.00	1.03	1.01	1.00	0.98

STANDARD DEVIATION 0.02

(a) Precision grid

1.00	0.97	0.98	0.98	1.00	0.97	0.98	1.01	0.93	1.00
1.02	1.04	1.01	1.03	1.04	1.03	1.04	1.00	1.00	1.04
1.01	0.99	0.96	0.96	0.95	0.98	0.96	0.98	0.99	0.95
1.06	1.02	1.00	0.98	1.00	0.99	1.00	1.02	0.97	1.00
1.00	0.97	0.96	1.00	0.96	0.97	0.99	0.96	0.95	0.98
1.01	1.04	1.02	1.02	1.00	1.03	1.01	1.01	0.98	0.97
0.99	1.01	0.90	1.00	0.96	0.97	0.99	1.07	0.97	0.95
0.97	1.05	0.92	1.01	0.98	0.97	0.97	1.00	0.97	1.00
1.04	1.02	0.89	1.00	1.01	1.02	0.97	1.03	0.98	1.02
1.02	1.03	0.98	1.03	1.00	1.00	0.97	1.01	0.96	0.98

STANDARD DEVIATION 0.03

(b) Aluminum mirror grid

Table 5.3.1 Determination of areas from digitized data

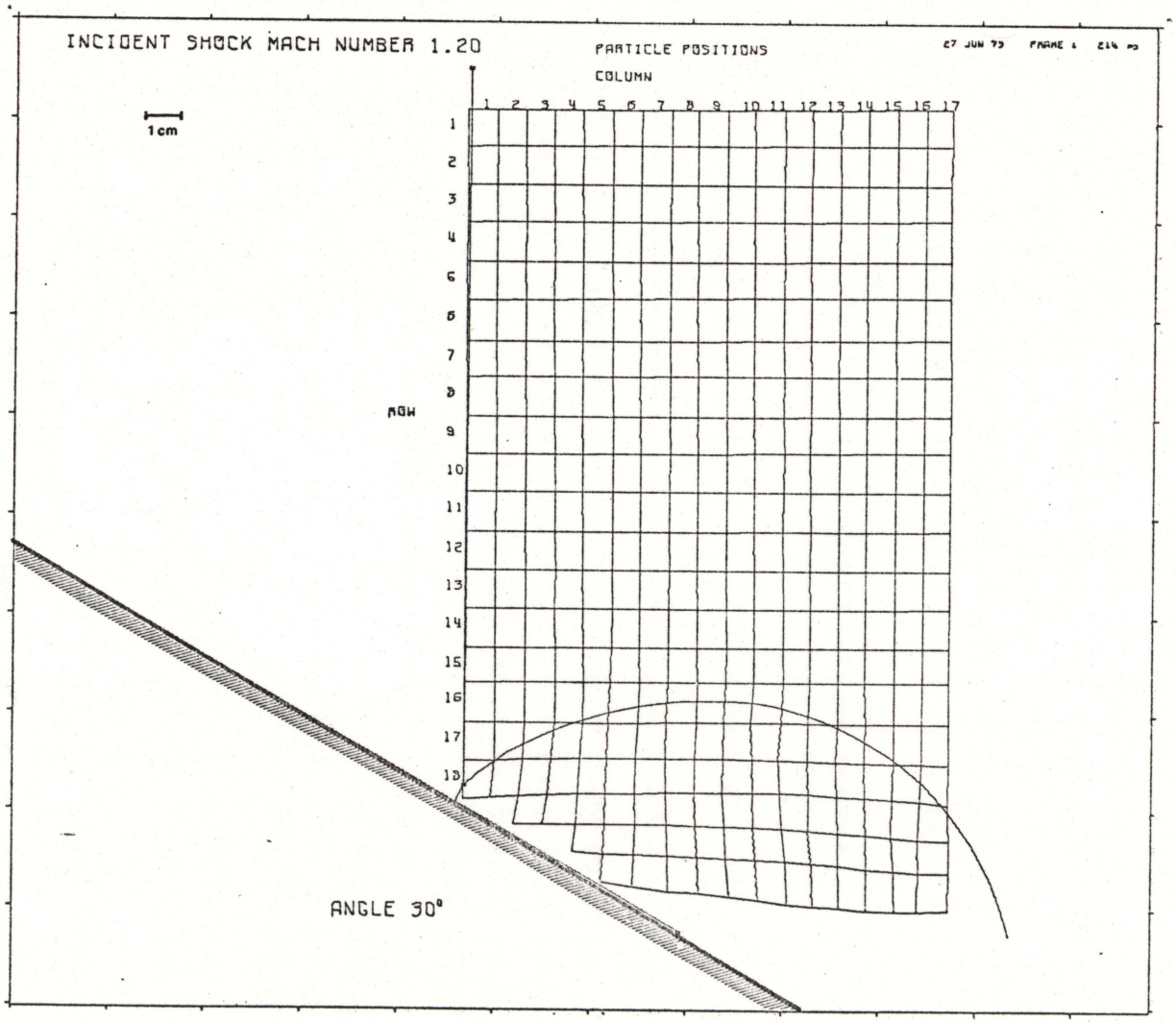

Fig. 5.3.1 Grid of particle tracers at 214 μs for the reflection of a Mach 1.20 shock at a 30° wedge.

	COLUMN																
	1	2	3	4	5	6	7	8	9	10	11	12	13	14	15	16	17
1	1.32	1.37	1.42	1.33	1.31	1.37	1.32	1.47	1.33	1.42	1.28	1.39	1.37	1.38	1.33	1.31	1.55
2	1.36	1.36	1.42	1.36	1.31	1.36	1.28	1.45	1.28	1.38	1.29	1.37	1.36	1.37	1.34	1.29	1.56
3	1.30	1.29	1.39	1.35	1.32	1.38	1.33	1.47	1.36	1.45	1.34	1.42	1.39	1.44	1.37	1.36	1.65
4	1.26	1.28	1.34	1.31	1.28	1.31	1.26	1.36	1.31	1.37	1.26	1.41	1.34	1.37	1.35	1.31	1.52
5	1.27	1.28	1.34	1.33	1.29	1.38	1.31	1.43	1.33	1.41	1.31	1.44	1.35	1.41	1.37	1.37	1.59
6	1.24	1.27	1.31	1.28	1.22	1.31	1.24	1.32	1.22	1.31	1.23	1.33	1.29	1.32	1.24	1.25	1.44
7	1.37	1.37	1.41	1.43	1.34	1.42	1.34	1.46	1.38	1.43	1.31	1.41	1.38	1.39	1.35	1.33	1.49
8	1.26	1.27	1.30	1.33	1.25	1.37	1.27	1.35	1.29	1.39	1.26	1.41	1.39	1.39	1.32	1.35	1.48
9	1.28	1.32	1.36	1.40	1.29	1.41	1.33	1.40	1.33	1.42	1.30	1.44	1.33	1.44	1.33	1.34	1.49
10	1.33	1.34	1.36	1.46	1.33	1.43	1.36	1.40	1.34	1.42	1.28	1.43	1.36	1.43	1.34	1.35	1.47
11	1.23	1.25	1.26	1.37	1.26	1.35	1.29	1.33	1.27	1.35	1.27	1.37	1.33	1.37	1.33	1.31	1.44
12	1.30	1.28	1.29	1.42	1.32	1.40	1.33	1.39	1.33	1.41	1.34	1.40	1.36	1.41	1.35	1.35	1.48
13	1.30	1.30	1.33	1.43	1.34	1.41	1.34	1.37	1.34	1.38	1.31	1.40	1.35	1.40	1.31	1.34	1.46
14	1.22	1.24	1.28	1.35	1.32	1.36	1.32	1.30	1.32	1.39	1.34	1.42	1.36	1.42	1.36	1.39	1.48
15	1.35	1.38	1.38	1.49	1.51	1.45	1.46	1.41	1.43	1.49	1.43	1.53	1.47	1.55	1.45	1.44	1.53
16	1.21	1.24	1.21	1.31	1.38	1.24	1.43	1.25	1.36	1.47	1.28	1.34	1.38	1.30	1.26	1.29	1.35
17	1.20	1.27	1.28	1.41	1.56	1.38	1.40	1.31	1.43	1.41	1.41	1.41	1.40	1.43	1.38	1.42	1.34
18	1.39	1.49	1.50	1.49	1.63	1.46	1.41	1.51	1.55	1.40	1.58	1.44	1.42	1.43	1.39	1.34	1.43
19			1.68	1.49	1.66	1.53	1.48	1.51	1.54	1.48	1.50	1.51	1.46	1.51	1.58	1.47	1.38
20					1.63	1.49	1.37	1.46	1.49	1.45	1.43	1.56	1.49	1.47	1.54	1.58	1.41
21						1.69	1.34	1.43	1.44	1.36	1.26	1.41	1.39	1.35	1.36	1.64	1.26

Table 5.3.2 Density values for Fig. 5.3.1.

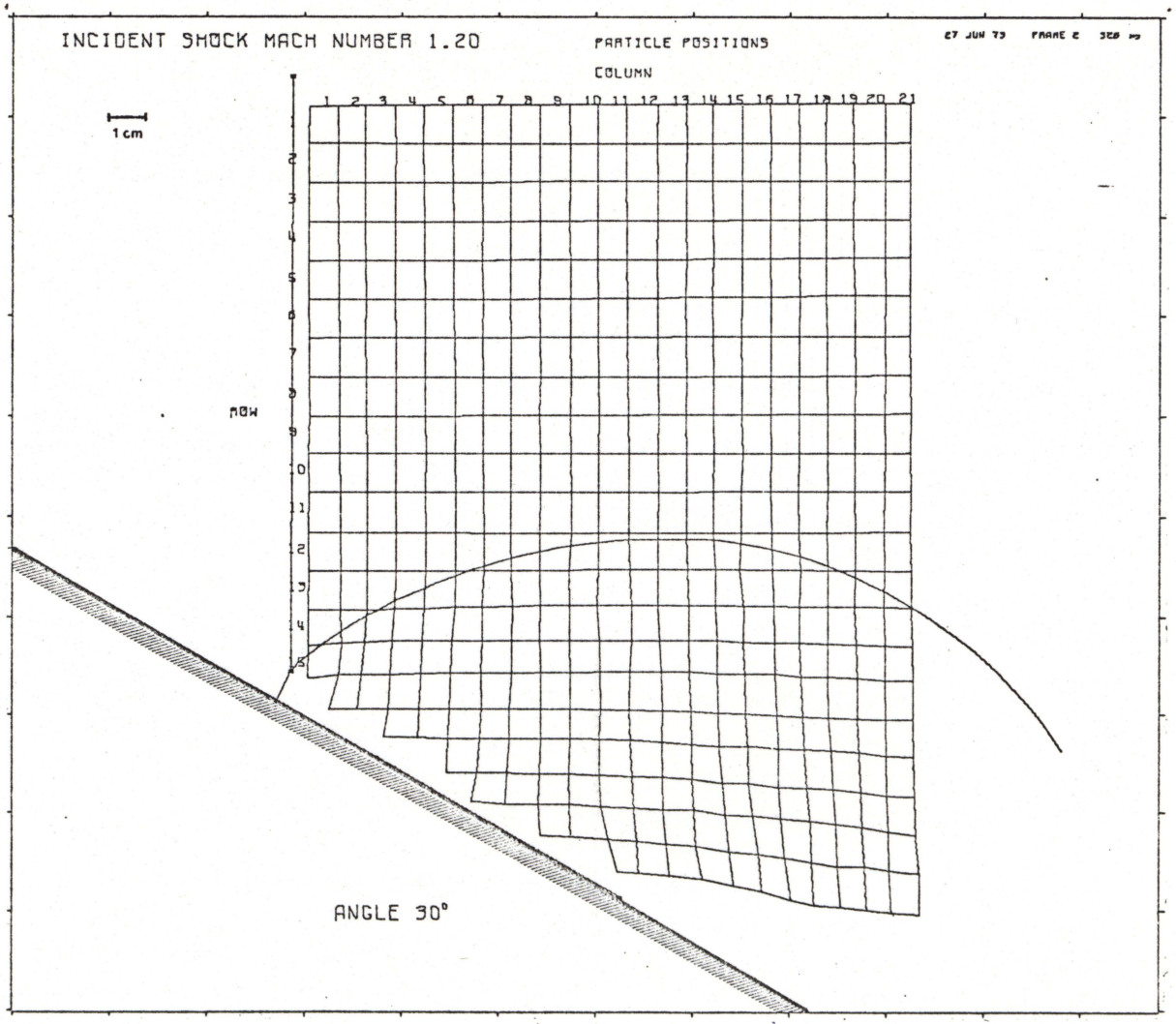

Fig. 5.3.2 Grid of particle tracers at 326 μs for the reflection of a Mach 1.20 shock at a 30° wedge.

	COLUMN																				
	1	2	3	5	5	6	7	8	9	10	11	12	13	14	15	16	17	18	19	20	21
1	1.39	1.46	1.28	1.38	1.35	1.31	1.37	1.33	1.30	1.42	1.38	1.26	1.35	1.48	1.31	1.37	1.34	1.45	1.39	1.21	1.55
2	1.29	1.44	1.28	1.38	1.33	1.30	1.35	1.32	1.30	1.45	1.39	1.25	1.36	1.52	1.30	1.33	1.33	1.45	1.40	1.24	1.55
3	1.32	1.45	1.29	1.36	1.35	1.35	1.40	1.35	1.33	1.41	1.39	1.27	1.38	1.50	1.36	1.41	1.40	1.51	1.47	1.29	1.61
4	1.25	1.41	1.25	1.29	1.28	1.29	1.30	1.24	1.25	1.32	1.25	1.19	1.25	1.37	1.28	1.29	1.26	1.37	1.35	1.20	1.52
5	1.30	1.50	1.37	1.37	1.38	1.40	1.44	1.37	1.32	1.49	1.41	1.36	1.46	1.55	1.41	1.45	1.41	1.59	1.48	1.33	1.63
6	1.25	1.42	1.27	1.30	1.29	1.30	1.34	1.27	1.21	1.35	1.26	1.21	1.29	1.36	1.25	1.23	1.25	1.30	1.26	1.20	1.46
7	1.31	1.49	1.33	1.37	1.33	1.41	1.45	1.37	1.32	1.47	1.39	1.32	1.41	1.51	1.43	1.37	1.42	1.43	1.42	1.37	1.63
8	1.27	1.42	1.29	1.30	1.26	1.34	1.36	1.31	1.24	1.36	1.28	1.24	1.35	1.37	1.33	1.28	1.34	1.35	1.35	1.26	1.48
9	1.29	1.48	1.37	1.34	1.37	1.45	1.42	1.35	1.28	1.46	1.36	1.33	1.42	1.45	1.38	1.37	1.41	1.37	1.40	1.31	1.55
10	1.25	1.46	1.37	1.30	1.30	1.41	1.43	1.35	1.29	1.45	1.28	1.32	1.38	1.43	1.39	1.35	1.43	1.36	1.45	1.33	1.50
11	1.15	1.40	1.29	1.27	1.25	1.31	1.34	1.26	1.19	1.40	1.23	1.25	1.31	1.42	1.34	1.21	1.34	1.28	1.34	1.28	1.47
12	1.24	1.54	1.38	1.34	1.33	1.44	1.40	1.32	1.32	1.44	1.34	1.31	1.46	1.56	1.40	1.41	1.47	1.44	1.43	1.38	1.45
13	1.17	1.44	1.31	1.37	1.39	1.55	1.50	1.58	1.54	1.54	1.30	1.56	1.34	1.48	1.51	1.27	1.46	1.40	1.46	1.31	1.55
14	1.29	1.42	1.65	1.47	1.46	1.47	1.38	1.50	1.40	1.41	1.21	1.53	1.41	1.56	1.57	1.37	1.68	1.50	1.47	1.38	1.44
15	1.53	2.09	1.71	1.54	1.58	1.57	1.58	1.67	1.62	1.66	1.62	1.67	1.69	1.55	1.60	1.44	1.65	1.48	1.45	1.47	1.49
16		1.59	1.43	1.30	1.35	1.29	1.41	1.33	1.36	1.33	1.33	1.17	1.35	1.40	1.42	1.24	1.48	1.45	1.27	1.39	1.38
17				1.51	1.62	1.40	1.57	1.48	1.62	1.55	1.54	1.36	1.43	1.51	1.46	1.34	1.53	1.60	1.44	1.47	1.43
18						1.41	1.54	1.36	1.50	1.47	1.34	1.43	1.52	1.56	1.51	1.35	1.50	1.56	1.42	1.54	1.39
19							1.45	1.38	1.57	1.43	1.35	1.47	1.43	1.45	1.58	1.49	1.47	1.61	1.45	1.54	1.38
20									1.61	1.44	1.59	1.63	1.49	1.37	1.46	1.49	1.38	1.49	1.46	1.62	1.40
21										1.36	1.69	1.46	1.38	1.33	1.37	1.31	1.35	1.29	1.29	1.36	1.19

Table 5.3.3 Density values for Fig. 5.3.2.

from (x_1, y_1) to (x_2, y_2), the magnitude of the component of velocity parallel to the incident flow (along the x-axis) is given by

$$u = (x_2 - x_1)/F$$

where F is the time between frames, recorded as explained in Section 4.6. The magnitude of the component of velocity perpendicular to the incident flow (along the y-axis) is

$$v = (y_2 - y_1)/F$$

The velocity vector thus has magnitude equal to $(u^2 + v^2)^{\frac{1}{2}}$ and makes an angle with the x-axis whose tangent is u/v. Typical results of these particle velocity calculations for two successive film frames are given in Fig. 5.4.1 and Table 5.4.1. The figure shows the positions of the shocks and of the particles in two successive frames. The table lists the longitudinal and transverse components of velocity (u and v), the total velocity (VEL) and the angle which the velocity vector makes with the x-axis (ANGLE). Other results are given in the Appendix.

5.5 Pressure and temperature

In order to estimate the accuracy of the particle trajectory analysis technique, the mean and standard deviation of the density values for the region behind the incident shock, and above the reflected shock were calculated. Interferometric records show that a uniform density field is to be expected in this area. The area was divided into vertical strips containing 20 - 40 density values for this calcu-

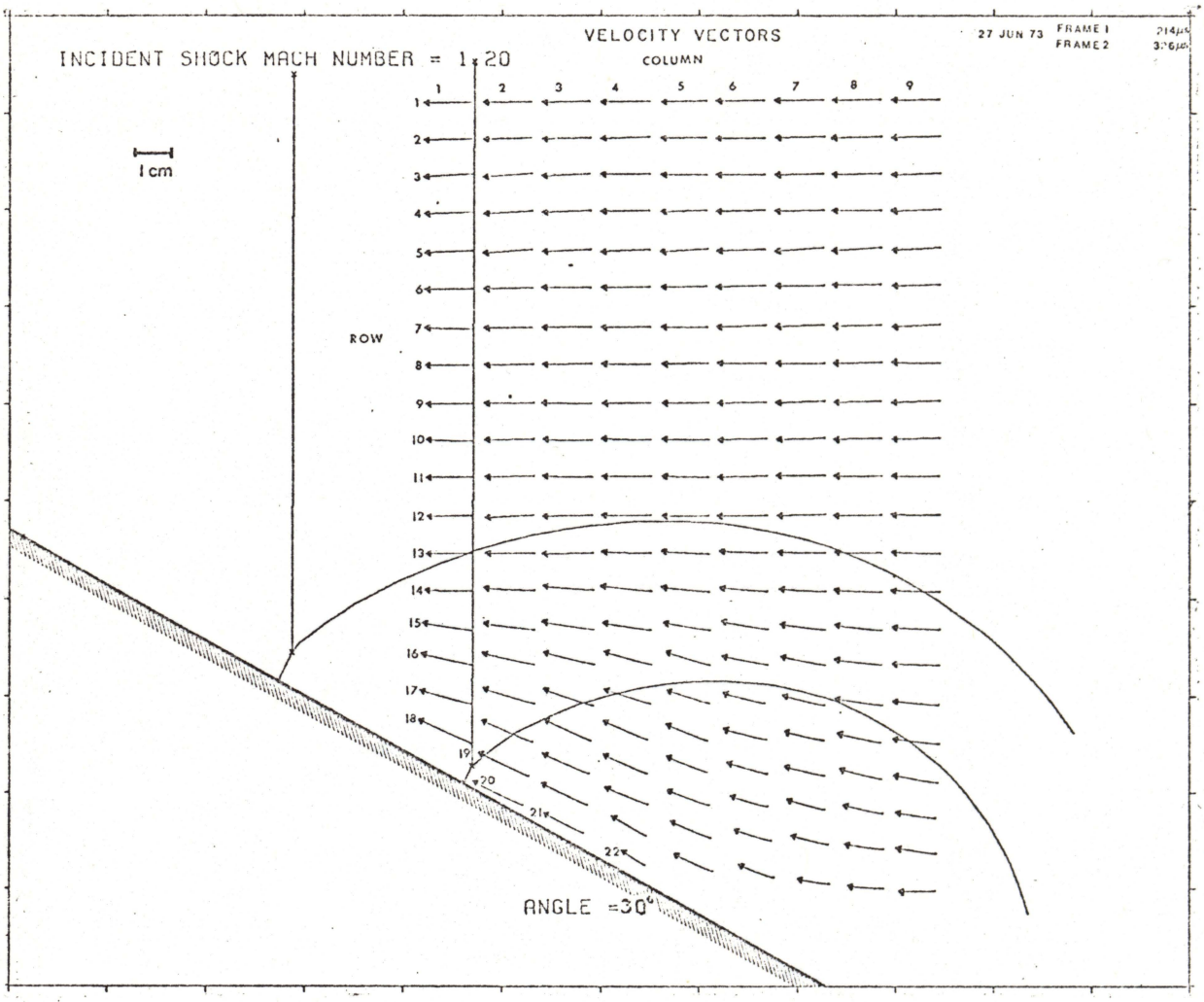

Fig. 5.4.1 Velocity vectors for the reflection of a Mach 1.20 shock at a 30° wedge.

COLUMN 1 — FRAME 1 - 2

ROW	U(M/S)	V(M/S)	VEL	ANGLE
1	103.29	-1.69	103.30	-0.94
2	102.61	-2.38	102.64	-1.33
3	103.30	-5.81	103.46	-3.22
4	102.61	-3.77	102.68	-2.11
5	100.56	-5.16	100.70	-2.94
6	100.55	-1.06	100.56	-0.61
7	101.23	1.66	101.25	0.94
8	101.92	-1.28	101.93	-0.71
9	100.55	-0.41	100.55	-0.23
10	99.86	3.00	99.91	1.72
11	99.19	-1.80	99.21	-1.04
12	97.82	-0.45	97.82	-0.26
13	99.19	-0.46	99.19	-0.26
14	101.92	2.28	101.94	1.28
15	107.35	16.64	108.64	8.81
16	110.07	25.53	112.99	13.06
17	112.79	31.68	117.15	15.69
18	116.84	54.24	128.82	24.90

COLUMN 2 — FRAME 1 - 2

ROW	U(M/S)	V(M/S)	VEL	ANGLE
1	103.96	-1.69	103.97	-0.93
2	103.28	-3.07	103.32	-1.70
3	105.34	-6.49	105.54	-3.53
4	104.65	-5.14	104.78	-2.81
5	106.02	-7.20	106.27	-3.88
6	103.96	-1.74	103.97	-0.96
7	103.96	-1.75	103.97	-0.95
8	105.33	-1.07	105.33	-0.58
9	106.69	-1.08	106.70	-0.58
10	105.32	-0.41	105.33	-0.22
11	105.33	-1.10	105.33	-0.60
12	103.97	-5.22	104.10	-2.88
13	105.33	-0.44	105.33	-0.24
14	108.73	6.39	108.92	3.37
15	110.08	15.28	111.13	7.90
16	111.42	25.53	114.31	12.91
17	110.71	34.41	115.94	17.26
18	110.00	48.07	120.04	23.61
19	109.30	53.53	121.71	26.09
20	109.30	54.89	122.31	26.67

COLUMN 3 — FRAME 1 - 2

ROW	U(M/S)	V(M/S)	VEL	ANGLE
1	102.58	-2.37	102.60	-1.33
2	102.58	-2.39	102.60	-1.33
3	102.53	-4.45	102.68	-2.48
4	103.26	-3.09	103.31	-1.71
5	103.27	-4.47	103.36	-2.48
6	104.62	0.31	104.62	0.17
7	104.62	-0.38	104.63	-0.21
8	104.63	-1.08	104.63	-0.59
9	107.36	0.97	107.36	0.52
10	105.30	2.32	105.33	1.25
11	105.99	1.63	106.00	0.88
12	107.36	-1.79	107.38	-0.96
13	108.73	-1.12	108.74	-0.59
14	108.02	9.81	108.47	5.19
15	111.42	17.33	112.76	8.84
16	109.35	26.89	112.61	13.82
17	107.27	36.45	113.30	18.77
18	101.69	48.05	111.93	25.42
19	100.42	45.31	110.16	24.28
20	98.36	48.71	109.76	26.35
21	86.06	45.25	97.23	27.74

COLUMN 4 — FRAME 1 - 2

ROW	U(M/S)	V(M/S)	VEL	ANGLE
1	106.65	-1.68	106.67	-0.90
2	105.30	-3.06	105.34	-1.67
3	105.29	-0.34	105.29	-0.18
4	104.61	-1.72	104.63	-0.94
5	105.30	-5.15	105.43	-2.80
6	104.61	-0.37	104.61	-0.20
7	105.98	-1.06	105.98	-0.57
8	104.61	0.98	104.61	0.53
9	104.61	-1.77	104.63	-0.97
10	107.33	3.70	107.40	1.97
11	105.97	0.95	105.98	0.51
12	106.66	0.25	106.66	0.14
13	106.65	3.66	106.71	1.97
14	109.37	12.55	110.08	6.55
15	104.57	16.63	105.88	9.04
16	102.49	28.93	106.49	15.79
17	99.74	33.61	105.06	18.31
18	95.62	41.88	104.39	23.65
19	95.62	43.24	104.94	24.33
20	92.21	38.44	99.90	22.63
21	73.73	44.54	86.14	31.14
22	47.77	32.16	57.59	33.95

COLUMN 5 — FRAME 1 - 2

ROW	U(M/S)	V(M/S)	VEL	ANGLE
1	97.76	-2.39	97.79	-1.40
2	98.44	-1.03	98.44	-0.60
3	98.43	0.33	98.44	0.19
4	99.81	-2.41	99.84	-1.38
5	101.87	-5.15	102.00	-2.90
6	98.44	-1.07	98.44	-0.62
7	100.49	-0.98	100.49	-0.56
8	99.81	-1.09	99.81	-0.62
9	99.81	-1.10	99.81	-0.63
10	101.85	0.95	101.86	0.53
11	100.48	1.62	100.50	0.92
12	101.17	-0.44	101.17	-0.25
13	102.53	6.39	102.72	3.57
14	104.57	9.80	105.03	5.36
15	100.45	16.62	101.82	9.40
16	96.32	29.60	100.76	17.08
17	92.90	29.58	97.49	17.66
18	90.14	37.08	97.47	22.36
19	88.78	35.70	95.69	21.91
20	89.47	34.33	95.83	20.99
21	87.40	39.10	95.75	24.10
22	82.62	39.08	91.39	25.32

COLUMN 6 — FRAME 1 - 2

ROW	U(M/S)	V(M/S)	VEL	ANGLE
1	106.60	-1.68	106.61	-0.90
2	107.97	-2.37	107.99	-1.26
3	105.91	-1.02	105.92	-0.55
4	105.91	0.34	105.91	0.18
5	106.61	-5.83	108.77	-3.13
6	105.22	1.00	105.23	0.54
7	103.87	-2.44	103.89	-1.34
8	103.86	-0.39	103.86	-0.22
9	101.81	-1.78	101.83	-1.00
10	103.18	-1.79	103.20	-0.99
11	102.49	0.94	102.49	0.52
12	103.86	-1.80	103.88	-1.00
13	101.80	2.28	101.83	1.28
14	102.48	5.01	102.60	2.80
15	101.78	11.15	102.39	6.25
16	101.10	11.14	101.71	6.29
17	101.77	15.23	102.91	8.51
18	92.19	21.35	94.63	13.04
19	90.13	23.39	93.12	14.55
20	84.67	19.27	86.83	12.82
21	83.31	13.10	84.34	8.93
22	75.12	6.23	75.38	4.74

COLUMN 7 — FRAME 1 - 2

ROW	U(M/S)	V(M/S)	VEL	ANGLE
1	104.56	-1.00	104.57	-0.55
2	105.25	-1.70	105.26	-0.92
3	103.88	-2.39	103.91	-1.32
4	104.55	-1.03	104.57	-0.57
5	103.89	-6.52	104.09	-3.59
6	103.88	-0.37	103.88	-0.21
7	103.88	-3.80	103.95	-2.10
8	104.56	0.97	104.56	0.53
9	104.57	-3.82	104.64	-2.09
10	102.51	-1.79	102.53	-1.00
11	105.24	0.26	105.24	0.14
12	103.20	-2.49	103.23	-1.38
13	101.82	1.60	101.83	0.90
14	98.39	5.68	98.56	3.31
15	97.01	12.51	97.81	7.35
16	95.62	19.33	97.56	11.43
17	88.78	22.04	91.48	13.94
18	83.31	20.65	85.93	13.92
19	84.68	20.65	87.16	13.70
20	79.89	22.68	83.04	15.85
21	78.53	19.93	81.01	14.24
22	66.92	11.00	67.82	9.33

COLUMN 9 — FRAME 1 - 2

ROW	U(M/S)	V(M/S)	VEL	ANGLE
1	104.53	-0.32	104.53	-0.18
2	105.90	-3.06	105.95	-1.66
3	105.22	-2.39	105.24	-1.30
4	105.22	-3.77	105.29	-2.05
5	104.54	-3.78	104.60	-2.07
6	103.85	-3.11	103.90	-1.71
7	103.17	-4.49	103.27	-2.49
8	103.84	2.34	103.86	1.29
9	103.85	-3.83	103.92	-2.11
10	103.95	-1.10	103.85	-0.61
11	103.16	0.94	103.16	0.52
12	105.21	2.30	105.23	1.25
13	104.52	2.97	104.56	1.63
14	105.89	3.65	105.95	1.97
15	102.46	5.68	102.62	3.17
16	101.79	3.62	101.85	2.04
17	99.04	9.76	99.52	5.63
18	99.71	12.48	100.49	7.14
19	94.23	17.25	95.80	10.37
20	86.03	13.80	87.13	9.11
21	84.67	13.10	85.68	8.90
22	76.49	-0.61	76.50	-0.45

Table 5.4.1 Velocity values for the vectors shown in Fig. 5.4.1.

lation. Using this average density value, the pressure and temperature in this same region were then calculated in the manner explained in Chapter 3. Typical results for these calculations for two successive film frames are given in Figs. 5.5.1 and 5.5.2. Other results are given in the Appendix.

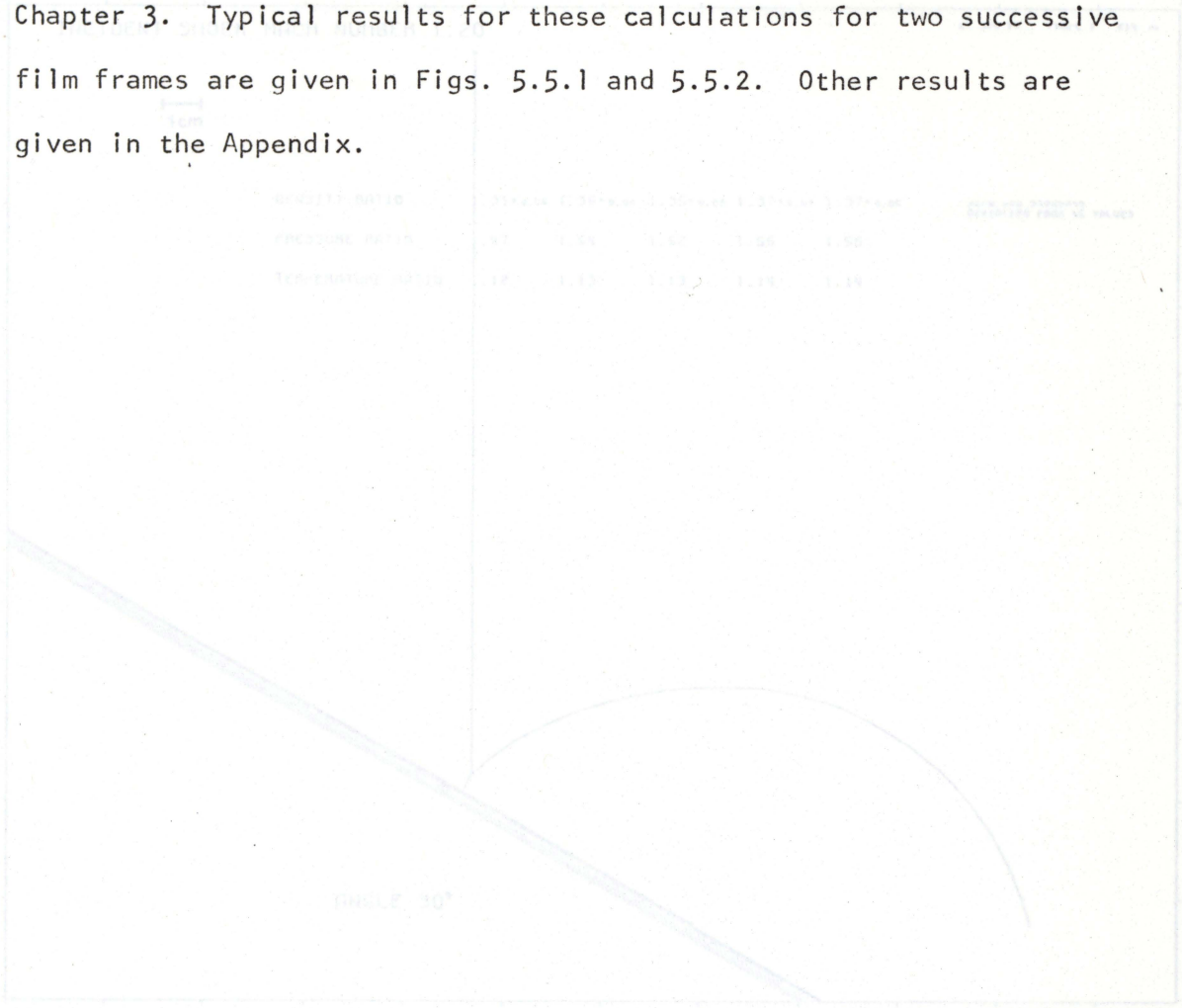

Fig. 5.5.1 Density, pressure, and temperature ratios behind a Mach 1.20 shock at 214 μs.

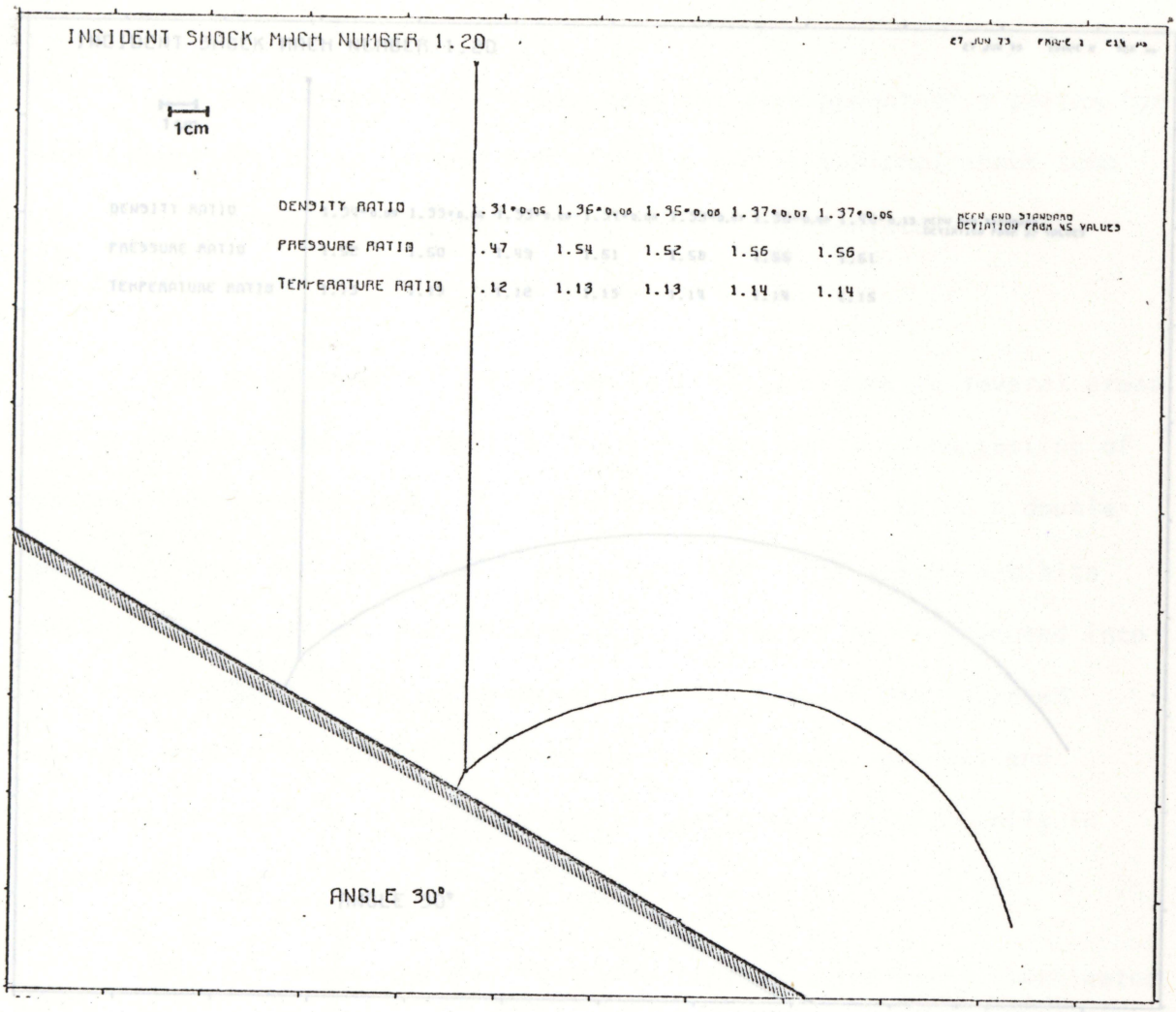

Fig. 5.5.1 Density, pressure, and temperature ratios behind a Mach 1.20 shock at 214 μs.

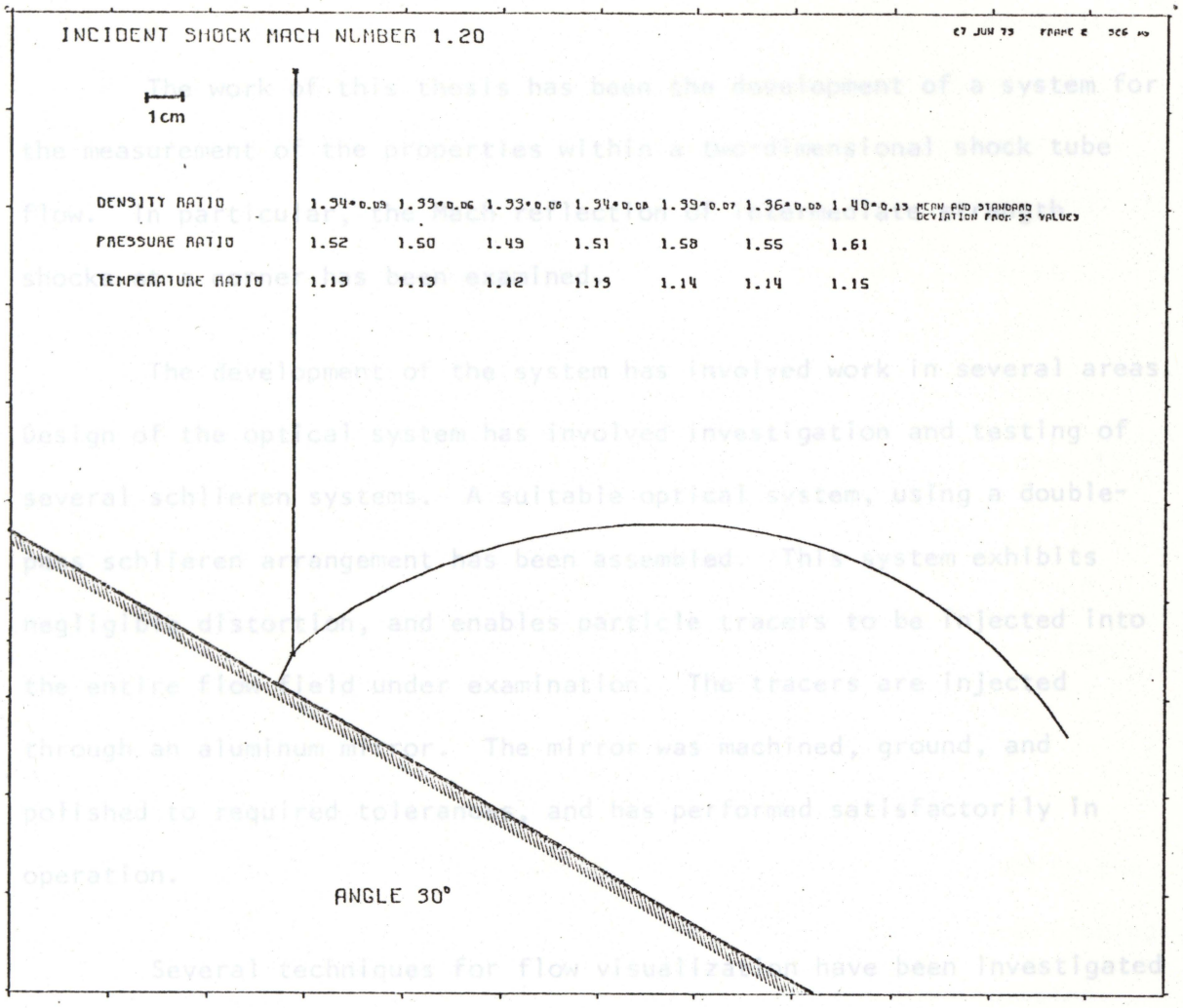

Fig. 5.5.2 Density, pressure, and temperature ratios behind a Mach 1.20 shock at 326 μs.

CHAPTER 6

DISCUSSION AND CONCLUSIONS

The work of this thesis has been the development of a system for the measurement of the properties within a two-dimensional shock tube flow. In particular, the Mach reflection of intermediate strength shocks at a corner has been examined.

The development of the system has involved work in several areas. Design of the optical system has involved investigation and testing of several schlieren systems. A suitable optical system, using a double-pass schlieren arrangement has been assembled. This system exhibits negligible distortion, and enables particle tracers to be injected into the entire flow field under examination. The tracers are injected through an aluminum mirror. The mirror was machined, ground, and polished to required tolerances, and has performed satisfactorily in operation.

Several techniques for flow visualization have been investigated and tested. The ammonium chloride tracers presently used have been shown to exhibit negligible inertia in flows involving intermediate strength shock waves. A system has been designed and built for the production of these tracers. The tracers, which are easily and cheaply produced, have been clearly visible on the photographic record. It would appear that in future work, both the size of the particles and the inter-particle spacing could be reduced considerably. This would increase the spatial resolution of the system.

The movement of the shocks and of the tracers is recorded simultaneously on a high speed film using a pulsed laser light source. Production of this light source has involved the building of an optical modulator, electronics to drive the modulator, and re-designing and aligning of the laser cavity components. The laser has performed reliably, and has been tested up to pulse repetition rates of 50,000 per second. The pulse width is typically 30 nanoseconds, which is approximately three hundred times less than that of a spark lamp. Variations in pulse intensity during a single laser firing have been observed, but these variations have not seriously affected the quality of the photographic record. The length of time for which pulses may be emitted is limited by the flashlamp pumping duration. This could be increased by the addition of further capacitors to the high voltage flashlamp supply unit. The laser now supplies pulses for a time approximately equal to the shock tube flow observation time.

The upper rate at which pictures may be taken is limited by the high speed camera to 11,000 full frames per second. This is approaching the upper capabilities of moving film cameras. Higher framing rates with the same camera could be obtained by reducing the frame size. This might, however, create problems with the film record when so much information is contained within such a small area. A rotating mirror camera and an image converter camera would both provide higher framing rates. Exposure time at higher framing rates would not be a limitation since shuttering in this system is provided by the laser light source itself.

In order to synchronize the various events taking place during an experiment, adjustable timing and delay circuits have been designed and built. Synchronization of laser, camera, and shock firing, for varying shock strengths and camera speeds, is routinely facilitated.

In order to analyse the large amount of data produced by the system, which for a single film frame approaches a thousand data points, semi-automated methods have been used. Digitization and computer analysis techniques have been developed to reduce the data, and produce plots of the properties within the flow field. As will be noted from Fig. 5.1.1 there are weak oblique shocks in the flow field. Attempts were made to eliminate these shocks by ensuring smooth joins between shock tube sections, between the shock tube windows and the wall of the shock tube, and between the wedge corner and the shock tube. These attempts to remove the weak oblique shocks were unsuccessful. The author has observed this type of weak oblique shock in schlieren photography taken by other workers using other shock tubes. It appears that the origin of these shocks may be at the diaphragm of the shock tube itself. However, the analysis carried through in this thesis gives the actual density field in the experimental flow, notwithstanding these oblique shocks.

The resolution of the technique depends on the size of the particle tracers, the inter-particle spacing, the accuracy of the recording system, and the accuracy of the analyser. The size of the particle tracers and the inter-particle spacing could both be decreased

with the manufacture of a new mirror. Also, the quality of the tracers could be improved with careful machining of the injector holes in the mirror. The recording system could be improved by the use of a larger format camera, and a more accurate and reliable digitizer could reduce the 2% error in area determination considerably. With these additions the technique would probably be capable of resolving 1% variations in density. At the present time, the density determination is accurate to within approximately 5%, and any conclusions about the detailed variations in density throughout the flow field would be premature.

From the plots showing the velocity vectors and successive positions of the shocks, the self-similarity of this type of flow has been confirmed. Clearly the parts of the reflected shock moving with and against the free stream are of different strengths. This is reflected in the magnitude of the velocity vectors behind these two portions of the reflected shock. As far as the author is aware this is the first time the velocity vectors have been mapped in this type of flow. The determination of the strength of the reflected shock along its entire length poses an interesting but complex problem.

It would appear that the system developed in this thesis could be a useful tool in the determination of particle velocity variation in various regions of the flow. Velocity variation across the slipstream would be of especial interest, but its determination was not attempted in the present work.

In summary, the system developed has recorded the motion of shock waves and particle tracers in the two-dimensional flow field created by the reflection of an intermediate strength shock, and the density field and particle velocity for several flows has been calculated. Improvements in the system could be made to increase the accuracy of the technique. The system also contains all the components theoretically necessary for the recording of motions in three dimensions. Using double pulses from the laser, holographic recording could be made. In this way, it might be possible to determine the properties within a three-dimensional flow.

REFERENCES

Bargmann, V., "On Nearly Glancing Reflection of Shocks", AMP Report 108.2R NDRC (1945)

Bleakney, W., "The Diffraction of Shock Waves Around Obstacles and the Transient Loading of Structures", Princeton University Department of Physics Technical Report II-3 (1950)

Bleakney, W. and A.H. Taub, "Interaction of Shock Waves", Reviews of Modern Physics 21 (1949) 584

Boys, C.V., "Photography of Flying Bullets", Photographic Journal, April 30,(1892)

Bradley, J.N., *Shock Waves in Chemistry and Physics* (John Wiley and Sons, Inc., New York, 1962)

Chisnell, R.F., "The Motion of a Shock Wave in a Channel, with Applications to Cylindrical and Spherical Shock Waves", Journal of Fluid Mechanics 2 (1957) 286

Cranz, C. and H. Schardin, "Kinematographic auf rukendem Film und mit extrem hoher Bildfrequenz", Zeitschrift Fur Physik, 56 (1929) 147

Dewey, J.M., "A Preliminary Investigation of the Use of Particle Trajectory Analysis for Studying the Interaction of a Shock Wave with a Structure", Ernst-Mach-Institut, Freiburg, Bericht Nr. 2 (1973)

Dewey, J.M., "The Properties of a Blast Wave Obtained from an Analysis of the Particle Trajectories", Proceedings of the Royal Society 324 (1971) 275

Dumitrescu, L.Z. and C. Popescu, "Experimental Studies of the Shock Reflection and Interaction in a Shock Tube", Shock Tubes--Proceedings of the Seventh International Shock Tube Symposium, University of Toronto Press (1970) 751

Fletcher, C.H., "The Mach Reflection of Weak Shock Waves", Princeton University Ph.D. thesis (1950)

Fletcher, C.H., A.H. Taub and W. Bleakney, "The Mach Reflection of Shock Waves at Nearly Glancing Incidence", Review of Modern Physics 23 (1951)

Fourney, M.E., "On the Application of a Laser to High Speed Photography", Ph.D. thesis California Institute of Technology, Pasadena, California (1963)

Gaydon, A.G. and I.R. Hurle, *The Shock Tube in High-Temperature Chemical Physics* (Chapman and Hall Ltd., London 1963)

Glasstone, S. and R.H. Lovberg, *Controlled Thermonuclear Reactions* (D. Van Nostrand Company, Inc., New Jersey, 1960)

Guderley, K.G., "Considerations of the Structure of Mixed Subsonic-Supersonic Flow Patterns", Wright Field Report F-TR-2168-ND (1947)

Gvozdeva, L.G., T.V. Bazhenova, O.A. Predvoditeleva and V.P. Fokeev, "Mach Reflection of Shock Waves in Real Gases", Astronautica Acta. 14 (1969) 503

Heilig, W., "Theoretische und Experimentelle Untersuchungen zur Beugung von Stobwellen an Kugeln und Zylindern", Ernst-Mach-Institut, Freiburg, Bericht Nr. 2/70 (1970)

Henderson, L.F., "The Refraction of a Plane Shock Wave at a Gas Interface", Journal of Fluid Mechnaics 26 (1966) 607

Hertzberg, A., "The Shock Tunnel and its Application to Hypersonic Flight", Cornell Aeronautical Lab. Report AD-1062-A-5 (1957)

Hoenig, S.A., "Acceleration of Dust Particles by Shock Waves", Journal of Applied Physics 28B (1957) 1218

Holsgrove, B.J. and R.A. Klymchuk, "Statically Oriented Smoke-Puff Grids", Suffield Technical Paper No. 352 (1970)

Holsgrove, B.J., R.A. Klymchuk and C.M. Myers, "Dynamically Oriented Smoke-Puff Grids", Suffield Technical Paper No. 360 (1971)

Hugoniot, H., Journal de l'Ecole Polytechnique, Paris 57 (1887) 1

Jahn, R.G., "Transition Processes in Shock Wave Interactions", Journal of Fluid Mechanics 2 (1956) 33

Jones, D.M., P. Moira, E. Martin and C.K. Thornhill, "A Note on the Pseudo-stationary Flow Behind a Strong Shock Diffracted or Reflected at a Corner", Proceedings of the Royal Society 209 (1951) 238

Kawamura, R. and H. Saito, "Reflection of Shock Waves-1 Pseudo-Stationary Case", Journal of the Physical Society of Japan 11 (1956)

Law, C.K., "Diffraction of Strong Shock Waves by a Sharp Compressive Corner", University of Toronto Institute for Aerospace Studies Technical Note No. 150 (1970)

Lean, G.H., "Report on Further Experiments on the Reflection of Inclined Shock Waves", National Physical Laboratory, London (1946)

Liepmann, H.W. and A. Roshko, *Elements of Gas Dynamics* (John Wiley and Sons, Inc., New York, 1957)

Lighthill, M.J., "The Diffraction of Blast. I", Proceedings of the Royal Society 198 (1949) 450

"The Diffraction of Blast. II", Proceedings of the Royal Society 200 (1950) 554

Ludloff, H.F. and M.B. Friedman, "Aerodynamics of Blasts--Diffraction of Blast Around Finite Corners", Journal of Aeronautical Sciences 22 (1955) 27

Mach, E., "Uber den Verlauf der Funkenwellen in der Ebene und im Raume", Vienna Academy Sitzungsberichte 78 (1878) 819

Male, D.H. and R.A. Chelsom, "Measurement of Peak Wall Pressure during Transition from Regular to Mach Reflection", Suffield Memorandum No. 130 (1968)

Mölder, S., "Head-on Interaction of Oblique Shock Waves", University of Toronto Institute of Aerophysics Technical Note No. 38 (1960)

Muirhead, J.C., "Smoke Streams as Tracers in Shock Tube Flows", Journal of Applied Physics 30 (1959) 789

Pack, D.C., "The Reflection and Diffraction of Shock Waves", Journal of Fluid Mechnaics 18 (1964) 549

Polacheck, H. and R.J. Seeger, "Regular Reflection of Shocks in Ideal Gases", Explosive Research Report No. 13, Navy Dept., Bureau of Ordnance Re2c, Washington, D.C. (1943)

Prasse, H.G., "Eine analytische Beschreibung der Ausbreitung des Reflektierten Stobes bei der Mach schen Reflexion an Keilen", Ernst-Mach-Institut, Freiburg, No. 4 (1972)

Prescott, R. and E.L. Gayhart, "A Method of Correction of Astigmatism in Schlieren Systems", Aeronautical Journal 18 (1951) 69

Rankine, R.J.M., "On the Thermodynamics Theory of Waves of Finite Longitudinal Disturbance", Philosophical Transactions of the Royal Society of London 160 (1870) 277

Rowlands, R.E., "A Sequentially Modulated Ruby Laser System for Transmitted and Scattered Light Dynamic Photoelasticity", Theoretical and Applied Mechanics Report, University of Illinois (1967)

Rudinger, G. and L.M. Somers, "Behaviour of Small Regions of Different Gases Carried in Accelerated Gas Flows", Journal of Fluid Mechanics 7 (1960) 161

Sakurai, A., "On the Problem of Weak Mach Reflection", MRC Technical Summary Report 460, Mathematics Research Centre, United States Army, Universtiy of Wisconsin (1964)

Scott, W.C. and M. de Wit, "Efficient Variable Threshold Acousto-optic Q-Switching of Flash Pumped Md:YAG Applied Physics Letters 20 (1972) 141

Shirley, B.V. and J.W. Sheldon, Particle Charging Behind Shock Waves in Suspensions", AIAA Journal 10 (1972) 1110

Skews, B.W., "Shock-Shock Reflection", Canadian Aerospace and Science Institute Transactions 4 (1971)

Smith, L.G., "Photographic Investigation of the Reflection of Plane Shocks in Air", Office of Scientific Research and Development No. 6271 (1945)

Smith, W.R., "Mutual Reflection of Two Waves of Arbitrary Strengths", The Physics of Fluids 2 (1959)

Smith, W.R., "Four-Shock Configuration", The Physics of Fluids 5 (1962)

Sternberg, J., "Triple-Shock-Wave Intersections", The Physics of Fluids 2 (1959)

Strehlow, R.A. and A. Cohen, "Initiation of Detonation", Physics of Fluids 5 (1962) 97

Ter-Minassiants, S.M., "The Diffraction Accompanying the Regular Reflection of a Plane Obliquely Impinging Shock Wave from the Walls of an Obtuse Wedge", Journal of Fluid Mechanics 35 (1969) 391

Ting, L. and H.F. Ludloff, "Aerodynamics of Blasts", Journal of Aeronautical Science 18 (1950) 143

Töepler, A., "Beobachtungen nach einer neuen optischen Methods", Poggendorf's Ann. d. Phys. u. Chem. 127 (1866) 556

Vieille, P., "Sur les Discontinuites Produites par la Detente Brusque de Gaz Comprimes", original in Comptes Rendus de l'Academie des Sciences 129 (1899) 1228 [re-appeared along with translation in Shock Tubes--Proceedings of the Seventh International Shock Tube Symposium 1969 ed. I.I. Glass, University of Toronto Press (1970)]

vom Stein, H.D. and H.J. Pfeifer, "Investigation of the Velocity Relaxation of Micron-Sized Particles in Shock Waves Using Laser Radiation", Applied Optics 11 (1972) 305

Von Neumann, J., "Oblique Reflection of Shocks", Explosive Research Report No. 12, Navy Department Bureau of Ordnance, Washington, D.C. (1943) [re-appears along with other articles on shock interaction in John von Neumann Collected Works Volume VI, Pergamon Press (1963)]

Von Neumann, J. and R.D. Richtmyer, "A Method for the Numerical Calculation of Hydrodynamic Shocks", Journal of Applied Physics 21 (1950) 232

Walker, D.K., "Particle Trajectory Analysis of a Two-dimensional Shock Tube Flow", M.Sc. thesis, University of Victoria (1970)

Warner, J., "Simulation of a Double 45° z-cut KD*P, Electro-optic Q-Switch by Desk-top computer", Optics and Laser Technology, November (1971) 215

Wentz, J.D., "Novel Laser Q-Switching Mechanism", IEEE Proceedings 52 (1964) 716

White, D.R., "An Experimental Survey of the Mach Reflection of Shock Waves", Princeton University Ph.D. thesis (1951)

Whitham, G.B., "A New Approach to Problems of Shock Dynamics--Part 1 Two-dimensional Problems", Journal of Fluid Mechanics 2 (1957) 145

Whitham, G.B., " New Approach to Problems of Shock Dynamics--Part 2 Three-dimensional Problems", Journal of Fluid Mechanics 5 (1959) 369

Whitten, B.T., "Calibration of a Shock Tube by Analysis of the Particle Trajectories", M.Sc. thesis University of Victoria (1969)

Yagla, J.J., "Machine Calculation of Unsteady Mach Reflections and Prandtl-Meyer Supersonic Flows", Naval Weapons Laboratory Technical Report (1973)

APPENDIX

This appendix contains the results of particle trajectory analysis for four different cases of Mach reflection:

1. incident shock Mach number 1.34, wedge angle 30°;
2. incident shock Mach number 1.35, wedge angle 10°;
3. incident shock Mach number 1.21, wedge angle 10°;
4. incident shock Mach number 1.20, wedge angle 30°.

For each of the four flows, the positions of the particle tracers are given for each film frame, and on the facing page, the density values corresponding to each quadrilateral formed by four tracers are given in a table. For each flow, a velocity vector plot for successive film frames is given, and a table of velocity values is given on the facing page. Finally, for each film frame, mean density, pressure, and temperature ratios calculated as explained in Section 5.5 are given.

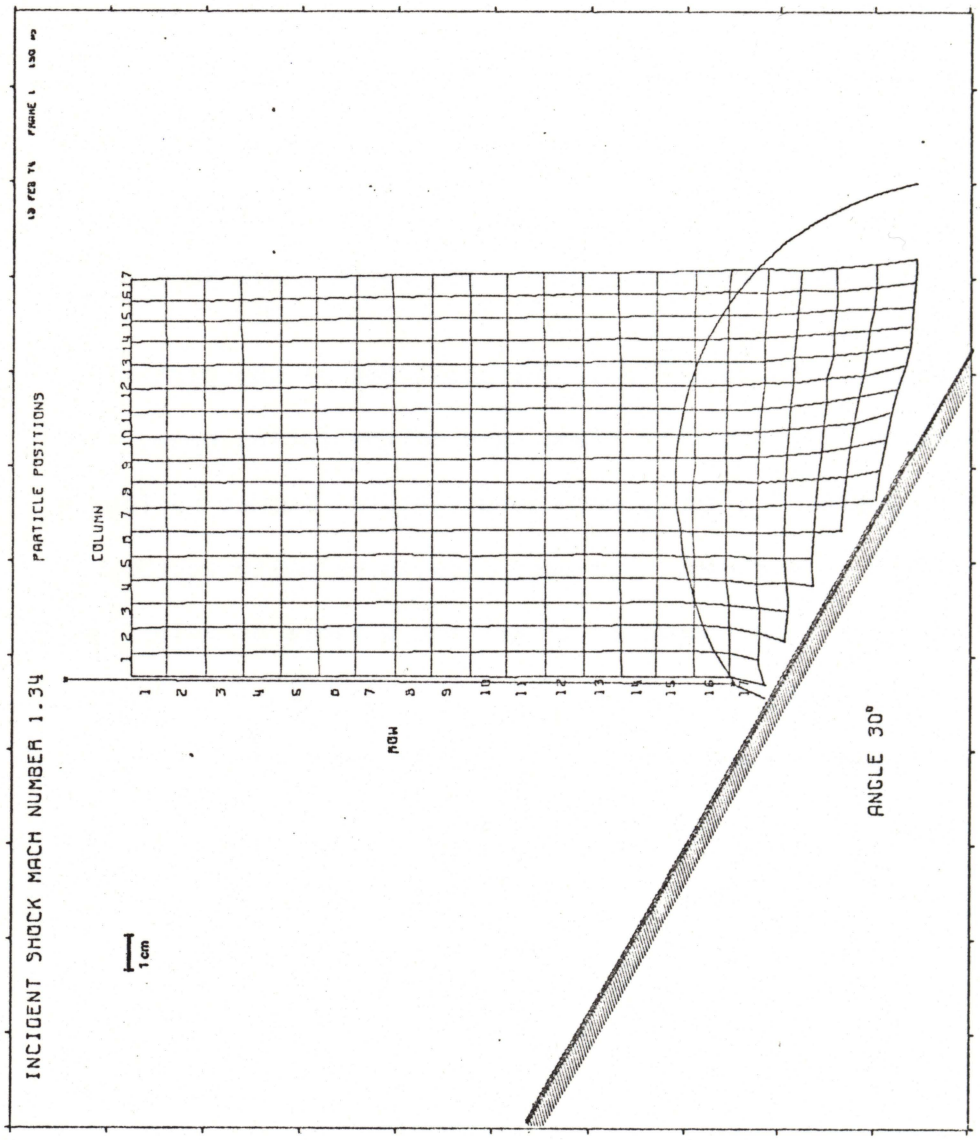

Fig. A.1.1 Tracers at 190 μs.

	COLUMN																
	1	2	3	5	5	6	7	8	9	10	11	12	13	14	15	16	17
1	1.66	1.53	1.63	1.66	1.66	1.56	1.67	1.53	1.81	1.62	1.53	1.71	1.71	1.60	1.93	2.04	1.83
2	1.56	1.44	1.51	1.60	1.56	1.51	1.57	1.43	1.70	1.53	1.49	1.69	1.63	1.55	1.90	1.89	1.66
3	1.53	1.39	1.50	1.56	1.59	1.57	1.60	1.45	1.67	1.52	1.42	1.60	1.50	1.55	1.78	1.75	1.67
4	1.52	1.49	1.64	1.60	1.62	1.54	1.57	1.43	1.67	1.60	1.50	1.63	1.60	1.60	1.75	1.74	1.68
5	1.51	1.48	1.56	1.56	1.61	1.57	1.58	1.51	1.67	1.58	1.54	1.66	1.72	1.67	1.87	1.83	1.84
6	1.60	1.49	1.60	1.60	1.57	1.54	1.52	1.49	1.60	1.50	1.40	1.54	1.58	1.46	1.58	1.65	1.64
7	1.46	1.35	1.59	1.56	1.45	1.46	1.54	1.45	1.60	1.50	1.43	1.61	1.68	1.65	1.69	1.78	1.83
8	1.59	1.46	1.67	1.66	1.63	1.66	1.72	1.49	1.68	1.55	1.48	1.62	1.65	1.62	1.69	1.70	1.69
9	1.48	1.41	1.57	1.57	1.55	1.41	1.58	1.44	1.61	1.50	1.42	1.57	1.61	1.55	1.63	1.68	1.72
10	1.55	1.49	1.64	1.65	1.67	1.50	1.70	1.51	1.65	1.60	1.52	1.71	1.75	1.69	1.73	1.84	1.77
11	1.41	1.41	1.57	1.53	1.58	1.49	1.64	1.48	1.54	1.50	1.42	1.59	1.59	1.62	1.61	1.70	1.66
12	1.48	1.45	1.62	1.55	1.61	1.53	1.61	1.50	1.60	1.53	1.51	1.66	1.60	1.75	1.65	1.70	1.68
13	1.50	1.46	1.65	1.55	1.64	1.58	1.64	1.49	1.57	1.56	1.49	1.65	1.53	1.64	1.61	1.69	1.81
14	1.60	1.51	1.71	1.65	1.72	1.59	1.72	1.54	1.61	1.62	1.48	1.70	1.62	1.77	1.71	1.73	1.69
15	1.40	1.40	1.64	1.58	1.63	1.48	1.61	1.57	1.53	1.56	1.45	1.56	1.48	1.65	1.57	1.66	1.60
16	1.56	1.54	1.81	1.80	1.94	1.78	1.70	1.65	1.74	1.85	1.73	1.66	1.73	1.79	1.63	1.70	1.73
17	1.81	1.84	1.85	1.80	1.80	1.82	1.69	1.84	1.80	1.71	1.82	1.58	1.71	1.67	1.68	1.69	1.65
18			1.74	1.78	1.92	1.91	1.75	1.87	1.76	1.74	1.83	1.79	1.85	1.84	1.82	1.81	1.81
19					1.94	1.89	1.79	1.91	1.71	1.66	1.82	1.80	1.79	1.76	1.76	1.86	1.82
20							1.71	1.77	1.62	1.73	1.65	1.63	1.65	1.69	1.61	1.71	1.47
21								1.65	1.48	1.66	1.69	1.72	1.70	1.63	1.77	1.65	1.58

FEB 19 1974

Table A.1.1 Density values for Fig. A.1.1.

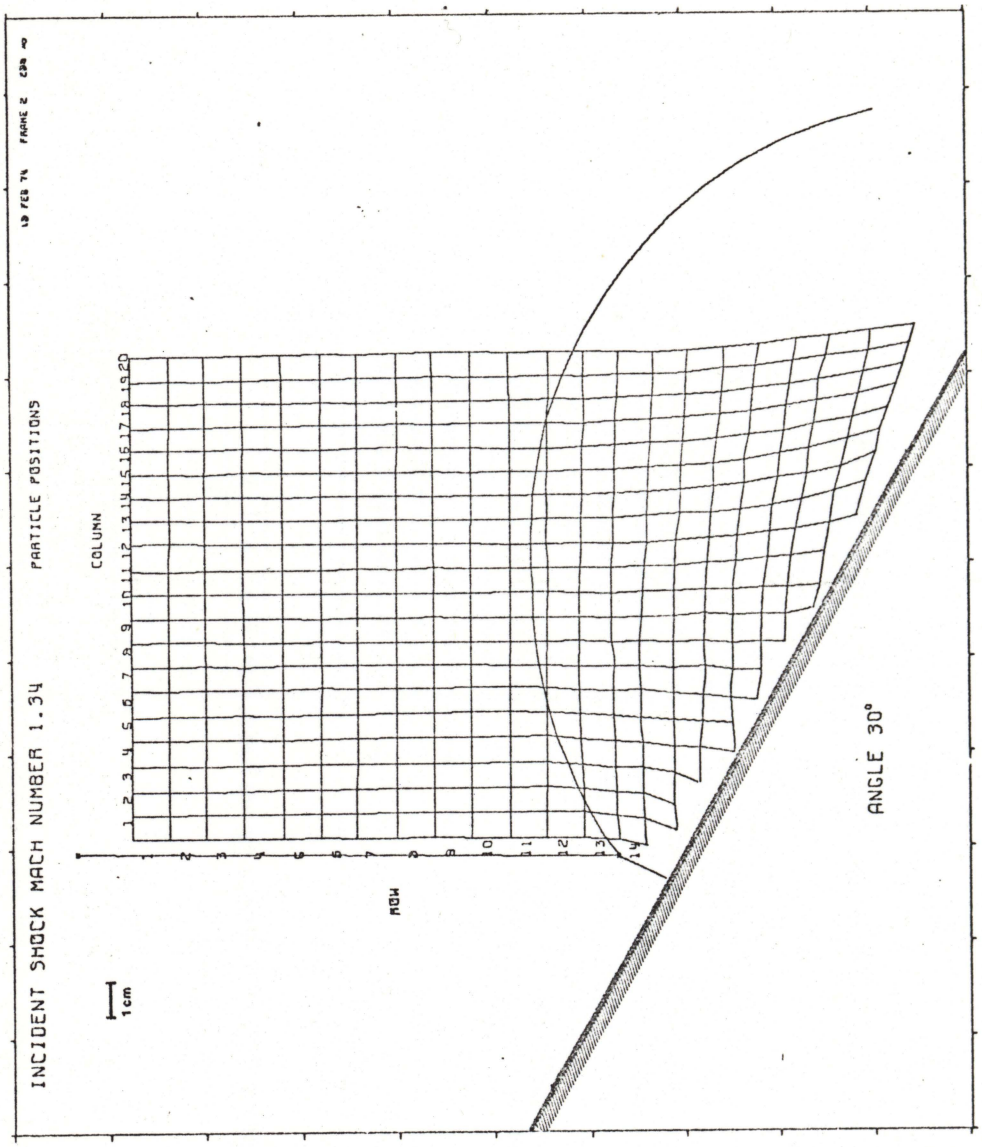

Fig. A.1.2 Tracers at 289 μs.

	COLUMN																			
	1	2	3	5	5	6	7	8	9	10	11	12	13	14	15	16	17	18	19	20
1	1.62	1.63	1.41	1.44	1.56	1.42	1.58	1.55	1.59	1.54	1.61	1.35	1.57	1.66	1.54	1.53	1.64	1.55	1.58	1.43
2	1.64	1.67	1.51	1.53	1.65	1.49	1.58	1.59	1.70	1.61	1.69	1.42	1.70	1.71	1.68	1.61	1.75	1.64	1.74	1.59
3	1.54	1.63	1.43	1.40	1.54	1.41	1.59	1.54	1.61	1.54	1.61	1.41	1.61	1.62	1.57	1.49	1.68	1.65	1.75	1.50
4	1.48	1.53	1.44	1.42	1.49	1.40	1.58	1.58	1.48	1.44	1.51	1.37	1.52	1.50	1.41	1.52	1.57	1.57	1.45	1.39
5	1.52	1.56	1.46	1.41	1.45	1.34	1.52	1.57	1.56	1.48	1.54	1.41	1.55	1.52	1.48	1.56	1.47	1.55	1.50	1.46
6	1.60	1.65	1.60	1.57	1.64	1.57	1.69	1.67	1.69	1.60	1.67	1.56	1.67	1.67	1.69	1.64	1.63	1.75	1.67	1.57
7	1.38	1.41	1.36	1.37	1.43	1.37	1.47	1.54	1.47	1.43	1.43	1.37	1.47	1.46	1.48	1.37	1.48	1.60	1.45	1.51
8	1.50	1.58	1.52	1.51	1.59	1.52	1.69	1.72	1.60	1.59	1.54	1.55	1.65	1.67	1.65	1.62	1.67	1.76	1.58	1.57
9	1.53	1.60	1.51	1.45	1.51	1.51	1.68	1.64	1.57	1.55	1.51	1.59	1.56	1.53	1.56	1.56	1.48	1.60	1.52	1.53
10	1.46	1.50	1.47	1.42	1.44	1.41	1.64	1.59	1.51	1.43	1.51	1.49	1.48	1.53	1.52	1.52	1.41	1.58	1.49	1.46
11	1.47	1.48	1.51	1.41	1.53	1.48	1.68	1.58	1.53	1.44	1.54	1.61	1.54	1.59	1.58	1.61	1.45	1.58	1.51	1.49
12	1.49	1.61	1.65	1.58	1.78	1.80	1.99	1.92	1.96	1.86	1.94	1.80	1.68	1.78	1.72	1.88	1.62	1.63	1.75	1.66
13	1.70	1.93	1.88	1.67	1.71	1.79	1.70	1.67	1.85	1.75	1.68	1.77	1.69	1.72	1.70	1.72	1.75	1.83	1.73	1.66
14	1.96	2.02	1.92	1.88	1.92	1.87	2.15	2.16	2.05	1.93	1.79	1.84	1.64	1.79	1.79	1.72	1.74	1.74	1.81	1.80
15		1.91	1.56	1.80	1.67	1.61	1.75	1.61	1.60	1.65	1.68	1.82	1.56	1.67	1.65	1.64	1.64	1.68	1.84	1.80
16				1.82	1.90	1.80	1.60	1.72	1.77	1.90	1.75	1.76	1.76	1.83	1.89	1.80	1.72	1.85	1.69	1.76
17					1.52	1.84	1.72	1.90	1.67	1.90	1.69	1.80	1.76	1.64	1.87	1.83	1.73	1.84	1.80	1.89
18							1.79	1.82	1.84	1.90	1.68	1.83	1.79	1.71	1.83	1.77	1.78	1.87	1.82	1.80
19									1.97	1.95	1.79	1.99	1.73	1.66	1.84	1.95	1.79	2.03	1.86	1.92
20										2.00	1.44	1.63	1.55	1.84	1.57	1.71	1.63	1.58	1.58	1.72
21													1.42	1.57	1.67	1.85	1.62	1.65	1.67	1.63

FEB 18 1974 z

Table A.1.2 Density values for Fig. A.1.2.

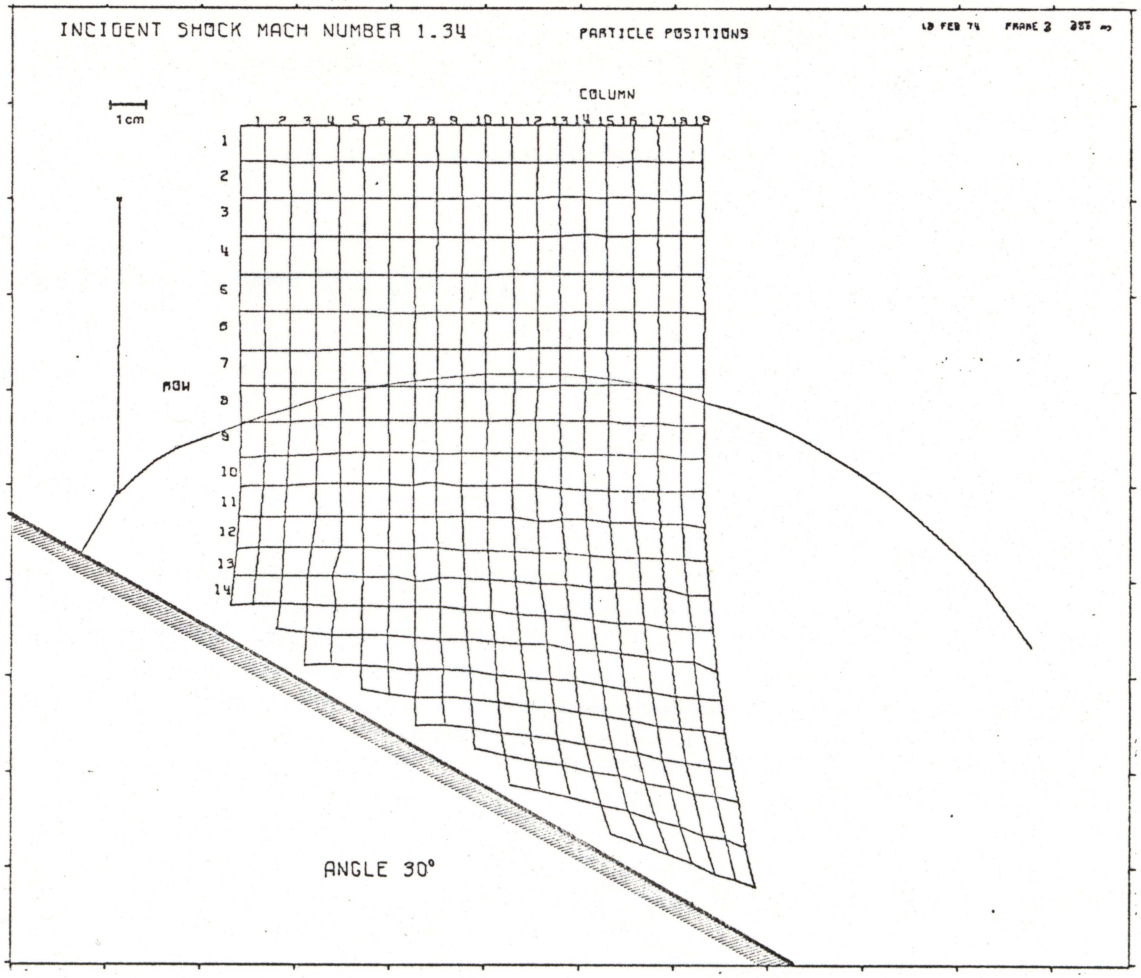

Fig. A.1.3 Tracers at 387 μs.

	COLUMN																		
	1	2	3	5	5	6	7	8	9	10	11	12	13	14	15	16	17	18	19
1	1.62	1.49	1.56	1.57	1.52	1.56	1.58	1.63	1.61	1.51	1.48	1.46	1.72	1.63	1.71	1.43	1.57	1.76	1.68
2	1.59	1.51	1.63	1.53	1.51	1.47	1.56	1.65	1.58	1.57	1.49	1.48	1.75	1.66	1.76	1.42	1.53	1.75	1.73
3	1.46	1.40	1.46	1.46	1.44	1.42	1.51	1.55	1.42	1.61	1.43	1.49	1.66	1.53	1.66	1.35	1.49	1.62	1.70
4	1.48	1.49	1.45	1.51	1.46	1.54	1.53	1.59	1.45	1.61	1.35	1.53	1.67	1.45	1.65	1.39	1.40	1.61	1.68
5	1.50	1.52	1.50	1.55	1.52	1.48	1.40	1.66	1.51	1.56	1.32	1.52	1.62	1.45	1.70	1.43	1.50	1.64	1.55
6	1.47	1.43	1.38	1.51	1.56	1.52	1.50	1.60	1.57	1.58	1.38	1.59	1.80	1.57	1.72	1.39	1.60	1.71	1.71
7	1.59	1.56	1.55	1.64	1.63	1.59	1.50	1.65	1.61	1.61	1.32	1.55	1.83	1.48	1.68	1.45	1.55	1.64	1.68
8	1.57	1.51	1.55	1.73	1.78	1.75	1.59	1.90	1.66	1.73	1.55	1.80	1.80	1.60	1.67	1.46	1.61	1.64	1.56
9	1.71	1.81	1.57	1.81	1.77	1.73	1.72	1.76	1.64	1.75	1.77	1.79	1.70	1.72	1.61	1.56	1.82	1.71	1.84
10	1.92	1.90	1.52	1.91	1.87	1.67	1.82	1.92	1.87	1.63	1.67	1.84	1.72	1.71	1.69	1.53	1.63	1.73	1.91
11	1.97	1.92	1.51	1.76	2.00	1.60	1.79	1.86	1.71	1.78	1.75	1.66	1.65	1.86	1.83	1.75	1.65	1.89	1.85
12	2.04	1.86	1.46	1.62	2.09	1.75	1.80	1.87	1.70	1.76	1.67	1.85	1.74	1.70	1.72	1.69	1.73	1.91	1.88
13	2.32	1.93	1.86	1.79	1.76	1.80	1.74	1.79	1.86	1.86	1.69	1.77	1.64	1.69	1.78	1.69	1.84	1.79	1.69
14	2.16	1.90	1.96	1.86	1.77	1.86	1.98	2.09	1.97	1.88	1.82	1.82	1.86	1.90	1.74	1.70	1.73	1.72	1.99
15			1.68	1.68	1.64	1.71	1.65	1.63	1.65	1.60	1.66	1.70	1.68	1.77	1.78	1.61	1.69	1.72	1.69
16				1.82	1.65	1.80	1.62	1.82	1.86	1.75	1.71	1.70	1.82	1.82	1.87	1.61	1.79	1.89	2.11
17						1.86	1.75	1.89	1.72	1.78	1.63	1.80	1.80	1.60	1.85	1.57	1.75	1.88	1.83
18								1.79	1.86	1.94	1.72	1.93	1.85	1.77	1.91	1.87	1.92	1.85	1.90
19										2.03	1.83	1.87	1.77	1.83	1.84	1.86	1.94	1.83	1.93
20											1.77	1.74	1.61	1.72	1.68	1.70	1.71	1.64	1.64
21														1.57	1.63	1.73	1.70	1.65	1.84

FEB 18 1974

Table A.1.3 Density values for Fig. A.1.3.

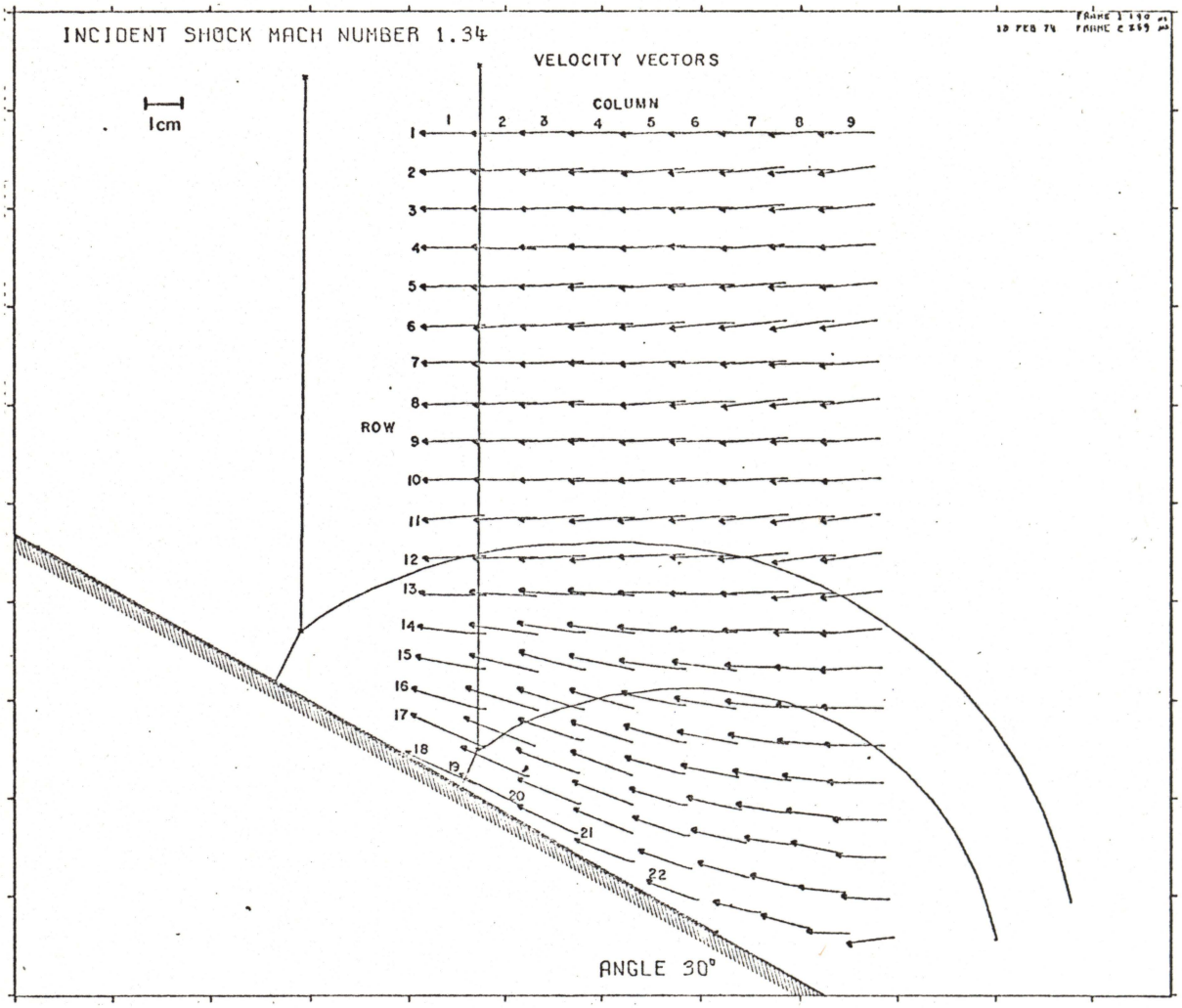

Fig. A.1.4 Velocity vectors 190 - 289 μs.

COLUMN 1 — FRAME 1 - 2

ROW	U(M/S)	V(M/S)	VEL	ANGLE
1	163.44	-1.59	163.45	-0.56
2	162.41	-7.66	162.59	-2.70
3	161.99	0.15	161.99	0.05
4	160.87	0.01	160.87	0.00
5	163.08	-2.97	163.11	-1.04
6	162.02	-5.80	162.12	-2.05
7	160.83	-2.97	160.85	-1.02
8	159.77	-4.89	159.85	-1.75
9	159.45	-5.23	159.54	-1.88
10	159.10	-1.49	159.11	-0.54
11	156.49	-10.85	156.86	-3.97
12	157.77	-7.12	157.93	-2.58
13	167.06	6.61	167.19	2.26
14	173.92	18.66	174.92	6.12
15	178.26	32.34	181.17	10.28
16	189.85	55.09	197.69	16.18
17	189.89	82.60	207.08	23.51
18	182.28	83.06	200.31	24.50

COLUMN 4 — FRAME 1 - 2

ROW	U(M/S)	V(M/S)	VEL	ANGLE
1	156.07	-5.33	156.16	-1.93
2	159.43	-7.29	159.60	-2.62
3	159.14	-1.90	159.05	-0.69
4	158.73	-1.44	158.73	-0.52
5	160.17	-7.49	160.35	-2.68
6	160.75	-11.91	161.19	-4.24
7	161.13	-3.26	161.16	-1.16
8	164.92	-1.94	164.93	-0.68
9	163.85	-6.36	163.97	-2.22
10	164.35	-4.27	164.40	-1.49
11	164.17	-12.79	164.67	-4.45
12	161.45	-14.81	162.13	-5.24
13	165.65	9.47	165.92	3.27
14	169.26	19.83	170.41	6.68
15	164.60	33.34	167.94	11.45
16	160.86	43.59	166.66	15.16
17	155.47	50.57	163.49	18.02
18	153.36	56.80	163.54	20.32
19	149.68	55.64	159.69	20.39
20	148.35	60.27	160.13	22.11
21	148.80	56.72	159.24	20.86

COLUMN 7 — FRAME 1 - 2

ROW	U(M/S)	V(M/S)	VEL	ANGLE
1	156.92	-4.91	156.00	-1.80
2	156.57	-15.05	157.29	-5.48
3	155.40	-12.13	155.87	-4.46
4	152.64	-10.90	153.02	-4.08
5	158.90	-12.79	159.42	-4.60
6	162.78	-18.86	163.86	-6.60
7	159.07	-9.40	159.34	-3.38
8	158.93	-19.58	160.13	-7.02
9	164.25	-13.29	164.78	-4.62
10	163.89	-8.74	164.12	-3.05
11	160.97	-16.38	167.77	-5.58
12	168.30	-15.89	169.25	-5.38
13	164.53	-4.84	164.60	-1.69
14	159.25	-1.18	159.25	-0.42
15	153.07	6.57	153.21	2.45
16	152.63	15.21	153.39	5.69
17	145.62	22.95	147.41	8.97
18	140.33	24.95	142.53	10.09
19	134.25	22.91	136.19	9.69
20	126.53	18.33	127.85	8.24
21	118.72	27.61	121.89	13.06
22	116.67	31.17	120.76	14.98

COLUMN 2 — FRAME 1 - 2

ROW	U(M/S)	V(M/S)	VEL	ANGLE
1	157.31	-4.00	157.36	-1.46
2	161.95	-8.36	162.17	-2.95
3	159.08	-0.57	159.08	-0.21
4	161.19	2.37	161.21	0.84
5	161.86	-7.77	162.05	-2.75
6	156.75	-13.11	157.30	-4.78
7	164.48	-5.16	164.56	-1.80
8	162.62	-8.82	162.86	-3.11
9	162.29	-7.52	162.46	-2.65
10	158.66	-3.83	158.71	-1.38
11	160.10	-10.70	160.46	-3.82
12	164.67	-7.71	164.85	-2.68
13	170.66	7.61	170.83	2.55
14	175.83	21.24	176.31	6.92
15	174.39	39.72	178.86	12.83
16	186.11	54.31	193.87	16.27
17	182.28	68.70	194.80	20.55
18	173.64	75.71	189.43	23.59
19	158.48	79.41	177.26	26.61

COLUMN 5 — FRAME 1 - 2

ROW	U(M/S)	V(M/S)	VEL	ANGLE
1	156.82	-6.86	156.97	-2.51
2	153.35	-13.80	153.97	-5.14
3	157.02	-6.72	157.17	-2.45
4	157.54	-7.06	157.70	-2.56
5	160.56	-9.81	160.86	-3.50
6	158.69	-13.45	159.26	-4.84
7	159.09	-6.43	159.22	-2.31
8	160.51	-10.86	160.98	-3.87
9	162.63	-9.52	162.91	-3.35
10	163.10	-5.78	163.20	-2.03
11	164.56	-13.44	165.10	-4.67
12	163.31	-5.63	163.40	-1.97
13	164.54	-0.23	164.54	-0.08
14	164.84	12.53	165.32	4.35
15	164.35	22.01	165.82	7.63
16	155.66	32.13	158.96	11.68
17	152.69	43.25	158.76	15.82
18	144.96	42.04	150.93	16.17
19	139.63	42.45	145.95	16.91
20	137.47	48.66	145.83	19.49
21	129.75	45.75	137.54	19.42
22	125.16	48.98	134.26	21.21

COLUMN 8 — FRAME 1 - 2

ROW	U(M/S)	V(M/S)	VEL	ANGLE
1	157.20	-10.46	157.55	-3.81
2	161.84	-13.18	162.33	-4.66
3	157.42	-11.95	157.87	-4.34
4	157.32	-4.11	157.87	-1.49
5	160.06	-9.33	160.33	-3.34
6	158.33	-23.61	160.08	-8.49
7	161.06	-6.75	161.20	-2.40
8	158.43	-14.50	159.09	-5.21
9	153.02	-8.31	158.24	-3.01
10	161.00	-7.80	161.19	-2.77
11	158.42	-19.62	159.63	-7.06
12	157.35	-22.45	158.94	-8.12
13	156.55	-17.06	157.87	-6.20
14	158.88	-4.31	158.93	-1.55
15	151.90	2.62	151.92	0.99
16	148.26	6.31	148.40	2.44
17	147.05	10.04	147.39	3.90
18	137.64	14.44	138.40	5.97
19	133.98	15.66	134.90	6.57
20	126.10	25.82	128.71	11.57
21	115.38	11.33	115.94	5.61
22	104.54	6.62	104.75	3.62

COLUMN 3 — FRAME 1 - 2

ROW	U(M/S)	V(M/S)	VEL	ANGLE
1	156.86	-4.67	156.93	-1.71
2	158.26	-9.08	158.52	-3.28
3	157.88	-4.53	157.95	-1.64
4	162.46	-2.35	162.47	-0.83
5	162.25	-8.42	162.47	-2.97
6	161.17	-10.43	161.51	-3.70
7	161.62	-6.67	161.76	-2.35
8	163.02	-9.45	163.30	-3.32
9	162.69	-8.16	162.89	-2.87
10	164.79	-4.39	164.85	-1.53
11	165.38	-9.62	165.66	-3.33
12	167.54	-9.14	167.79	-3.12
13	166.90	10.15	167.21	3.48
14	171.26	24.62	173.02	8.18
15	169.77	44.72	175.56	14.76
16	163.55	51.73	176.31	17.06
17	154.85	53.86	173.43	18.09
18	160.33	54.46	170.65	20.03
19	152.02	64.67	171.36	21.88
20	153.58	71.73	169.50	25.04

COLUMN 6 — FRAME 1 - 2

ROW	U(M/S)	V(M/S)	VEL	ANGLE
1	153.95	-7.54	154.14	-2.80
2	157.80	-11.91	158.25	-4.32
3	153.36	-9.56	153.68	-3.68
4	155.40	-2.01	155.41	-0.74
5	159.32	-10.47	159.66	-3.75
6	157.49	-17.40	158.44	-6.30
7	158.48	-7.90	159.08	-2.84
8	159.29	-13.16	159.83	-4.72
9	161.33	-6.93	161.48	-2.46
10	161.07	-8.92	161.32	-3.17
11	162.49	-14.90	163.18	-5.26
12	162.88	-7.13	163.04	-2.51
13	163.31	-2.55	163.33	-0.90
14	159.59	5.23	159.68	1.88
15	154.96	19.94	156.18	7.19
16	149.65	24.84	151.70	9.43
17	145.16	26.60	147.63	10.56
18	139.05	27.30	141.70	11.11
19	132.07	29.20	135.28	12.51
20	132.45	30.59	135.94	13.00
21	123.00	34.99	127.88	15.85
22	109.61	26.92	112.87	13.60

COLUMN 9 — FRAME 1 - 2

ROW	U(M/S)	V(M/S)	VEL	ANGLE
1	137.96	-7.26	138.15	-3.01
2	134.63	-19.03	136.93	-7.82
3	139.06	-14.46	139.81	-5.93
4	139.49	-8.27	139.73	-3.39
5	140.88	-11.88	141.38	-4.82
6	142.33	-19.57	143.66	-7.83
7	140.81	-10.87	147.21	-4.23
8	145.75	-15.32	146.56	-6.00
9	146.18	-9.94	146.52	-3.89
10	140.69	-8.65	140.94	-3.58
11	147.35	-18.79	148.54	-7.27
12	149.53	-20.75	150.95	-7.90
13	153.23	-16.13	154.08	-6.01
14	134.00	-13.17	135.05	-4.87
15	135.71	-0.12	135.83	-2.25
16	153.64	2.47	153.66	0.92
17	157.05	2.06	150.06	0.78
18	138.27	3.18	138.31	1.32
19	131.41	1.06	131.42	0.46
20	122.84	6.31	123.00	2.94
21	110.26	6.64	110.45	3.14
22	117.68	-16.71	118.86	-8.08

Table A.1.4 Velocity values for Fig. A.1.4.

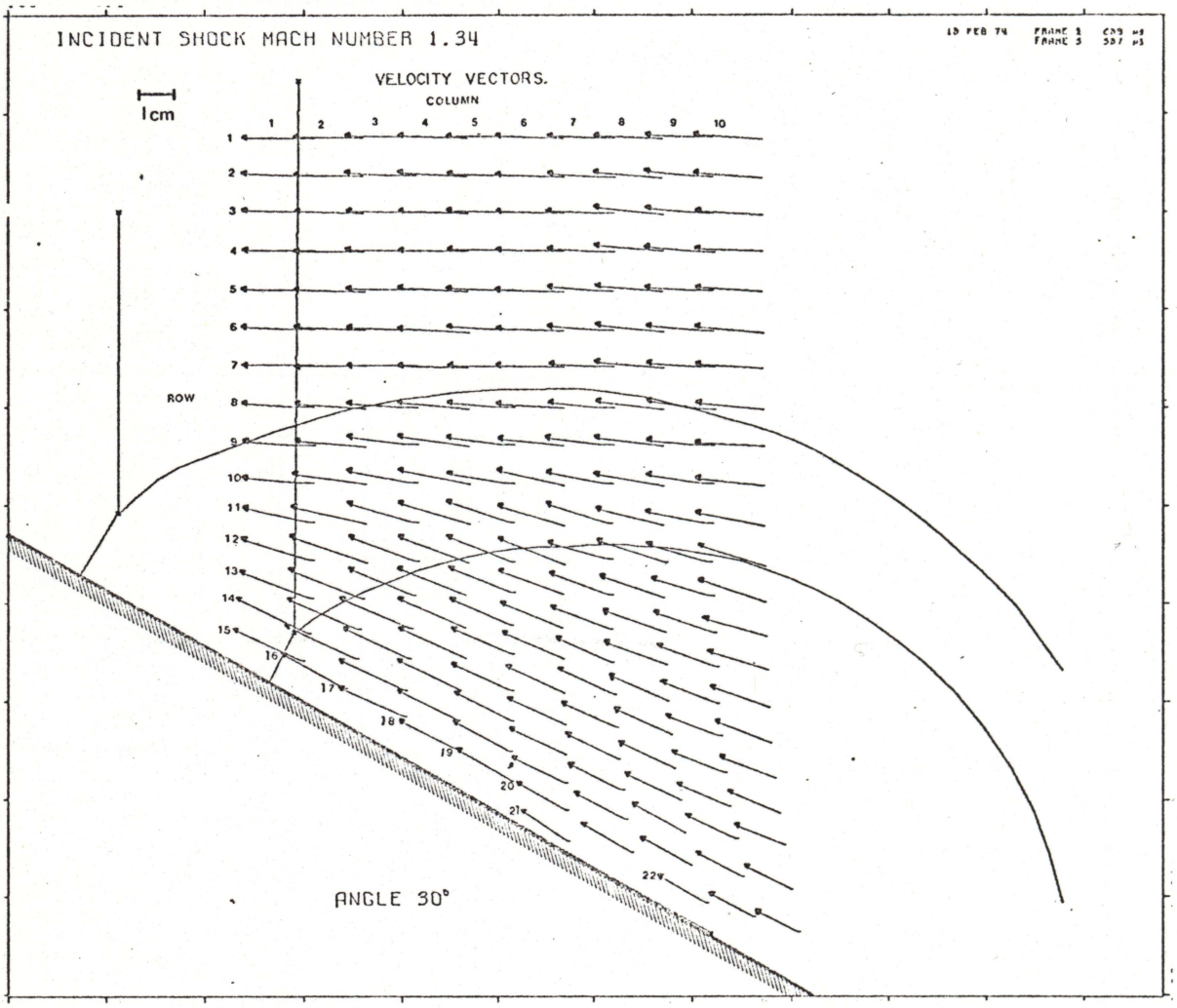

Fig. A.1.5 Velocity vectors 289 - 387 μs.

COLUMN 1 — FRAME 2 - 3

ROW	U(M/S)	V(M/S)	VEL	ANGLE
1	180.06	0.66	180.06	0.21
2	181.44	8.36	181.63	2.64
3	178.91	6.20	179.01	1.98
4	179.42	3.28	179.55	1.05
5	180.29	5.28	180.36	1.68
6	182.56	8.11	182.74	2.54
7	178.43	0.20	178.45	0.37
8	178.38	12.00	179.38	3.84
9	179.64	13.98	180.19	4.45
10	178.65	16.74	179.43	5.35
11	178.15	39.92	182.57	12.63
12	182.63	58.27	191.70	17.69
13	185.58	70.06	198.36	20.68
14	186.70	93.22	208.68	26.53
15	178.55	83.53	197.12	25.07

COLUMN 2 — FRAME 2 - 3

ROW	U(M/S)	V(M/S)	VEL	ANGLE
1	171.49	2.31	171.50	0.77
2	171.35	2.65	171.37	0.89
3	169.57	4.58	169.63	1.55
4	171.96	0.07	171.96	0.02
5	170.68	3.76	170.72	1.22
6	174.85	8.16	175.04	2.67
7	170.58	-5.37	170.66	-1.74
8	176.98	12.14	177.40	3.92
9	176.82	14.13	177.38	4.56
10	183.87	25.15	185.58	7.79
11	187.54	42.68	192.33	12.82
12	195.19	66.81	206.31	18.89
13	190.82	75.02	205.41	21.72
14	184.88	81.91	202.21	23.89
15	185.50	87.06	204.92	25.14
16	164.82	92.67	189.09	29.35

COLUMN 3 — FRAME 2 - 3

ROW	U(M/S)	V(M/S)	VEL	ANGLE
1	177.62	-5.03	177.69	1.62
2	179.86	10.31	180.15	3.28
3	176.34	6.50	176.66	2.11
4	179.69	5.36	179.77	1.68
5	176.29	5.56	176.38	1.81
6	176.92	9.19	177.16	2.97
7	178.56	1.37	178.57	0.44
8	179.87	13.18	180.36	4.19
9	179.61	22.47	181.01	7.13
10	180.12	33.42	183.20	10.51
11	179.69	52.53	187.21	16.29
12	178.53	66.72	190.59	20.47
13	178.17	75.14	184.06	22.49
14	186.20	79.65	202.52	23.16
15	172.22	73.68	189.76	24.83
16	172.07	79.95	189.74	24.92
17	172.86	76.11	188.87	23.76

COLUMN 4 — FRAME 2 - 3

ROW	U(M/S)	V(M/S)	VEL	ANGLE
1	176.42	6.83	176.55	2.22
2	176.24	10.42	176.54	3.38
3	177.02	5.05	177.09	1.63
4	177.77	1.32	177.77	0.43
5	179.14	9.04	179.37	2.89
6	184.72	9.50	184.97	2.94
7	179.79	4.02	179.83	1.24
8	185.17	16.70	185.92	5.15
9	183.29	24.34	184.90	7.56
10	183.01	34.45	186.23	10.66
11	184.18	59.22	192.28	17.89
12	180.61	66.11	192.33	20.10
13	174.74	67.92	187.47	21.24
14	172.06	75.51	187.90	23.69
15	171.94	76.59	188.23	24.01
16	164.43	78.37	182.15	25.44
17	159.43	77.74	177.37	25.99
18	148.74	75.37	166.75	26.87

COLUMN 5 — FRAME 2 - 3

ROW	U(M/S)	V(M/S)	VEL	ANGLE
1	179.36	3.77	179.40	1.20
2	176.71	8.15	176.90	2.64
3	179.85	8.53	180.05	2.72
4	174.87	5.52	174.95	1.81
5	177.16	6.73	177.29	2.17
6	175.60	11.18	176.05	3.58
7	174.49	4.91	174.56	1.61
8	175.01	15.07	175.66	4.92
9	178.86	21.98	180.20	7.01
10	175.37	27.97	177.59	9.06
11	170.41	56.88	185.35	17.87
12	170.91	68.66	189.77	21.21
13	172.76	67.23	185.38	21.26
14	154.44	69.83	178.65	23.01
15	163.56	64.44	177.30	22.71
16	160.13	70.34	174.90	23.71
17	154.25	75.41	171.69	26.05
18	152.43	79.72	172.02	27.61
19	147.39	83.17	169.24	29.43

COLUMN 6 — FRAME 2 - 3

ROW	U(M/S)	V(M/S)	VEL	ANGLE
1	176.50	5.53	176.59	1.79
2	177.19	5.88	177.28	1.90
3	174.65	3.71	174.69	1.22
4	176.99	2.46	177.01	0.80
5	176.81	5.26	176.89	1.70
6	175.02	7.21	175.17	2.36
7	176.60	2.66	176.62	0.86
8	175.36	9.54	176.62	3.10
9	169.60	16.28	170.38	5.48
10	174.04	37.10	177.95	12.03
11	172.91	48.85	179.67	15.78
12	174.13	66.35	186.35	20.80
13	168.43	59.17	178.52	19.36
14	160.08	63.42	172.19	21.61
15	159.94	66.95	173.39	22.72
16	156.87	66.30	164.79	23.72
17	150.78	65.76	164.50	23.56
18	144.96	66.75	159.59	24.73
19	144.02	69.46	159.89	25.75
20	132.45	73.60	151.52	29.06
21	125.70	81.92	150.04	33.09

COLUMN 7 — FRAME 2 - 3

ROW	U(M/S)	V(M/S)	VEL	ANGLE
1	172.02	8.08	172.21	2.69
2	174.08	12.55	174.73	4.12
3	174.21	8.78	174.43	2.89
4	171.62	9.90	171.90	3.30
5	170.60	13.58	171.14	4.52
6	171.31	12.22	171.75	4.08
7	166.34	9.20	166.60	3.17
8	170.18	16.15	170.94	5.42
9	175.66	22.27	177.07	7.23
10	172.12	31.52	174.99	10.38
11	170.80	54.09	179.34	17.76
12	166.75	45.97	172.97	15.41
13	163.97	59.30	174.36	19.84
14	158.97	55.70	169.46	20.27
15	147.34	65.34	161.18	23.91
16	148.86	67.28	163.36	24.32
17	144.73	65.97	158.68	24.21
18	138.10	55.06	153.08	23.56
19	141.21	71.30	158.19	26.79
20	133.82	59.81	150.94	27.55
21	129.60	74.95	149.71	30.04

COLUMN 8 — FRAME 2 - 3

ROW	U(M/S)	V(M/S)	VEL	ANGLE
1	172.46	7.43	172.62	2.47
2	173.04	14.31	173.62	4.72
3	174.49	17.92	175.41	5.86
4	173.61	14.16	174.19	4.65
5	168.59	13.62	169.14	4.62
6	170.85	17.28	171.72	5.77
7	173.22	14.37	173.82	4.74
8	169.73	20.36	170.95	6.83
9	172.86	20.75	174.10	6.88
10	174.23	29.28	176.67	9.54
11	169.02	40.56	173.91	13.67
12	169.52	53.53	177.77	17.53
13	159.61	53.69	168.40	18.59
14	155.23	54.77	165.55	19.31
15	156.90	57.52	167.11	20.17
16	148.52	65.05	162.14	23.95
17	143.55	64.46	157.36	24.18
18	141.01	65.54	155.50	24.93
19	140.10	67.46	155.50	25.71
20	130.97	73.33	150.10	29.24
21	125.24	71.10	144.22	29.57
22	124.39	73.94	144.71	30.71

COLUMN 9 — FRAME 2 - 3

ROW	U(M/S)	V(M/S)	VEL	ANGLE
1	166.36	8.31	166.56	2.86
2	170.17	16.88	171.00	5.66
3	167.62	15.53	168.34	5.29
4	174.02	15.98	174.76	5.25
5	169.08	10.53	169.40	3.57
6	164.79	14.90	165.46	5.17
7	167.97	13.64	168.52	4.64
8	170.09	25.47	171.99	8.52
9	166.03	15.93	166.73	5.48
10	166.55	20.88	168.70	9.17
11	167.11	33.76	170.49	11.42
12	162.67	48.71	169.80	16.67
13	155.24	48.08	162.52	17.21
14	154.21	54.92	163.70	19.60
15	152.45	57.65	162.98	20.71
16	142.56	56.18	153.23	21.61
17	139.24	54.80	149.64	21.43
18	139.09	54.25	149.57	21.83
19	130.87	57.75	143.05	23.81
20	127.50	62.10	141.82	25.97
21	118.44	63.12	134.21	28.06
22	111.09	60.95	126.71	28.75

COLUMN 10 — FRAME 2 - 3

ROW	U(M/S)	V(M/S)	VEL	ANGLE
1	169.16	12.61	169.63	4.26
2	166.57	12.90	167.07	4.43
3	165.69	9.96	165.99	3.44
4	166.47	4.58	166.53	1.58
5	162.98	9.78	163.28	3.43
6	169.30	15.14	169.98	5.11
7	164.36	9.66	164.65	3.36
8	165.77	15.76	166.52	5.43
9	169.86	7.99	170.05	2.69
10	167.93	18.09	168.90	6.15
11	159.18	33.97	172.56	11.39
12	156.31	53.04	174.57	17.59
13	163.70	55.76	172.94	18.81
14	155.63	43.79	161.65	15.64
15	148.95	47.17	156.24	17.57
16	145.51	51.52	154.36	19.53
17	138.84	54.18	149.04	21.32
18	137.97	52.86	147.75	20.96
19	128.07	54.66	139.25	23.11
20	124.80	50.83	134.76	22.14
21	118.88	59.31	132.85	26.53
22	110.68	57.15	124.57	27.31

Table A.1.5 Velocity values for Fig. A.1.5.

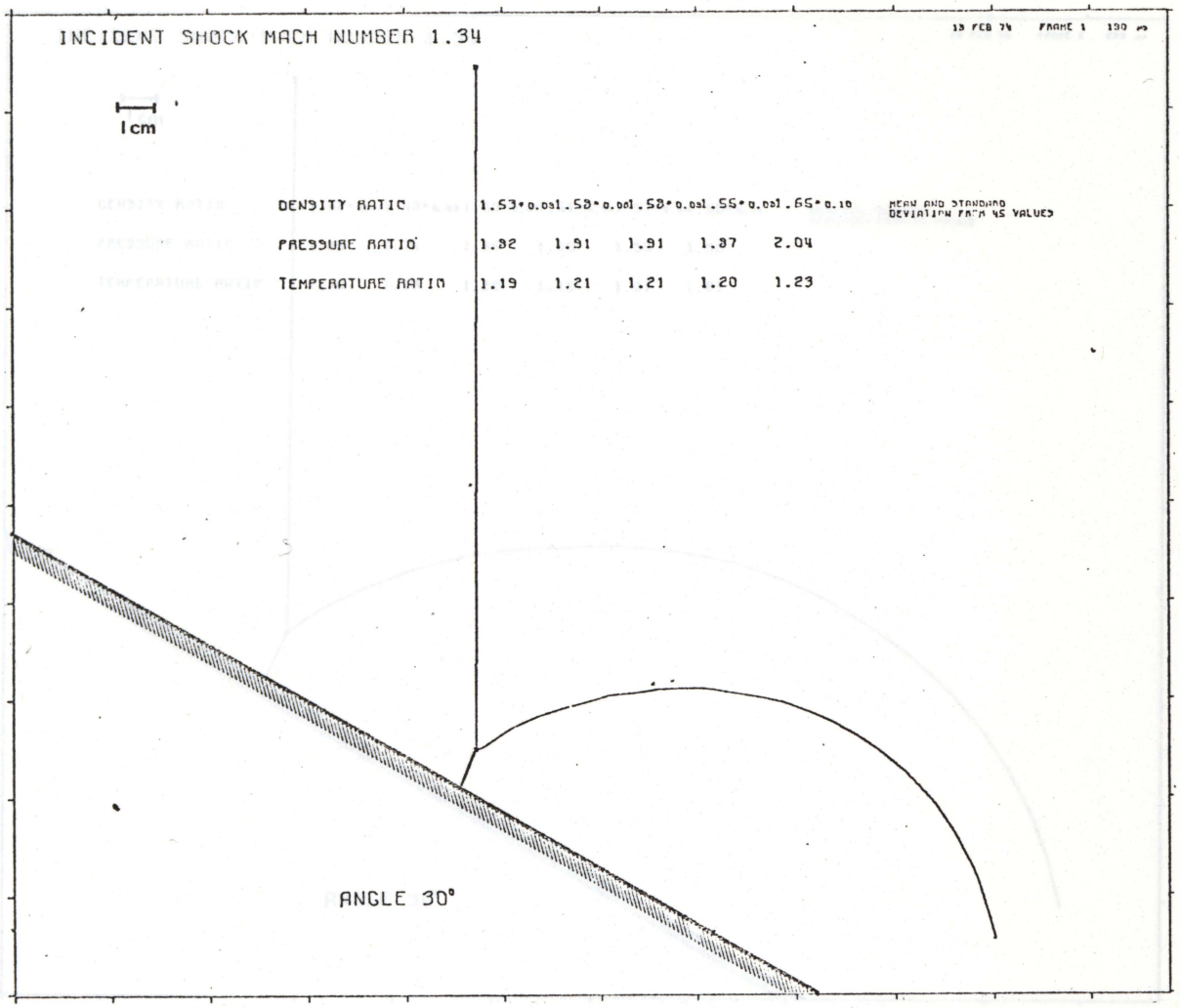

Fig. A.1.6 Mean ratios 190 μs.

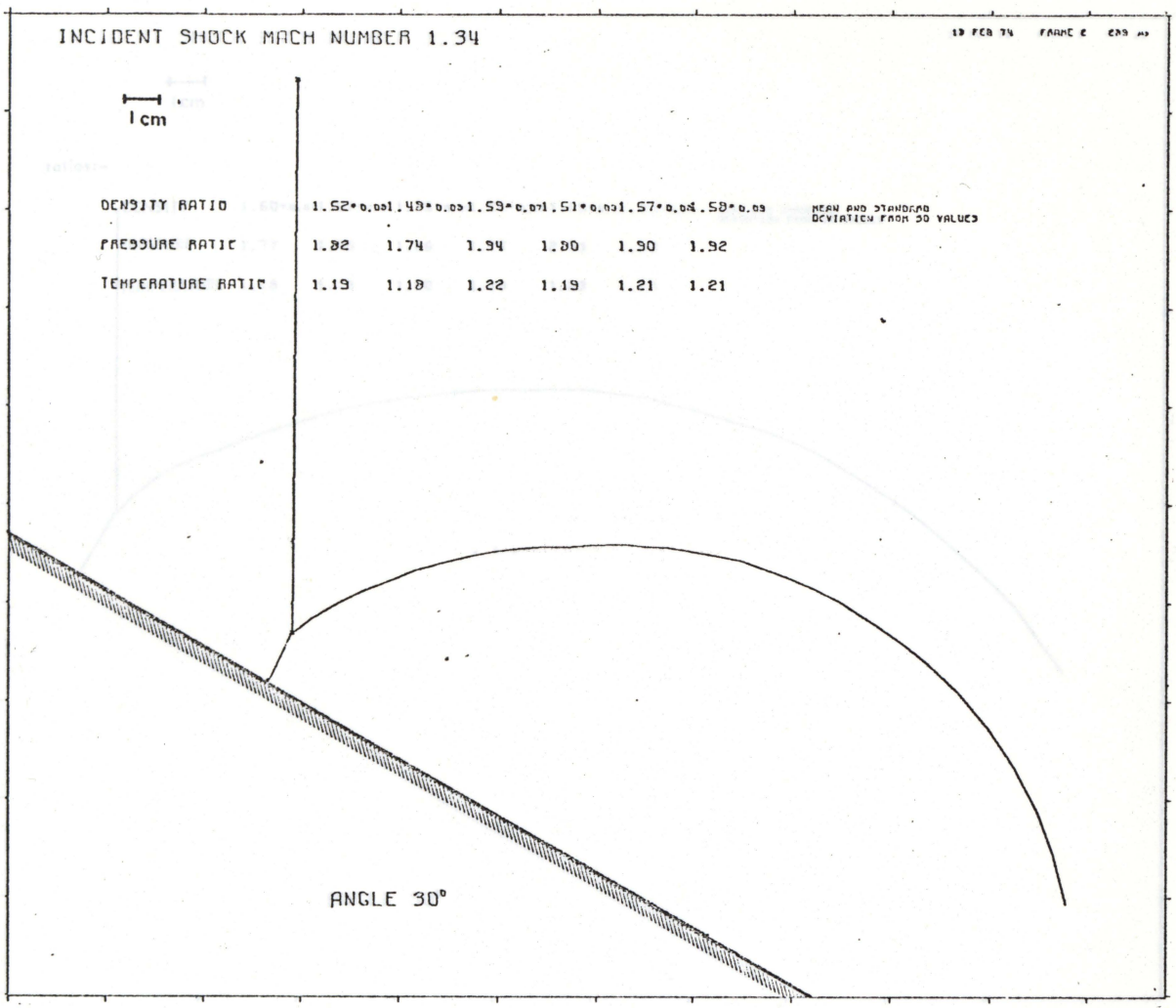

Fig. A,1.7 Mean ratios 289 μs.

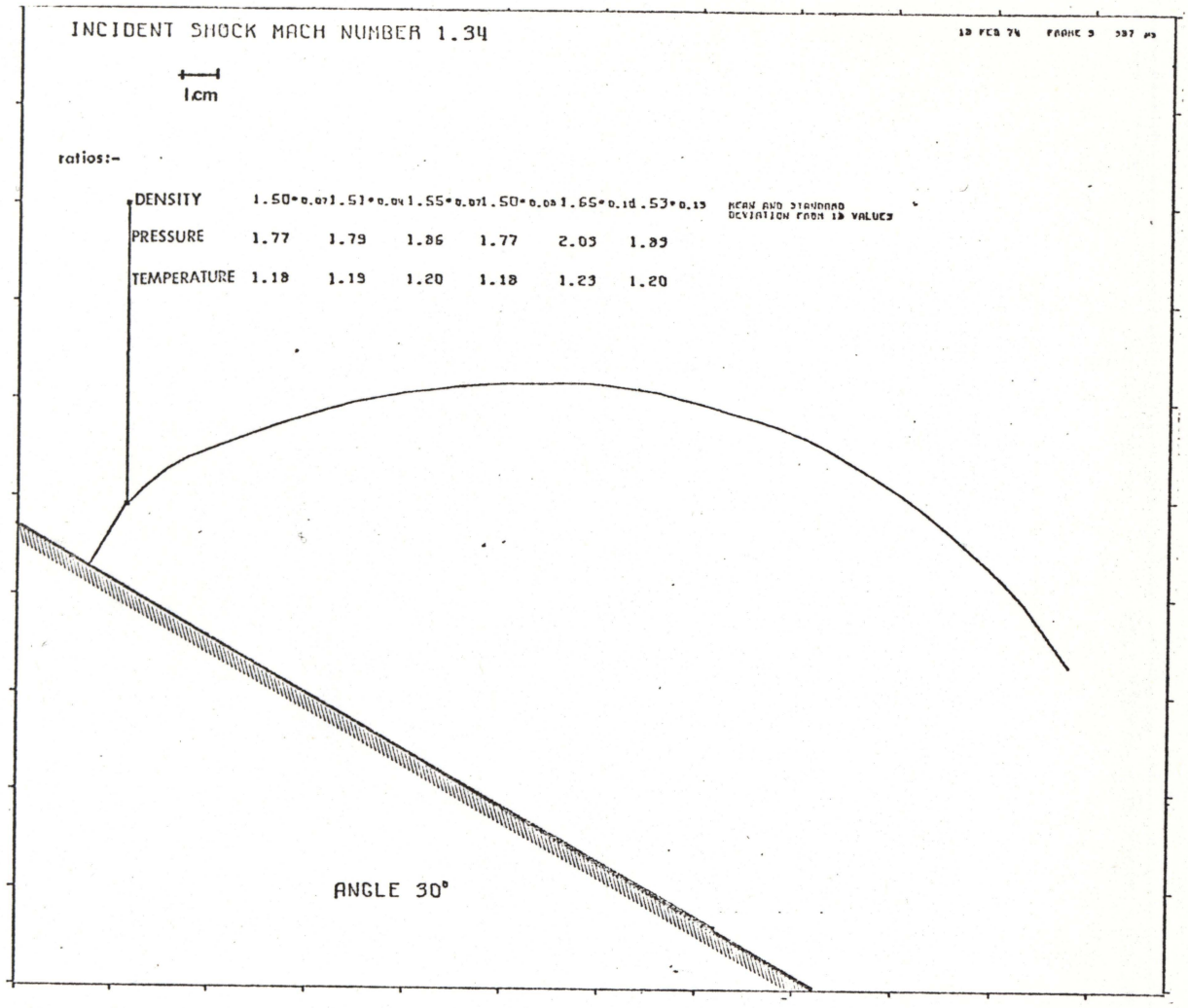

Fig. A.1.8 Mean ratios 387 μs.

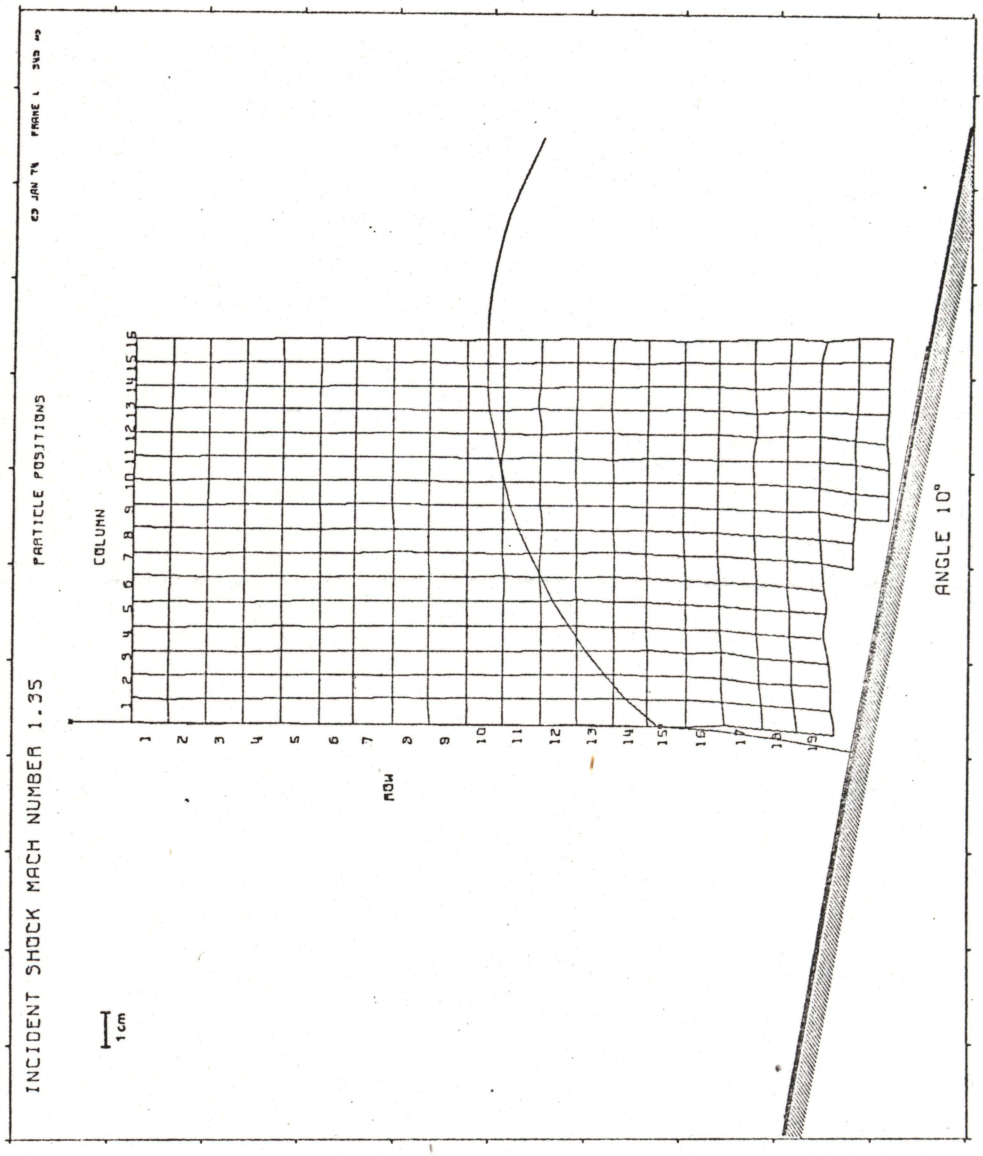

Fig. A.2.1 Tracers at 349 µs.

	COLUMN															
	1	2	3	5	5	6	7	8	9	10	11	12	13	14	15	16
1	1.60	1.65	1.63	1.59	1.52	1.46	1.71	1.50	1.66	1.57	1.62	1.59	1.52	1.67	1.54	1.61
2	1.52	1.55	1.61	1.59	1.51	1.48	1.68	1.50	1.67	1.49	1.60	1.58	1.53	1.76	1.62	1.66
3	1.48	1.56	1.66	1.51	1.52	1.49	1.67	1.54	1.59	1.50	1.60	1.65	1.51	1.69	1.55	1.69
4	1.51	1.56	1.62	1.47	1.53	1.52	1.62	1.56	1.56	1.55	1.60	1.63	1.53	1.72	1.57	1.69
5	1.44	1.52	1.57	1.47	1.46	1.50	1.55	1.53	1.52	1.51	1.54	1.57	1.53	1.69	1.51	1.60
6	1.60	1.72	1.75	1.69	1.61	1.74	1.78	1.76	1.63	1.65	1.76	1.77	1.63	1.71	1.67	1.71
7	1.40	1.65	1.55	1.47	1.43	1.53	1.49	1.55	1.48	1.60	1.59	1.53	1.57	1.65	1.65	1.66
8	1.44	1.68	1.57	1.48	1.52	1.60	1.56	1.74	1.48	1.61	1.60	1.56	1.58	1.61	1.55	1.64
9	1.43	1.65	1.64	1.55	1.56	1.64	1.57	1.64	1.53	1.63	1.57	1.59	1.62	1.62	1.65	1.73
10	1.45	1.64	1.62	1.55	1.48	1.54	1.60	1.63	1.56	1.60	1.66	1.57	1.56	1.59	1.53	1.53
11	1.41	1.60	1.55	1.52	1.51	1.67	1.70	1.51	1.52	1.69	1.57	1.54	1.63	1.86	1.53	1.59
12	1.48	1.65	1.58	1.58	1.51	1.67	1.60	1.79	1.57	1.66	1.60	1.66	1.59	1.72	1.56	1.71
13	1.42	1.61	1.60	1.60	1.50	1.61	1.53	1.78	1.59	1.73	1.60	1.52	1.71	1.74	1.64	1.64
14	1.56	1.77	1.68	1.78	1.70	1.77	1.72	1.92	1.69	1.72	1.71	1.59	1.56	1.65	1.70	1.69
15	1.33	1.51	1.52	1.65	1.45	1.56	1.53	1.61	1.59	1.58	1.59	1.64	1.53	1.66	1.63	1.71
16	1.48	1.66	1.59	1.72	1.61	1.66	1.54	1.71	1.66	1.62	1.73	1.62	1.60	1.72	1.70	1.83
17	1.65	1.69	1.54	1.82	1.70	1.64	1.57	1.73	1.61	1.54	1.78	1.50	1.55	1.67	1.66	1.74
18	1.69	1.82	1.67	1.67	1.63	1.63	1.68	1.77	1.70	1.62	1.74	1.86	1.86	1.80	1.62	1.69
19	1.65	1.68	1.72	1.69	1.67	1.67	1.58	1.86	1.71	1.73	1.67	1.74	1.70	1.78	1.66	1.76
20								1.72	1.52	1.61	1.39	1.58	1.57	1.55	1.50	1.84
21										1.64	1.55	1.76	1.50	1.68	1.69	1.80

JAN 2 3 1974

Table A.2.1 Density values for Fig. A.2.1.

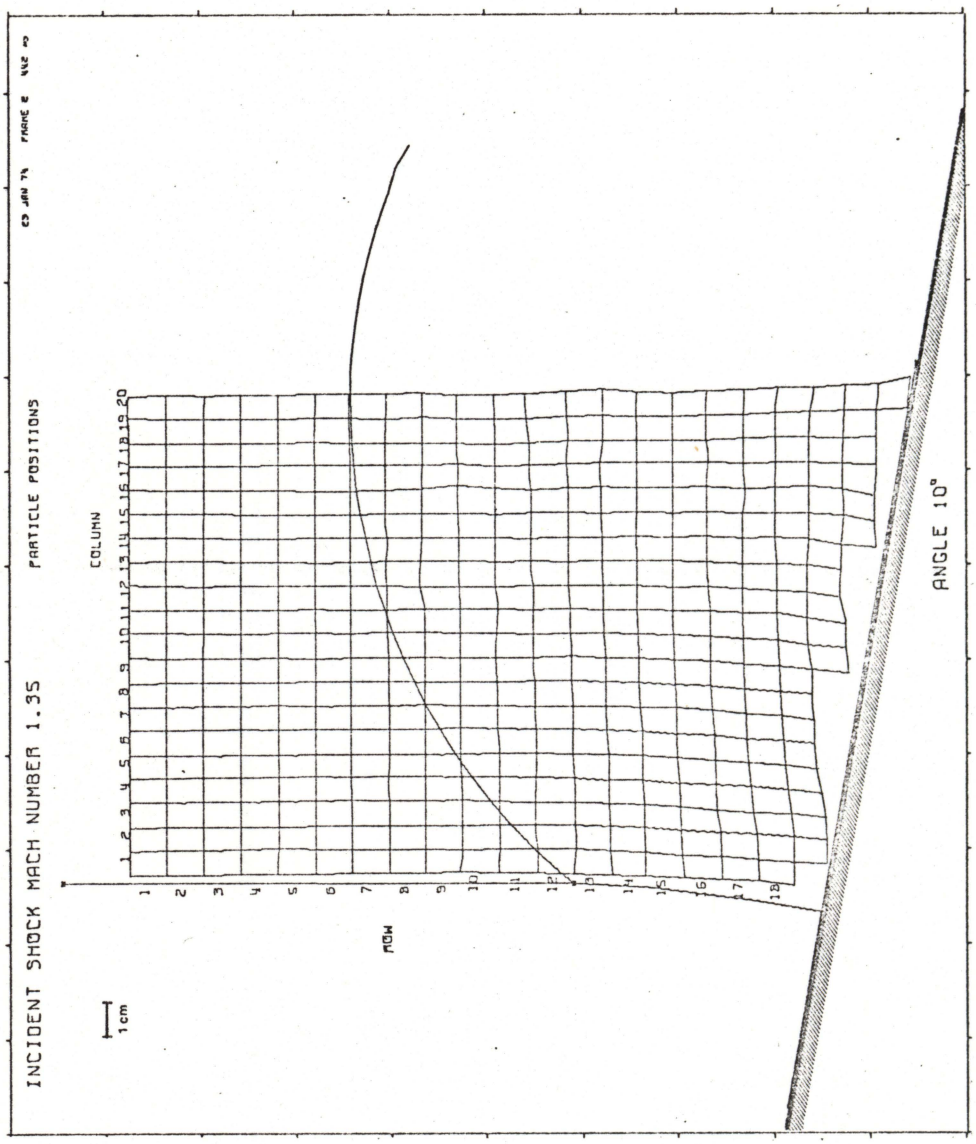

Fig. A.2.2 Tracers at 442 μs.

	COLUMN																		
	1	2	3	5	5	6	7	8	9	10	11	12	13	14	15	16	17	18	19	20
1	1.58	1.70	1.51	1.58	1.70	1.52	1.68	1.55	1.54	1.56	1.65	1.55	1.60	1.60	1.56	1.60	1.57	1.51	1.45	1.60
2	1.49	1.62	1.49	1.56	1.70	1.46	1.60	1.56	1.52	1.45	1.53	1.60	1.47	1.55	1.52	1.57	1.55	1.59	1.50	1.52
3	1.53	1.63	1.48	1.58	1.70	1.45	1.59	1.58	1.55	1.57	1.61	1.56	1.56	1.65	1.56	1.63	1.54	1.70	1.60	1.65
4	1.41	1.62	1.41	1.50	1.65	1.42	1.56	1.55	1.52	1.52	1.58	1.54	1.57	1.59	1.55	1.56	1.50	1.64	1.51	1.54
5	1.49	1.75	1.47	1.56	1.67	1.44	1.57	1.58	1.57	1.43	1.57	1.57	1.59	1.54	1.60	1.56	1.43	1.71	1.58	1.53
6	1.57	1.66	1.52	1.70	1.79	1.58	1.68	1.61	1.75	1.62	1.78	1.71	1.75	1.70	1.77	1.72	1.57	1.83	1.65	1.71
7	1.53	1.58	1.45	1.55	1.64	1.45	1.53	1.48	1.57	1.43	1.66	1.58	1.59	1.59	1.62	1.71	1.52	1.78	1.60	1.49
8	1.60	1.62	1.53	1.60	1.75	1.53	1.62	1.66	1.62	1.53	1.70	1.81	1.64	1.67	1.60	1.56	1.52	1.76	1.49	1.57
9	1.76	1.61	1.49	1.58	1.71	1.51	1.64	1.69	1.66	1.54	1.64	1.60	1.38	1.69	1.54	1.48	1.73	1.90	1.58	1.66
10	1.53	1.53	1.52	1.60	1.55	1.43	1.68	1.60	1.65	1.56	1.55	1.72	1.50	1.64	1.57	1.38	1.74	1.79	1.48	1.55
11	1.56	1.57	1.71	1.67	1.64	1.47	1.60	1.48	1.63	1.58	1.66	1.64	1.51	1.78	1.62	1.63	1.65	1.80	1.62	1.68
12	1.52	1.54	1.57	1.45	1.57	1.64	1.67	1.53	1.62	1.68	1.60	1.74	1.66	1.59	1.50	1.70	1.58	1.68	1.50	1.48
13	1.54	1.67	1.70	1.69	1.56	1.62	1.74	1.61	1.67	1.69	1.68	1.67	1.61	1.71	1.67	1.64	1.73	1.87	1.60	1.49
14	1.70	1.73	1.82	1.73	1.66	1.75	1.74	1.73	1.81	1.76	1.84	1.82	1.69	1.76	1.67	1.58	1.55	1.72	1.69	1.59
15	1.56	1.46	1.57	1.54	1.49	1.61	1.49	1.51	1.52	1.56	1.57	1.63	1.49	1.59	1.58	1.58	1.50	1.67	1.61	1.60
16	1.65	1.53	1.70	1.68	1.61	1.60	1.57	1.78	1.68	1.62	1.55	1.68	1.66	1.75	1.72	1.72	1.66	1.91	1.80	1.75
17	1.68	1.53	1.69	1.46	1.66	1.71	1.61	1.62	1.65	1.69	1.64	1.74	1.61	1.52	1.56	1.54	1.54	1.65	1.52	1.55
18	1.81	1.62	1.77	1.60	1.69	1.66	1.63	1.69	1.66	1.65	1.62	1.84	1.60	1.65	1.75	1.90	1.77	1.74	1.86	1.70
19		1.67	1.71	1.62	1.66	1.69	1.74	1.67	1.67	1.70	1.64	1.87	1.69	1.66	1.68	1.66	1.77	1.71	1.68	1.64
20										1.62	1.47	1.55	1.51	1.55	1.41	1.49	1.66	1.54	1.44	1.66
21															1.57	1.77	1.54	1.59	1.63	1.73
22	23 JAN 74																			1.51

Table A.2.2 Density values for Fig. A.2.2.

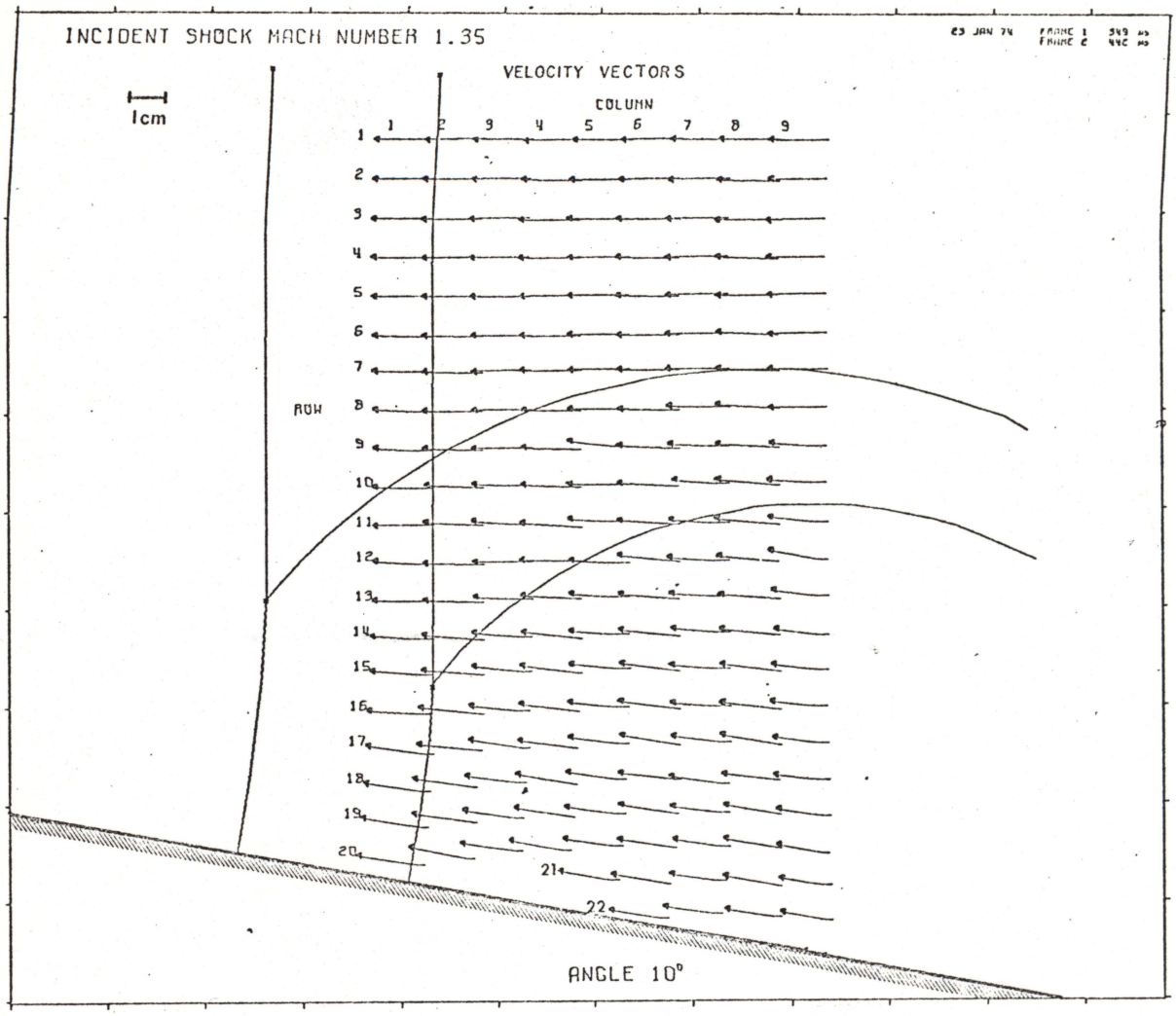

Fig. A.2.3 Velocity vectors 349 - 442 μs.

COLUMN 1			FRAME 1 - 2	
ROW	U(M/S)	V(M/S)	VEL	ANGLE
1	165.29	1.14	165.30	0.40
2	162.32	1.81	162.33	0.64
3	159.35	2.48	159.37	0.89
4	160.69	4.11	160.74	1.46
5	160.37	1.37	160.38	0.49
6	158.18	5.51	158.27	2.00
7	158.71	5.40	158.80	1.95
8	158.25	9.58	158.54	3.46
9	157.02	9.42	157.30	3.43
10	158.45	6.71	158.59	2.43
11	159.97	-0.31	159.97	-0.11
12	158.52	10.78	158.88	3.90
13	161.73	5.52	161.82	1.95
14	167.31	14.56	167.71	3.95
15	165.22	13.11	165.74	4.54
16	172.64	13.11	173.14	4.34
17	181.50	27.02	183.50	8.47
18	178.57	26.80	180.57	8.54
19	176.18	29.23	180.57	9.32
20	181.30	29.13	183.63	9.13

COLUMN 4			FRAME 1 - 2	
ROW	U(M/S)	V(M/S)	VEL	ANGLE
1	165.66	-0.89	165.67	-0.31
2	163.51	2.40	163.53	0.84
3	163.20	-0.35	163.20	-0.12
4	166.35	-2.14	166.36	-0.74
5	164.31	-4.91	164.38	-1.71
6	162.98	-0.75	162.98	-0.26
7	165.21	0.91	165.21	0.31
8	159.63	1.52	159.64	0.55
9	160.93	4.87	161.00	1.73
10	163.15	5.65	163.25	1.98
11	168.75	9.96	169.04	3.38
12	166.87	1.14	166.88	0.39
13	165.51	7.91	165.70	2.73
14	164.95	17.28	165.85	5.98
15	167.17	19.80	168.34	6.75
16	163.36	19.56	164.53	6.83
17	162.99	21.14	164.35	7.39
18	166.88	26.28	168.93	8.95
19	163.15	24.33	164.96	8.48
20	168.73	32.08	171.75	10.76

COLUMN 7			FRAME 1 - 2	
ROW	U(M/S)	V(M/S)	VEL	ANGLE
1	159.88	2.98	159.91	1.07
2	162.19	-0.56	162.19	-0.20
3	163.52	1.06	163.52	0.37
4	164.08	-1.66	164.09	-0.58
5	164.58	-0.91	164.58	-0.32
6	165.00	2.42	165.02	0.84
7	167.30	0.62	167.30	0.21
8	165.97	5.66	166.07	1.95
9	162.07	8.90	162.32	3.14
10	156.39	12.87	156.94	4.89
11	160.40	12.93	160.92	4.61
12	162.64	12.63	163.15	4.51
13	163.22	10.14	163.54	3.56
14	158.47	14.25	159.11	5.14
15	158.15	13.23	158.70	4.78
16	156.95	12.22	157.43	4.45
17	157.32	19.90	158.56	7.21
18	156.89	22.32	158.47	8.10
19	154.92	20.45	156.26	7.52
20	151.08	22.86	152.80	8.60
21	149.90	22.67	151.61	8.50
22	156.52	23.52	158.27	8.55

COLUMN 2			FRAME 1 - 2	
ROW	U(M/S)	V(M/S)	VEL	ANGLE
1	162.57	-1.04	162.57	-0.37
2	162.20	-0.32	162.20	-0.11
3	161.86	-1.32	161.86	-0.47
4	161.53	-3.19	161.56	-1.13
5	161.93	-0.72	161.98	-0.25
6	163.28	1.77	163.29	0.62
7	161.23	0.73	161.23	0.26
8	160.88	-0.28	160.88	-0.10
9	162.18	3.08	162.21	1.09
10	158.30	6.34	158.42	2.29
11	159.64	7.96	159.84	2.85
12	163.73	3.99	163.74	0.35
13	164.17	4.33	164.23	1.51
14	168.84	12.95	169.33	4.39
15	169.40	11.96	169.82	4.04
16	175.83	18.01	176.75	5.85
17	175.53	16.13	176.27	5.25
18	172.43	24.54	174.17	8.10
19	172.97	24.42	174.68	8.04
20	175.88	34.71	179.27	11.16

COLUMN 5			FRAME 1 - 2	
ROW	U(M/S)	V(M/S)	VEL	ANGLE
1	162.83	2.12	162.85	0.75
2	165.05	2.89	165.08	1.00
3	165.54	3.63	165.58	1.26
4	162.64	0.84	162.65	0.30
5	163.17	-0.15	163.17	-0.05
6	162.75	2.30	162.76	0.81
7	164.18	0.48	164.18	0.17
8	163.76	2.93	163.79	1.02
9	165.70	18.42	166.72	6.34
10	166.46	5.32	166.55	1.83
11	167.76	9.55	168.03	3.26
12	163.89	10.19	164.20	3.56
13	161.81	11.75	162.23	4.15
14	163.19	11.65	163.60	4.08
15	164.51	15.89	165.27	5.52
16	165.07	16.62	165.84	5.75
17	161.98	20.75	163.30	7.30
18	161.60	23.19	163.26	8.17
19	153.87	23.11	165.49	8.03
20	161.83	23.72	163.57	8.36
21	164.90	28.03	167.26	9.55

COLUMN 8			FRAME 1 - 2	
ROW	U(M/S)	V(M/S)	VEL	ANGLE
1	161.45	2.61	161.47	0.93
2	161.93	3.35	161.96	1.19
3	161.68	-1.98	161.69	-0.70
4	162.88	5.70	162.98	2.01
5	160.93	-0.53	160.93	-0.19
6	161.27	7.14	161.43	2.53
7	164.41	6.22	164.52	2.17
8	165.70	10.44	165.03	3.60
9	166.20	10.31	166.52	3.55
10	164.88	15.35	165.59	5.32
11	157.13	14.35	167.75	4.92
12	159.84	14.97	160.54	5.35
13	160.40	12.27	160.87	4.37
14	158.22	17.29	159.17	6.24
15	160.41	20.68	161.73	7.35
16	159.21	19.65	160.41	7.04
17	159.57	28.19	162.04	10.02
18	150.79	17.49	151.80	6.62
19	148.57	25.99	150.82	9.92
20	151.68	26.81	154.03	10.02
21	152.18	27.55	154.65	10.20
22	148.49	23.90	153.40	9.14

COLUMN 3			FRAME 1 - 2	
ROW	U(M/S)	V(M/S)	VEL	ANGLE
1	164.08	1.18	164.08	0.41
2	160.28	0.10	160.28	0.04
3	162.52	0.02	162.52	0.01
4	161.27	0.73	161.27	0.26
5	165.20	1.55	165.21	0.54
6	161.34	3.06	161.37	1.09
7	161.97	-1.37	161.97	-0.49
8	162.41	1.10	162.41	0.39
9	165.49	1.89	165.50	0.66
10	163.31	6.91	163.45	2.42
11	164.57	12.00	165.01	4.17
12	162.65	3.17	162.68	1.12
13	163.05	9.11	163.31	3.20
14	163.48	13.31	164.02	4.65
15	164.78	18.40	165.80	6.47
16	165.30	17.39	166.22	6.00
17	169.11	26.00	171.10	8.74
18	168.00	22.35	169.48	7.58
19	168.47	23.68	170.41	8.57
20	169.94	23.84	171.60	7.99

COLUMN 6			FRAME 1 - 2	
ROW	U(M/S)	V(M/S)	VEL	ANGLE
1	164.46	-0.84	164.46	-0.29
2	161.59	-4.50	161.65	-1.60
3	167.18	-0.18	167.18	-0.06
4	167.63	2.28	167.65	0.79
5	167.27	2.14	167.29	0.73
6	165.23	-0.63	165.23	-0.22
7	168.33	1.04	168.33	0.36
8	164.47	1.99	164.48	0.69
9	164.88	6.76	165.02	2.35
10	162.78	7.44	162.95	2.62
11	164.95	10.22	165.30	3.75
12	165.34	16.75	166.19	5.79
13	159.89	12.18	160.35	4.36
14	161.16	17.27	162.09	6.12
15	159.92	19.73	161.13	7.03
16	162.99	21.38	164.39	7.47
17	159.68	25.53	162.00	9.07
18	164.13	17.69	165.08	6.15
19	157.00	29.22	159.60	9.09
20	155.61	22.44	157.22	8.21
21	152.97	24.88	158.93	9.01
22	157.49	25.61	159.56	9.24

COLUMN 9			FRAME 1 - 2	
ROW	U(M/S)	V(M/S)	VEL	ANGLE
1	159.52	3.99	159.56	1.46
2	155.71	2.82	155.74	1.04
3	158.07	-3.33	158.10	-1.21
4	155.01	1.67	155.02	0.62
5	157.31	-1.00	157.31	-0.36
6	156.92	-0.28	156.92	-0.10
7	159.93	4.86	160.01	1.74
8	155.31	2.03	155.32	0.75
9	153.89	11.39	154.31	4.23
10	154.74	11.35	155.15	4.02
11	159.58	17.31	160.91	6.15
12	158.50	30.13	161.34	10.76
13	154.90	19.55	156.13	7.19
14	147.61	19.28	148.87	7.44
15	153.38	17.53	154.38	6.52
16	153.92	16.54	154.91	6.13
17	150.91	19.82	152.20	7.43
18	151.48	17.12	152.44	6.45
19	147.57	22.12	149.22	8.52
20	141.94	20.18	144.34	10.45
21	142.55	23.51	144.47	9.37
22	140.44	25.95	142.81	10.47

Table A.2.3 Velocity values for Fig. A.2.3.

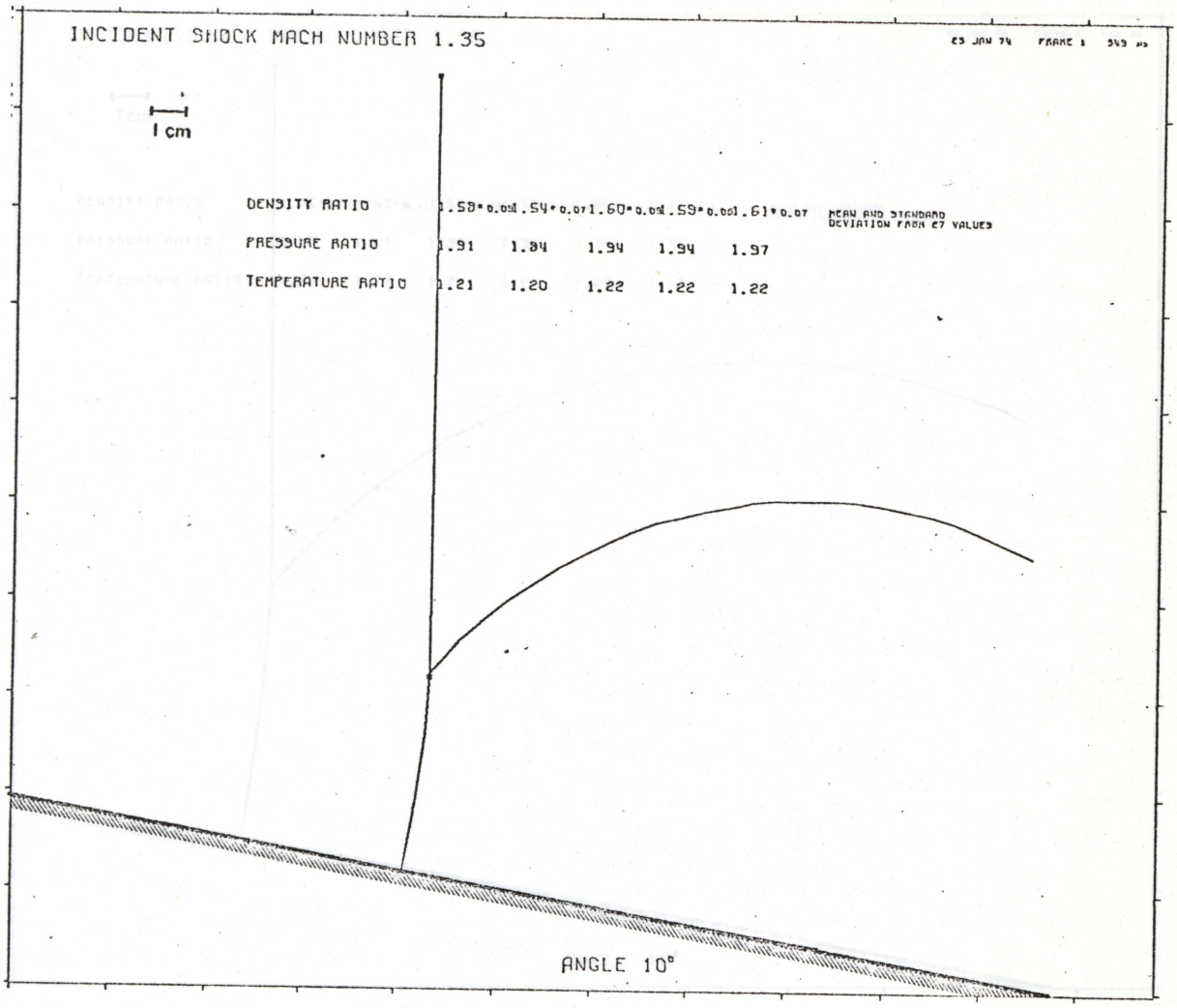

Fig. A.2.4 Mean ratios 349 μs.

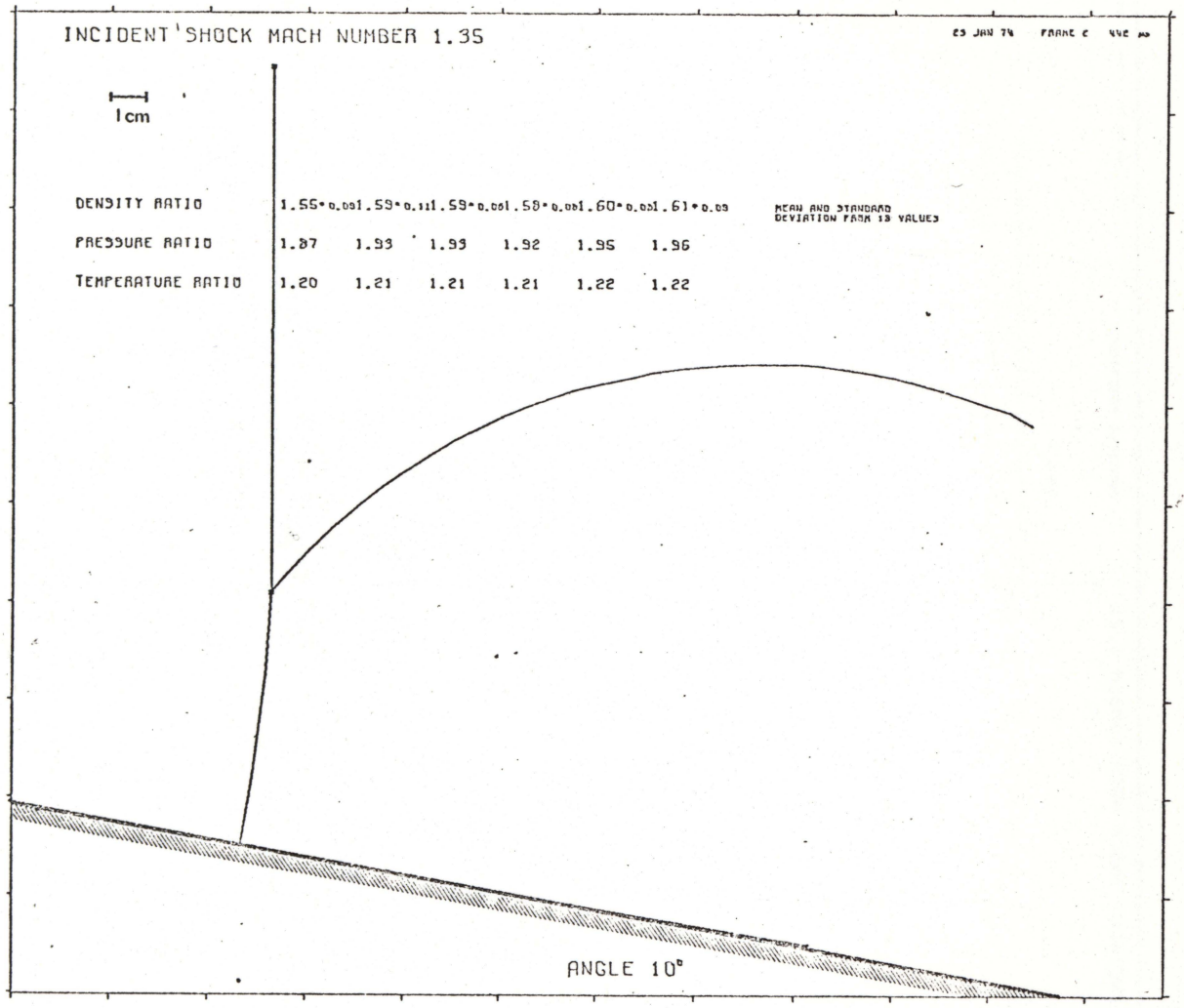

Fig. A.2.5 Mean ratios 442 μs.

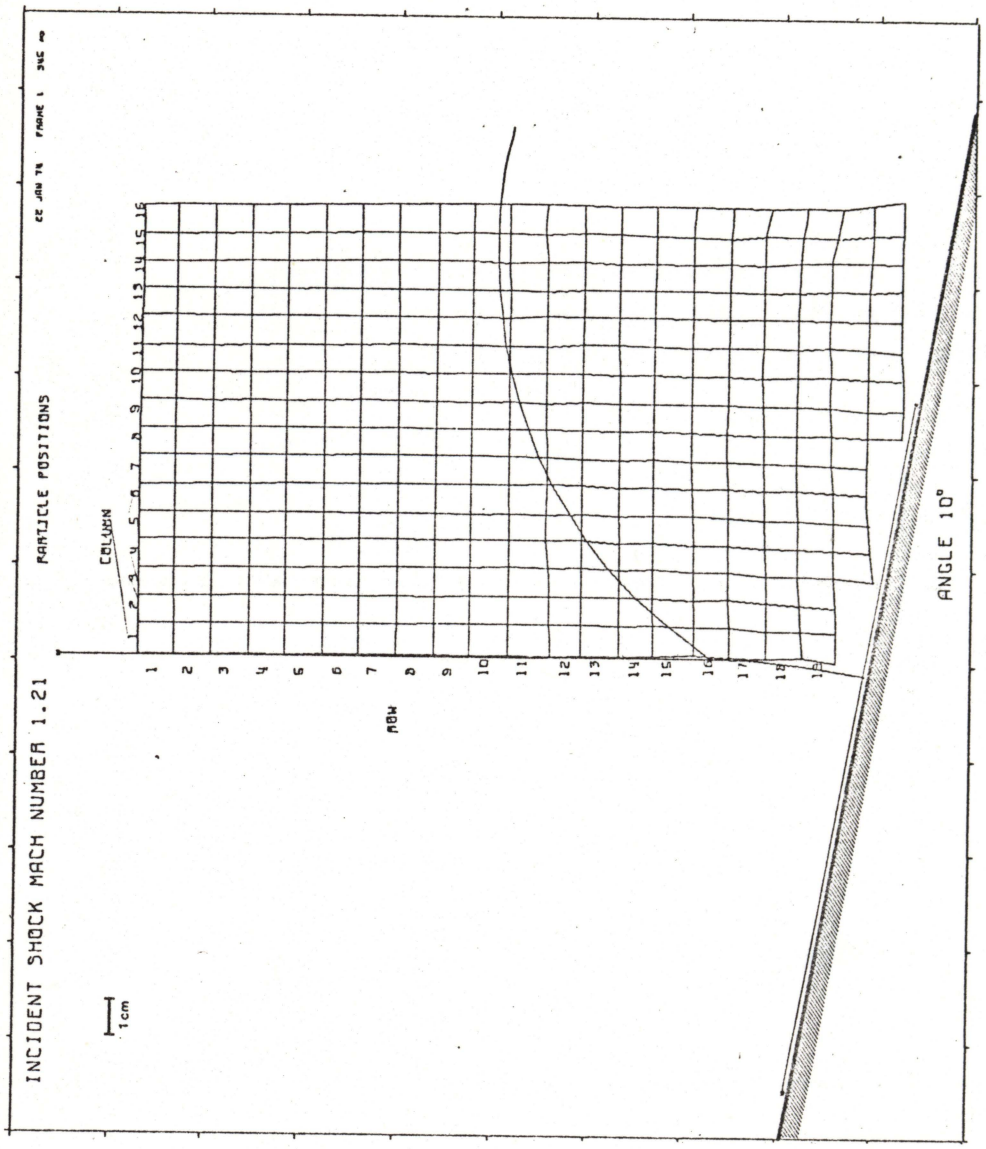

Fig. A.3.1 Tracers at 345 μs.

	COLUMN															
	1	2	3	5	5	6	7	8	9	10	11	12	13	14	15	16
1	1.25	1.47	1.41	1.33	1.46	1.45	1.33	1.42	1.37	1.39	1.55	1.32	1.47	1.55	1.46	1.40
2	1.22	1.36	1.30	1.29	1.38	1.31	1.27	1.33	1.41	1.33	1.48	1.25	1.38	1.44	1.38	1.29
3	1.20	1.35	1.33	1.33	1.40	1.34	1.31	1.37	1.45	1.34	1.45	1.29	1.40	1.38	1.36	1.36
4	1.24	1.39	1.40	1.33	1.40	1.33	1.31	1.35	1.40	1.35	1.40	1.31	1.41	1.39	1.39	1.33
5	1.15	1.31	1.33	1.31	1.40	1.30	1.31	1.32	1.39	1.33	1.40	1.31	1.41	1.38	1.35	1.34
6	1.28	1.45	1.39	1.40	1.47	1.30	1.33	1.41	1.38	1.36	1.39	1.33	1.41	1.36	1.34	1.33
7	1.22	1.34	1.27	1.34	1.46	1.28	1.30	1.39	1.38	1.39	1.38	1.36	1.41	1.35	1.39	1.36
8	1.24	1.41	1.32	1.37	1.48	1.27	1.28	1.41	1.38	1.33	1.33	1.33	1.34	1.20	1.28	1.24
9	1.24	1.44	1.34	1.39	1.47	1.30	1.34	1.44	1.43	1.37	1.40	1.37	1.46	1.35	1.44	1.35
10	1.17	1.33	1.27	1.37	1.39	1.21	1.29	1.37	1.33	1.31	1.39	1.36	1.39	1.33	1.35	1.33
11	1.07	1.29	1.25	1.42	1.53	1.28	1.35	1.43	1.53	1.37	1.42	1.34	1.49	1.40	1.42	1.33
12	1.40	1.55	1.44	1.41	1.50	1.35	1.52	1.36	1.36	1.28	1.38	1.32	1.41	1.29	1.23	1.23
13	1.18	1.36	1.31	1.38	1.43	1.34	1.38	1.29	1.38	1.37	1.36	1.41	1.44	1.48	1.32	1.43
14	1.31	1.46	1.47	1.56	1.49	1.43	1.48	1.45	1.49	1.42	1.35	1.41	1.49	1.57	1.38	1.40
15	1.19	1.30	1.22	1.32	1.28	1.35	1.35	1.32	1.31	1.26	1.27	1.26	1.33	1.40	1.33	1.22
16	1.36	1.42	1.39	1.45	1.36	1.36	1.34	1.36	1.43	1.44	1.40	1.42	1.42	1.44	1.46	1.27
17	1.33	1.37	1.41	1.45	1.42	1.38	1.47	1.38	1.30	1.45	1.34	1.37	1.47	1.42	1.40	1.29
18	1.44	1.45	1.47	1.47	1.40	1.33	1.48	1.47	1.41	1.42	1.41	1.49	1.54	1.45	1.44	1.41
19	1.51	1.60	1.40	1.55	1.48	1.36	1.54	1.43	1.45	1.40	1.48	1.55	1.47	1.46	1.60	1.32
20				1.24	1.30	1.29	1.45	1.26	1.33	1.19	1.24	1.30	1.27	1.25	1.45	1.46
21									1.40	1.23	1.44	1.39	1.34	1.50	1.54	1.45

Table A.3.1 Density values for Fig. A.3.1.

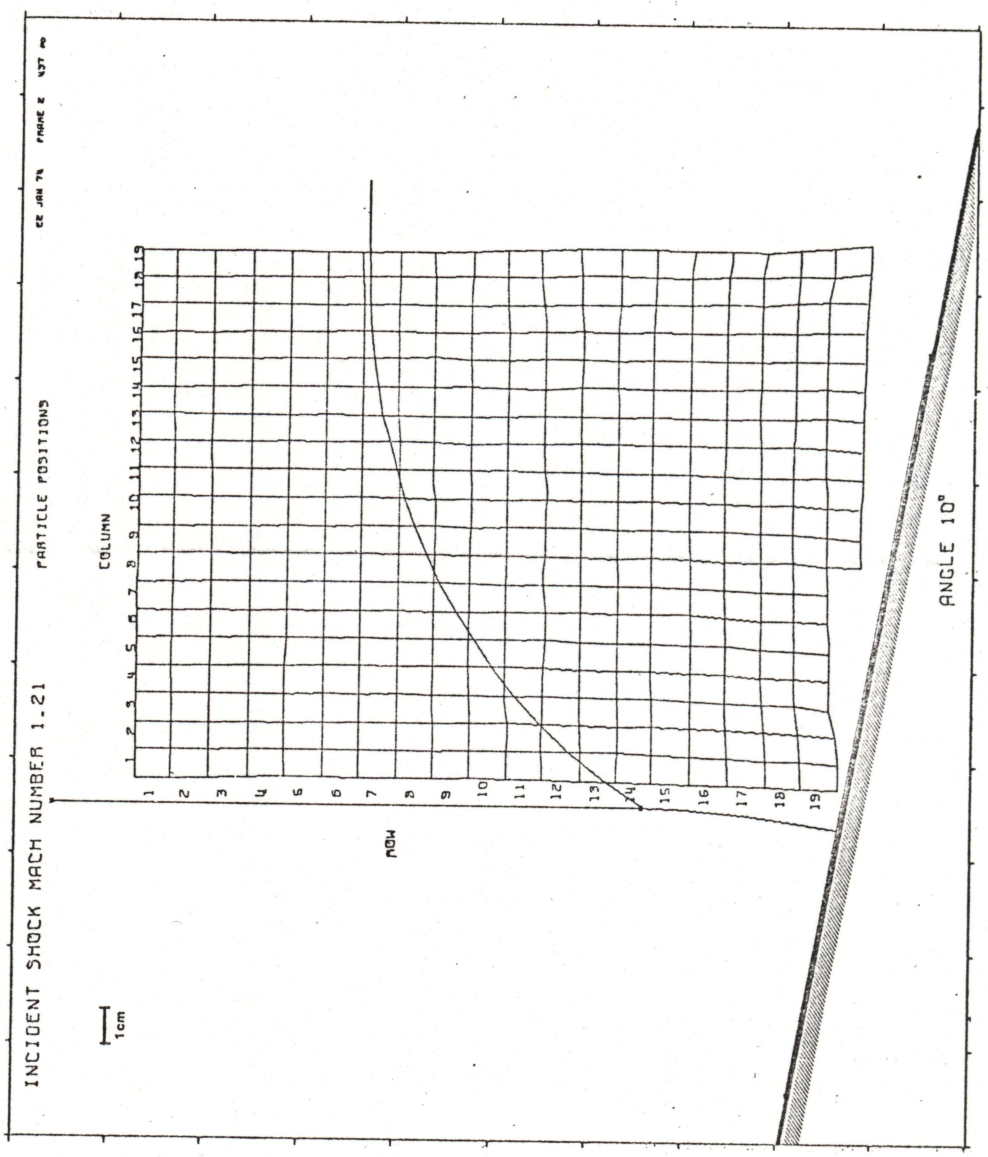

Fig. A.3.2 Tracers at 437 μs.

	COLUMN																		
	1	2	3	5	5	6	7	8	9	10	11	12	13	14	15	16	17	18	19
1	1.33	1.44	1.35	1.48	1.38	1.47	1.32	1.27	1.43	1.26	1.38	1.45	1.46	1.59	1.37	1.53	1.34	1.57	1.50
2	1.31	1.46	1.30	1.32	1.28	1.40	1.31	1.33	1.44	1.28	1.34	1.40	1.34	1.36	1.32	1.44	1.28	1.42	1.42
3	1.24	1.31	1.20	1.25	1.26	1.37	1.24	1.29	1.35	1.25	1.29	1.30	1.29	1.30	1.31	1.39	1.33	1.38	1.42
4	1.43	1.50	1.41	1.43	1.44	1.47	1.32	1.38	1.41	1.35	1.37	1.42	1.42	1.32	1.35	1.40	1.37	1.39	1.43
5	1.32	1.34	1.26	1.26	1.27	1.33	1.25	1.30	1.33	1.26	1.29	1.35	1.40	1.30	1.31	1.43	1.40	1.39	1.53
6	1.41	1.48	1.35	1.34	1.42	1.50	1.39	1.41	1.43	1.38	1.42	1.41	1.44	1.38	1.35	1.41	1.40	1.36	1.55
7	1.34	1.37	1.27	1.31	1.37	1.38	1.28	1.32	1.33	1.33	1.33	1.34	1.46	1.38	1.38	1.60	1.55	1.43	1.60
8	1.44	1.42	1.36	1.44	1.44	1.50	1.41	1.46	1.38	1.40	1.37	1.48	1.46	1.30	1.31	1.50	1.36	1.37	1.65
9	1.37	1.42	1.39	1.37	1.44	1.44	1.32	1.38	1.37	1.46	1.34	1.41	1.44	1.32	1.41	1.62	1.46	1.39	1.52
10	1.37	1.33	1.33	1.29	1.36	1.41	1.41	1.36	1.37	1.43	1.28	1.40	1.37	1.27	1.30	1.32	1.34	1.36	1.56
11	1.39	1.47	1.41	1.28	1.27	1.33	1.35	1.30	1.25	1.32	1.29	1.49	1.44	1.39	1.31	1.43	1.53	1.56	1.66
12	1.21	1.36	1.34	1.45	1.44	1.45	1.37	1.36	1.37	1.49	1.39	1.29	1.36	1.43	1.32	1.36	1.35	1.22	1.25
13	1.27	1.46	1.31	1.39	1.34	1.28	1.43	1.41	1.32	1.39	1.36	1.37	1.39	1.27	1.39	1.47	1.39	1.26	1.36
14	1.41	1.55	1.37	1.47	1.51	1.46	1.51	1.46	1.46	1.46	1.45	1.40	1.47	1.42	1.40	1.48	1.51	1.56	1.44
15	1.26	1.31	1.37	1.34	1.26	1.19	1.37	1.27	1.32	1.33	1.33	1.32	1.33	1.30	1.25	1.33	1.33	1.47	1.34
16	1.31	1.32	1.41	1.44	1.39	1.32	1.44	1.38	1.31	1.38	1.42	1.37	1.46	1.39	1.38	1.48	1.39	1.46	1.43
17	1.38	1.33	1.41	1.44	1.37	1.41	1.39	1.41	1.33	1.45	1.40	1.26	1.45	1.33	1.35	1.37	1.36	1.41	1.51
18	1.45	1.36	1.39	1.50	1.42	1.44	1.44	1.36	1.43	1.50	1.58	1.39	1.44	1.36	1.48	1.49	1.50	1.51	1.63
19	1.40	1.43	1.53	1.49	1.47	1.41	1.56	1.50	1.46	1.39	1.43	1.41	1.46	1.51	1.54	1.50	1.39	1.55	1.46
20									1.40	1.41	1.33	1.29	1.22	1.29	1.30	1.29	1.22	1.44	1.33

Table A.3.2 Density values for Fig. A.3.2.

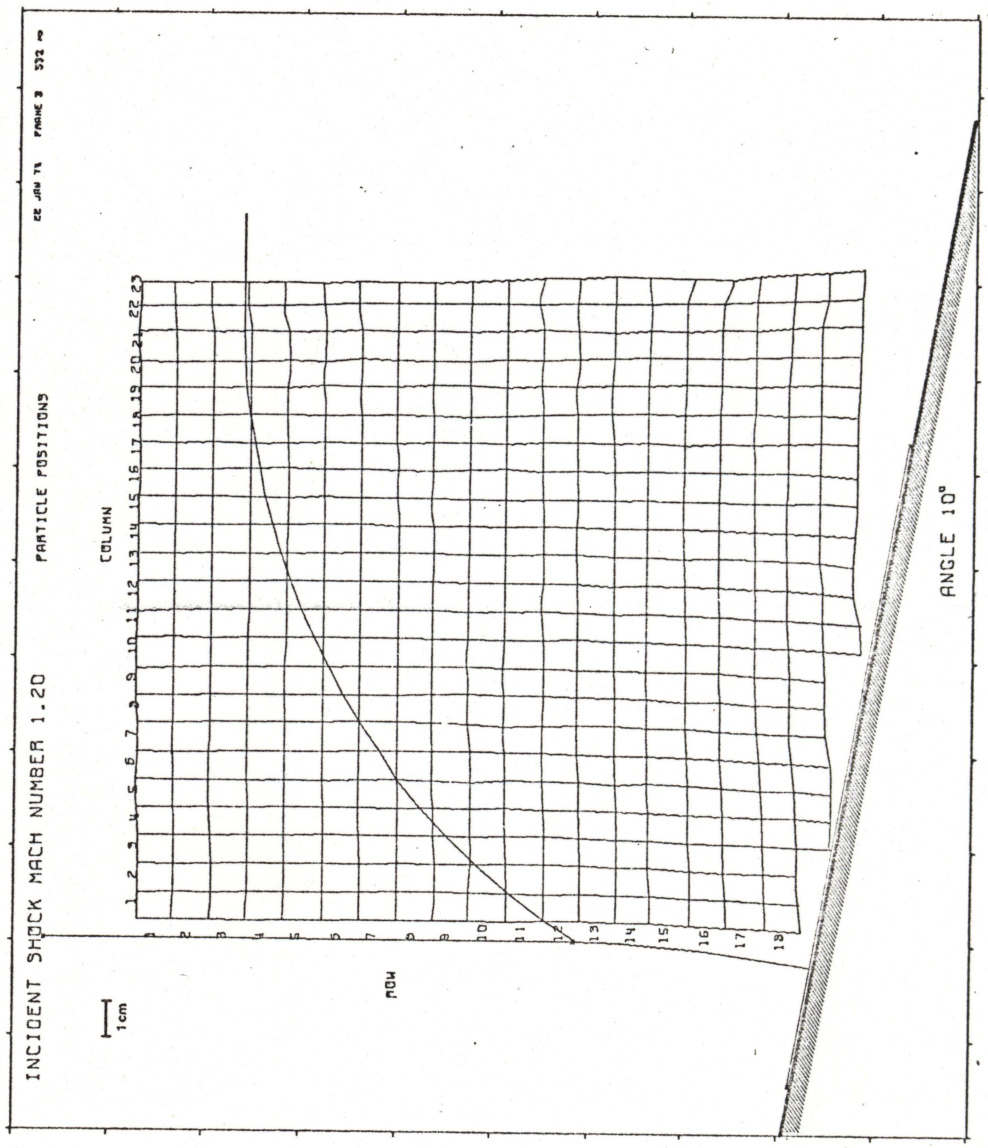

Fig. A.3.3 Tracers at 532 µs.

	COLUMN																						
	1	2	3	5	5	6	7	8	9	10	11	12	13	14	15	16	17	18	19	20	21	22	23
1	1.39	1.33	1.34	1.40	1.39	1.36	1.35	1.40	1.41	1.23	1.38	1.31	1.42	1.30	1.31	1.39	1.50	1.44	1.33	1.58	1.25	1.57	1.31
2	1.39	1.34	1.34	1.33	1.42	1.39	1.29	1.39	1.36	1.29	1.37	1.32	1.36	1.35	1.39	1.40	1.42	1.43	1.36	1.46	1.16	1.41	1.58
3	1.36	1.34	1.41	1.34	1.39	1.27	1.28	1.43	1.41	1.31	1.30	1.31	1.36	1.31	1.33	1.32	1.44	1.37	1.39	1.51	1.28	1.56	1.77
4	1.38	1.36	1.37	1.37	1.39	1.28	1.30	1.38	1.32	1.31	1.36	1.32	1.41	1.33	1.36	1.25	1.48	1.29	1.39	1.43	1.22	1.47	1.68
5	1.23	1.24	1.30	1.33	1.36	1.28	1.27	1.37	1.27	1.25	1.39	1.30	1.36	1.28	1.41	1.40	1.53	1.36	1.32	1.53	1.33	1.37	1.64
6	1.38	1.35	1.33	1.39	1.42	1.31	1.28	1.45	1.38	1.32	1.36	1.37	1.41	1.33	1.40	1.36	1.42	1.36	1.31	1.48	1.34	1.47	1.80
7	1.31	1.35	1.35	1.34	1.28	1.27	1.28	1.47	1.33	1.33	1.37	1.33	1.30	1.38	1.46	1.36	1.51	1.52	1.41	1.46	1.39	1.40	1.77
8	1.33	1.28	1.33	1.38	1.35	1.32	1.33	1.45	1.42	1.42	1.40	1.47	1.37	1.46	1.39	1.49	1.41	1.38	1.30	1.56	1.35	1.43	1.82
9	1.38	1.44	1.43	1.44	1.43	1.28	1.46	1.38	1.45	1.49	1.37	1.35	1.39	1.47	1.38	1.30	1.32	1.44	1.23	1.62	1.31	1.37	1.77
10	1.32	1.33	1.38	1.39	1.45	1.30	1.45	1.25	1.42	1.42	1.42	1.34	1.34	1.40	1.40	1.23	1.49	1.45	1.28	1.43	1.27	1.41	1.74
11	1.39	1.30	1.34	1.40	1.38	1.42	1.41	1.16	1.28	1.27	1.34	1.38	1.31	1.37	1.40	1.34	1.44	1.44	1.40	1.49	1.32	1.59	1.66
12	1.40	1.29	1.37	1.39	1.28	1.29	1.40	1.42	1.53	1.40	1.37	1.39	1.39	1.53	1.51	1.34	1.35	1.42	1.40	1.51	1.33	1.42	1.52
13	1.37	1.34	1.42	1.39	1.45	1.40	1.31	1.36	1.40	1.32	1.46	1.42	1.32	1.36	1.35	1.38	1.39	1.43	1.41	1.40	1.47	1.32	1.37
14	1.53	1.52	1.53	1.49	1.47	1.43	1.42	1.48	1.51	1.49	1.54	1.50	1.45	1.50	1.46	1.46	1.42	1.32	1.38	1.49	1.55	1.45	1.47
15	1.30	1.26	1.31	1.34	1.24	1.33	1.30	1.34	1.24	1.21	1.29	1.30	1.32	1.37	1.36	1.28	1.33	1.25	1.23	1.33	1.39	1.42	1.37
16	1.36	1.42	1.36	1.33	1.31	1.37	1.36	1.38	1.38	1.49	1.40	1.35	1.38	1.35	1.41	1.38	1.46	1.38	1.41	1.57	1.48	1.45	1.63
17	1.35	1.36	1.28	1.33	1.35	1.30	1.37	1.44	1.42	1.40	1.38	1.35	1.33	1.42	1.37	1.29	1.39	1.28	1.35	1.43	1.40	1.41	1.84
18	1.40	1.41	1.41	1.36	1.47	1.42	1.40	1.45	1.36	1.38	1.48	1.40	1.38	1.56	1.48	1.41	1.43	1.44	1.52	1.49	1.46	1.45	1.52
19				1.43	1.42	1.37	1.32	1.46	1.51	1.46	1.51	1.42	1.45	1.60	1.39	1.43	1.40	1.55	1.42	1.57	1.54	1.58	1.52
20											1.23	1.35	1.40	1.38	1.24	1.31	1.15	1.37	1.21	1.27	1.20	1.45	1.46

Table A.3.3 Density values for Fig. A.3.3.

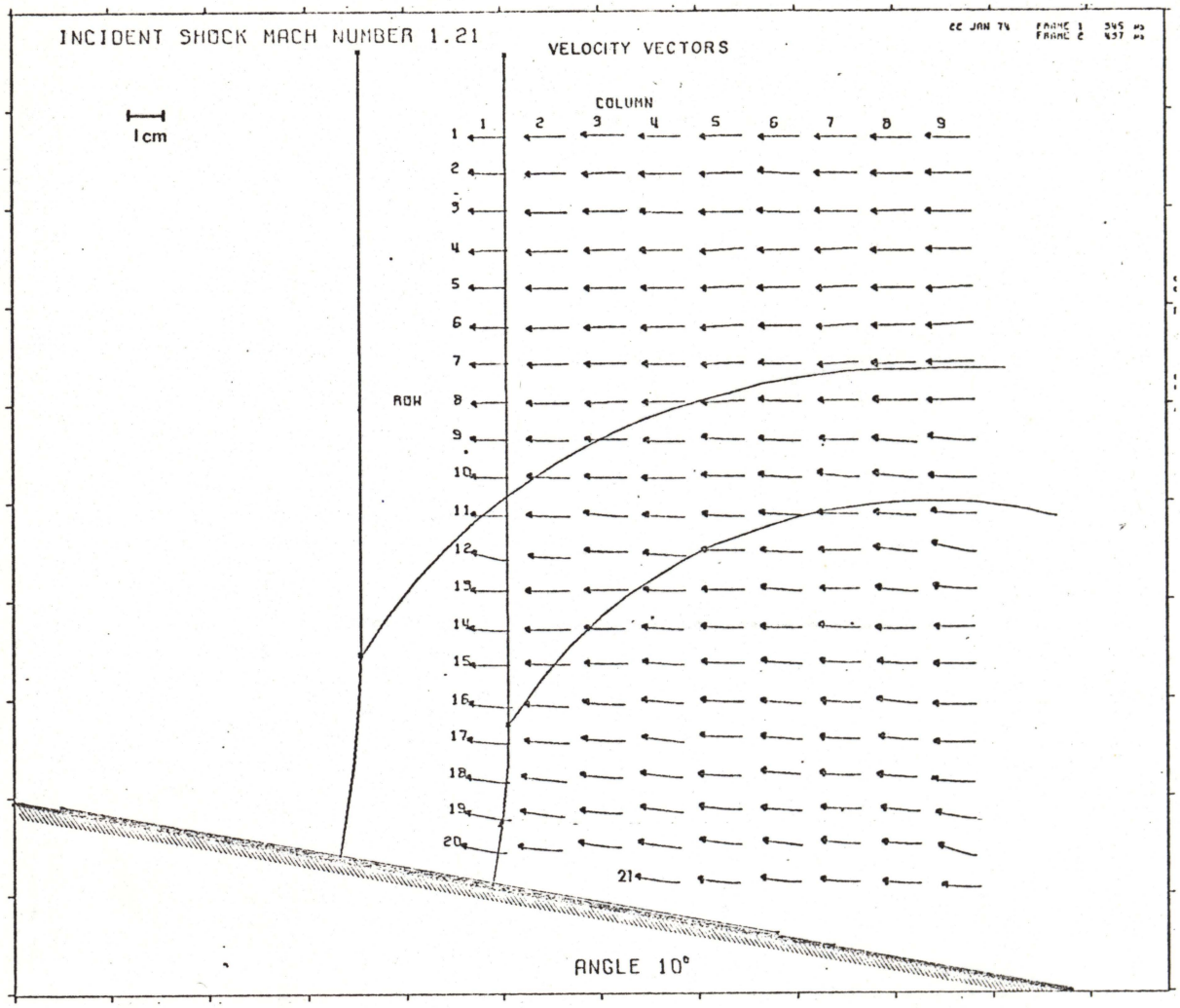

Fig. A.3.4 Velocity vectors 345 - 437 μs.

COLUMN 1 FRAME 1 - 2

ROW	U(M/S)	V(M/S)	VEL	ANGLE
1	100.24	-0.35	100.24	-0.20
2	99.96	4.96	100.08	2.84
3	100.91	1.65	100.92	0.94
4	101.06	-3.41	101.12	-1.93
5	99.94	0.99	99.95	0.57
6	99.81	2.85	99.85	1.64
7	101.62	-0.42	101.62	-0.24
8	99.07	-3.01	99.11	-1.74
9	101.23	5.87	101.40	3.32
10	100.34	5.09	100.47	2.90
11	102.00	5.28	102.14	2.96
12	99.47	22.65	102.01	12.83
13	102.81	1.82	102.88	2.13
14	105.16	8.38	105.49	4.56
15	106.26	1.60	106.27	0.87
16	117.87	12.63	118.54	6.12
17	115.20	12.64	115.89	6.26
18	117.55	17.19	118.80	8.32
19	123.32	22.76	125.41	10.46
20	122.35	23.69	124.62	10.96

COLUMN 2 FRAME 1 - 2

ROW	U(M/S)	V(M/S)	VEL	ANGLE
1	105.66	-0.89	105.66	-0.48
2	104.91	-5.14	105.04	-2.81
3	105.60	-2.36	105.63	-1.29
4	106.01	-4.82	106.02	-2.59
5	107.17	-1.21	107.18	-0.64
6	104.11	-4.51	104.21	-2.39
7	105.45	-4.50	105.55	-2.45
8	107.80	0.06	107.80	0.03
9	106.69	4.46	106.78	2.40
10	110.12	3.66	110.19	2.01
11	110.06	3.98	110.13	2.07
12	107.35	4.87	107.46	2.60
13	114.35	1.80	114.38	0.90
14	116.97	0.30	116.97	0.15
15	114.16	3.76	114.22	1.89
16	113.58	6.49	114.16	3.26
17	116.48	7.58	116.72	3.72
18	117.88	13.83	119.68	6.69
19	115.10	16.42	116.27	8.12
20	113.97	14.83	116.92	7.29

COLUMN 3 FRAME 1 - 2

ROW	U(M/S)	V(M/S)	VEL	ANGLE
1	112.59	3.83	112.65	1.95
2	111.99	-3.88	112.05	-1.98
3	108.20	2.15	108.22	1.14
4	107.49	-2.95	107.53	-1.57
5	109.08	-1.03	109.09	-0.54
6	107.39	-3.58	107.45	-1.91
7	109.82	-0.75	109.82	-0.39
8	110.77	-4.06	110.84	-2.10
9	109.54	2.94	109.58	1.54
10	112.04	4.04	112.11	2.06
11	114.24	12.06	114.87	6.03
12	114.40	6.98	114.61	3.49
13	115.52	-0.66	115.53	-0.33
14	108.31	4.36	108.39	2.31
15	112.61	3.79	112.68	1.93
16	107.99	8.93	108.36	4.72
17	111.35	10.05	111.80	5.16
18	110.42	10.12	110.88	5.24
19	110.28	11.97	110.92	6.19
20	110.07	15.53	111.16	8.03

COLUMN 4 FRAME 1 - 2

ROW	U(M/S)	V(M/S)	VEL	ANGLE
1	106.78	1.94	106.79	1.04
2	108.67	-3.06	108.71	-1.61
3	109.25	2.29	109.27	1.20
4	107.63	-1.99	107.65	-1.06
5	108.40	-0.97	108.40	-0.51
6	111.08	-4.20	111.15	-2.16
7	107.44	-1.63	107.45	-0.87
8	108.35	-4.07	108.43	-2.15
9	105.43	2.00	105.45	1.09
10	111.57	-1.09	111.58	-0.56
11	107.75	5.81	107.91	3.09
12	110.25	6.91	110.46	3.58
13	108.56	4.35	108.65	2.29
14	106.65	6.99	106.88	3.75
15	106.55	7.96	106.85	4.27
16	105.58	8.91	105.95	4.82
17	107.93	14.30	107.98	7.61
18	107.11	10.94	107.66	5.83
19	109.50	14.63	110.47	7.61
20	111.12	15.67	112.22	8.03
21	115.27	18.56	116.76	9.15

COLUMN 5 FRAME 1 - 2

ROW	U(M/S)	V(M/S)	VEL	ANGLE
1	105.45	-3.22	105.50	-1.75
2	106.25	-3.07	106.30	-1.65
3	108.71	-1.10	108.72	-0.58
4	108.11	-8.81	108.47	-4.66
5	106.17	-5.30	106.30	-2.86
6	108.77	-6.80	108.98	-3.58
7	106.94	-5.89	107.10	-3.15
8	108.57	-4.34	108.68	-2.55
9	106.22	8.19	106.54	4.41
10	107.14	5.75	107.29	3.07
11	104.36	8.36	104.69	4.58
12	107.94	4.29	108.03	2.27
13	106.14	4.34	106.23	2.34
14	106.87	6.22	107.05	3.33
15	106.88	4.60	106.98	2.47
16	107.61	6.49	107.80	3.45
17	107.54	6.60	107.74	3.51
18	107.47	6.72	107.68	3.58
19	107.19	12.02	107.86	6.40
20	105.26	15.51	106.39	8.39
21	106.99	13.98	107.90	7.44

COLUMN 6 FRAME 1 - 2

ROW	U(M/S)	V(M/S)	VEL	ANGLE
1	106.35	0.38	106.35	0.21
2	107.77	6.63	107.97	3.52
3	110.44	3.39	110.49	1.76
4	107.20	-3.56	107.26	-1.90
5	109.77	-4.19	109.85	-2.19
6	109.64	-2.34	109.66	-1.22
7	109.42	1.24	109.43	0.65
8	110.95	4.89	111.05	2.52
9	109.97	5.84	110.13	3.04
10	112.47	6.93	112.69	3.53
11	109.02	5.17	109.14	2.72
12	108.05	6.12	108.22	3.24
13	108.67	10.61	109.19	5.57
14	106.37	1.96	106.39	1.05
15	106.09	7.26	106.34	3.92
16	105.15	7.35	105.41	4.00
17	107.62	9.30	108.02	4.94
18	101.53	8.29	101.87	4.67
19	105.87	6.86	106.09	3.70
20	102.09	12.88	102.90	7.19
21	104.58	13.97	105.51	7.61

COLUMN 7 FRAME 1 - 2

ROW	U(M/S)	V(M/S)	VEL	ANGLE
1	107.47	-1.21	107.48	-0.65
2	110.84	-0.09	110.84	-0.05
3	109.00	0.83	109.00	0.43
4	108.33	-5.15	108.45	-2.72
5	106.53	-5.11	106.65	-2.74
6	106.50	-5.85	106.66	-3.14
7	104.78	-7.54	105.05	-4.11
8	103.56	-6.53	103.56	-3.29
9	98.94	4.60	99.05	2.66
10	108.07	12.01	108.84	6.31
11	104.91	4.22	104.99	2.31
12	106.65	2.69	106.69	1.44
13	103.95	3.56	104.01	1.96
14	108.03	8.19	108.34	4.34
15	104.51	8.16	104.83	4.45
16	102.67	9.07	103.07	5.05
17	102.61	9.19	103.02	5.12
18	104.35	7.64	104.63	4.19
19	101.73	6.78	101.96	3.81
20	100.69	9.44	101.14	5.36
21	99.76	9.53	100.21	5.46

COLUMN 8 FRAME 1 - 2

ROW	U(M/S)	V(M/S)	VEL	ANGLE
1	104.90	2.24	104.93	1.22
2	104.99	-1.11	104.99	-0.61
3	105.11	-5.32	105.24	-2.90
4	110.12	-2.38	110.15	-1.24
5	108.49	-4.07	108.48	-2.15
6	110.93	-3.84	111.00	-1.98
7	110.98	-6.31	111.16	-3.29
8	112.54	-3.93	112.60	-1.90
9	113.69	8.79	114.03	4.42
10	112.73	9.73	113.14	4.93
11	106.78	5.26	106.91	2.82
12	108.16	12.38	108.86	6.53
13	106.43	10.70	106.97	5.74
14	105.71	1.04	105.71	0.59
15	98.70	6.27	98.90	3.63
16	100.18	10.79	100.76	6.15
17	97.63	8.20	97.97	4.80
18	98.50	6.62	98.72	3.85
19	98.30	10.20	98.83	5.92
20	97.53	6.91	97.77	3.99
21	98.49	9.49	98.95	5.52

COLUMN 9 FRAME 1 - 2

ROW	U(M/S)	V(M/S)	VEL	ANGLE
1	115.32	6.24	115.49	3.10
2	118.08	1.27	118.09	0.62
3	118.01	1.39	118.02	0.67
4	117.23	-1.99	117.25	-0.97
5	119.94	-6.09	120.10	-2.91
6	121.65	-6.76	121.84	-3.18
7	123.93	-0.48	123.93	-0.22
8	124.76	-1.19	124.77	-0.54
9	125.02	11.95	125.59	5.46
10	125.25	5.15	125.35	2.39
11	118.11	8.44	118.41	4.09
12	116.49	24.96	119.13	12.10
13	110.87	12.71	111.60	6.54
14	105.22	1.32	105.23	0.72
15	108.66	0.72	108.66	0.38
16	111.94	3.59	112.00	1.84
17	107.62	1.79	107.63	0.95
18	108.91	10.64	109.43	5.58
19	104.16	19.23	105.92	10.46
20	95.83	30.27	100.50	17.53
21	98.51	7.08	98.76	4.11

Table A.3.4 Velocity values for Fig. A.3.4.

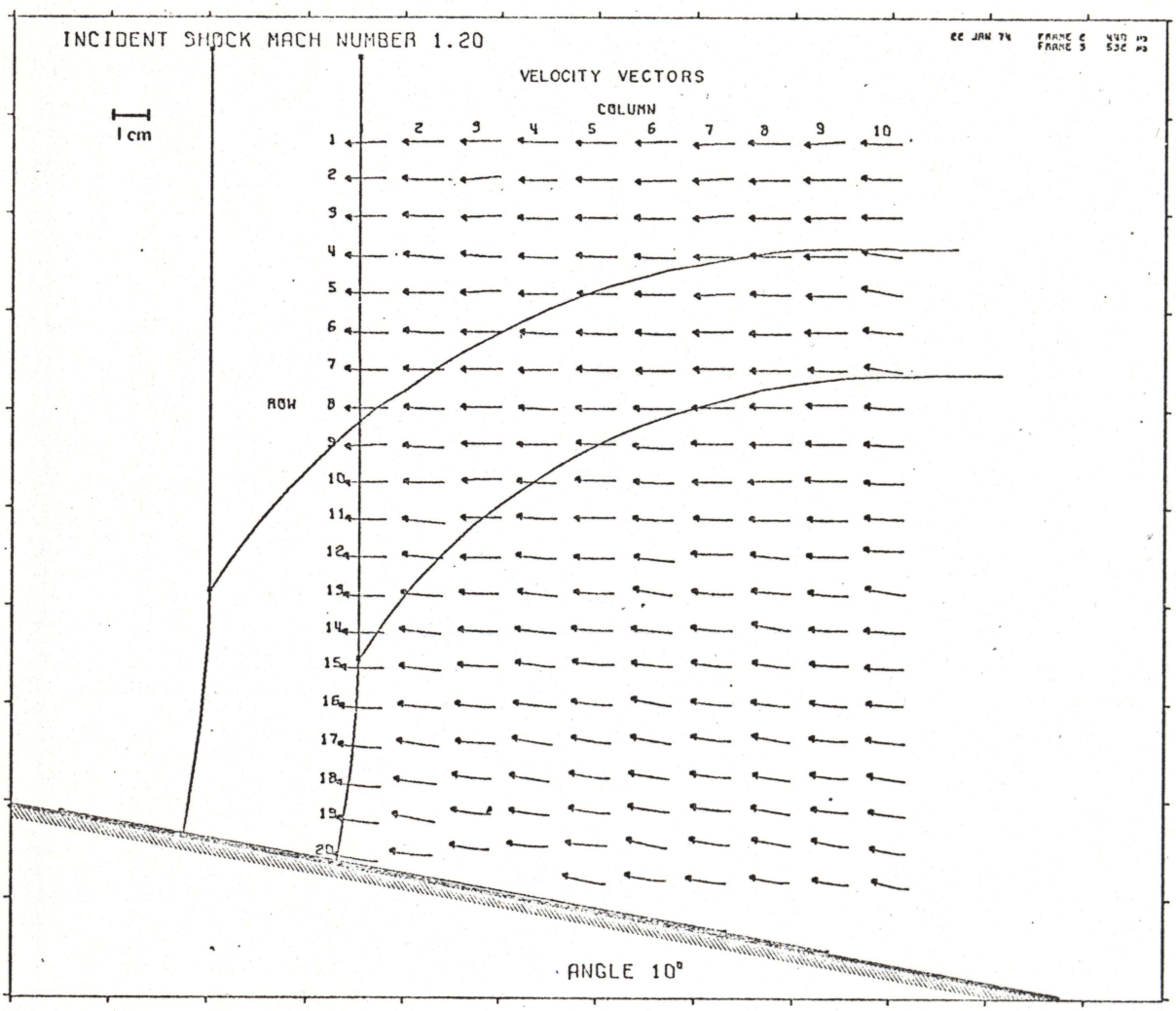

Fig. A.3.5 Velocity vectors 437 - 532 μs.

COLUMN 1 — FRAME 2 - 3

ROW	U(M/S)	V(M/S)	VEL	ANGLE
1	105.07	-3.67	105.14	-2.00
2	104.76	-1.25	104.97	-0.68
3	105.86	-2.26	105.88	-1.22
4	109.03	4.62	109.12	2.43
5	112.48	4.59	112.58	2.34
6	110.68	6.06	110.85	3.13
7	109.85	4.98	109.96	2.60
8	111.76	6.53	111.76	0.27
9	109.38	-4.95	109.49	-2.59
10	113.56	-1.48	113.57	-0.75
11	106.37	4.11	106.45	2.21
12	112.48	3.32	112.52	1.69
13	108.04	5.55	108.18	2.94
14	108.94	4.54	109.03	2.39
15	110.64	5.31	110.76	2.75
16	111.36	8.62	111.70	4.43
17	112.92	12.84	113.64	6.49
18	114.61	13.59	115.42	6.76
19	109.31	19.79	110.44	8.22
20	116.06	20.23	117.81	9.89

COLUMN 2 — FRAME 2 - 3

ROW	U(M/S)	V(M/S)	VEL	ANGLE
1	104.68	-1.06	104.69	-0.58
2	106.20	4.03	106.27	2.17
3	104.50	2.91	104.54	1.60
4	104.23	8.78	104.60	4.81
5	103.69	0.77	103.70	0.43
6	105.20	5.85	105.37	3.18
7	104.52	1.30	104.53	0.72
8	102.67	3.64	102.74	2.03
9	105.27	3.57	105.33	1.94
10	104.47	1.63	104.48	0.89
11	110.17	10.36	110.65	5.37
12	105.34	10.00	105.31	5.40
13	107.65	8.16	107.95	4.33
14	107.47	12.31	108.17	6.53
15	109.20	12.21	109.88	6.38
16	110.17	9.45	110.53	4.91
17	109.96	14.48	110.91	7.50
18	111.81	11.77	112.43	6.01
19	110.62	19.35	112.30	9.92
20	109.98	13.94	110.86	7.22

COLUMN 3 — FRAME 2 - 3

ROW	U(M/S)	V(M/S)	VEL	ANGLE
1	106.17	-1.85	106.19	-1.00
2	106.53	-10.69	107.07	-5.73
3	104.54	-4.89	104.65	-2.68
4	107.45	8.07	107.76	4.23
5	108.03	-5.57	108.20	-3.16
6	107.81	-0.97	107.81	-0.51
7	108.67	-1.11	108.68	-0.59
8	107.70	1.27	107.70	0.67
9	104.26	0.08	104.26	0.04
10	102.64	-2.77	102.67	-1.54
11	106.78	1.57	106.80	0.84
12	104.11	2.99	104.16	1.65
13	103.14	5.39	103.28	2.99
14	103.94	6.97	104.17	3.84
15	104.80	6.84	105.03	3.74
16	108.09	11.13	108.65	5.88
17	103.91	7.30	104.16	4.02
18	104.53	13.24	105.37	7.22
19	105.36	13.57	106.28	7.55
20	105.33	14.66	106.35	7.93

COLUMN 4 — FRAME 2 - 3

ROW	U(M/S)	V(M/S)	VEL	ANGLE
1	101.19	6.63	101.41	3.75
2	97.22	-2.40	97.25	-1.41
3	102.31	0.24	102.31	0.13
4	99.60	2.54	99.63	1.46
5	101.43	-0.17	101.43	-0.09
6	97.71	5.56	97.87	3.26
7	101.50	-2.27	101.53	-1.28
8	100.38	3.58	100.44	2.04
9	102.26	0.01	102.26	0.01
10	102.07	4.16	102.16	2.33
11	103.73	5.79	103.89	3.20
12	105.28	10.01	105.75	5.43
13	102.64	10.59	103.18	5.89
14	105.24	10.52	105.76	5.71
15	104.19	12.65	104.99	6.59
16	112.17	10.45	112.65	5.32
17	104.92	17.78	106.41	9.62
18	104.16	16.73	105.43	9.11
19	105.07	18.97	107.00	7.57
20	100.88	12.15	101.57	6.49

COLUMN 5 — FRAME 2 - 3

ROW	U(M/S)	V(M/S)	VEL	ANGLE
1	103.84	-1.05	103.84	-0.58
2	104.55	2.27	104.58	1.24
3	104.59	1.22	104.59	0.67
4	101.80	5.25	101.94	2.95
5	100.21	1.33	100.22	0.83
6	101.00	3.11	101.05	1.76
7	101.83	3.84	101.90	2.16
8	101.85	2.79	101.90	1.57
9	101.72	6.08	101.90	3.42
10	103.52	4.24	103.61	2.35
11	104.53	0.63	104.53	0.35
12	100.85	5.49	101.00	3.12
13	102.54	6.26	102.73	3.50
14	104.21	7.39	104.51	4.33
15	105.79	11.26	106.38	6.03
16	104.85	12.77	105.62	6.94
17	99.47	16.70	100.87	9.53
18	102.94	16.68	104.28	9.20
19	100.41	16.65	107.70	8.89
20	104.91	11.22	105.50	6.10
21	109.60	23.39	112.07	12.05

COLUMN 6 — FRAME 2 - 3

ROW	U(M/S)	V(M/S)	VEL	ANGLE
1	104.45	-1.86	104.47	-1.03
2	103.73	-5.56	103.88	-3.07
3	103.48	0.32	103.48	0.18
4	102.46	3.55	102.52	1.99
5	100.83	0.71	100.84	0.40
6	100.65	4.85	100.76	2.76
7	99.16	-1.47	99.17	-0.85
8	105.12	1.20	105.13	0.66
9	102.34	5.24	102.48	2.93
10	101.51	4.17	101.59	2.35
11	102.34	4.89	102.46	2.74
12	102.64	11.63	102.70	6.50
13	99.26	15.66	100.49	8.98
14	104.71	9.66	105.16	5.27
15	103.81	10.32	104.32	5.68
16	101.75	17.87	103.31	9.96
17	101.75	17.69	103.27	9.86
18	103.60	14.39	104.67	8.23
19	105.16	15.80	107.33	8.47
20	103.24	23.32	105.84	12.73
21	105.19	18.03	106.72	9.72

COLUMN 7 — FRAME 2 - 3

ROW	U(M/S)	V(M/S)	VEL	ANGLE
1	102.52	-3.59	102.58	-2.05
2	101.69	-4.76	101.80	-2.68
3	100.10	-8.48	100.46	-4.84
4	98.93	-1.78	98.95	-1.03
5	100.01	-7.13	100.27	-4.08
6	100.63	-1.21	100.63	-0.69
7	101.49	-1.35	101.49	-0.76
8	106.65	-0.45	106.65	-0.24
9	105.56	4.54	105.66	2.46
10	97.91	0.96	97.91	0.33
11	97.65	6.44	97.86	3.78
12	102.96	3.90	103.03	2.17
13	103.56	9.81	104.02	5.41
14	104.43	9.67	104.88	5.29
15	100.78	13.68	101.70	7.73
16	101.72	11.80	102.40	6.62
17	99.87	14.16	100.87	8.07
18	101.71	11.45	102.36	6.42
19	100.74	13.85	101.68	7.83
20	100.63	16.29	101.94	9.20
21	100.72	14.37	101.74	8.12

COLUMN 8 — FRAME 2 - 3

ROW	U(M/S)	V(M/S)	VEL	ANGLE
1	105.42	3.46	105.48	1.88
2	103.11	-3.82	103.18	-2.12
3	105.60	-1.30	105.60	-0.70
4	104.54	2.81	104.58	1.54
5	104.57	1.76	104.59	0.97
6	107.21	3.91	107.21	2.09
7	103.85	-2.11	103.87	-1.16
8	106.26	2.16	106.28	1.16
9	106.44	-3.35	106.47	-1.80
10	110.84	-4.38	110.92	-2.11
11	104.45	3.27	104.50	1.80
12	98.96	9.81	99.44	5.66
13	101.69	6.28	101.88	3.53
14	100.35	17.33	101.83	9.80
15	95.33	12.60	96.16	7.53
16	98.83	11.69	99.52	6.75
17	96.05	15.75	97.33	9.31
18	96.98	13.87	97.97	8.14
19	101.17	17.35	102.64	9.73
20	100.33	16.29	101.65	9.22
21	102.00	17.91	103.56	9.96

COLUMN 9 — FRAME 2 - 3

ROW	U(M/S)	V(M/S)	VEL	ANGLE
1	105.59	-7.00	105.82	-3.79
2	108.83	-1.83	108.85	-0.96
3	106.30	-3.86	106.37	-2.08
4	111.31	0.51	111.31	0.25
5	105.31	-1.67	105.33	-0.91
6	109.50	1.80	109.51	0.94
7	102.37	5.65	102.53	3.15
8	106.13	-1.29	106.14	-0.70
9	105.01	4.55	105.11	2.48
10	106.74	4.44	106.83	2.38
11	104.02	6.74	104.24	3.71
12	106.69	4.94	106.81	2.65
13	104.66	11.61	105.30	6.33
14	97.91	6.82	98.15	3.98
15	99.56	8.46	99.92	4.85
16	96.82	11.62	97.51	6.84
17	99.49	9.83	99.97	5.64
18	99.33	13.12	100.20	7.52
19	95.03	11.90	95.78	7.14
20	95.57	19.57	97.55	11.57
21	93.15	14.95	94.34	9.12

COLUMN 10 — FRAME 2 - 3

ROW	U(M/S)	V(M/S)	VEL	ANGLE
1	106.53	5.21	106.66	2.80
2	103.97	4.06	104.05	2.24
3	104.94	1.31	104.95	0.72
4	105.29	13.30	106.13	7.20
5	106.76	19.25	108.45	10.22
6	102.87	8.48	103.22	4.71
7	100.01	14.26	101.02	8.11
8	101.19	6.31	101.39	3.57
9	102.19	5.30	102.23	2.97
10	101.30	3.35	101.35	1.90
11	100.35	4.01	100.47	2.29
12	102.09	4.80	102.20	2.69
13	105.07	16.00	106.28	8.56
14	107.16	7.22	107.40	3.85
15	101.21	4.19	101.29	2.37
16	94.99	7.22	95.27	4.35
17	100.04	10.73	100.61	6.12
18	97.29	13.91	98.28	8.14
19	96.45	12.83	97.30	7.58
20	92.00	15.07	93.23	9.30
21	96.86	22.91	99.53	13.21

Table A.3.5 Velocity values for Fig. A.3.5.

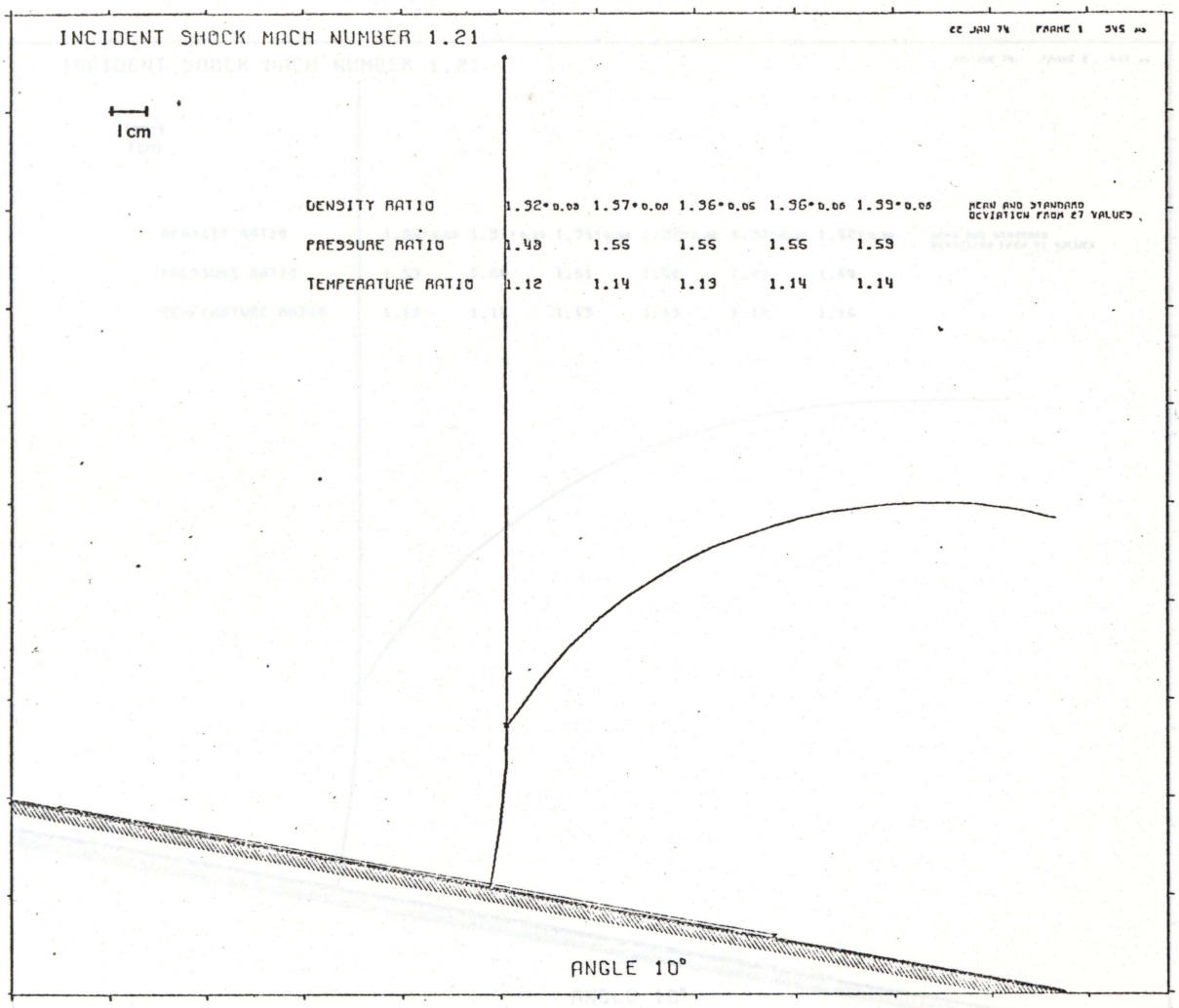

Fig. A.3.6 Mean ratios 345 µs.

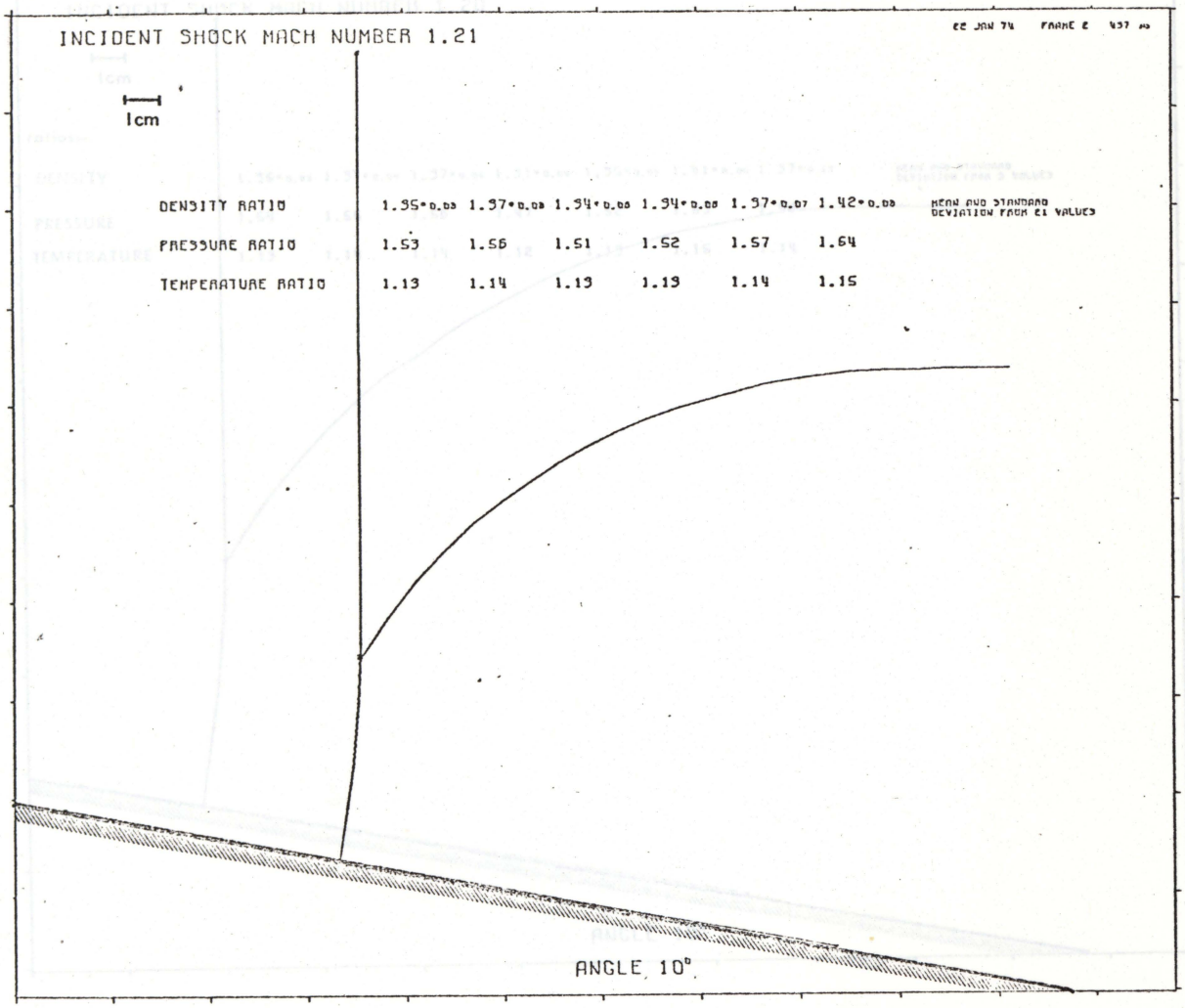

Fig. A.3.7 Mean ratios 437 μs.

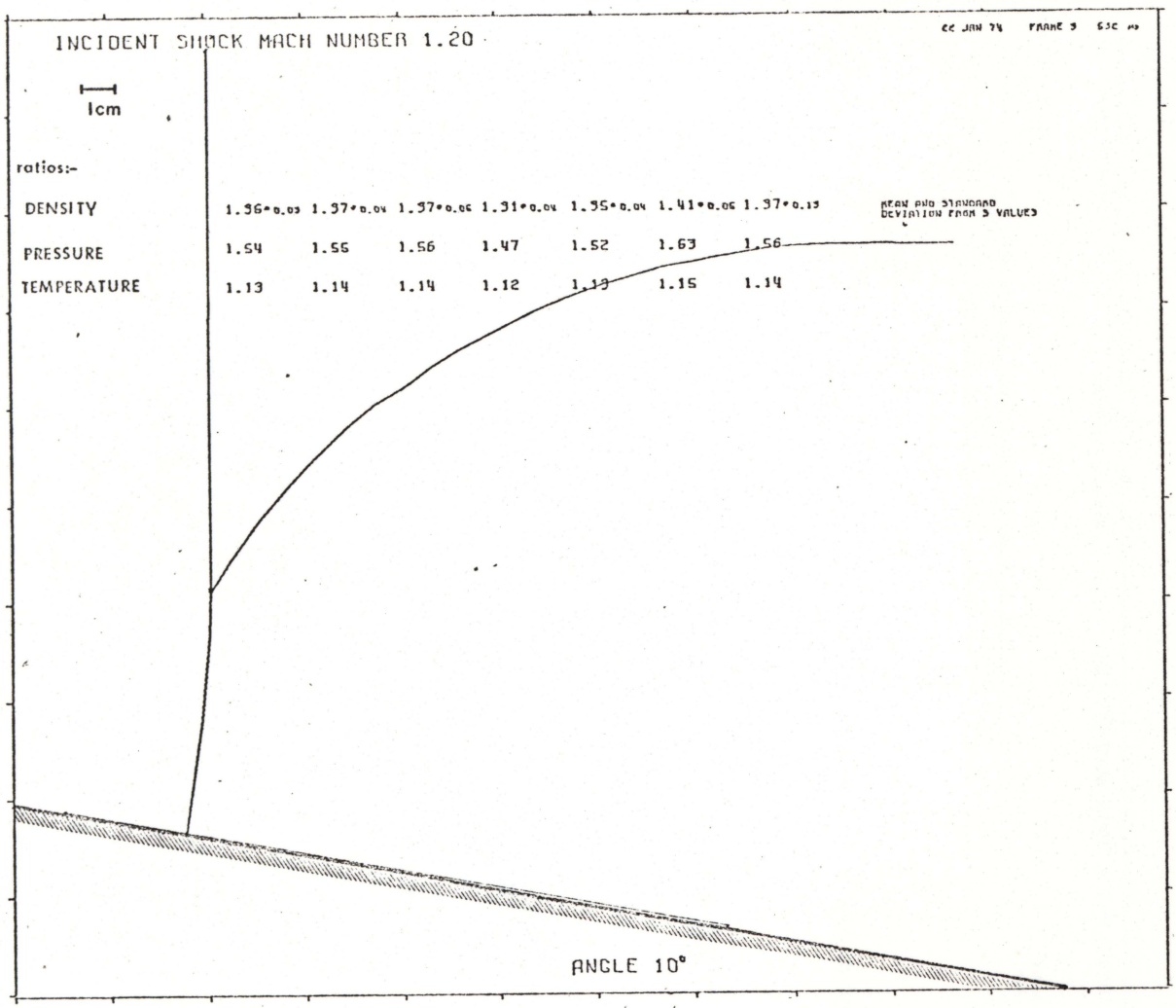

Fig. A.3.8 Mean ratios 532 μs.

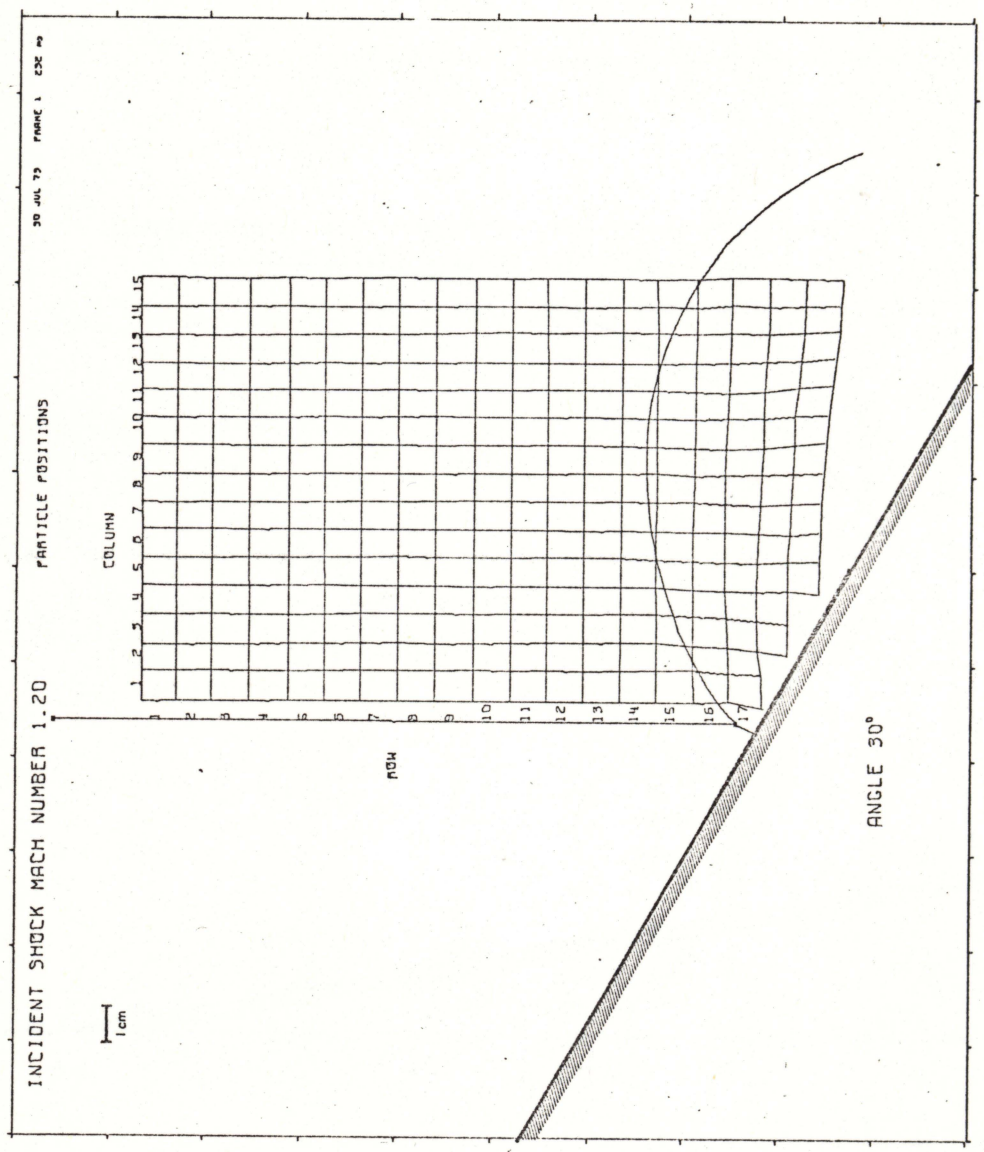

Fig. A.4.1 Tracers at 232 μs.

	COLUMN														
	1	2	3	5	5	6	7	8	9	10	11	12	13	14	15
1	1.29	1.53	1.30	1.33	1.43	1.35	1.50	1.39	1.30	1.39	1.38	1.45	1.33	1.33	1.28
2	1.29	1.52	1.32	1.37	1.41	1.34	1.46	1.39	1.32	1.39	1.39	1.44	1.35	1.37	1.33
3	1.23	1.44	1.27	1.28	1.34	1.34	1.41	1.36	1.28	1.35	1.41	1.47	1.34	1.33	1.37
4	1.16	1.29	1.21	1.23	1.29	1.28	1.34	1.29	1.27	1.27	1.32	1.38	1.26	1.28	1.32
5	1.25	1.39	1.31	1.29	1.33	1.34	1.37	1.29	1.33	1.32	1.37	1.40	1.29	1.33	1.31
6	1.29	1.46	1.32	1.36	1.38	1.42	1.42	1.39	1.38	1.37	1.44	1.45	1.35	1.47	1.36
7	1.23	1.37	1.29	1.38	1.30	1.39	1.36	1.37	1.29	1.33	1.41	1.40	1.28	1.40	1.29
8	1.24	1.42	1.30	1.39	1.32	1.41	1.35	1.38	1.34	1.33	1.42	1.43	1.32	1.42	1.33
9	1.22	1.42	1.27	1.38	1.33	1.35	1.31	1.40	1.32	1.29	1.39	1.34	1.22	1.38	1.27
10	1.19	1.37	1.29	1.33	1.28	1.32	1.26	1.36	1.33	1.36	1.37	1.36	1.23	1.45	1.36
11	1.28	1.43	1.37	1.43	1.42	1.46	1.38	1.44	1.34	1.35	1.41	1.44	1.29	1.54	1.42
12	1.23	1.36	1.35	1.38	1.33	1.42	1.33	1.36	1.33	1.37	1.39	1.43	1.25	1.52	1.34
13	1.25	1.39	1.36	1.37	1.32	1.42	1.31	1.36	1.38	1.37	1.41	1.42	1.24	1.49	1.28
14	1.20	1.33	1.33	1.44	1.45	1.40	1.32	1.37	1.45	1.38	1.39	1.45	1.27	1.60	1.51
15	1.13	1.46	1.32	1.33	1.31	1.33	1.35	1.41	1.35	1.26	1.32	1.37	1.20	1.33	1.21
16	1.33	1.59	1.41	1.67	1.55	1.45	1.43	1.57	1.55	1.38	1.52	1.30	1.27	1.44	1.37
17	1.34	1.71	1.49	1.58	1.51	1.43	1.42	1.36	1.49	1.33	1.61	1.37	1.40	1.40	1.34
18			1.50	1.41	1.52	1.55	1.41	1.40	1.52	1.42	1.48	1.33	1.37	1.42	1.36
19					1.52	1.67	1.64	1.63	1.62	1.58	1.50	1.61	1.56	1.63	1.53

Table A.4.1 Density values for Fig. A.4.1

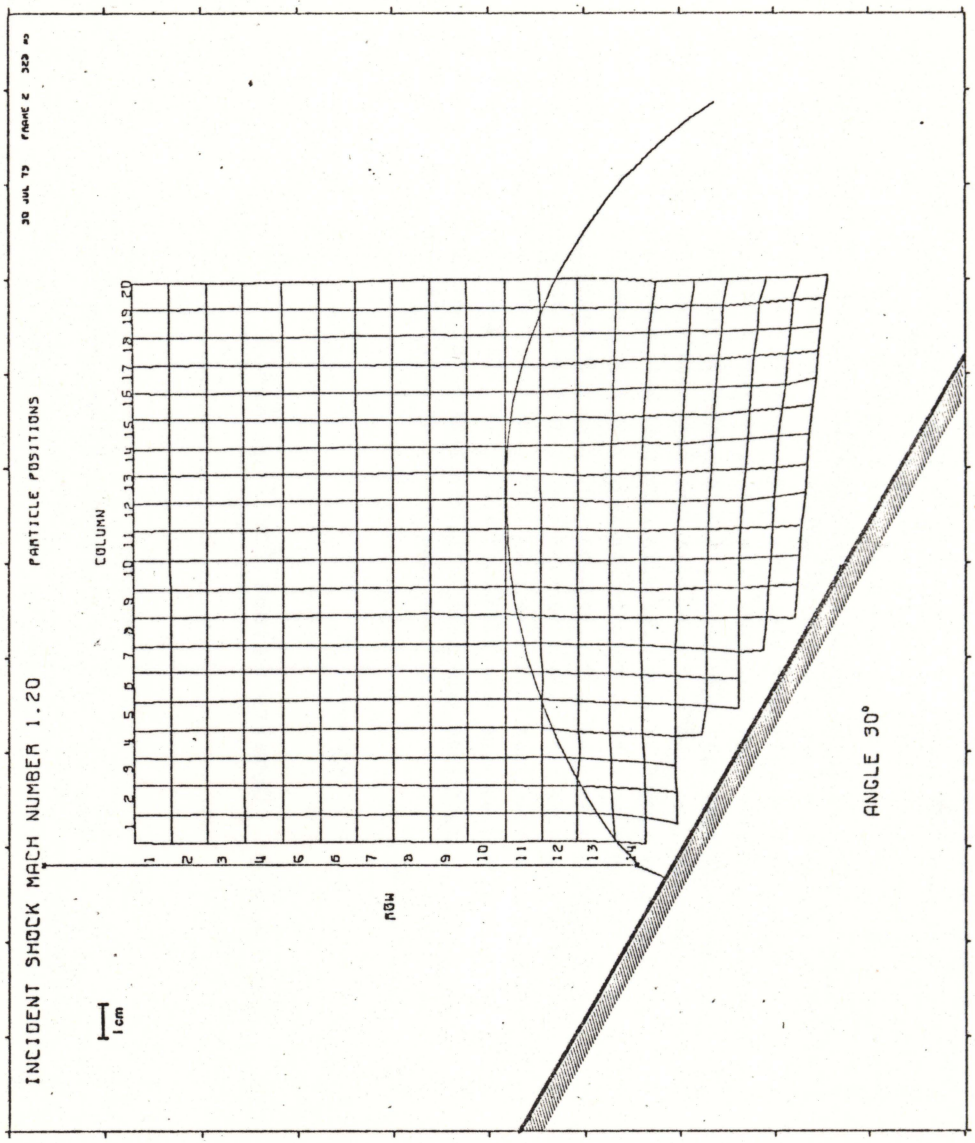

Fig. A.4.2 Tracers at 328 µs.

	COLUMN																			
	1	2	3	5	5	6	7	8	9	10	11	12	13	14	15	16	17	18	19	20
1	1.31	1.25	1.38	1.32	1.29	1.25	1.44	1.29	1.31	1.29	1.28	1.39	1.40	1.47	1.26	1.44	1.34	1.34	1.31	1.42
2	1.40	1.37	1.50	1.41	1.37	1.33	1.51	1.39	1.45	1.35	1.29	1.42	1.41	1.51	1.33	1.47	1.37	1.39	1.34	1.47
3	1.30	1.25	1.36	1.31	1.29	1.31	1.44	1.31	1.40	1.33	1.26	1.37	1.38	1.48	1.31	1.39	1.34	1.35	1.34	1.50
4	1.35	1.25	1.33	1.26	1.22	1.24	1.34	1.23	1.30	1.25	1.20	1.25	1.33	1.39	1.26	1.34	1.32	1.30	1.29	1.40
5	1.31	1.26	1.38	1.27	1.28	1.26	1.40	1.28	1.37	1.30	1.24	1.33	1.36	1.44	1.39	1.39	1.33	1.33	1.32	1.33
6	1.39	1.35	1.43	1.31	1.38	1.39	1.44	1.30	1.46	1.42	1.29	1.38	1.44	1.47	1.43	1.43	1.42	1.35	1.45	1.42
7	1.43	1.35	1.43	1.31	1.31	1.35	1.40	1.30	1.44	1.36	1.24	1.31	1.40	1.45	1.39	1.37	1.35	1.28	1.41	1.31
8	1.32	1.30	1.36	1.28	1.30	1.35	1.41	1.29	1.45	1.38	1.29	1.30	1.40	1.51	1.38	1.37	1.37	1.30	1.45	1.31
9	1.34	1.36	1.36	1.27	1.34	1.35	1.36	1.26	1.38	1.37	1.27	1.26	1.38	1.44	1.34	1.35	1.31	1.23	1.38	1.27
10	1.28	1.30	1.29	1.23	1.30	1.34	1.33	1.29	1.35	1.36	1.22	1.25	1.45	1.42	1.38	1.35	1.33	1.25	1.41	1.32
11	1.36	1.42	1.37	1.30	1.36	1.35	1.33	1.42	1.43	1.50	1.30	1.31	1.51	1.47	1.51	1.46	1.45	1.32	1.43	1.37
12	1.39	1.46	1.37	1.37	1.33	1.46	1.39	1.39	1.35	1.43	1.26	1.29	1.51	1.31	1.32	1.36	1.38	1.27	1.45	1.35
13	1.31	1.48	1.54	1.62	1.39	1.56	1.54	1.63	1.52	1.60	1.46	1.51	1.61	1.43	1.58	1.50	1.44	1.37	1.45	1.22
14	1.69	1.61	1.63	1.60	1.43	1.49	1.51	1.65	1.58	1.56	1.48	1.56	1.59	1.37	1.60	1.44	1.39	1.43	1.47	1.29
15		1.44	1.63	1.48	1.34	1.45	1.39	1.41	1.42	1.30	1.33	1.35	1.30	1.26	1.38	1.39	1.35	1.36	1.52	1.50
16					1.49	1.48	1.44	1.37	1.46	1.49	1.43	1.49	1.46	1.44	1.51	1.48	1.44	1.46	1.53	1.51
17						1.58	1.63	1.41	1.52	1.55	1.55	1.60	1.45	1.44	1.57	1.55	1.44	1.59	1.54	1.56
18								1.46	1.49	1.45	1.36	1.43	1.36	1.38	1.49	1.61	1.25	1.52	1.36	1.63
19									1.59	1.77	1.76	1.60	1.63	1.57	1.70	1.97	1.71	2.05	1.77	2.27

Table A.4.2 Density values for Fig. A.4.2.

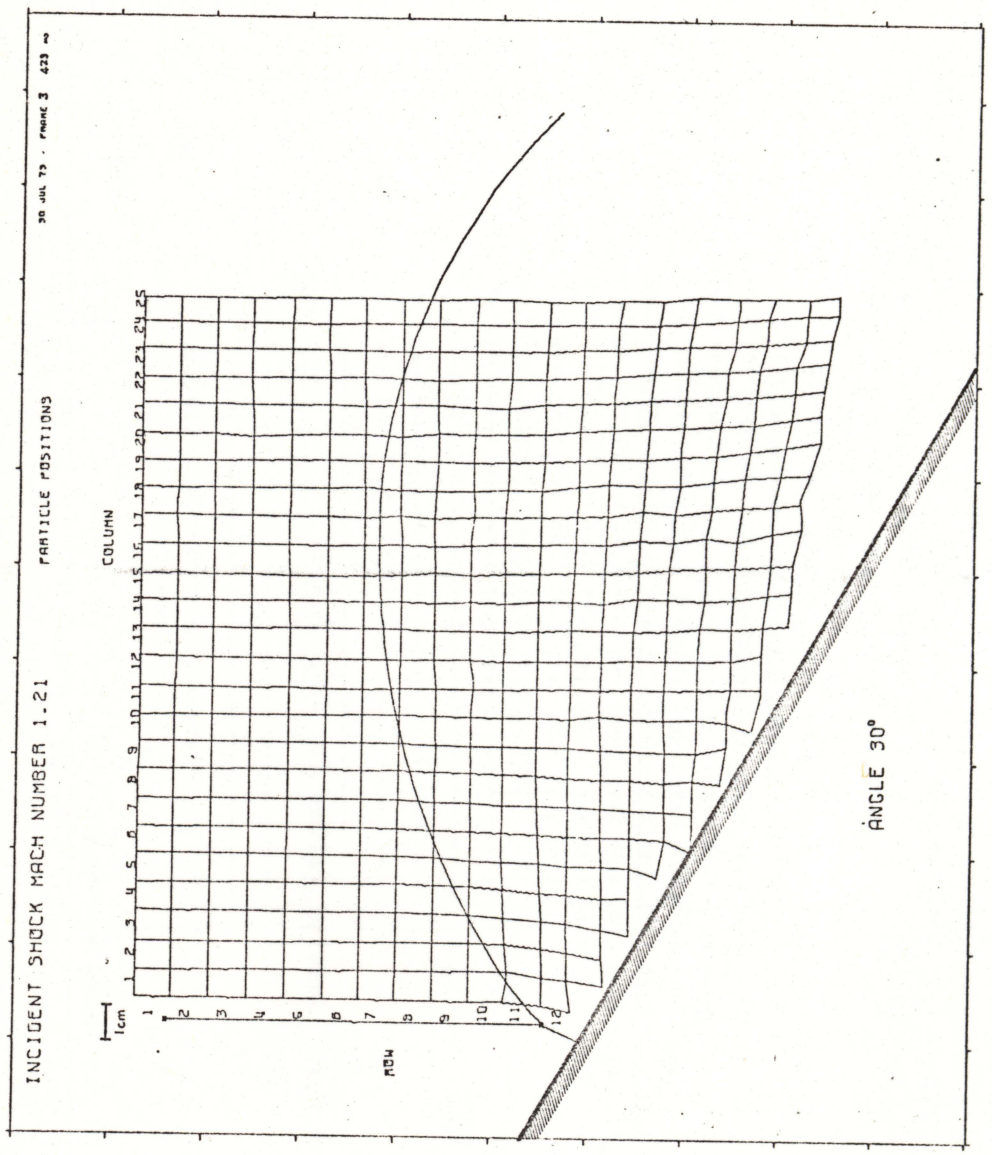

Fig. A.4.3 Tracers at 423 µs.

	COLUMN																								
	1	2	3	5	5	6	7	8	9	10	11	12	13	14	15	16	17	18	19	20	21	22	23	24	25
1	1.41	1.36	1.23	1.41	1.28	1.45	1.36	1.29	1.40	1.50	1.36	1.32	1.31	1.43	1.49	1.32	1.38	1.47	1.40	1.43	1.24	1.48	1.27	1.47	1.58
2	1.34	1.35	1.24	1.36	1.27	1.43	1.33	1.28	1.35	1.38	1.38	1.33	1.33	1.49	1.47	1.32	1.28	1.40	1.47	1.44	1.27	1.52	1.33	1.45	1.53
3	1.28	1.32	1.17	1.29	1.25	1.37	1.30	1.27	1.32	1.38	1.35	1.29	1.28	1.40	1.42	1.27	1.32	1.36	1.38	1.45	1.24	1.47	1.40	1.49	1.55
4	1.33	1.40	1.23	1.32	1.34	1.43	1.31	1.28	1.34	1.32	1.34	1.24	1.19	1.32	1.38	1.21	1.34	1.31	1.37	1.46	1.15	1.27	1.27	1.43	1.45
5	1.28	1.33	1.23	1.32	1.30	1.40	1.31	1.28	1.35	1.36	1.39	1.24	1.21	1.43	1.51	1.19	1.26	1.29	1.39	1.47	1.26	1.34	1.37	1.47	1.44
6	1.36	1.35	1.27	1.36	1.30	1.40	1.33	1.34	1.42	1.41	1.51	1.34	1.26	1.43	1.49	1.30	1.35	1.28	1.44	1.48	1.33	1.35	1.42	1.48	1.57
7	1.28	1.32	1.23	1.33	1.32	1.38	1.28	1.31	1.36	1.33	1.44	1.29	1.23	1.41	1.42	1.25	1.37	1.44	1.39	1.49	1.27	1.35	1.40	1.35	1.49
8	1.30	1.37	1.30	1.38	1.38	1.42	1.32	1.34	1.43	1.37	1.45	1.40	1.43	1.53	1.44	1.45	1.45	1.57	1.38	1.49	1.27	1.50	1.41	1.47	1.65
9	1.27	1.37	1.32	1.36	1.39	1.42	1.43	1.36	1.52	1.43	1.40	1.37	1.44	1.45	1.43	1.46	1.30	1.33	1.32	1.38	1.37	1.44	1.36	1.37	1.46
10	1.26	1.32	1.41	1.43	1.61	1.55	1.53	1.36	1.50	1.49	1.67	1.54	1.36	1.35	1.39	1.36	1.62	1.65	1.42	1.42	1.61	1.44	1.41	1.44	1.53
11	1.28	1.48	1.50	1.41	1.41	1.37	1.43	1.46	1.53	1.42	1.46	1.42	1.38	1.48	1.44	1.36	1.43	1.40	1.37	1.38	1.37	1.42	1.41	1.45	1.53
12	1.74	1.86	1.91	1.88	1.72	1.61	1.49	1.46	1.50	1.57	1.50	1.59	1.44	1.54	1.53	1.46	1.51	1.40	1.48	1.44	1.40	1.52	1.48	1.58	1.74
13		1.53	1.47	1.36	1.38	1.49	1.51	1.57	1.45	1.44	1.66	1.56	1.39	1.56	1.46	1.52	1.53	1.45	1.77	1.37	1.50	1.55	1.46	1.61	1.63
14				1.44	1.61	1.59	1.62	1.58	1.58	1.32	1.62	1.68	1.62	1.52	1.57	1.50	1.51	1.48	1.62	1.38	1.48	1.54	1.50	1.60	1.55
15						1.25	1.43	1.41	1.39	1.34	1.43	1.36	1.38	1.28	1.52	1.38	1.33	1.43	1.41	1.30	1.31	1.42	1.50	1.71	1.53
16							1.64	1.59	1.64	1.29	1.42	1.58	1.49	1.44	1.26	1.48	1.56	1.52	1.56	1.40	1.38	1.36	1.33	1.37	1.42
17									1.37	1.54	1.33	1.38	1.27	1.51	1.41	1.53	1.36	1.46	1.50	1.36	1.46	1.59	1.62	1.66	1.99
18											1.36	1.55	1.61	1.52	1.42	1.48	1.49	1.53	1.54	1.56	1.41	1.48	1.59	1.48	2.20
19														1.66	1.94	1.52	1.79	1.61	1.33	1.55	1.71	1.57	1.89	1.87	2.46

Table A.4.3 Density values for Fig. A.4.3.

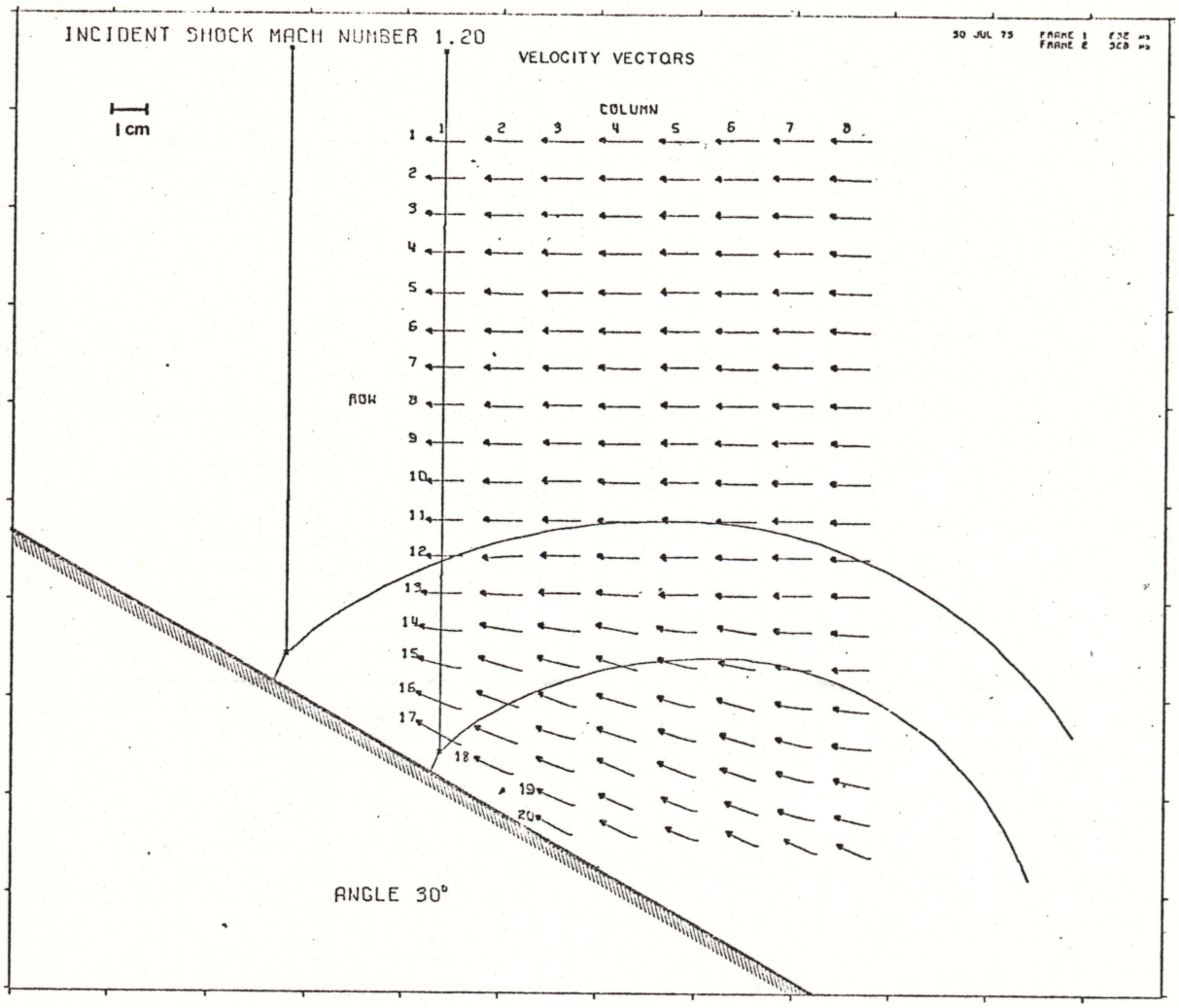

Fig. A.4.4 Velocity vectors 232 - 328 μs.

COLUMN 1 — FRAME 1 - 2

ROW	U(M/S)	V(M/S)	VEL	ANGLE
1	96.62	7.21	96.89	4.27
2	93.84	2.58	93.87	1.54
3	93.45	3.48	93.71	2.07
4	94.75	1.97	94.77	1.19
5	94.52	3.66	94.59	2.22
6	96.92	-0.21	96.92	-0.13
7	92.70	1.45	92.71	0.90
8	91.72	2.32	91.75	1.45
9	90.83	0.82	90.83	0.52
10	94.45	0.95	91.45	0.60
11	91.25	1.84	91.27	1.16
12	89.57	0.32	89.57	0.21
13	101.88	3.20	101.93	1.80
14	107.67	12.92	108.42	6.84
15	102.57	27.87	112.12	14.45
16	114.93	44.00	123.06	20.95
17	116.52	62.22	132.09	28.10

COLUMN 2 — FRAME 1 - 2

ROW	U(M/S)	V(M/S)	VEL	ANGLE
1	89.73	7.23	90.02	4.61
2	90.59	0.30	90.59	0.19
3	92.55	-1.11	92.66	-0.69
4	91.05	0.53	91.05	0.34
5	93.09	4.65	93.20	2.86
6	91.51	-0.01	91.51	-0.00
7	95.27	0.23	95.27	0.14
8	94.27	1.88	94.29	1.14
9	93.35	1.16	93.35	0.71
10	94.75	1.32	94.76	0.80
11	95.36	1.46	95.38	0.87
12	97.85	-6.99	98.09	-4.09
13	103.64	2.73	103.67	1.51
14	100.41	15.46	101.54	8.84
15	108.63	31.38	113.07	16.11
16	105.17	36.07	111.18	18.93
17	107.23	40.16	114.50	20.53
18	98.32	43.86	107.66	24.04

COLUMN 3 — FRAME 1 - 2

ROW	U(M/S)	V(M/S)	VEL	ANGLE
1	104.85	6.43	105.04	3.51
2	104.08	1.02	104.09	0.56
3	101.55	1.82	101.54	1.03
4	99.73	4.23	99.82	2.43
5	100.50	-0.34	100.50	-0.19
6	98.73	0.50	98.73	0.29
7	96.24	-0.27	96.24	-0.16
8	94.46	1.35	94.47	0.82
9	91.89	2.04	91.93	1.83
10	94.96	0.01	94.96	0.01
11	94.71	2.48	94.74	1.50
12	98.50	1.92	98.52	1.12
13	103.09	0.41	103.09	0.24
14	103.97	16.45	105.26	8.99
15	105.09	25.22	108.08	13.50
16	97.48	36.07	103.64	20.30
17	98.82	28.28	100.86	16.28
18	93.67	36.10	100.02	21.16
19	94.51	41.74	103.32	23.83
20	91.76	44.57	104.29	28.38

COLUMN 4 — FRAME 1 - 2

ROW	U(M/S)	V(M/S)	VEL	ANGLE
1	104.25	5.88	104.42	3.23
2	104.22	2.06	104.24	1.13
3	102.57	-0.25	102.57	-0.14
4	100.83	-0.20	100.83	-0.11
5	101.39	1.51	101.40	0.85
6	99.66	0.78	99.68	0.45
7	101.03	2.50	101.06	1.42
8	98.59	0.17	98.59	0.10
9	99.21	0.30	99.21	0.17
10	98.96	2.76	99.00	1.59
11	99.63	1.32	99.63	0.76
12	100.20	3.01	100.24	1.72
13	100.74	5.49	100.89	3.12
14	103.26	19.03	105.00	10.44
15	99.57	30.79	104.22	17.18
16	97.16	27.67	101.02	15.90
17	94.58	30.03	99.23	17.62
18	89.40	39.37	97.66	23.77
19	81.51	36.06	89.13	23.87
20	86.24	42.67	98.02	25.81

COLUMN 5 — FRAME 1 - 2

ROW	U(M/S)	V(M/S)	VEL	ANGLE
1	95.86	3.48	95.92	2.08
2	94.20	1.16	94.21	0.72
3	94.07	0.50	94.07	0.30
4	92.23	3.69	92.30	2.29
5	91.32	2.20	91.35	1.38
6	92.70	3.15	92.75	1.95
7	90.21	2.38	90.24	1.51
8	90.01	3.27	90.07	2.08
9	89.09	2.57	89.13	1.65
10	88.95	1.89	88.97	1.21
11	87.16	3.51	87.22	2.31
12	90.29	-0.99	90.80	-0.63
13	94.00	0.81	94.00	0.50
14	98.20	11.26	98.84	6.64
15	97.59	24.70	100.67	14.20
16	92.63	26.99	96.48	16.24
17	90.89	27.82	95.05	17.02
18	94.31	38.24	101.77	22.07
19	88.00	35.00	94.70	21.69
20	79.33	32.44	85.70	22.24

COLUMN 6 — FRAME 1 - 2

ROW	U(M/S)	V(M/S)	VEL	ANGLE
1	106.40	-1.41	106.41	-0.76
2	103.10	-1.41	103.11	-0.78
3	103.61	1.86	103.63	1.03
4	103.46	1.19	103.48	0.65
5	101.81	-1.12	101.82	-0.63
6	102.35	1.37	102.36	0.77
7	101.40	1.44	101.41	0.82
8	100.51	-0.05	100.51	-0.03
9	103.40	2.51	103.43	1.39
10	100.09	2.51	100.12	1.44
11	99.27	-1.33	99.28	-0.77
12	98.19	2.67	98.23	1.56
13	98.06	1.20	98.08	0.70
14	93.57	13.72	94.57	8.24
15	87.01	17.52	88.75	11.39
16	90.49	25.60	94.04	15.80
17	84.09	24.71	87.64	16.38
18	81.51	27.08	85.89	18.38
19	79.77	27.92	84.51	19.29
20	77.01	35.77	84.91	24.92

COLUMN 7 — FRAME 1 - 2

ROW	U(M/S)	V(M/S)	VEL	ANGLE
1	98.64	0.93	98.64	0.54
2	99.25	1.06	99.26	0.61
3	98.28	1.92	98.29	1.12
4	95.89	-1.98	95.91	-1.18
5	98.78	2.56	98.78	1.49
6	99.37	1.51	99.38	0.87
7	99.12	3.07	99.20	1.78
8	98.25	1.69	98.27	0.98
9	99.79	-3.08	99.81	-1.19
10	100.32	0.41	100.32	0.23
11	99.34	1.27	99.35	0.73
12	97.53	3.67	97.60	2.16
13	94.31	1.32	94.32	0.80
14	93.12	8.45	93.51	5.19
15	86.01	10.69	87.26	7.04
16	88.47	14.04	90.57	9.02
17	86.26	21.97	90.95	14.06
18	91.19	23.74	94.23	14.56
19	90.22	24.61	93.52	15.24
20	81.85	36.22	90.50	23.87

COLUMN 8 — FRAME 1 - 2

ROW	U(M/S)	V(M/S)	VEL	ANGLE
1	100.28	3.59	100.35	2.05
2	99.33	3.67	99.40	2.11
3	99.95	3.80	100.02	2.18
4	100.54	4.72	100.65	2.69
5	101.18	4.06	101.28	2.30
6	98.69	3.31	98.74	1.92
7	94.66	1.70	94.67	1.03
8	97.68	0.35	97.68	0.20
9	94.33	1.91	94.34	1.16
10	95.75	1.29	95.76	0.77
11	95.60	0.61	95.61	0.37
12	94.66	0.66	94.66	0.41
13	91.38	-0.10	91.38	-0.06
14	91.84	4.74	91.96	2.95
15	91.14	-2.26	91.17	-1.41
16	85.91	7.90	86.27	5.25
17	95.11	9.00	95.62	5.64
18	86.81	18.36	88.73	11.94
19	85.81	20.00	88.11	13.12
20	82.00	35.68	90.42	23.52

Table A.4.4 Velocity values for Fig. A.4.4.

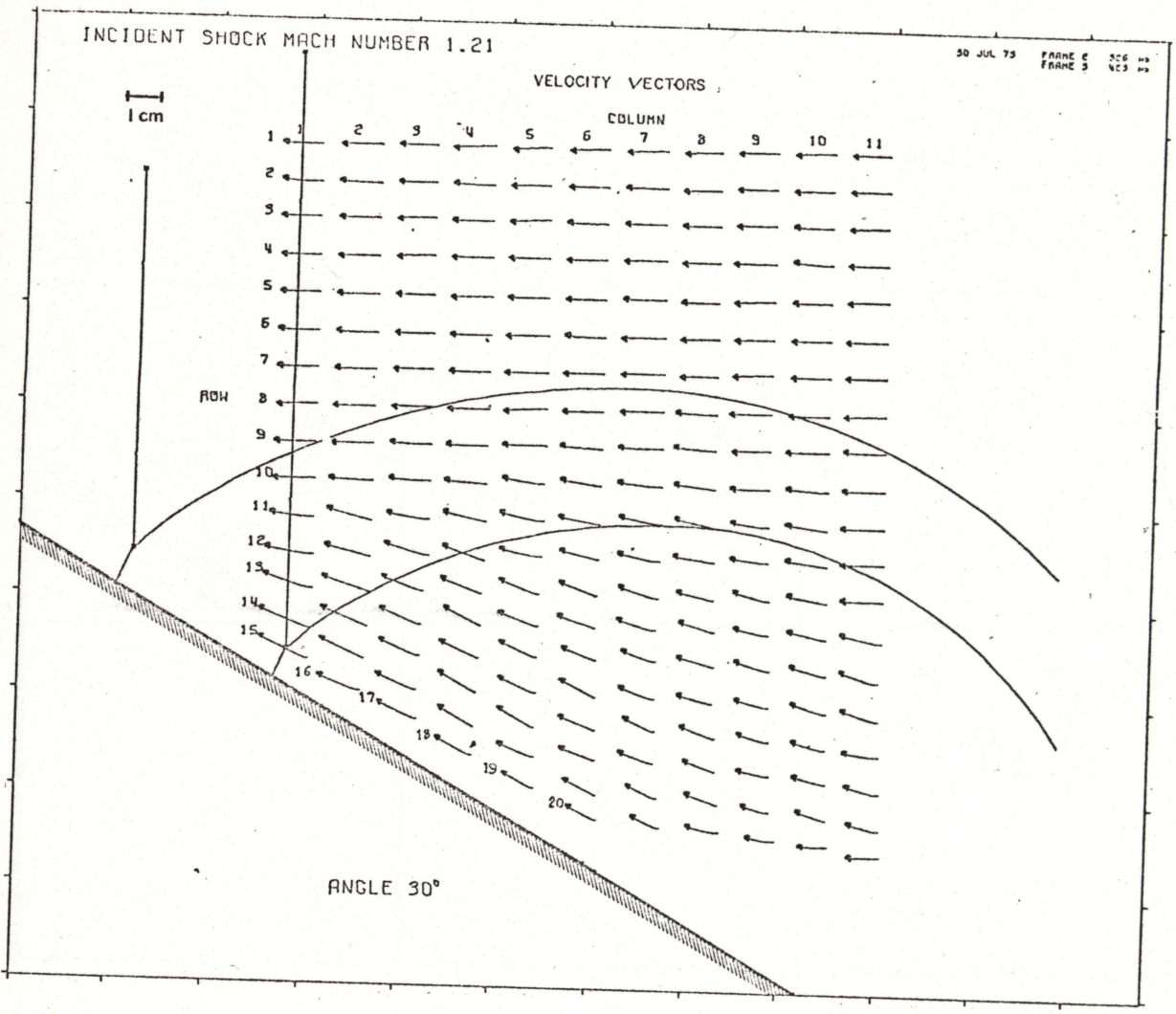

Fig. A.4.5 Velocity vectors 328 - 423 μs.

COLUMN 1			FRAME 2 - 3	
ROW	U(M/S)	V(M/S)	VEL	ANGLE
1	101.26	6.01	101.44	3.40
2	99.71	8.19	100.64	4.70
3	98.44	1.75	98.48	1.02
4	98.56	0.84	98.57	0.49
5	98.60	2.29	98.63	1.33
6	101.81	3.07	101.86	1.72
7	101.90	2.95	101.96	1.66
8	101.37	-1.90	101.38	-1.08
9	103.66	2.77	103.70	1.53
10	105.38	1.14	105.39	0.62
11	111.30	14.58	112.25	7.46
12	122.22	10.65	123.77	4.99
13	125.50	40.77	131.96	18.01
14	134.59	53.53	144.85	21.69
15	128.15	60.29	141.63	25.20

COLUMN 2			FRAME 2 - 3	
ROW	U(M/S)	V(M/S)	VEL	ANGLE
1	102.83	0.42	102.83	0.24
2	105.12	5.09	105.24	2.77
3	103.07	-1.38	103.08	-0.76
4	103.98	-2.26	104.00	-1.24
5	104.73	1.57	104.74	0.86
6	103.98	3.00	104.02	1.65
7	104.16	0.53	104.16	0.29
8	105.11	-1.91	105.13	-1.04
9	106.73	-0.41	106.73	-0.22
10	109.80	4.30	109.88	2.24
11	113.01	27.96	116.40	13.85
12	114.70	27.02	117.94	13.25
13	119.94	37.30	125.60	17.27
14	116.54	47.29	125.77	22.09
15	112.57	50.98	123.57	24.37
16	109.01	42.90	117.14	21.48

COLUMN 3			FRAME 2 - 3	
ROW	U(M/S)	V(M/S)	VEL	ANGLE
1	96.29	2.42	96.32	1.44
2	97.15	3.11	97.20	1.84
3	98.26	-4.02	98.35	-2.35
4	97.57	-4.18	97.66	-2.45
5	99.05	1.24	99.06	0.72
6	100.69	1.96	100.71	1.11
7	101.65	-0.48	101.65	-0.27
8	102.52	-0.57	102.53	-0.32
9	105.52	6.48	105.71	3.52
10	107.10	8.78	107.46	4.68
11	110.64	17.40	111.40	8.99
12	114.32	32.36	118.82	15.81
13	108.66	39.92	115.76	20.17
14	100.26	42.67	114.89	22.74
15	109.53	44.33	114.46	22.78
16	105.65	43.46	114.24	22.35
17	101.69	46.35	111.76	24.50

COLUMN 4			FRAME 2 - 3	
ROW	U(M/S)	V(M/S)	VEL	ANGLE
1	109.69	-4.33	109.78	-2.26
2	106.35	4.07	106.43	2.19
3	107.37	0.01	107.37	0.03
4	108.32	-2.38	108.36	-1.26
5	106.85	-3.35	106.95	-1.79
6	107.63	0.48	107.63	0.26
7	105.39	-0.40	105.39	-0.27
8	107.08	-1.34	107.09	-0.72
9	107.82	2.40	107.85	1.22
10	108.57	6.33	108.76	3.34
11	111.26	22.02	113.42	11.19
12	108.55	35.16	114.10	17.95
13	106.93	38.93	113.60	20.01
14	95.81	44.73	105.74	25.03
15	100.71	41.66	108.99	22.47
16	98.12	50.89	110.64	27.41
17	90.42	48.99	102.82	28.43
18	95.99	49.09	107.80	27.06

COLUMN 5			FRAME 2 - 3	
ROW	U(M/S)	V(M/S)	VEL	ANGLE
1	96.18	-4.93	96.30	-2.94
2	98.52	-1.83	98.54	-1.07
3	101.86	-2.41	101.86	-1.35
4	104.17	-1.06	104.17	-0.60
5	104.16	1.14	104.19	0.62
6	109.86	-1.15	109.86	-0.60
7	110.68	0.33	110.68	0.17
8	111.74	-5.25	111.96	-2.69
9	113.08	4.10	113.15	2.08
10	107.22	17.14	108.56	9.08
11	114.11	25.17	116.84	12.41
12	108.79	22.47	111.16	11.67
13	102.62	39.41	109.36	21.12
14	101.42	36.14	107.47	19.61
15	95.01	42.11	103.02	23.80
16	98.64	42.83	105.71	23.91
17	93.26	52.04	106.80	29.16
18	93.09	36.22	99.85	21.28
19	79.63	41.16	89.64	27.33

COLUMN 6			FRAME 2 - 3	
ROW	U(M/S)	V(M/S)	VEL	ANGLE
1	98.35	-5.00	98.48	-2.91
2	99.15	-2.72	99.19	-1.58
3	101.48	1.15	101.47	0.65
4	101.63	-1.32	101.64	-0.74
5	100.92	-0.69	100.92	-0.39
6	101.61	4.72	101.72	2.66
7	102.73	-2.43	102.76	-1.36
8	102.82	-2.55	102.86	-1.42
9	106.54	6.10	106.72	3.28
10	101.66	13.68	102.57	7.66
11	103.17	18.32	104.75	10.07
12	97.65	21.16	99.92	12.23
13	94.96	33.52	100.70	19.45
14	95.93	30.32	100.61	17.54
15	84.99	30.62	90.34	19.81
16	87.62	42.39	97.52	25.76
17	91.34	33.75	97.28	20.28
18	86.56	31.19	93.70	19.45
19	80.32	38.58	89.14	25.70
20	75.62	39.98	85.54	27.87

COLUMN 7			FRAME 2 - 3	
ROW	U(M/S)	V(M/S)	VEL	ANGLE
1	101.25	-3.47	101.31	-1.96
2	105.11	1.26	105.12	0.68
3	104.42	1.11	104.42	0.61
4	106.21	-2.87	106.25	-1.55
5	108.50	1.79	108.52	0.95
6	111.11	-2.06	111.15	-1.52
7	109.58	-1.56	109.59	-0.81
8	109.67	-1.67	109.68	-0.87
9	112.64	6.17	112.80	3.13
10	111.70	12.09	112.47	6.48
11	108.38	20.71	110.24	10.82
12	106.05	22.87	108.48	12.17
13	99.56	31.17	104.33	17.39
14	97.30	31.00	102.11	17.67
15	84.84	29.68	89.88	19.25
16	88.75	32.05	94.30	19.85
17	79.25	37.12	87.51	25.10
18	87.37	31.80	92.97	20.00
19	75.51	35.98	83.64	25.48
20	72.56	31.84	79.24	23.99

COLUMN 8			FRAME 2 - 3	
ROW	U(M/S)	V(M/S)	VEL	ANGLE
1	96.96	-2.28	96.99	-1.39
2	97.24	-3.08	97.27	-1.81
3	96.47	-1.65	96.49	-0.98
4	96.65	-4.12	96.74	-2.44
5	97.40	-0.29	97.40	-0.17
6	98.35	-2.74	98.39	-1.60
7	96.09	-2.94	96.14	-1.75
8	105.42	2.76	105.45	1.50
9	106.86	8.98	107.24	4.81
10	105.31	11.16	105.90	6.06
11	102.70	21.17	104.86	11.65
12	100.09	16.45	101.35	8.82
13	94.26	21.42	96.62	12.81
14	90.23	25.11	93.44	15.55
15	98.19	24.48	101.20	14.00
16	90.55	20.94	92.64	13.03
17	88.73	20.21	91.72	12.80
18	81.82	27.57	86.32	18.58
19	84.23	28.26	88.84	18.66
20	83.78	20.28	86.20	13.61

COLUMN 9			FRAME 2 - 3	
ROW	U(M/S)	V(M/S)	VEL	ANGLE
1	101.65	-2.15	101.65	-1.21
2	101.64	0.00	101.64	0.00
3	100.19	-0.87	100.20	-0.50
4	100.06	0.12	100.08	0.06
5	103.61	-2.36	103.64	-1.30
6	101.52	-2.77	101.56	-1.57
7	102.25	-4.43	102.34	-2.48
8	100.27	-0.38	100.27	-0.20
9	98.38	-0.87	98.39	-0.51
10	100.61	5.36	100.76	3.05
11	98.81	14.61	99.89	8.41
12	98.95	12.93	99.80	7.44
13	92.33	25.15	99.70	15.24
14	89.47	19.44	91.56	12.26
15	96.91	25.65	94.48	15.78
16	87.21	21.48	89.91	13.84
17	81.72	23.54	85.04	16.07
18	80.50	15.52	81.08	10.92
19	76.22	19.76	78.95	15.72
20	72.87	12.67	73.97	9.87

COLUMN 10			FRAME 2 - 3	
ROW	U(M/S)	V(M/S)	VEL	ANGLE
1	100.72	-3.89	100.79	-2.21
2	100.76	-2.44	100.79	-1.39
3	99.91	2.13	99.93	1.22
4	99.84	6.72	100.06	3.85
5	97.82	-0.55	97.82	-0.32
6	100.27	-0.69	100.27	-0.39
7	100.39	-1.49	100.40	-0.85
8	102.84	-1.53	102.85	-0.86
9	110.72	6.19	110.72	3.20
10	105.84	7.76	106.13	4.19
11	104.16	13.08	106.06	7.15
12	104.24	13.75	106.18	7.52
13	101.06	17.45	102.66	9.80
14	97.93	19.58	99.67	11.31
15	91.58	23.96	94.66	14.66
16	89.99	24.92	93.93	16.66
17	83.96	21.89	86.77	14.61
18	82.56	19.37	84.80	13.26
19	74.83	23.69	78.36	17.41
20	69.55	4.57	70.00	3.74

COLUMN 11			FRAME 2 - 3	
ROW	U(M/S)	V(M/S)	VEL	ANGLE
1	96.49	-0.24	96.49	-0.15
2	99.75	-1.04	99.75	-0.60
3	99.11	-2.75	99.15	-1.59
4	101.50	-1.22	101.51	-0.69
5	104.09	-2.93	104.14	-1.61
6	105.59	-0.54	105.59	-0.29
7	103.30	0.05	103.30	0.03
8	106.64	-3.10	106.68	-1.67
9	107.24	4.66	107.35	2.49
10	108.15	3.77	108.22	2.00
11	109.82	3.71	109.88	1.94
12	109.26	1.22	109.21	0.64
13	108.37	5.00	108.44	2.64
14	107.09	23.68	109.62	12.47
15	98.25	31.90	103.28	17.99
16	95.23	30.10	99.87	17.54
17	90.36	14.10	91.46	8.87
18	85.42	23.23	88.62	15.22
19	79.31	20.55	81.93	14.52
20	80.80	1.64	80.82	1.17

Table A.4.5 Velocity values for Fig. A.4.5.

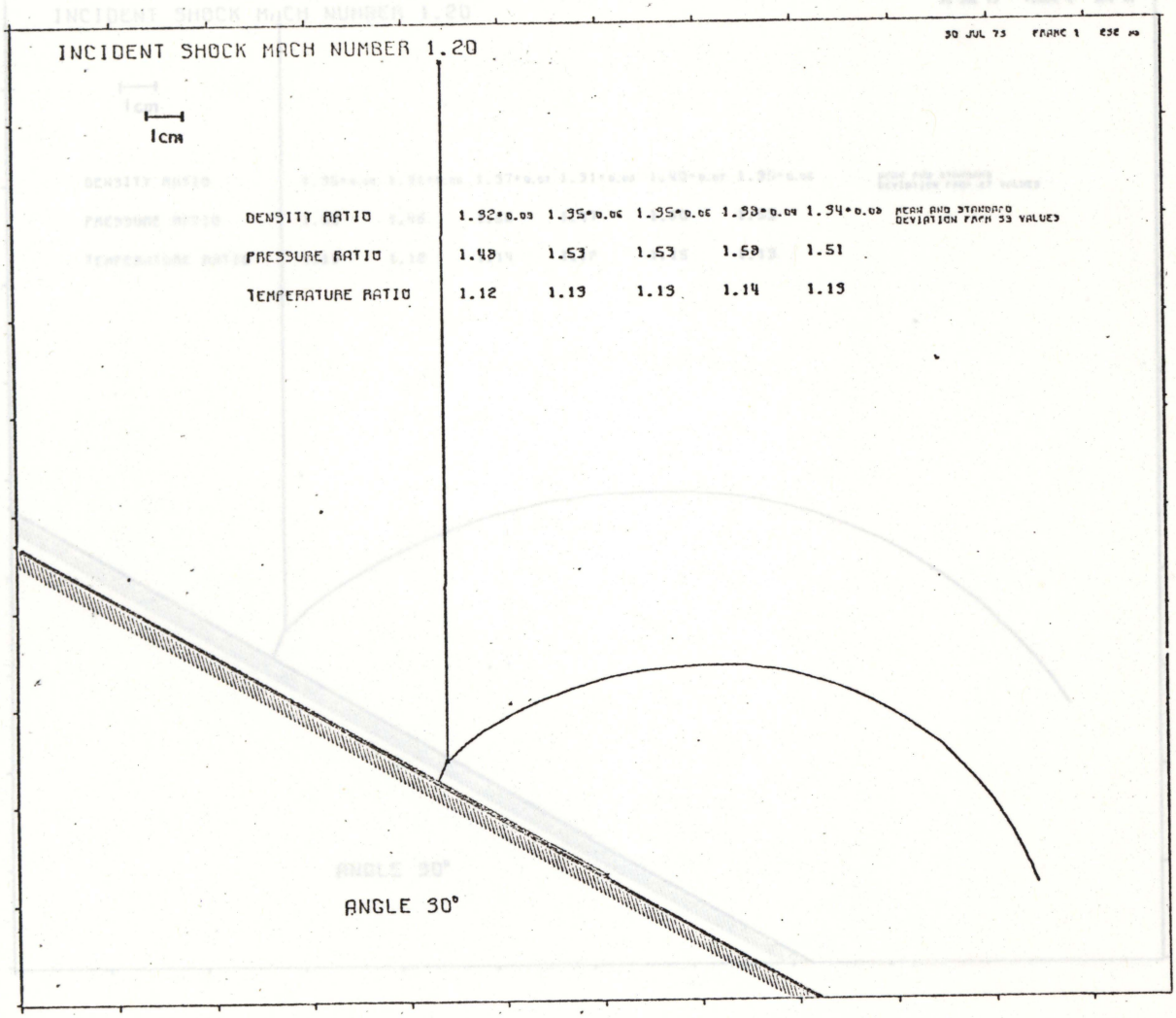

Fig. A.4.6 Mean ratios 232 μs.

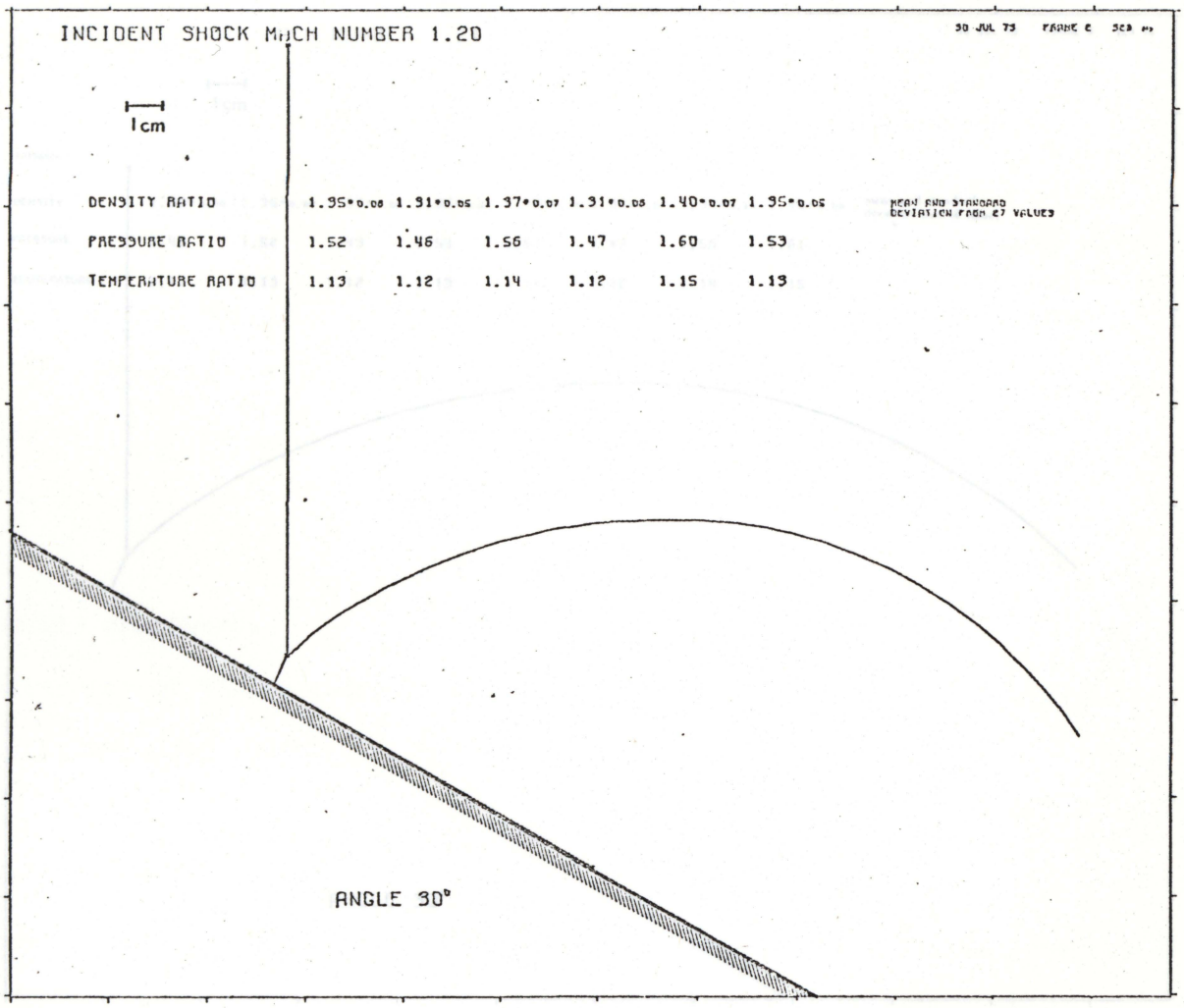

Fig. A.4.7 Mean ratios 328 µs.

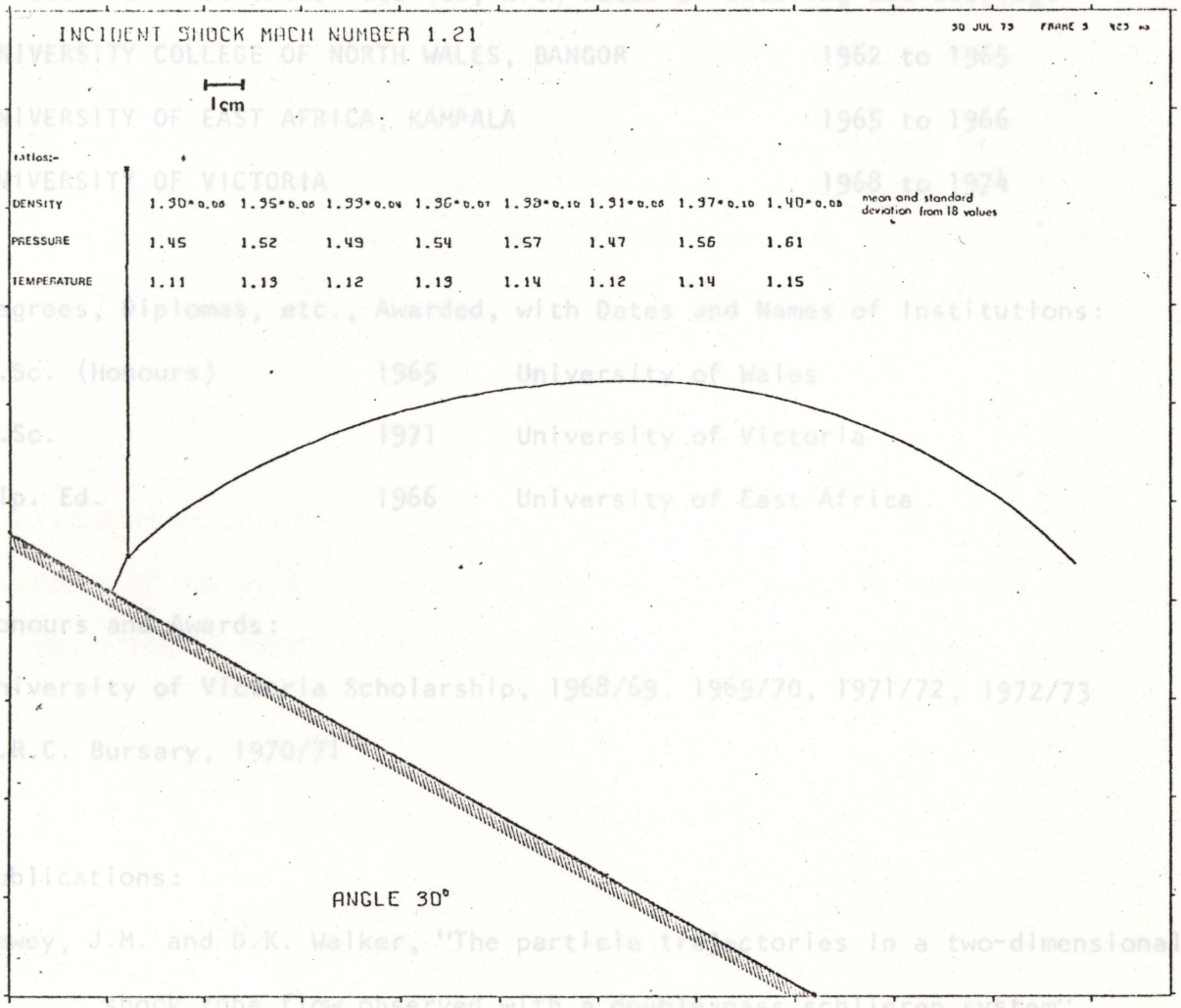

Fig. A.4.8 Mean ratios 423 μs.

Surname: WALKER Given Names: David Keith

Place of Birth: BIRMINGHAM, U.K. Date of Birth: December 16, 1944

Educational Institutes Attended, with Dates of Entering and Leaving:

UNIVERSITY COLLEGE OF NORTH WALES, BANGOR	1962 to 1965
UNIVERSITY OF EAST AFRICA, KAMPALA	1965 to 1966
UNIVERSITY OF VICTORIA	1968 to 1974

Degrees, Diplomas, etc., Awarded, with Dates and Names of Institutions:

B.Sc. (Honours)	1965	University of Wales
M.Sc.	1971	University of Victoria
Dip. Ed.	1966	University of East Africa

Honours and Awards:

University of Victoria Scholarship, 1968/69, 1969/70, 1971/72, 1972/73

N.R.C. Bursary, 1970/71

Publications:

Dewey, J.M. and D.K. Walker, "The particle trajectories in a two-dimensional shock tube flow observed with a double-pass schlieren system". Published in *Recent Developments in Shock Tube Research*, Proceedings of the Ninth International Shock Tube Symposium, Stanford University, 1973 (Stanford University Press, 1973)

PARTIAL COPYRIGHT LICENSE

I hereby grant the right to lend my dissertation (the title of which is shown below) to users of the University of Victoria Library, and to make *single copies only* for such users or in response to a request from the library of any other university, or similar institution, on its behalf or for one of its users. I further agree that permission for extensive copying of this dissertation for scholarly purposes may be granted by me or a member of the University designated by me. It is understood that copying or publication of this dissertation for financial gain shall not be allowed without my written permission.

Title of Dissertation:

STUDY OF TWO-DIMENSIONAL SHOCK TUBE FLOWS BY FOLLOWING PARTICLE TRAJECTORIES USING A MULTIPLY PULSED LASER SCHLIEREN SYSTEM

Author .....

David Keith Walker

May 1974